Non-Dissociative Sequential Metabolism of Enoxacin to a Metabolic Intermediate Complex with Cytochrome P450 1A2

Ryan P. Seguin

A dissertation

submitted in partial fulfillment of the

requirements for the degree of

Doctor of Philosophy

University of Washington

2017

Reading Committee:

Kent L. Kunze, Chair

Rheem A. Totah

William M. Atkins

Program Authorized to Offer Degree:

Medicinal Chemistry

University of Washington

Abstract

Non-Dissociative Sequential Metabolism of Enoxacin to a Metabolic Intermediate Complex with Cytochrome P450 1A2

Ryan P. Seguin

Chair of the Supervisory Committee:

Assoc. Professor Kent L. Kunze

Medicinal Chemistry

Cytochrome P450 enzymes constitute a superfamily of isoforms which accelerate the removal of foreign compounds from the body through oxidative biotransformation to generate polar metabolites that are more readily excreted from the body. Hence, susceptibility to oxidation by cytochrome P450 may largely determine the in vivo half-life, plasma level, and tissue exposure of small molecule drugs. As the P450 isoforms involved in drug metabolism contain large, flexible, and promiscuous active sites which can bind and metabolize multiple drugs, it is common for one drug to interfere with the metabolism of another. Inhibition of a specific P450 isoform may lead to drug-drug interactions (DDIs) through impairment of metabolic clearance of a coadministered drug and the build-up of this drug or its metabolites to toxic levels in the body. The use of in vitro data to predict, rationalize and, ultimately, prevent DDIs is a top priority in drug development. Accordingly, emphasis in this field of study has been placed on understanding which drug structures inhibit P450 and the mechanism by which inhibition occurs.

This dissertation explores the mechanism of inhibition of cytochrome P450 1A2 (CYP1A2) by the fluoroquinolone antibacterial enoxacin. Enoxacin elicits clinically-significant DDIs with

theophylline and caffeine due to potent CYP1A2 inhibition in vivo. However, enoxacin is characterized as a weak reversible inhibitor of CYP1A2 in vitro leading to severe underprediction of the DDIs with theophylline and caffeine. Herein, we have clarified the mechanism of inhibition as a time-dependent irreversible process where enoxacin is sequentially metabolized within the CYP1A2 active site to a mechanism-based inhibitor. Thus, CYP1A2 is inactivated by a metabolite of enoxacin through formation of a metabolic-intermediate (MI) complex. The mechanism of MI complex formation requires N-hydroxylation of the piperazine ring of enoxacin followed by α-carbon hydroxylation and oxidative ring-opening to a nitroso metabolite that strongly ligates to the ferrous heme iron of CYP1A2.

We elucidated the mechanism of CYP1A2 inactivation as sequential metabolism of the piperazine ring to an MI complex in recombinant CYP1A2 and confirmed that this mechanism is still viable in human liver microsomes. Circumstantial evidence was provided for MI complex formation with CYP1A2 in primary human hepatocytes. The DDIs with theophylline and caffeine were well-predicted by in vitro to in vivo predictions using apparent CYP1A2 inactivation parameters for the parent drug, enoxacin. Our results suggest that enoxacin is sequentially metabolized to an MI complex non-dissociatively within the CYP1A2 active site and that released metabolite intermediates do not significantly contribute to MI complex formation. The non-dissociative nature of the sequential metabolic inactivation process accounts for our success in predicting the DDIs with theophylline and caffeine using apparent inactivation parameters of the parent drug.

Although enoxacin requires multiple CYP1A2-mediated oxidations to inactivate CYP1A2, enoxacin can be treated as a single-step inactivator (i.e. a true mechanism-based inhibitor) for DDI prediction purposes. In our view, non-dissociative sequential inactivation accounts not only for the success of our prediction, but also the potent inhibition of CYP1A2 in vivo. Our observation that N-hydroxy enoxacin, an intermediate hydroxylamine metabolite, is reduced

back to enoxacin in human liver microsomes and human hepatocytes calls into question whether a dissociative sequential inactivation process would be viable in vivo. Futile cycling between enoxacin and the N-hydroxy enoxacin metabolite could theoretically prevent the sequential metabolic process from progressing beyond the hydroxylamine, thus highlighting the importance of non-dissociative sequential metabolism.

In summary, we proposed enoxacin is a time-dependent inhibitor of CYP1A2 through non-dissociative sequential metabolism of the piperazine ring to an MI complex. This is the first report of sequential metabolism of a piperazine by a cytochrome P450 to an MI complex. It is suggested that MI complex formation may result from sequential metabolism of other alicyclic amine-containing substrates and that alicyclic amines may be a new structural alert for MI complex formation.

Table of Contents

List of Figures

List of Tables

Acknowledgements

Thank you to:

Kent Kunze for a great deal of patience, guidance, and advice. Thank you for putting me back on the trail when I, all too often, strayed away from it. At the same time, thank you for giving me the freedom to explore and create my own trails.

Doctoral Committee Members: Rheem Totah, Bill Atkins, and Allan Rettie, thank you for serving on my committee. I have learned an immense amount from each of you over the course of graduate school. Thank you Christophe Verlinde for serving as my GSR.

Wendel Nelson for inspiring me to join the Department of Medicinal Chemistry.

Members of the Kunze Lab: Kelsey Hanson, Cristina Fernandez, and Rob Pelletier; all good people whom I have learned from and enjoyed spending time with. I want to acknowledge former Kunze lab member Dustin Smith who made an important contribution to the research topic of this dissertation. His work allowed me to hit the ground running. Also, Kantipudi Babu for synthesizing many compounds for the Kunze lab and for all the sweets from India!

I want to thank my Med Chem "cohort": Wynton McClary, Amanda Johnson, and Shannon Lambert for all the good times during the first few years of struggling through classes and not knowing what we were doing. Somehow we made it through.

I have met many wonderful people during graduation school. To name just a few:
Eric Evangelista, you are reliably entertaining.
Mariko Nakano, I look forward to future trips to Japan with you.
Natalie Garcia, for being a wonderful friend. You will always be my Tabata instructor.
Nancy Hom, it has been fun riding bikes, growing plants, and visiting bats with you.
Natalie and Nancy again, for going on many walks to you know where.
Mike Guttman, thanks for helping me move a couch. And probably a few other things too.
Tad Davenport, for helping me pursue Quality in life.
Thank you Kelly Lee and Lee lab for letting me be an unofficial lab member. I've learned so much about viruses.

Mass spectrometry: Dale Whittington, Ross Lawrence, Scott Edgar, Tauri Senn. Thanks for keeping things running. In particular, thank you Dale for coming in on weekends to help out and, further, hosting us all on weekends at the cabin.

I want to acknowledge Michele Scian for so many hours spent helping me record and interpret NMR spectra of synthesized material and never failing to let me know when I didn't make what I thought I did.

Medicinal Chemistry staff: Jeanine Kanov, Caryl Corsi, Meg Running, Judi Morris, Erik Lee, Sarah Lenti, and all the staff over the years for the work you do that has kept everything running. I have relied on and been helped by each of you many times.

Thank you Mom and Dad, my brother Alex, my niece Alexis, Uncle Brian and Aunt Elaine, Grandma Dickie and the rest of my Ohio family. I am grateful for all of you.

Dedication

To my parents,
for always supporting me
from the beginning.

Chapter 1: Introduction

1.1 Dissertation Purpose and Organization

The primary purpose of this dissertation is to elucidate the mechanism of CYP1A2 inhibition by the fluoroquinolone antibacterial enoxacin (ENX) and to further characterize inhibition in multiple in vitro systems. Secondarily, it is hoped that the results and discussion presented are helpful to those studying metabolite-mediated enzyme inactivation and drug-drug interactions (DDIs), in particular those involving sequential metabolism of the parent drug.

The current chapter (Chapter 1) provides the reader with useful background information concerning the role of cytochrome P450 inhibition in DDIs. An emphasis has been placed on mechanism-based (irreversible) inhibition of cytochrome P450 and the use of in vitro data to study inhibition mechanisms and predict DDIs. In addition, some background on fluoroquinolone antibacterials will be presented. Studies related to inhibition of CYP1A2 by fluoroquinolones in vivo and in vitro will be reviewed, especially with regard to ENX.

In Chapter 2, the mechanism by which (a metabolite of) ENX inactivates CYP1A2 was studied. The enzyme system used for all experiments in Chapter 2 is CYP1A2 bactosomes. Bactosomes are a commercially-available preparation of bacterial membranes containing human cytochrome P450 reductase and a single human cytochrome P450 isoform. Both proteins are of the native, full-length unmodified sequence. This enzyme system greatly facilitated our mechanistic studies as it only contains a single cytochrome P450 isoform. More importantly, the specific CYP1A2 content (pmol CYP1A2/mg protein) in this system is ~20-fold higher than in human liver microsomes which allowed us to complete spectrophotometric studies that were critical to elucidating the mechanism of inhibition.

In Chapter 3, the inactivation of CYP1A2 by (a metabolite of) ENX was further characterized in human liver microsomes (HLM) and primary human hepatocytes. Compared with CYP1A2 bactosomes, HLM and hepatocytes are more relevant systems for the prediction of DDIs as the enzyme environment and lipid content are more consistent with that of a human liver. Thus, the properties of CYP1A2 may differ across systems thereby affecting the interaction of CYP1A2 with ENX. Differences between bactosomes, HLM, and hepatocytes might also affect the metabolic fate and stability of ENX and its metabolites which may in turn alter the inhibitory effect upon CYP1A2. Finally, note that hepatocytes are whole cells. The multitude of cellular processes taking place while inhibition of CYP1A2 is being characterized in hepatocytes suggests that the results of studies performed in hepatocytes should be interpreted with caution. These results are additionally complicated by an uncertainty in the intracellular concentration of ENX and its metabolites relative to the nominal concentrations dosed.

In Chapter 4, the major findings of the above studies are briefly summarized and distilled down to a few key points. Where appropriate, the results of our studies are discussed in the larger context of metabolite-mediated enzyme inactivation and DDI. For example, we suggest that our specific finding of sequential metabolism of the piperazine moiety of ENX to a metabolic-intermediate (MI) complex with CYP1A2 may, more generally speaking, indicate that alicyclic amines contained within other substrate molecules can be sequentially metabolized to MI complexes with other cytochrome P450 isoforms. If true, this conclusion would form the basis for a new structural alert for MI complex formation (alicyclic amines). Another key point made in Chapter 4 is that while *dissociative* sequential metabolic inactivation processes may operate more or less efficiently depending upon the enzyme environment (be it bactosomes, HLM, hepatocytes, or in vivo), *non-dissociative* sequential metabolic processes are contained within the enzyme active site and are, therefore, more likely to be conserved across enzyme environments.

1.2 Drug-Drug Interactions

The US Food and Drug Administration (FDA) estimates that over 2 million adverse drug reactions occur each year resulting in approximately 100,000 deaths (FDA, 2016). By this estimate, adverse drug reactions are the 4th leading cause of death in the United States and cost the healthcare system $136 billion annually. Notably, it has been estimated that 26% of adverse drug reactions are due to drug-drug interactions (DDIs) which are avoidable (Wienkers and Heath, 2005). Therefore, to protect the safety of patients, it is a crucial mission for pharmaceutical scientists (in both academia and industry) to understand how DDIs occur. In particular, this means we must understand how the structural features of drugs interact with the enzymes and proteins that control the metabolic fate of drugs.

It is well established that inhibition of drug-metabolizing cytochrome P450 enzymes presents one of the greatest risks for precipitation of a DDI (Soars et al., 2007). An analysis of the top 200 most prescribed drugs revealed that the majority of drugs are cleared via metabolism and further, that the majority of the metabolic activity can be attributed to just five cytochrome P450 isoforms: CYP1A2, CYP2C9, CYP2C19, CYP2D6, and CYP3A4 (Wienkers and Heath, 2005). The distribution of the metabolic load across this small handful of drug-metabolizing enzymes creates a reasonable expectation that one drug may interfere with the metabolism of another co-administered drug. Many drugs in use today cause mild, moderate, or potent inhibition of one or more CYP isoforms (Rendic, 2002), thereby compromising metabolic clearance and potentially exposing patients to toxic levels of coadministered drugs. The fluoroquinolone antibacterial enoxacin (ENX), the drug studied in this dissertation, is a known inhibitor of CYP1A2 and toxicity experienced by patients that received both ENX and theophylline, a CYP1A2 substrate, has been documented (Wijnands et al., 1984). The severity of the interaction between ENX and CYP1A2 substrates in vivo was among the reasons for the removal of ENX from the US market.

Hence, DDIs not only compromise the safety of patients, but also pose a significant challenge in drug development. Drug developers must ensure that drug candidate molecules in their pipeline which may cause unacceptable DDIs are screened out before being moved forward to more costly stages of development (i.e. clinical trials) and, ultimately, onto the market. Development of a drug requires an immense amount of scientific effort, time, resources, and financial investment. Identifying those molecules which pose a high risk of causing DDIs allows a drug company to manage risk and avoid wasting resources or incurring a significant financial loss later on. To that end, it is imperative that we are able to use in vitro data to predict when a molecule will cause a DDI in vivo. Our understanding of in vitro data, having the correct experimental approaches to generate the most relevant in vitro data, and our ability to utilize in vitro data to accurately predict DDIs will determine our success in choosing the correct molecules to develop as drugs.

1.3 Prediction of Drug-Drug Interactions from in vitro Cytochrome P450 Inhibition Data

Drugs are known to inhibit P450 enzymes by binding reversibly or irreversibly to the enzyme. A variety of in vitro systems and experimental approaches are used to measure reversible and irreversible inhibition of P450 (Fowler and Zhang, 2008). The most common in vitro systems used are recombinant individually-expressed P450, liver microsomes, and hepatocytes. These are the three in vitro systems utilized in this dissertation. Probe substrates (Tucker et al., 2001) are routinely used to assay the activity of specific P450 isoforms in the presence or absence of an inhibitor. For example, in this dissertation, phenacetin is used as a probe substrate of CYP1A2. At the appropriate concentration of phenacetin, phenacetin o-deethylation is a specific probe reaction of CYP1A2 activity in HLM with minimal contribution

from other CYP isoforms (Venkatakrishnan et al., 1998). Therefore, even in complex systems such as HLM and hepatocytes, we can assay for inhibition of specific CYP isoforms.

For reversible inhibition, the inhibitor is co-incubated with the probe substrate to measure inhibition constants such as the IC_{50} value (the inhibitor concentration causing half-maximal inhibition of probe substrate turnover) which will depend upon the concentration of probe substrate and possibly the substrate used. Through the more intensive approach of varying both inhibitor and probe substrate concentrations, one may obtain the K_i value which has greater utility in DDI prediction since it is a more robust binding constant. With an estimate or knowledge of the inhibitor concentration, [I], at which a drug will circulate in vivo, the ratio $[I]/K_i$ can then be determined. With this simple ratio, a crude DDI risk assessment is relatively straightforward as molecules with $[I]/K_i$ ratio below and above a cut-off value (typically 2) will be considered low and high risk molecules, respectively, for precipitating a DDI involving the particular CYP isoform for which the K_i value was measured (Tucker et al., 2001). A detailed discussion of the potential complexities encountered when predicting DDIs for reversible CYP inhibition is outside the scope of this dissertation. It suffices to say that early prediction efforts were centered on reversible CYP inhibition (Ito et al., 2005) and much progress has been made in successfully predicting DDIs based upon reversible inhibition (Obach et al., 2006).

For the purpose of this dissertation, prediction of DDIs based upon *irreversible* CYP inhibition or "time-dependent" inhibition is more relevant and the most reliable methodology for assessing these predictions is still unclear (Burt et al., 2012; Fujioka et al., 2012; Yates et al., 2012). A critical feature of irreversible CYP inhibition is the time-dependent loss of CYP activity in the presence of the inhibitor and NADPH. The experimental method for measuring irreversible (time-dependent) CYP inhibition is to pre-incubate the in vitro system with the inhibitor molecule and NADPH for increasing pre-incubation times followed by measurement of the remaining CYP activity with a probe substrate. The rate of CYP activity loss (λ) caused by

pre-incubation with the inhibitor is generally saturable at increasing concentrations of inhibitor yielding an apparent maximal inactivation rate (k_{inact}) and a concentration at which the inactivation rate is half-maximal (K_I). The apparent inactivation parameters, k_{inact} and K_I, can be used to calculate the enzyme inactivation rate, λ, at a given inhibitor concentration (Tudela et al., 1987) by use of Equation 1:

$$\lambda = \frac{k_{inact}\,[I]}{K_I + [I]} \qquad (1)$$

By considering the magnitude of λ at the circulating concentration of inhibitor present in vivo compared with the natural in vivo degradation rate of the CYP enzyme, k_{deg}, Mayhew et al. (2000) developed the theoretical model for how a time-dependent inhibitor affects the steady-state level of active enzyme in vivo (Figure 1.1) and further extrapolated these enzyme inactivation kinetics to the prediction of a DDI for the first time. Essentially, the introduction of the "exogenous" inactivation rate λ augments the apparent in vivo CYP degradation rate thus lowering the amount of active enzyme pool to a new steady-state. For a substrate dependent on clearance solely by the affected enzyme, this decrease in active enzyme results in a proportional decrease in the intrinsic clearance for that substrate and, therefore, an inversely proportional increase in the magnitude of a DDI (exposure increase) for that substrate. The equations developed by Mayhew et al. (2000) have since been refined to include additional parameters including the fraction of the metabolic clearance of the substrate due to the affected enzyme, f_m. Hence, prediction of the fold AUC increase for a victim substrate (AUC'/AUC) in the presence of the inhibitor is given by Equation 2 (Grimm et al., 2009):

$$\frac{AUC'}{AUC} = \frac{1}{\left(\frac{f_m}{1+\lambda/k_{deg}}\right)+(1-f_m)} \qquad (2)$$

Equation 2 will be used in this dissertation to predict fold AUC increases for theophylline and caffeine in the presence of circulating concentrations of ENX from the in vitro enzyme

inactivation parameters obtained from three in vitro systems and the accuracy of the predictions will be compared with literature values. The DDI magnitude between ENX and CYP1A2 substrates is severely underpredicted when the CYP inhibition mechanism is assumed to be reversible (Obach et al., 2006) highlighting the importance of understanding the inhibition mechanism to accurate DDI prediction. In this dissertation, evidence will be provided for irreversible (time-dependent) inhibition of CYP1A2 by ENX and, ultimately, mechanism-based inhibition of CYP1A2 by a metabolite of ENX. The next section covers the topic of mechanism-based inhibition.

1.4 Mechanism-Based (Time-Dependent) Inhibition

Mechanism-based inhibition is a form of irreversible enzyme inhibition that requires a catalytic step in the enzyme active site. The concept of mechanism-based enzyme inactivation has been around for nearly a century. However, the first clear example and well-defined mechanism of a mechanism-based inhibitor (MBI) did not appear in the literature until 1970. In this seminal paper, inhibition of the *Escherichia coli* enzyme β-hydroxydecanoyl thioester dehydrase by a substrate analogue, 3-decynoyl-N-acetylcysteamine, required a catalytic step by the enzyme in "a rather unique case of an enzyme promoting its own destruction by catalyzing the transformation of a substrate analogue to an active site probe of extreme chemical reactivity" (Endo et al., 1970). A general framework for understanding mechanism-based enzyme inactivation was later developed by Silverman (1988). In his authoritative text, Richard Silverman describes an MBI as "a relatively unreactive compound, having a structural similarity to the substrate or product for a particular enzyme that, via its normal catalytic mechanism of action, converts the inactivator molecule into a species which, without prior release from the active site, binds most often covalently, to that enzyme." Silverman goes on to define a set of

seven criteria which has assisted experimentalists in distinguishing mechanism-based inhibition from other modes of enzyme inhibition:

1. Time-dependent loss of enzyme activity
2. The rate of enzyme inactivation is saturable at high concentrations of inactivator
3. Inactivation is slowed in the presence of an alternative substrate
4. Dialysis does not restore enzyme activity (inactivation is irreversible)
5. A 1:1 stoichiometry of inhibitor bound to enzyme is observed
6. A catalytic step by the enzyme is required for inactivation to occur
7. Inactivation exhibits no lag and is unaffected by addition of trapping agents

In order to fully understand mechanism-based inactivation in the context of P450 enzymes, some knowledge of the mechanism of the catalytic cycle of cytochrome P450 is required. The following three subsections will cover (1) details of the P450 catalytic cycle, (2) mechanism-based inactivation of cytochrome P450, and (3) a type of mechanism-based inactivation, termed “metabolic-intermediate complex formation”, unique to cytochrome P450.

1.4.1 The Cytochrome P450 Catalytic Cycle

Cytochrome P450, a superfamily of b-type heme-containing enzymes found in organisms from all domains of life (Nelson, 2013), are mixed-function oxidases that catalyze the heterolytic cleavage of molecular oxygen to produce one molecule of water and a highly reactive Fe^{V}=O oxene intermediate capable of oxidizing a wide array of substrates. The chemistry catalyzed by cytochrome P450 is varied (Guengerich, 2001) but largely includes oxygen insertion and

desaturation reactions. Each cytochrome P450 isoform contains a unique active site architecture which determines its substrate profile. If a small molecule is a substrate of a given P450 isoform, the site of oxidation on the substrate is then determined by the binding orientation(s) in the P450 active site and, further, by both the steric accessibility and reactivity of sites on the substrate which orient towards the active oxidizing species of P450. Generation of the active oxidizing species of P450 is a multi-step process. These individual steps (labeled a-f) are listed below and correspond to the labels provided in Figure 1.2:

a) The resting state of P450: low-spin, water-bound ferric heme

b) Binding of a substrate molecule (RH) induces a shift to high-spin heme

c) Delivery of the first electron by cytochrome P450 reductase yields ferrous heme

d) Ferrous heme iron binds molecular oxygen

e) Delivery of the second electron by cytochrome b5 or cytochrome P450 reductase yields a ferric peroxy anion species (*) which can also be protonated once on the distal oxygen atom to yield a ferric hydroperoxo species (*)

f) Double protonation of the distal oxygen atom followed by heterolytic O-O bond cleavage yields a highly reactive Fe^{V}=O oxene species (*), also known as Compound I, the principal intermediate in P450 catalysis responsible for substrate oxidation (ROH, oxygen insertion product)

All species marked with an asterisk (*) in the list above are believed to be capable of performing oxidative chemistry on the substrate (Coon et al., 1998). Red arrows in Figure 1.2 indicate “leaks” in the catalytic cycle where uncoupling to produce reactive oxygen species can occur (production of superoxide and peroxide). For further reading on the cytochrome P450 catalytic cycle, the reader is referred to Ortiz de Montellano (2005) and references therein.

1.4.2 Mechanism-Based Inactivation of Cytochrome P450

Through the catalytic cycle described above, cytochrome P450 can convert an innocuous substrate molecule into a reactive intermediate (bioactivation) capable of irreversibly modifying the prosthetic heme group or apoprotein of P450, thus rendering the enzyme catalytically incompetent (Hollenberg et al., 2008). Inhibition is time-dependent and NADPH-dependent (i.e. requires catalysis). It should, therefore, also require an oxygen-containing atmosphere and interaction with the electron-delivery accessory protein cytochrome P450 reductase. Certain organic functional groups and structural motifs are recognized as “bioactivatable” by P450 such as acetylenes, furans, thiophenes, aminophenols and hydrazines to name a few (Orr et al., 2012). In fact, understanding which structures can be bioactivated by P450 to cause enzyme inactivation is a key objective to accomplish in order to move towards an improved drug development process.

In the context of DDIs, a drug which causes mechanism-based inactivation is of serious concern as the inhibition will persist for days beyond drug excretion and until the *de novo* synthesis of new enzyme is complete (Figure 1.1). A study comparing reversible and mechanism-based inhibitors of CYP3A4 found that MBI drugs more frequently produce clinically-significant DDIs (Zhou et al., 2005). These DDIs have led to some fatalities with, for example, drugs such as terfenadine which cause life-threatening torsades de pointes (arrhythmia and QT prolongation). Due to this serious risk, lead candidate molecules are routinely screened for mechanism-based inactivation of P450 during preclinical drug development.

1.4.3 Metabolic-Intermediate Complex Formation with Cytochrome P450

Another example of mechanism-based inactivation of cytochrome P450 is the formation of metabolic-intermediate (MI) complexes. MI complex formation results in “quasi-irreversible” inhibition due to a metabolite ligand strongly coordinating to the ferrous heme iron. The “quasi-irreversible” term refers to the ability of the chemical oxidant potassium ferricyanide ($K_3Fe(CN)_6$) to destroy MI complexes by oxidizing the heme iron to the ferric state thereby releasing the inhibitory ligand (Delaforge et al., 1984). MI complexes can also be destroyed by absorption of high-intensity blue light (Ullrich and Schnabel, 1973). Both of these processes restore the catalytic activity of the P450. The “quasi-irreversibility” of MI complexes may make this seem like an unusual case of mechanism-based inactivation. However, mechanism-based inactivation of CYP2B6 by 2-oxo-clopidogrel is also reversible by treatment with a common laboratory chemical (DTT) due to the nature of the bond between the inhibitory ligand and the P450 (disulfide bond) (Zhang et al., 2011). The stability of MI complexes in humans in vivo has been directly demonstrated as MI complexes were still present in liver microsomes prepared from human liver biopsies of patients administered drugs known to form MI complexes with CYP3A4 (Pessayre et al., 1982; Larrey et al., 1983). Therefore, while “quasi-irreversible” in nature, MI complexes are irreversible in vivo.

Aliphatic alkylamines are a structural alert for MI complex formation where P450-mediated sequential oxidation to a nitrosoalkane (Mansuy et al., 1977) leads to strong binding to the ferrous heme iron through the nitrogen lone pair of electrons (Figure 1.3). The pathway to MI complex formation has been described (Jeffery and Mannering, 1983) and the role of individual metabolites further evaluated (Hanson et al., 2010). An important branching point exists at the secondary amine where oxidation can proceed either through N-dealkylation to a primary amine or N-hydroxylation to a secondary hydroxylamine (Figure 1.3). The primary amine may then be N-hydroxylated and dehydrogenated to a nitrosoalkane, however, primary amines may also be

potent reversible inhibitors and oppose (protect against) MI complex formation (Hanson et al., 2010) and multiple studies have suggested that MI complex formation likely proceeds through the secondary hydroxylamine to a nitrone (Cerny and Hanzlik, 2005; Hanson et al., 2010; Barbara et al., 2013).

Nitrosoalkane MI complexes exhibit a Soret peak near 455 nm with an approximate extinction coefficient of 65 $mM^{-1}cm^{-1}$ (Franklin, 1974; Pershing and Franklin, 1982). Due to their signature Soret absorbance, sensitivity to ferricyanide, and ability to block the binding of carbon-monoxide, there are a variety of in vitro diagnostic tools for revealing MI complexes which we have leveraged in this dissertation.

In a previous dissertation out of this laboratory (Smith, 2007), it was proposed (but not confirmed) that the fluoroquinolone ENX forms an MI complex with CYP1A2. Sequential N-oxidation and eventual ring-opening to a nitroso-aldehyde metabolite was proposed to account for MI complex formation from ENX. The current dissertation seeks to confirm whether an MI complex is formed with CYP1A2 by sequential metabolism of the piperazine ring of ENX and potentially identify a new structural alert for MI complex formation (alicyclic amine).

1.5 Discovery, Development, and Use of Fluoroquinolone Antibacterials

Nalidixic acid (Figure 1.4), the original “quinolone” antibacterial, was first discovered by George Lesher and coworkers at Sterling-Winthrop Research Institute in New York in 1962 in the distillate of a chloroquine synthesis (Lesher et al., 1962). Nalidixic acid is technically a naphthyridone (not a quinolone). It has a 4-oxo-1,8-naphthyridin-3-carboxylic acid nucleus and it was found to have antibacterial activity against a wide range of gram-negative bacteria. The bactericidal mechanism of action was later found to be inhibition of bacterial type II topoisomerases (DNA gyrase, aka Topoisomerase II, and Topoisomerase IV). DNA gyrase

introduces and removes negative supercoils in bacterial DNA by cleaving a specific region of DNA allowing one section of DNA to pass through another section and then resealing of the cleavage site (Stein, 1988) in a process essential for bacterial DNA replication to occur. Quinolone antibacterials bind to DNA gyrase during the passage of an uncleaved DNA strand through the opening introduced in the cleaved DNA strand, thus locking DNA gyrase and the DNA strands in a ternary complex (Drlica and Zhao, 1997). The resulting inhibition of DNA synthesis and cell growth leads to death of the bacteria.

The development of newer quinolones was driven by the need for more potent antibacterials with a broader spectrum of activity against gram-negative and gram-positive bacteria. After nalidixic acid was approved for treatment of urinary tract infections (UTI) in the mid 1960s, little progress was made to improve this class of antibacterials until the 1980s. However, during the 1970's, two important "stepping stone" structural groups were added to the quinolone repertoire with flumequine (first C6-fluoro) and pipemidic acid (first C7-piperazinyl group). Norfloxacin (patented 1979) was the first quinolone to combine the C6-fluoro and C7-piperazinyl groups resulting in a dramatic increase in antibacterial potency and the birth of the second-generation fluoroquinolone antibacterials (Figure 1.4). The fluoroquinolones ENX and ciprofloxacin came into development immediately afterwards in the early 1980s. Ciprofloxacin became the most successful and widely used of the second-generation fluoroquinolone due to its superior potency against most gram-negative bacteria, including *Pseudomonas aeruginosa* which is a multidrug resistant pathogen.

While the earlier quinolones were indicated only for the treatment of UTI, newer fluoroquinolones, having gone on to the third- and fourth-generation (Figure 1.4), are indicated for treatment of a variety of infections including bone and joint infections, abdominal & GI tract infections, infectious diarrhea, respiratory tract infections, tuberculosis, skin infections, and typhoid fever (Vincent, 2005). Fluoroquinolone antibacterials continue to be developed (Naeem

et al., 2016) due to good oral bioavailability, low incidence of toxicity, favorable pharmacokinetics, and broad-spectrum activity against gram-positive and gram-negative bacteria

1.6 The Fluoroquinolone Enoxacin

The fluoroquinolone antibacterial enoxacin (ENX) was used for the treatment of infections, including respiratory tract infections, for a relatively short period of time (mid 1980s to early 1990s) before it became obsolete relative to other fluoroquinolones, such as ciprofloxacin which has superior antibacterial activity and a lower incidence of adverse effects, and ENX was subsequently withdrawn from the US market. Among the reasons for removal of ENX from the US market was an unacceptable DDI magnitude with CYP1A2 substrates such as caffeine and theophylline (Wijnands et al., 1984; Harder et al., 1988).

Some of the pharmacokinetic characteristics of ENX are outlined in Figure 1.5 (Nakamura et al., 1983). ENX, administered orally at 200 or 400 mg (bid), is well-absorbed from the GI tract. The parent drug reaches C_{max} values in the range of 2-4 mg/L (~6-12 μM with ~35% bound to serum proteins) in blood with a T_{max} of 1-2 hours and an elimination half-life of ~5 hours. ENX is metabolized at the piperazinyl ring to form the lactam oxo-ENX (which circulates in blood at ~10% the level of ENX) and four additional metabolites (Figure 1.5) which are excreted into urine at levels constituting 1% or less of the dose. More than half of the dose is recovered in urine as the unchanged parent with a significant percentage (5-10%) presenting as oxo-ENX.

1.7 Interaction of Fluoroquinolones with Cytochrome P450 1A2

ENX was reported to raise the plasma concentration of theophylline (a narrow therapeutic index drug) to levels where patients reported adverse effects (nausea, vomiting, tachycardia, and headaches) (Wijnands et al., 1984). Subsequently, it was found in a later study that the fluoroquinolones ciprofloxacin and pefloxacin, in addition to ENX, can increase theophylline plasma concentrations, although the interactions were weaker than that of ENX (Wijnands et al., 1986). The authors noted that the DDI magnitude (fold AUC increase for theophylline) observed for each study subject was positively correlated with the urinary recovery of the oxo (lactam) metabolite and further suggested that the oxo metabolite was responsible for inhibiting the clearance of theophylline. This was the first suggestion that metabolism of fluoroquinolones may be linked to the DDI.

Harder et al. (1988) examined the interaction of various quinolones (enoxacin, ciprofloxacin, norfloxacin, ofloxacin, and pipemidic acid) with caffeine in human subjects. Again, the DDI magnitude was greatest with ENX (caffeine AUC increase of ~5-fold) followed by pipemidic acid (~3-fold) and only weak interactions were observed with ciprofloxacin and norfloxacin. The authors of this study addressed the previous suggestion that the oxo-metabolite mediates the DDI by noting that pipemidic acid, which caused a substantial DDI in this study, does not form an oxo-metabolite. It has also been shown that rats dosed with oxo-ENX directly show no interaction with theophylline even though rats dosed with ENX experience the same DDI magnitude with theophylline as humans (when dosed orally at equivalent mg/kg dosages) (Mizuki et al., 1989). Additional reports have found oxo-ENX to be a weaker inhibitor of CYP1A2 than ENX in vitro in human liver microsomes and rat hepatocytes (Mulder et al., 1988; Sarkar et al., 1990; Fuhr et al., 1993).

To date, the in vitro and in vivo inhibition studies on the fluoroquinolone enoxacin have not provided adequate information to rationalize the DDI magnitude observed in vivo (Obach et al., 2006). Reversible inhibitory constants for ENX and its metabolites are weak in microsomes, hepatocytes, and rats (Mulder et al., 1988; Mizuki et al., 1989; Fuhr et al., 1990; Sarkar et al., 1990; Fuhr et al., 1992; Fuhr et al., 1993; Mizuki et al., 1996b; Brown et al., 2010). One study (Spaldin et al., 1994), outside of the experiments conducted in this laboratory (Smith, 2007), has noted that the inhibitory effect of ENX upon CYP1A2 in HLM increases with pre-incubation time and depends on NADPH. Thus, we have hypothesized that ENX is a time-dependent inhibitor of CYP1A2 and that the interaction with CYP1A2 substrates involves mechanism-based inactivation of this P450 enzyme.

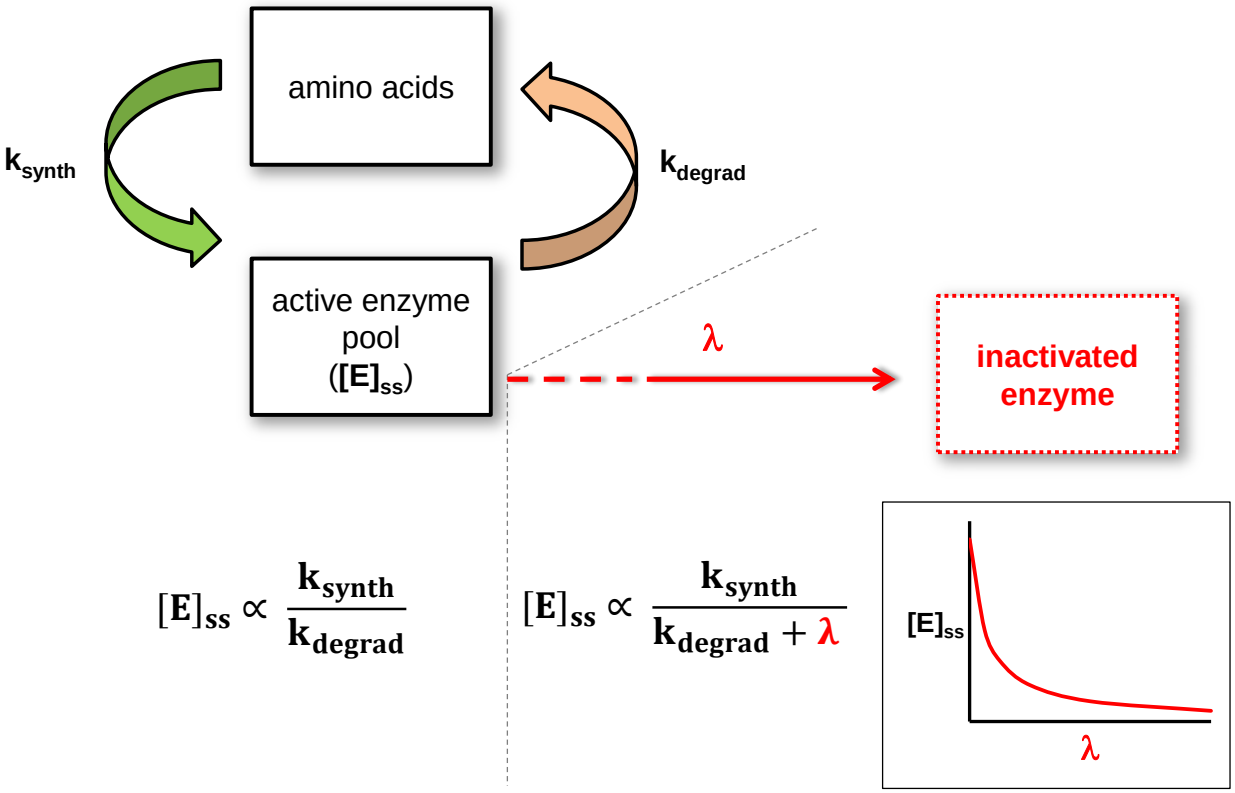

Figure 1.1 – The effect of mechanism-based inactivation on active enzyme level in vivo
Active enzyme level ($[E]_{ss}$), kept stable by normal enzyme synthesis (k_{synth}) and degradation (k_{degrad}), can be perturbed in the presence of a mechanism-based inactivator molecule through introduction of an inactivation rate, λ. The mathematical relationship between increasing λ and reduction in steady-state active enzyme, $[E]_{ss}$, is shown (lower-right). This figure and the equations given within were adapted from the seminal work of Mayhew et al. (2000); see References.

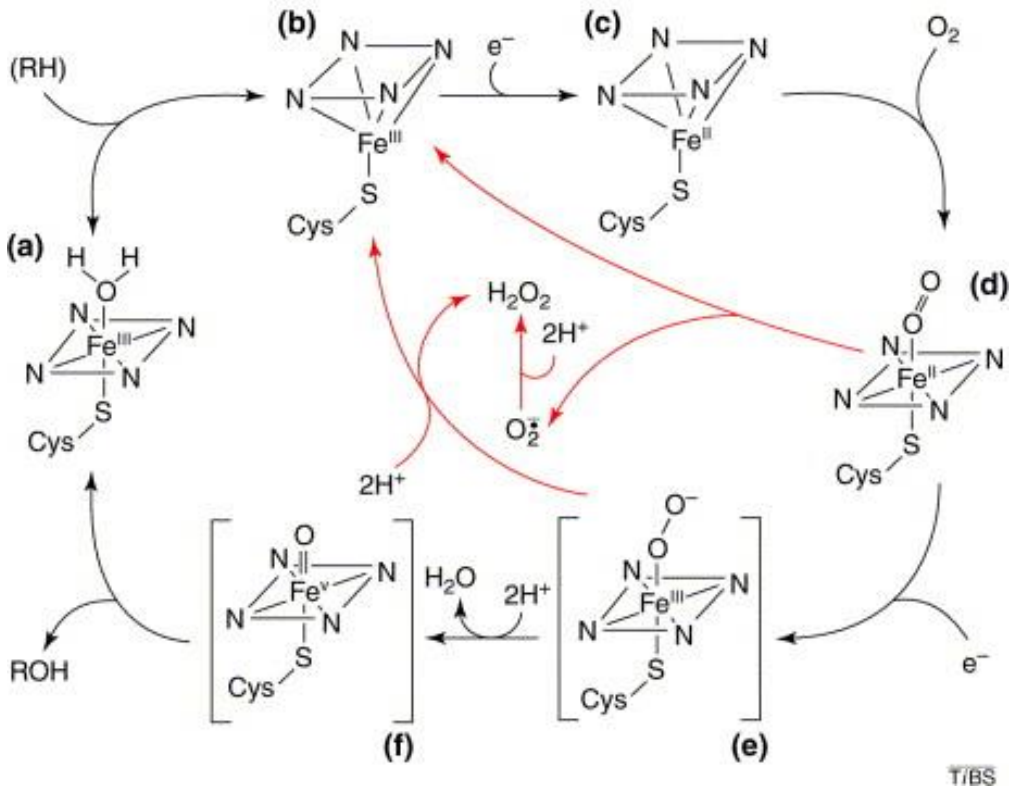

Figure 1.2 – The cytochrome P450 catalytic cycle
Intermediates in the P450 catalytic cycle (labeled **a** through **f**) are discussed in the text. This figure was taken from Davydov (2001); see References.

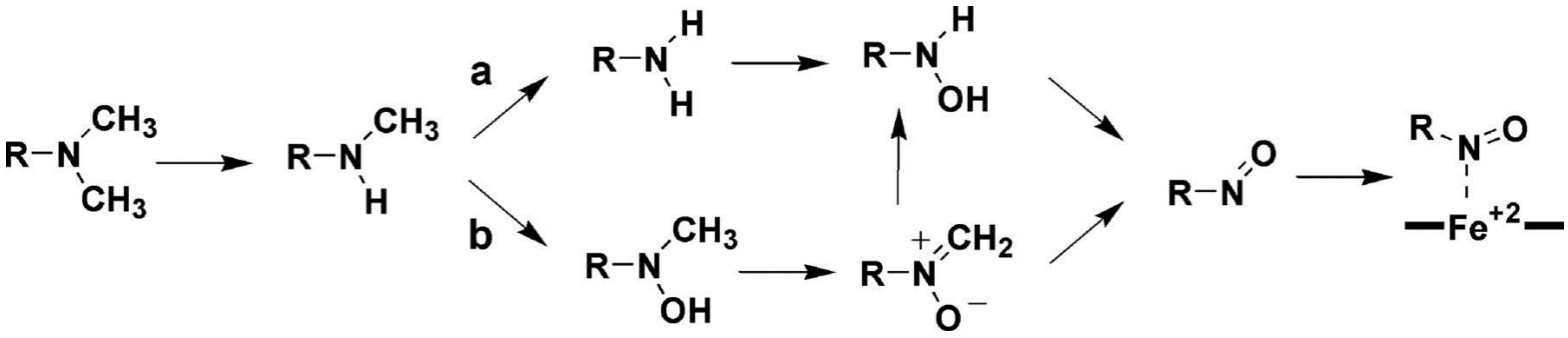

Figure 1.3 – Sequential metabolism of alkylamines to metabolic intermediate complex
Sequential metabolism of a tertiary amine (left) through either the primary amine pathway (a) or the secondary hydroxylamine pathway (b) can result in a nitroso metabolite coordinated to the ferrous heme iron of a cytochrome P450 (i.e. formation of a metabolic-intermediate complex). This figure was taken from Hanson et al. (2010); see References.

First generation:

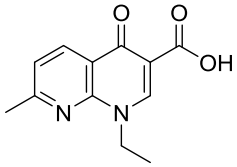

Nalidixic acid

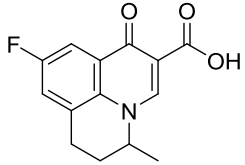

Flumequine

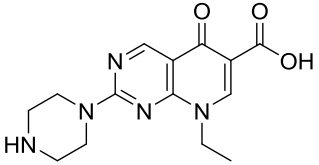

Pipemidic acid

Second generation:

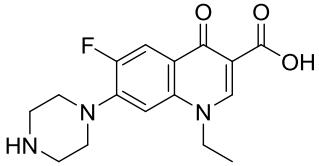

Norfloxacin

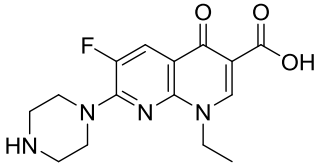

Enoxacin

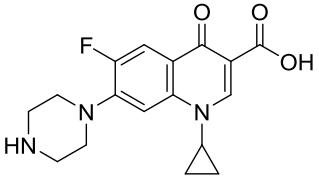

Ciprofloxacin

Third generation: Sparfloxacin, Gatifloxacin, Grepafloxacin

Fourth generation: Trovafloxacin, Moxifloxacin, Gemifloxacin

…more in development

Figure 1.4 – The development of fluoroquinolone antibacterials across generations
Various fluoroquinolone drug structures are shown beginning with nalidixic acid, the first "quinolone." The structural changes which led to development of enoxacin are evident and are further discussed in the text.

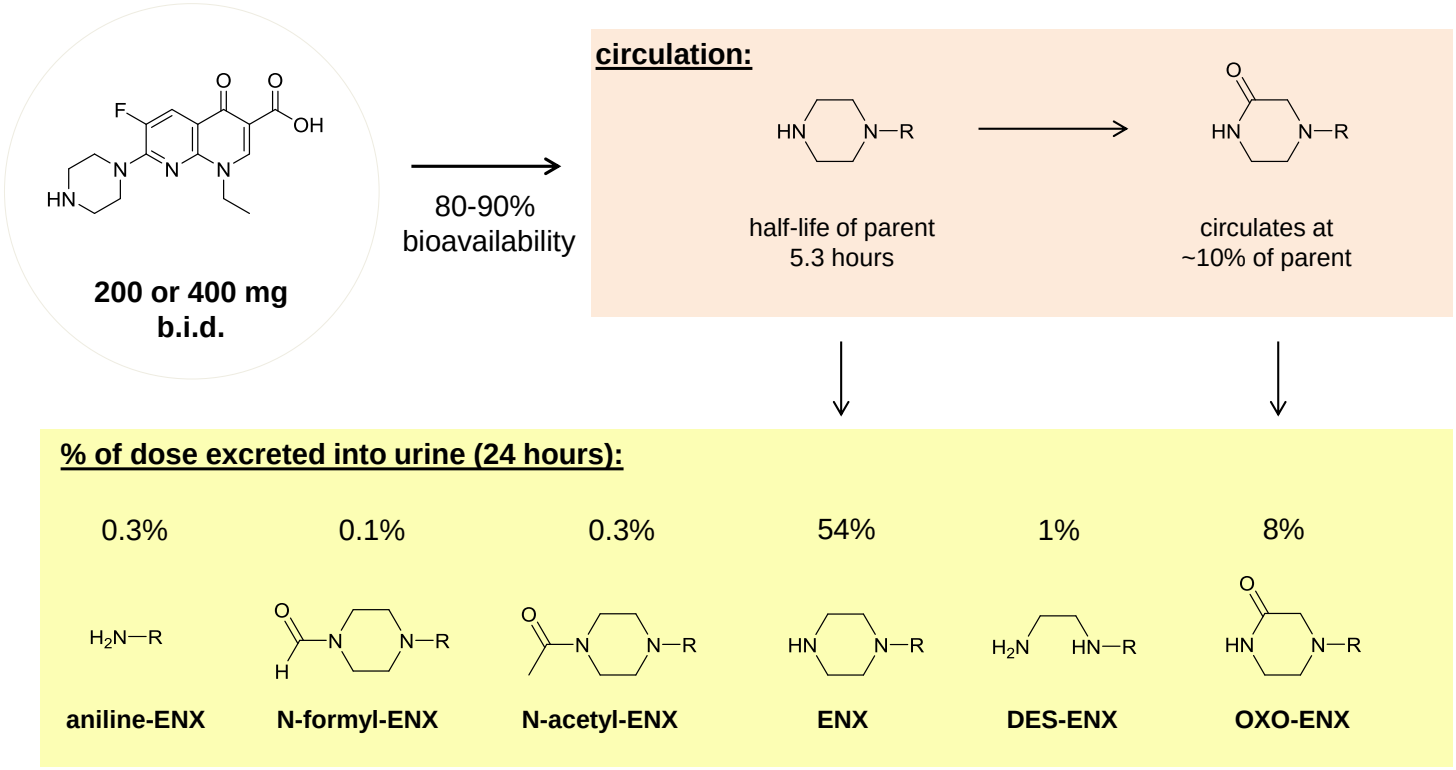

Figure 1.5 – Pharmacokinetic description of enoxacin absorption, metabolism, and excretion
The values in this figure are taken from Nakamura et al. (1983); see References.

Chapter 2: The Mechanism of CYP1A2 Inactivation by Enoxacin

2.1 Introduction

Enoxacin (ENX, structure 1 in Figure 2.1) causes moderate to severe drug-drug interactions (DDI) with the cytochrome P450 1A2 (CYP1A2) substrates theophylline and caffeine (Wijnands et al., 1984; Wijnands et al., 1986; Kinzig-Schippers et al., 1999). Inhibition studies conducted in vitro have reported weak reversible affinity for CYP1A2 in rat and human liver microsomes [IC50 and K_i values > 100 μM ENX] (Fuhr et al., 1990; Brown et al., 2010). Predictions of the DDI magnitude with theophylline based upon competitive CYP1A2 inhibition by ENX grossly underpredict even when maximal hepatic inlet concentrations of ENX are applied (Obach et al., 2006). The discrepancy between the inhibition potency in vitro and in vivo suggests that inhibition may rely on metabolism of ENX.

Five in vivo metabolites of ENX have been reported in humans (Yamaguchi et al., 1984). Desethylene enoxacin, aniline enoxacin, N-acetyl enoxacin, N-formyl enoxacin, and oxo-enoxacin are all found in patient urine while only oxo-enoxacin has been detected in circulation (structures 3 - 7 in Figure 2.1). Inhibition of CYP1A2 by oxo-enoxacin, the major metabolite of ENX, was weaker than that of ENX in both human liver microsomes and rat hepatocytes (Mulder et al., 1988; Sarkar et al., 1990; Fuhr et al., 1993). Inhibition of CYP1A2 by desethylene enoxacin, the second most abundant metabolite of ENX in patient urine, was similar to that of ENX (Fuhr et al., 1993). The other three reported metabolites are found in the urine of patients at very low levels. Of these three, only N-acetyl enoxacin has been assessed for inhibition of CYP1A2 and it was found to be a very weak inhibitor in rat liver microsomes (Mizuki et al., 1996b). To date, there is no evidence to link the in vivo metabolites of ENX to the observed DDI with CYP1A2 substrates.

Evidence for time-dependent inhibition (TDI) of CYP1A2 by ENX has appeared in the literature (Spaldin et al., 1994). ENX was found to block the formation of protein-reactive and stable metabolites of tacrine in human liver microsomes. Inhibition was significantly enhanced by pre-incubating microsomes with ENX and NADPH. These results suggested that metabolism of ENX may enhance the inhibition of CYP1A2, the major isoform responsible for metabolism of tacrine.

In a previous dissertation out of this laboratory, a mechanism to account for the TDI of CYP1A2 by ENX was proposed (Smith, 2007). The secondary hydroxylamine, N-hydroxy enoxacin (N-OH-ENX, structure 2 in Figure 2.1), was identified as a metabolite of ENX and found to cause NADPH-dependent TDI of CYP1A2 at a considerably faster rate than that of ENX. In one instance, spectral evidence for the formation of a metabolic-intermediate (MI) complex was captured upon incubating N-OH-ENX in human liver microsomes with NADPH. Unfortunately, the MI complex could not be demonstrated reproducibly and evidence for formation of the MI complex from the parent drug was lacking. Nonetheless, these results suggested that ENX may be sequentially metabolized by CYP1A2 to an MI complex through the secondary hydroxylamine intermediate, N-OH-ENX.

The aim of this study was to further characterize TDI of CYP1A2 by ENX and to determine the mechanism of inhibition. By use of CYP1A2 bactosomes (a system with high specific CYP1A2 content) we sought to confirm that metabolism of ENX leads to MI complex formation. The pathway leading to MI complex formation may then be elucidated. It is hypothesized that inhibition of CYP1A2 by ENX is due to MI complex formation and that this process can account for the DDI with CYP1A2 substrates observed in vivo.

2.2 Experimental

2.2.1 Materials.

All chemicals from commercial sources were of analytical grade. Acetonitrile and water used in liquid chromatography were of Optima LC-MS grade and purchased from Fisher-Scientific (Santa Clara, CA). Human CYP1A2 bactosomes co-expressed with cytochrome P450 reductase were purchased from XenoTech LLC (Lenexa, KS). Slide-A-Lyzer MINI dialysis units were purchased from Thermo Scientific (Rockford, IL). Enoxacin (1) sesquihydrate, enrofloxacin (internal standard), phenacetin, acetaminophen, NADPH co-factor, potassium ferricyanide and potassium cyanide were purchased from Sigma-Aldrich (St. Louis, MO). Isotopically-labeled potassium cyanide-(^{13}C, ^{15}N) was purchased from Toronto Research Chemicals (Toronto, ON, Canada). The internal standard, methyl-labeled acetaminophen-d_3, was purchased from TLC PharmaChem (Vaughan, ON, Canada). N-hydroxy enoxacin (2), desethylene enoxacin (3), aniline enoxacin (4), N-formyl enoxacin (6), and the internally and externally N-formylated analogues of desethylene enoxacin (8 and 9) were synthesized in house by Dr. Kantipudi N. Babu and their identities were confirmed by NMR and mass spectrometry. The cyclic nitrone of enoxacin (11) and labeled N-hydroxy enoxacin (2; oxygen-18 label in the N-hydroxy group) were synthesized as described below. Oxygen-18 gas (99%, Stohler Isotope Chemicals) was a gift from the laboratory of Dr. Sid Nelson. The numbers in parentheses correspond to the structures in Figure 2.1. All other chemicals were from Sigma-Aldrich unless specified.

2.2.2 ^{1}H NMR Spectroscopy.

Analysis of synthetic products and intermediates was performed on an Agilent DD2 500 MHz spectrometer equipped with a 5-mm HCN triple resonance z-axis PFG probe. Deuterated solvents were purchased from Cambridge Isotopes (Andover, MA, USA).

2.2.3 Organic Synthesis.

Preparation of N-hydroxy-enoxacin (Uno et al., 1990; O'Neil et al., 2001):

N-cyanoethyl-enoxacin intermediate: To a round-bottom flask with a stir bar was added 3.00 g (9.38 mmol) of enoxacin (Sigma) and 100 mL of anhydrous methanol. With stirring at room temperature, 3.00 g (56.5 mmol) of acrylonitrile was added in one portion. The flask was then equipped with a water condenser and warmed to 60 °C in an oil bath. The reaction slurry was stirred for 24 hours and then cooled to room temperature. Methanol was evaporated under reduced pressure and the yellow solid obtained was recrystallized from $CHCl_3$:EtOH (1:1) yielding 2.99 g (85%) as pale yellow needles. The intermediate, N-cyanoethyl-enoxacin, was confirmed by mass spectrometry and proton NMR. ^{1}H-NMR (500 MHz) $CDCl_3$ δ: 1.53 (t, 3H, J = 7 Hz, -N-CH_2-$\underline{CH_3}$), 2.59 (t, 2H, J = 6.5 Hz, CH_2-piperazine ring), 2.71 (t, 4H, J = 6 Hz, -N-$\underline{CH_2}$-$\underline{CH_2}$-CN), 2.79 (t, 2H, J = 6.5 Hz, CH_2-piperazine ring), 3.92 (t, 4H, J = 6.5 Hz, CH_2-piperazine ring), 4.42 (q, 2H, J = 7.5 Hz, -N-$\underline{CH_2}$-CH_3), 8.12 (d, 1H, J_{HF} = 13.5 Hz, C5-H), 8.72 (s, 1H, C2-H); MS [MH+] 374.1 ($C_{18}H_{20}FN_5O_3$, requires 373.1550).

N-hydroxy-enoxacin: A stirred solution of N-cyanoethyl-enoxacin (2.05 g, 5.5 mmol) in dry $CHCl_3$ (100 mL) was cooled to 0 °C and m-CPBA (77%, 1.23 g, 5.5 mmol) was then added in small portions over 10 minutes. The flask was sealed with a rubber septum and stirred for 2 hours at 0 °C followed by 10 hours at room temperature. The mixture was concentrated under reduced pressure to half the initial volume and the resulting precipitate was filtered and washed thoroughly with cold $CHCl_3$. The solid obtained was dried and recrystallized from DMF:H_2O (2:1) yielding 1.42 g (76%) as yellow needles. ^{1}H-NMR (500 MHz) DMSO-d_6 δ: 1.38 (t, 3H, J = 7.5 Hz, -N-CH_2-$\underline{CH_3}$), 2.57 (m, 2H, CH_2-piperazine ring), 3.17 (m, 2H, CH_2-piperazine ring), 3.33 (bs, 2H, CH_2-piperazine ring), 4.36 (bd, 2H, J = 7.5 Hz, CH_2-piperazine ring), 4.47 (q, 2H, J = 7

Hz, -N-$\underline{CH_2}$-CH_3), 8.08 (d, 1H, J_{HF} = 13.5 Hz, C5-H), 8.28 (s, 1H, C2-H), 8.98 (s, 1H, -N-OH); TOF-MS [MH+] 337.1312 (calculated m/z: 337.1312).

Microscale preparation of an aqueous solution of the cyclic nitrone of enoxacin:

Ferricyanide-mediated oxidation of N-hydroxy-enoxacin: First, 995 μL of 1 M aqueous HCl solution was added to 18 mL of water resulting in an acidic solution. [N-hydroxy]-enoxacin (8 mg, 23.8 μmol) was dissolved in 1000 μL of aqueous 1 M NaOH and then forcefully added to the acidic solution via pipet followed by immediate vortexing of the solution. This immediate mixing was found to prevent N-hydroxy-enoxacin from precipitating out of solution under the initially acidic conditions. The pH of the resulting solution was within the range of 10-11 once mixed. To this basic solution, solid potassium ferricyanide (15 mg, 45.5 μmol) was added and mixed to dissolve. The reaction proceeded at room temperature for 2 hours during which the yellow color of the solution faded slightly as ferricyanide was converted to ferrocyanide. At this point, the reaction had reached approximately 50% completion as determined by HPLC-UV (280 nm) and the cyclic nitrone of enoxacin was partially purified by solid-phase extraction as described below.

Solid-Phase Extraction: An Oasis HLB (200 mg, 30 μm particle, Part# WAT106202) SPE cartridge was conditioned with methanol and equilibrated with water. The above reaction mixture was applied and drawn slowly through the cartridge using a vacuum manifold to control the flow rate. The cartridge was then washed with water (3x 5 mL) followed by D_2O (3x 5 mL). The SPE cartridge was then eluted with D_2O containing 20% methanol. The collected fractions were analyzed by HPLC-UV and the product-containing fractions were combined. Under reduced pressure, the methanol was removed and the resulting solution of the cyclic nitrone of enoxacin in D_2O was concentrated for analysis by proton NMR. ^{1}H-NMR (500 MHz) D_2O δ: 1.44

(t, 3H, J = 7 Hz, -N-CH_2-$\underline{CH_3}$), 4.08 (bs, 2H, CH_2-piperazine ring), 4.26 (m, 2H, CH_2-piperazine ring), 4.42 (q, 2H, J = 7 Hz, -N-$\underline{CH_2}$-CH_3), 7.60 (bs, 1H, HC=N), 7.84 (d, 1H, J_{HF} = 12.9 Hz, C5-H), 8.65 (s, 1H, C2-H); TOF-MS [MH+] 335.1149 (calculated m/z: 335.1156).

Special Notes on Structural Confirmation of the cyclic nitrone of enoxacin: The NMR signals for two protons from a methylene (CH_2-piperazine) group were obscured underneath the water (HDO) signal at 4.79 ppm. 2D-COSY proton NMR confirmed the presence of this group of protons as a clear coupling was observed between the proton of the sp^2-carbon of the nitrone (7.60 ppm) and a proton signal located underneath HDO. The proton signal underneath the water was also clearly coupled to the CH_2-piperazine protons at 4.08 ppm, further confirming these protons are on the piperazine ring. Additional chemical tests were performed to characterize the cyclic nitrone of enoxacin and to further confirm its identity (see Results).

Preparation of oxygen-18 labeled N-hydroxy-enoxacin:

^{18}O-labeled peroxide (adapted from Rosenthal (1976)): Silica gel (5 grams) was added to a round-bottom flask and baked in an oven for 3 days at 180 °C before cooling to room temperature under vacuum in a dessicator. Anhydrous benzene (100 mL, Sigma) was added to the silica-containing flask and the flask was sealed with a rubber septum and purged with dry argon gas. The benzene was dried over silica for 2 days before use. On the day of the reaction, a second round-bottom flask was flame-dried and cooled under vacuum. This flask was opened briefly to introduce 2.2 g (12 mmol) of benzhydrol which had been stored for several days in a vacuum dessicator. The flask was then resealed with a septum and evacuated. Dry, argon-purged benzene (20 mL) was added via syringe to this flask to dissolve the benzhydrol. A third round-bottom flask (hereafter, the reaction flask) was flame-dried and cooled under vacuum and then opened briefly to introduce a stir bar and 1.3 g (12 mmol) of potassium tert-butoxide (t-BuOK). A breakseal flask containing $^{18}O_2$ gas (250 mL, 10.3 mmol) was attached to the reaction

flask via Tygon tubing. This reaction set-up was evacuated and then the glass seal of the breakseal flask was broken to introduce $^{18}O_2$ gas into the reaction flask. At this point, the solution of benzhydrol in dry, argon-purged benzene was taken up into a syringe by applying positive pressure with dry argon. The entire 20 mL of benzhydrol solution was then transferred into the reaction flask to react with the t-BuOK and $^{18}O_2$ gas. This mixture was stirred vigorously at room temperature for 2 hours with dry benzene being periodically added to the $^{18}O_2$ flask to maintain 1 atm pressure and to drive $^{18}O_2$ gas into the reaction flask. After 2 hours had elapsed, the reaction flask was cooled in an ice water bath, poured off into a pre-chilled separatory funnel, and extracted with ice-cold water (5 mL) to isolate $K^{18}O^{18}OH$ as an aqueous solution. The aqueous $K^{18}O^{18}OH$ extract was washed with fresh benzene (10 mL) and then used immediately and without characterization in the synthesis of ^{18}O m-CPBA (see below).

^{18}O-labeled m-CPBA: To an Erlenmeyer flask with a stir bar was added $MgSO_4 \cdot 7H_2O$ (17 mg, 68.9 μmol), NaOH (200 mg, 5 mmol), an aqueous $K^{18}O^{18}OH$ solution (5 mL, uncharacterized, see above), and dioxane (5 mL). The flask was chilled to O °C and 3-chlorobenzoyl chloride (583 mg, 3.33 mmol, Sigma) was added in one portion with vigorous stirring. The reaction was stirred at O °C for 15 minutes before adding ice-cold 20% H_2SO_4 solution (10 mL) and transferring the reaction to a pre-chilled separatory funnel. The reaction was extracted with CH_2Cl_2 (10 mL) and the CH_2Cl_2 extract was dried over anhydrous MgSO4 and filtered. Evaporation of CH_2Cl_2 under reduced pressure yielded 542 mg of flaky white solid. This solid was used immediately and without characterization in the synthesis of N-^{18}OH-enoxacin.

N-^{18}OH-enoxacin: A stirred solution of N-cyanoethyl-enoxacin (100 mg, 0.268 mmol) in $CHCl_3$ (10 mL) was chilled to 0 °C and ^{18}O-m-CPBA (%activity unknown, 400 mg) was added in portions over 10 minutes. The mixture was stirred for 2 hours at 0 °C followed by 10 hours at room temperature. The reaction was then extracted with pH 6.0 potassium phosphate buffer (5x

20 mL) to remove the m-CBA byproduct and evaporated to dryness under reduced pressure to yield an orange solid. Recrystallization from hot methanol yielded ~40 mg (~45%) of orange solid product. The product gave 1H-NMR signals matching those of the unlabeled [N-hydroxy]-enoxacin (see above) and had a matching HPLC retention time (see Results). Accurate mass measurement indicated a mixture of ^{18}O-labeled (77.4%) and ^{16}O-unlabeled (22.6%) product. TOF-MS of ^{18}O-labeled parent ion [MH+] 339.1352 (calculated m/z: 339.1354).

2.2.4 HPLC-MS/MS (MRM) Method for Quantification of Acetaminophen (APAP).

After work-up, samples from phenacetin o-deethylase activity assays were injected onto a Thermo Hypersil GOLD C_{18} column (100 x 2.1 mm, 1.9- µm particle) attached to a Waters ACQUITY UPLC pump (Waters Corp., Milford, MA). Separation was performed at a flow rate of 0.4 mL/min with a mixture of mobile phases (A: 0.1% formic acid in water; B: 0.1% formic acid in acetonitrile). Initially, mobile phase composition consisted of 90% A / 10% B and the %B was linearly increased to 40% over 2 minutes. The %B was then increased to 80% for 0.7 minutes before returning to the initial conditions and re-equilibrating. The total run time for each injection was 4.7 minutes. Acetaminophen and acetaminophen-d_3 eluted at 1.5 minutes and were detected by tandem mass spectrometry on an API-4000 Q-Trap triple-quadrupole mass spectrometer (AB Sciex, Foster City, CA). The instrument was operated in ESI-(+) mode with a source temperature of 550°C and an ion spray voltage of 5000 V. The declustering potential, collision energy and collision cell exit potential were 60 V, 23 eV and 6 V, respectively, with mass transitions being monitored at 152 > 110 (m/z) for acetaminophen and 155 > 111 (m/z) for acetaminophen-d3. Peak areas were normalized to that of the deuterated internal standard during data work-up.

2.2.5 HPLC-MS/MS (MRM) Method for Quantification of Enoxacin and Metabolites.

After work-up, samples from incubations were injected onto a Thermo Hypersil GOLD C_{18} column (100 x 2.1 mm, 1.9- µm particle) attached to a Waters ACQUITY UPLC pump (Waters Corp., Milford, MA). Separation was performed at a flow rate of 0.4 mL/min with a mixture of mobile phases (A: 0.1% formic acid in water, pH adjusted to 3.0 with ammonium hydroxide; B: 0.1% formic acid in acetonitrile). Initially, mobile phase composition consisted of 95% A / 5 % B and the %B was linearly increased to 34% over 7.5 minutes. The %B was then increased to 80% for 2.4 minutes before returning to the initial conditions and re-equilibrating. The total run time for each injection was 11.9 minutes. Analytes were detected by tandem mass spectrometry on an API-4000 Q-Trap triple-quadrupole mass spectrometer (AB Sciex, Foster City, CA). The instrument was operated in ESI-(+) mode with a source temperature of 400°C and an ion spray voltage of 4200 V. Mass transitions for each analyte along with instrument parameters are listed below in order of increasing retention time (RT). DP, CE, and CXP stand for declustering potential, collision energy, and collision cell exit potential, respectively.

[ANALYTE, RT; (*m/z* mass transition); DP, CE, CXP]: [desethylene enoxacin, 3.36 min; (295→257); 61, 35, 10], [enoxacin, 3.73 min; (321→234); 86, 31, 16], [nitrone enoxacin, 4.52 min; (335→246); 60, 30, 20], [nitrone+water enoxacin, 4.52 min; (353→246); 60, 30, 20], [enrofloxacin, 4.58 min; (360→316); 66, 27, 22], [aniline enoxacin, 5.25 min; (252→123); 61, 61, 10], [N-hydroxy enoxacin, 5.74 min; (337→274); 71, 43, 24], [N-formyl enoxacin, 6.46 min; (349→231); 61, 51, 12], [CN-nitrone enoxacin, 6.68 min; (362→246); 60, 30, 20]. The following channel was left open to search for the nitroso enoxacin metabolite (structure 12 in Figure 2.1): [nitroso enoxacin, retention time unknown; (351→333); 60, 30, 20]. Peak areas were normalized to that of the internal standard, enrofloxacin, during data work-up.

2.2.6 Identification of Metabolites by High-Resolution Mass Spectrometry.

Samples for metabolite identification were prepared by incubating CYP1A2 bactosomes (0.5 µM) with substrates in 0.1 M potassium phosphate buffer (pH 7.4) in the presence or absence of NADPH (1 mM). Another set of incubations was performed in the presence of 0.5 mM potassium cyanide / 0.5 mM potassium cyanide-(^{13}C, ^{15}N) both with and without NADPH. The total incubation volume was 0.4 mL. DMSO was present at 0.5% (v/v). All incubations were performed at 25°C for 60 minutes and then quenched by addition of 200 µL of ice-cold acetonitrile. Samples were centrifuged and 250 µL of supernatant was transferred to 750 µL of water in an LC vial. The samples were injected onto a Waters Synapt G2 Q-TOF mass spectrometer coupled to a Waters ACQUITY UPLC system equipped with a Thermo Hypersil GOLD (100 x 2.1 mm, 1.9- µm particle) C_{18} column. The mobile phase flow rate was set at 0.4 mL/min. Initial conditions for the LC gradient were 95% A (0.1% formic acid in water, pH adjusted to 3.0 with ammonium hydroxide) and 5% B (0.1% formic acid in acetonitrile). The %B was linearly increased to 55% over 8 minutes. The %B was then returned to 5% and the column re-equilibrated. The total run time for each injection was 10 minutes. Samples were ionized by electrospray ionization in positive ion mode. The source conditions were as follows: capillary voltage of 3.5 kV, cone voltage of 30 V, source temperature at 120°C, and desolvation temperature at 350°C. Ion m/z values were recorded in the 50 – 1000 m/z range. The instrument was calibrated immediately prior to analysis by infusion of sodium formate solution. Leu-enkephalin lock mass (556.2771 m/z) solution was simultaneously infused during each data collection and automatically-applied as a mass correction reference. Note that the retention times for some analytes shifted (≤0.25 minutes) across datasets due to the purchasing of new columns and slight reconfigurations of the HPLC system which occurred over the course of this study.

2.2.7 Oxidation of N-OH-ENX by Potassium Ferricyanide.

To support metabolite identification studies, N-OH-ENX was chemically oxidized by potassium ferricyanide, $K_3Fe(CN)_6$, by the following method. A solution of N-OH-ENX was prepared in 0.1 M potassium phosphate buffer (pH 7.4) by addition of N-OH-ENX from a concentrated DMSO stock. The solution was distributed equally into four tubes. Water (vehicle) was added to the first tube. Aqueous potassium ferricyanide was added to the second tube. Aqueous potassium cyanide was added to the third tube. Both potassium ferricyanide and potassium cyanide were added to the fourth tube. Where present, the final concentrations of potassium ferricyanide and potassium cyanide were 0.1 mM and 1 mM, respectively. The final concentration of N-OH-ENX was 10 μM and DMSO was present at 0.5% (v/v). These solutions were incubated for 1 hour at 25°C before addition of 200 μL of ice-cold acetonitrile. These samples were then vortexed, diluted into water, and analyzed by high-resolution mass spectrometry as described above.

2.2.8 Time-Dependent Inhibition of CYP1A2 Activity (*Phenacetin o-deethylase*).

Assays were carried out in 96-well polypropylene plates in a 37°C water incubator. Each inhibitor concentration was carried out in triplicate. Pre-incubation wells containing inhibitor and CYP1A2 bactosomes (usually 10 pmol, unless stated otherwise) in 0.1 M potassium phosphate buffer (pH 7.4) were warmed to 37°C for 3 minutes. The incubation was initiated by addition of 20 μL of 10 mM NADPH dissolved in phosphate buffer. The final pre-incubation volume was 200 μL per well and contained 0.5% DMSO (v/v). At specified time points (generally 0.2, 1, 2, 4, 8, and 16 minutes), an aliquot (20 μL) of the pre-incubation mixture was diluted 10-fold into a CYP1A2 activity assay. Activity assays consisted of 300 μM phenacetin and 1 mM NADPH in phosphate buffer in a final volume of 200 μL per well. After 5 minutes, an aliquot (150 μL) of activity assay was quenched into 75 μL of ice cold ACN containing 15 pmol of acetaminophen-

d_3. The quenched samples were centrifuged at 13,000 x g for 10 minutes at 4°C. An aliquot (60 µL) of supernatant was transferred to a clean 96-well plate containing 140 µL of water per well and the samples were analyzed for APAP and d_3-APAP by HPLC-MS/MS as described above.

2.2.9 Reversibility of CYP1A2 Inhibition to Dialysis and Ferricyanide Treatments.

CYP1A2 bactosomes (0.1 µM CYP1A2) and NADPH (1 mM) were pre-incubated in the presence of vehicle (0.5% DMSO, 0.5% 1 M NaOH and 0.5% 1 M HCl (v/v)) or inhibitor at 25°C in a final volume of 150 µL. Incubations were performed in quadruplicate. At 30 minutes, an aliquot (20 µL) of pre-incubation was diluted 10-fold into activity assay and the activity assay was run for 8 minutes before being quenched by addition of ice cold acetonitrile containing acetaminophen-d_3. These samples were designated as “Before Dialysis.” Aliquots (100 µL each) of the remaining pre-incubation mixtures were transferred to Slide-A-Lyzer MINI dialysis units (3.5 kDa MWCO) which were pre-loaded into individual tubes containing 1.2 mL of 0.1 M potassium phosphate buffer (pH 7.4). Samples were allowed to dialyze at 4°C against 1.2 mL of buffer for 90 minutes with the buffer being replaced with fresh buffer at 30 and 60 minutes. This initial dialysis was performed in individual tubes to avoid cross-contamination of inhibitors between pre-incubation aliquots (particularly the potent inhibitor furafylline). Finally, the pre-incubation aliquots were further dialyzed against 0.5 L of phosphate buffer in a shared beaker for a further 90 minutes. Two separate aliquots (20 µL) of the dialyzed enzyme from each dialysis unit were transferred to individual wells of a 96-well polypropylene plate and warmed to 25°C for 3 minutes. Water (20 µL) was added to one of the aliquots while 2 mM potassium ferricyanide (20 µL) was added to the other and these mixtures were incubated for 5 minutes. Activity assay solution (160 µL) which had been pre-warmed to 25°C was then added to yield a final concentration of 300 µM phenacetin and 1 mM NADPH in potassium phosphate buffer in a final volume of 200 µL per well. The activity assay was run for 8 minutes before being quenched

by addition of ice cold acetonitrile containing acetaminophen-d_3. These samples were designated as “Dialyzed” and “Dialyzed + Ferricyanide.” Samples were processed for mass spectrometry analysis and acetaminophen and acetaminophen-d_3 were quantified by LC-MS/MS as described above.

2.2.10 Ferricyanide Reversal of the MI Complex: LC-MS Analysis of the Released Ligand.

Without dialysis:

CYP1A2 bactosomes (0.5 µM CYP1A2) and NADPH (1 mM) were incubated with N-OH-ENX or N-^{18}OH-ENX (40 µM, 1% DMSO (v/v)) at 37°C in polypropylene tubes at a final volume of 50 µL (0.1 M potassium phosphate buffer, pH 7.4). After 40 minutes of incubation, either water (0.5 µL) or potassium ferricyanide in water (0.5 µL, final concentration of 100 µM ferricyanide) was added and the incubation was continued for 5 further minutes before being quenched by addition of ice cold acetonitrile (25 µL). The tubes were then vortexed, chilled on ice, and centrifuged (16,000g, 5 min). Supernatant (50 µL) was diluted into water (100 µL) and an aliquot of each sample (25 µL) was analyzed by HPLC-MS (full scan) and HPLC-MS/MS (targeted) on a Waters Synapt G2 Q-TOF mass spectrometer as described above. Control incubations were performed either in the absence of NADPH or in the presence of furafylline (10 µM).

With dialysis:

CYP1A2 bactosomes (0.5 µM CYP1A2) and NADPH (1 mM) were incubated with N-OH-ENX (40 µM, 1% DMSO (v/v)) at 37°C in polypropylene tubes at a final volume of 400 µL (0.1 M potassium phosphate buffer, pH 7.4). After 40 minutes of incubation, an aliquot (50 µL) of incubation was quenched into ice-cold acetonitrile (25 µL) containing internal standard (200 nM enrofloxacin). This sample was designated as “Before Dialysis.” The remaining 350 µL of

incubation volume was then chilled on ice for 5 minutes before the transfer of three individual aliquots (110 μL per aliquot) to three individual Slide-A-Lyzer MINI dialysis units (3.5 kDa MWCO) which were pre-loaded into individual tubes containing 1.2 mL of 0.1 M potassium phosphate buffer (pH 7.4). Dialysis was performed at 4°C as already described (see above). Briefly, fresh 1.2 mL buffer exchanges were made at 30 and 60 minutes. At 90 minutes, the dialysis units were placed in a shared beaker containing 0.5 L of buffer and dialyzed for a further 90 minutes. After dialysis, two aliquots (50 μL each) were removed from each of the three dialysis units, placed in polypropylene tubes, and warmed to 37°C in a water bath. Either water (0.5 μL) or potassium ferricyanide in water (0.5 μL, final concentration of 100 μM ferricyanide) was added and the incubation was continued for 5 further minutes before being quenched by addition of ice cold acetonitrile (25 μL). The tubes were then vortexed, chilled on ice, and centrifuged (16,000g, 5 min). Supernatant (50 μL) was diluted into water (100 μL) and an aliquot of each sample (10 μL) was analyzed by HPLC-MS/MS (MRM method) on an API-4000 Q-Trap triple-quadrupole mass spectrometer. The LC conditions were as described above for quantification of ENX metabolites with the exception that the %B was ramped from 5% to 55% over the first 8 minutes. The instrument parameters were as described above with the exception that three additional MRM transitions corresponding to fragments of the putative nitroso/oxime metabolite: (351→315), (351→246), and (351→218) with collision energies of 30, 35, and 40 eV, respectively were also monitored. Peak areas were normalized to that of the internal standard (enrofloxacin) during data work-up.

2.2.11 Spectral Scanning for MI Complex Formation and CO Binding to Residual P450.

UV-Vis spectroscopy was performed on an Olis-modernized Aminco DW-2 spectrophotometer (Olis, Bogart, GA) operated in split-beam mode. The sample temperature was maintained at 25°C by a Julabo F30-C compact refrigerated circulator (Julabo USA, Inc.,

Allentown, PA). CYP1A2 bactosomes were thawed on ice and diluted into 0.1 M potassium phosphate buffer (pH 7.4) containing NADPH (except for ENX, see below). The solution was split into two 1-cm pathlength quartz cuvettes which were loaded into the spectrophotometer and the temperature was allowed to equilibrate for 5 minutes. Meanwhile, scans were taken to ensure a stable baseline. Scans were performed from 500- to 400-nm wavelength light at 1-nm intervals at a scan rate of ~1 scan per minute. To initiate the reaction, vehicle was added to the reference cuvette and inhibitor stock was added to the sample cuvette (N-OH-ENX or DES-ENX), OR, NADPH solution was added to both cuvettes where only the sample cuvette contained inhibitor (ENX) [Since ENX stocks were prepared in aqueous 1 M NaOH solution, it was necessary to add an equivalent volume of aqueous 1 M HCl to offset any pH change and thus, for practical reasons, experiments involving ENX were initiated with NADPH after the appropriate additions of ENX stock and 1 M HCl (sample cuvette), or 1 M NaOH and 1 M HCl (reference cuvette) had been made]. In all cases, the total volume in each cuvette was 0.4 mL. The final concentrations of CYP1A2 and NADPH were 0.5 µM and 1.5 mM, respectively. DMSO was present at 0.5% (v/v) in all cases. Spectra were recorded repetitively over the course of about 70 minutes followed by addition of a few crystals of dithionite to each cuvette to stop the reaction. A new baseline scan was taken and the spectrum was blanked. Carbon monoxide (CO) gas was then gently bubbled into the sample cuvette and the resulting spectrum recorded. This procedure allowed for determination of the residual amount of P450 capable of binding CO in the inhibitor-containing cuvette. The positions of the sample and reference cuvettes were then reversed and a new baseline scan recorded. The spectrum was blanked and the procedure for bubbling CO gas was repeated. This second measurement allowed for determination of the residual amount of P450 capable of binding CO in the vehicle-containing cuvette. For all recorded spectra, the absorbance at 490 nm was set to 0 Abs by subtraction in order to correct for instrument signal drift. Extinction coefficients of 65 $mM^{-1}cm^{-1}$ (Pershing and Franklin, 1982)

and 91 $mM^{-1}cm^{-1}$ (Omura and Sato, 1964) were applied to the absorbance maxima to quantify the amount of MI-complexed and CO-bound P450, respectively.

In one experiment, aliquots (10 μL) were withdrawn from the cuvettes at 0, 4, 7.5, 15, 30, 45, and 70 minutes and diluted 20-fold into phenacetin o-deethylase activity assay (see above). The activity assay was run for 2 minutes at 25°C before being quenched by addition of ice-cold acetonitrile containing acetaminophen-d_3. Samples were processed as described under "phenacetin o-deethylase" and analyzed by HPLC-MS/MS for acetaminophen and acetaminophen-d_3 as described above.

2.2.12 Spectral Ferricyanide Reversal in CYP1A2 Bactosomes.

The spectrophotometer used and the mode of operation are described above. This procedure was adapted and modified from procedures reported in the literature (Larrey et al., 1983; Wrighton et al., 1985; Jones et al., 1999). CYP1A2 bactosomes were thawed over ice and added to 0.1 M potassium phosphate buffer (pH 7.4) containing ENX (500 μM), N-OH-ENX (50 μM), or DES-ENX (50 μM). Experiments with each test substrate were carried out in triplicate. The enzyme-substrate mixture was warmed to 25°C in a water bath incubator and the reaction initiated by addition of NADPH stock solution. The final solution contained 0.5 μM CYP1A2, 1.5 mM NADPH, and one of the above three test substrates in a total volume of 0.9 mL. DMSO was present at 0.5% (v/v). The incubation was continued at 25°C for 70 minutes. Equal volume aliquots (430 μL) of this pre-incubated mixture were then transferred to sample and reference cuvettes pre-loaded into the spectrophotometer which was at 25°C. A baseline scan was recorded and the spectrum blanked. At this stage, 20 μL of water was added to the sample cuvette and 20 μL of 2 mM potassium ferricyanide dissolved in water was added to the reference cuvette (89 μM f.c.). The resulting spectrum was recorded from 500- to 400-nm

wavelength light at 1-nm intervals. A few crystals of sodium dithionite were then added to each cuvette and CO binding was quantified as described above.

2.2.13 Substrate Depletion and CYP1A2 Activity Remaining (Partition Ratio).

ENX (50 μM) or N-OH-ENX (25 μM) were pre-incubated with CYP1A2 bactosomes (0.5 μM) and NADPH (1 mM) in 0.1 M potassium phosphate buffer (pH 7.4) at 37°C in a water bath incubator. The final incubation volume was 200 μL and DMSO was present at 0.5% (v/v). Identical control incubations were run for ENX and N-OH-ENX which lacked NADPH. All incubations were performed in triplicate. At 0.33 and 45 minutes, an aliquot (20 μL) of pre-incubation mixture was diluted into 180 μL phenacetin o-deethylase activity assay mixture (described above). The activity assay was run for 2 minutes before transferring an aliquot (100 μL) of this mixture into 50 μL of ice-cold acetonitrile containing acetaminophen-d_3 (200 nM). To the remaining 100 μL of activity assay mixture was added 100 μL of ice-cold acetonitrile containing enrofloxacin (1 μM). Samples were centrifuged and the supernatants diluted into water prior to analysis by HPLC-MS/MS for APAP (phenacetin o-deethylase activity) or ENX and N-OH-ENX remaining. The HPLC-MS/MS methods for quantification of APAP, ENX, and N-OH-ENX are described above. NADPH-dependent consumption of ENX or N-OH-ENX and NADPH-dependent loss of CYP1A2 activity were used in estimating the partition ratios.

2.2.14 Metabolite Formation Time Courses.

ENX was incubated with CYP1A2 bactosomes (0.1 or 0.5 μM) and NADPH (1 or 1.5 mM) in 0.1 M potassium phosphate buffer (pH 7.4) at 37°C in a water bath incubator. At specified time points (usually 1, 2, 4, 8, 16, 32, and 64 minutes) an aliquot of the incubation was removed and quenched into an equal volume of ice-cold acetonitrile containing enrofloxacin (200 nM).

Samples were then centrifuged at 13,000 x g for 10 minutes at 4°C. An aliquot (60 µL) of supernatant was transferred to a clean 96-well plate containing 140 µL of water per well and the samples were analyzed for metabolites of ENX by HPLC-MS/MS as described above. Standard curves of the analytes were constructed by diluting concentrated stocks of authentic standards into phosphate buffer. These samples were warmed to 37°C before being quenched and processed by the same procedure as was done for incubations. After analysis by HPLC-MS/MS, analyte peak areas were normalized to that of the internal standard, enrofloxacin.

2.2.15 Data analysis.

Mass spectral data was processed using MassLynx 4.10 (Micromass Ltd., Milford, MA) for high-resolution TOF data (Synapt G2 mass spectrometer) or Analyst software (AB SCIEX, Framingham, MA) for multiple-reaction monitoring (MRM) data (API-4000 mass spectrometer). Spectrophotometric data was processed using Olis Globalworks (Bogart, GA) and no smoothing was applied (Digital-Filter [Savitzky-Golay] = 0).

For time-dependent inhibition analysis, natural log of residual CYP1A2 activity remaining was plotted against pre-incubation time in the presence or absence of inhibitor. The slope of the linear portion of the resulting line was calculated in Microsoft Excel (Redmond, WA). As described by equations 1 and 2, this slope is equal to the enzyme inactivation rate, λ.

$$\mathrm{A_t} = \mathrm{A_o} * \mathrm{e}^{-\lambda \mathrm{t}} \qquad (1)$$

$$LN\left(\frac{A_t}{A_o}\right) = -\lambda * t \qquad (2)$$

The enzyme inactivation rate, after correcting for background inactivation in the absence of inhibitor, was plotted against concentration of inhibitor in GraphPad Prism (San Diego, CA). The apparent inactivation parameters, k_{inact} and K_I, were estimated by non-linear regression using equation 3:

$$\lambda = \frac{k_{inact}\,[I]}{K_I + [I]} \qquad (3)$$

Errors, where displayed, are the standard deviation of the mean (typically, N=3). Standard practices for propagation of error were applied. Tests for statistical significance were performed in Microsoft Excel using Student's t-test (two-tailed, unpaired). Statistical significance was assumed at $P<0.05$. The use of asterisks in figures follows the convention: * ($P<0.05$), ** ($P<0.01$), and *** ($P<0.001$).

2.2.16 Static Prediction of CYP1A2 MBI on Active Enzyme and AUC_i/AUC.

Inactivation parameters K_I and k_{inact} were used to calculate an estimate of active CYP1A2 levels in a human liver exposed to circulating concentrations of enoxacin at a therapeutic dose. The maximal effect on active CYP1A2 levels is described by Equation 4 (Mayhew et al., 2000):

$$\frac{E'}{E} = \frac{k_{deg}}{k_{deg} + \lambda} \qquad (4)$$

The corresponding maximal effect on the fold-increase in AUC of a victim drug is described by Equation 5 (Mayhew et al., 2000):

$$\frac{\mathrm{AUC}'}{\mathrm{AUC}} = 1 + \frac{\lambda}{k_{deg}} \qquad (5)$$

AUC' and AUC are the area under the plasma concentration vs time curve for a victim drug in the presence and absence of inhibitor, respectively. The predicted AUC increase of specific victim drugs was then calculated by using the corresponding literature value for fraction metabolized by CYP1A2, $f_{m,\,CYP1A2}$, and equation 6 (Grimm et al., 2009):

$$\frac{\mathrm{AUC}'}{\mathrm{AUC}} = \frac{1}{\left(\frac{f_m}{1+\lambda/k_{\mathrm{deg}}}\right)+(1-\mathrm{f_m})} \qquad (6)$$

All predictions were carried out using the above equations in Microsoft Excel.

2.3 Results

2.3.1 Synthesis of N-OH-ENX and ^{18}O-labeled N-OH-ENX.

The secondary hydroxylamine, N-OH-ENX, was synthesized by the method of O'Neil et al. (2001) where oxidation of a β-cyanoethyl tertiary amine with mCPBA gives the corresponding N-oxide which subsequently undergoes Cope elimination to afford the secondary hydroxylamine. The above procedure presents a synthetic route to N-^{18}OH-ENX by substitution of ^{18}O-labeled mCPBA for mCPBA. Labeled mCPBA was synthesized in two steps. First, $^{18}O_2$ gas was reduced to the peroxide by oxidation of benzhydrol to benzophenone and converted to the potassium salt in dry benzene with potassium tert-butoxide (Rosenthal, 1976). The resulting potassium peroxide salt (K^{18}O^{18}OH) was extracted into cold water and used to synthesize ^{18}O-labeled mCPBA from 3-chlorobenzoyl chloride. N-oxidation of β-cyanoethyl-enoxacin with ^{18}O-labeled mCPBA yielded N-^{18}OH-ENX (77.4% enrichment of oxygen-18).

2.3.2 Isolation of an Aqueous Solution of the Cyclic Nitrone of Enoxacin.

The N-hydroxy-piperazine moiety of N-OH-ENX was dehydrogenated by oxidation with alkaline potassium ferricyanide to yield the cyclic nitrone of enoxacin (structure 11 in Figure 2.1, abbreviated NITRONE-ENX). An analogous oxidation of N-hydroxy-piperidine by alkaline potassium ferricyanide to give cyclic nitrone piperidine (2,3,4,5-tetrahydropyridine N-oxide) has been reported (Thesing and Mayer, 1957). NITRONE-ENX has not been reported in the literature previously. We were unable to isolate pure solid product due to decomposition but were able to prepare an aqueous solution of NITRONE-ENX in D_2O for NMR. Proton NMR (including ^{1}H-^{1}H COSY NMR) analysis of this D_2O solution confirmed the product identity as the cyclic nitrone. Desethylene enoxacin (DES-ENX, Figure 2.1) was the major side product of this reaction (confirmed by LC/MS/MS and comparison with authentic compound). This side

product, which appeared to form late in the reaction and continued to increase past peak nitrone concentration, may be a product of further oxidation of the nitrone. Further characterization of NITRONE-ENX is presented under “Metabolite Identification Studies” (Section 2.3.7), including results of the ^{1}H-^{1}H COSY experiment, accurate mass fragmentation, and chemical reactivity.

2.3.3 CYP1A2 MI Complex Formation from ENX and N-OH-ENX, but not DES-ENX.

Incubation of ENX (640 μM, sesquihydrate) with CYP1A2 bactosomes and NADPH resulted in the time-dependent formation of a 452 nm peak in UV-Vis difference spectra (Figure 2.2, A). The intensity of this species increased over time and reached completion at roughly 70 minutes (Figure 2.2, B). The initial scans were consistently marked by a rapid increase of a broad absorbance at 420 – 440 nm which was gradually replaced by the final peak at 452 nm by 16 minutes. The CYP1A2 CO complexes (λ_{max}=448) in the sample and reference cuvettes were determined by treatment with dithionite and carbon monoxide (Figure 2.2, C). The concentration of ferrous CO complex was reduced by approximately 60% in the sample cuvette (Figure 2.2, D). Based on these findings and other confirmatory studies to be presented later in this section, the 452 nm peak was designated as a type of metabolite intermediate complex (MI complex) where the P450 prosthetic heme iron is ligated to a nitroso group derived from a metabolite of enoxacin.

The above results suggested that a population of CYP1A2 (40%) survived enoxacin treatment and conversion to the MI complex. Possible reasons for this finding may include: a) instability of the MI complex to dithionite treatment, b) a portion of the CYP1A2 is catalytically-inactive and therefore incapable of forming MI complexes, or, c) protection from MI complex formation by the presence of a competing ligand (potentially a metabolite of ENX) in the CYP1A2 active site. Depletion of oxygen during MI complex formation was ruled out by bubbling of oxygen gas at 30 minutes, which did not enhance the yield of MI complex (data not shown).

Further, NADPH and ENX are present in great excess (3000:1 and 1280:1 ratio with CYP1A2, respectively). Thus depletion of these substrates does not appear to account for the incomplete conversion to the MI complex.

The result of MI complex formation from enoxacin suggested, structurally, a nitroso metabolite coordinating to the P450 ferrous heme iron. The piperazine moiety of enoxacin, a secondary alkylamine, is separated from a nitroso moiety by three two-electron oxidations accompanied by a ring opening reaction at some point in the sequence. Thus intermediate metabolites would be expected to occur in the incubations. Two known metabolites of enoxacin, the primary amine urinary metabolite DES-ENX (structure 3 in Figure 2.1) and the secondary hydroxylamine N-OH-ENX (structure 2 in Figure 2.1), were observed in incubations with CYP1A2 (see Section 2.3.7). These compounds were tested in bactosomes for their ability to cause MI complex formation with CYP1A2.

Incubation with N-OH-ENX resulted in rapid appearance of an MI complex with a λ_{max} of 452 nm (Figure 2.3, A). This is the same wavelength observed for MI complex formation from ENX, suggesting that the same complex was being formed from N-OH-ENX. Further, MI complex formation from N-OH-ENX was markedly (5-fold) faster than complex formation from ENX. Incubation with either ENX or N-OH-ENX resulted in similar yields of MI complexes as judged by comparison of the intensities of the 452 nm absorbance. The shoulder observed with enoxacin was not observed. Thus, MI complex formation did not go to completion which was confirmed by the observation of a P448 peak after treatment of the sample cuvette with dithionite and CO. These results are consistent with the possibility that the N-OH-ENX metabolite of enoxacin is likely an intermediate in the formation of an MI complex.

Incubation with DES-ENX, on the other hand, did not result in MI complex formation with CYP1A2. A rapid increase in absorbance occurred at 425 nm wavelength light (Figure 2.3, B). This Soret peak remained at the 425 nm position and no appreciable absorbance in the

wavelength range that might suggest MI complex formation (450 – 460 nm) was generated. Since the reaction was initiated with substrate, the NADPH-dependence of the peak at 425 nm was not confirmed. Of note, it has been reported that ENX binding to rat CYP1A generates a λ_{max} at 425 nm (Mizuki et al., 1989). In contrast to incubations with either ENX or N-OH-ENX, when the sample and reference cuvettes were assayed for P448, similar quantities of CO complex were observed (Figure 2.3, D). These results indicate that DES-ENX does not form an MI complex with CYP1A2 and secondarily that it does not interfere with the binding of CO to CYP1A2.

In summary, MI complex formation proceeds from ENX and, at a markedly faster rate, from N-OH-ENX whereas the primary amine metabolite DES-ENX does not produce an MI complex. MI complex cannot be due to generation of carbon monoxide as the CO complex with CYP1A2 absorbs maximally at 448 nm and the spectral complex is significantly red-shifted relative to the CO complex. These results suggest metabolism of ENX and its metabolite N-OH-ENX result in the generation of a nitroso metabolite that coordinates to the CYP1A2 heme iron. While the extinction coefficient for this MI complex is not known, the extinction coefficient determined for other MI complexes (65 $mM^{-1}cm^{-1}$; Pershing and Franklin (1982)) was applied to obtain estimates of the MI complex concentrations to compare with the concentrations obtained using the CO complex extinction coefficient (91 $mM^{-1}cm^{-1}$; Omura and Sato (1964)). These calculations are summarized in Table 2.1 and provide good agreement with the expected mass balance.

2.3.4 Confirmation of the MI Complex by Spectral Ferricyanide Reversal.

To further confirm that the absorbance generated at 452 nm wavelength light is due to the formation of MI complexes, the stability of the complex to potassium ferricyanide treatment was determined. Nitroso MI complexes are decomposed by treatment with ferricyanide to release

the ligand from ferrous heme iron by converting the heme iron to the ferric state. Reversal by potassium ferricyanide is usually accompanied by restoration of enzyme activity and the ability to bind CO in the presence of dithionite. Thus ferricyanide treatment is a diagnostic tool that can be used to verify MI complexes.

MI complex was formed with CYP1A2 by incubating with N-OH-ENX and NADPH for 70 minutes in a test tube. The contents were then divided into sample and reference cuvettes and the absorbance spectrum was recorded and zeroed. Addition of a potassium ferricyanide solution to the reference cuvette to destroy the MI complex provided a positive peak with maximal absorbance at 452 nm (Figure 2.4, A). This experiment showed that the putative MI complex is decomposed by ferricyanide. The CO complexes produced by subsequent addition of dithionite and bubbling of CO gas to the ferricyanide-treated (reference) cuvette and the untreated sample cuvette were quantified (Figure 2.4, C). This experiment demonstrates that ferricyanide treatment released the ligand of the MI complex and restored the ability of the heme-iron to bind CO. Interestingly, the yield of MI complex as a fraction of initial P450 was higher in this experiment. Notably, the incubation to form the complex took place in a heated water bath rather than in a cuvette subject to continuous scanning of the Soret region as described previously. Also the quantity of CO complex formed subsequent to release of the ligand by ferricyanide treatment was higher in this experimental design (Figure 2.4, C) indicating that a greater proportion of CYP1A2 existed as the MI complex after incubating in the water bath as compared to a reaction which had been repetitively scanned with 400- to 500-nm wavelength light. A possible explanation for this difference may lie with the effect of blue light on P450 activity or the sensitivity of the MI complex to blue light. In the latter case, persistent scanning in the 400- to 500-nm wavelength region may cause some degree of photolysis and a decrease in the MI complex yield. Enhanced yield of MI complex and a greater loss of enzyme

activity might then be expected when incubations are not performed in a scanning spectrophotometer.

The above procedure was repeated where DES-ENX served as the test substrate, essentially a negative control experiment where no MI complex formation was expected. CYP1A2 incubated with DES-ENX and NADPH for 70 minutes was split into the sample and reference cuvettes. The spectrum was recorded and zeroed. Addition of potassium ferricyanide solution to the reference cuvette did not reveal the presence of an MI complex (Figure 2.4, B). This result supported our conclusion that no MI complex formation occurs from DES-ENX. This control experiment also validated that the Soret peak observed in the previous experiment was due to reversal of an MI complex and not a spectral artifact that occurs upon addition of ferricyanide to the reference cuvette. As expected, both cuvettes formed similar quantities of CO complex in the experiment run with DES-ENX as substrate (Figure 2.4, D). These results are consistent with MI complex formation from N-OH-ENX, but not DES-ENX.

Finally, this study was repeated (N=3 for each substrate) and extended to include the parent drug, ENX. The results are summarized in Table 2.2. In the case of N-OH-ENX, the concentration of MI complex as judged by the intensity of the 452 nm absorbance after ferricyanide treatment of the reference cuvette as in Figure 2.4 (Panel A) was 290 ± 16 nM using an extinction coefficient of 65 $mM^{-1}cm^{-1}$. The concentration of the MI complex as judged by the concentration of MI complex converted to the CO complex after ferricyanide induced release of the ligand was not significantly different (295 ± 35 nM). The amount of CO complex in the N-OH-ENX treated incubations without ferricyanide treatment was low (30 ± 17 nM)

The presence of MI complex was consistently revealed for incubations beginning from N-OH-ENX. On the other hand, there was no statistically significant difference in CO-binding between ferricyanide- and water-treated cuvettes when DES-ENX served as the test substrate,

in agreement with the observation that no MI complex was revealed following incubation with DES-ENX.

The incubations with ENX as substrate provided an identical MI complex with the same λ_{max} (452 nm) to that of N-OH-ENX. However, the estimated yield of the MI complex revealed by ferricyanide treatment of the reference cuvette (128 ± 9 nM) was roughly half of that revealed following incubation with N-OH-ENX (290 ± 16 nM, above). The difference in MI complex yields determined by this method was statistically significant and is at variance with the observation of similar final MI complex yields when MI complex formation was scanned repetitively (Table 2.1). The concentration of the MI complex as judged by the concentration of MI complex converted to the CO complex after ferricyanide-induced release of the ligand in the ENX incubations was 204 ± 46 nM. We did not detect a significant difference in CO complex between the ferricyanide-treated (204 ± 46 nM) and water-treated (156 ± 18 nM) cuvettes following incubation with ENX, perhaps due to the modest MI complex yield, whereas the difference in CO complex between the ferricyanide-treated (295 ± 35 nM) and water-treated (30 ± 17 nM) cuvettes following incubation with N-OH-ENX was statistically-significant. These results support MI complex formation from ENX and N-OH-ENX with the complex formation from the latter species exhibiting a higher yield of MI complex.

2.3.5 Evaluation of ENX, N-OH-ENX, and DES-ENX as Time-Dependent Inhibitors of CYP1A2.

To assess the time-dependent loss of enzyme activity and the kinetics of enzyme inactivation, CYP1A2 was pre-incubated with ENX, N-OH-ENX, or DES-ENX with and without NADPH. Aliquots were removed at various time points and added to tubes containing the activity assay components phenacetin, a probe substrate for CYP1A2 activity, and NADPH. After a fixed period of incubation the activity assays were quenched and assayed for

acetaminophen by LC/MS/MS. Time- and NADPH-dependent inhibition of CYP1A2 by N-OH-ENX (50 μM) was observed at a rate of approximately 0.074 min^{-1} (half-life of about 9 minutes) (Figure 2.5, A). Modest loss of enzyme activity was observed in the NADPH only inactivation assays. Control incubations with CYP1A2 but no NADPH revealed no significant loss of activity. By contrast, CYP1A2 activity was unaffected in incubations with DES-ENX both in the presence or absence of NADPH (Figure 2.5, B). In (-NADPH) control incubations, DES-ENX and N-OH-ENX exhibited a modest initial rate of CYP1A2 activity loss of about 0.010 min^{-1} (half-life of about 70 minutes). From our experience, the NADPH only loss of activity observed is typical in CYP1A2 bactosomes. Thus DES-ENX does not affect CYP1A2 stability with or without NADPH, and N-OH-ENX markedly accelerates CYP1A2 activity loss that is observed in the presence of NADPH alone. These results indicate the ENX metabolite N-OH-ENX is an intermediate that is "on-path" for MI complex formation and that DES-ENX is off-path and not a time-dependent inhibitor.

Comparisons of the initial rates of CYP1A2 inactivation by ENX and N-OH-ENX were made using three concentrations of each inhibitor (40, 80, and 160 μM; triplicates) spanning a 4-fold concentration range. Rates observed in vehicle controls were used to correct the background rates of CYP1A2 degradation in an effort to isolate the inactivation due to the metabolism of the inhibitors. Incubation with N-OH-ENX displayed significantly faster ($p<0.05$) CYP1A2 inactivation rates than ENX at all three concentrations of inhibitor (Figure 2.6). Overall, inactivation by N-OH-ENX was 6-fold to 8-fold faster than the same concentration of ENX (Figure 2.6). Both compounds produced concentration-dependent increases in the inactivation rates with only modest evidence of saturation of effect in the case of NOH-ENX. Due to solubility limitations, concentrations of N-OH-ENX above 160 μM could not be tested. However, at the concentrations tested we found evidence of approaching saturation as the enzyme inactivation rate only increased 2.77-fold (± 0.32; 95% CI 2.41 to 3.13) across a 4-fold increase

in nominal inhibitor concentration suggesting that the kinetics were significantly less than first-order. In combination with the NADPH-dependence, these results suggest that CYP1A2 inactivation from N-OH-ENX requires both substrate binding and catalysis.

Full characterization of the apparent inactivation parameters, K_I and k_{inact}, for ENX was carried out by determining rates of CYP1A2 inactivation at 9 concentrations of ENX ranging from 20 to 1000 μM. The natural log transformed plots of activity loss over time for four concentrations of ENX and the vehicle control are shown in Figure 2.7 (Panel A). No appreciable lag in CYP1A2 inactivation was detected, even at the highest concentration of ENX tested (1 mM). The rates of enzyme inactivation were plotted against concentration of ENX (Figure 2.7.B) and the rates appeared to reach saturation at the highest concentrations of inhibitor tested. Non-linear regression analysis was performed to estimate the apparent inactivation parameters K_I and k_{inact} at 132 μM and 0.05 min^{-1}. The maximal rate of inactivation by ENX was approximately 5-fold faster than the innate rate of enzyme degradation in CYP1A2 bactosomes due to NADPH alone.

For comparison, the apparent inactivation parameters K_I and k_{inact} were estimated for N-OH-ENX using the available rate data within the solubility limit above (reported in Table 2.3). The data set was analyzed by non-linear regression of the standard MBI equation (Figure 2.8, B). Estimated apparent inactivation parameters were K_I = 211 μM and k_{inact} = 0.44 min^{-1}. The estimated K_I value for N-OH-ENX is slightly higher than that of ENX and the estimated maximal rate of inactivation by N-OH-ENX is approximately 9-fold faster than ENX (Table 2.3). Finally, we could detect no significant lag for ENX and N-OH-ENX which is consistent with the spectral results.

2.3.6 Reversibility to Dialysis and Ferricyanide: Assessing the Contribution of MI Complex Formation to CYP1A2 Activity Loss.

Further studies of the inactive enzyme generated from incubation with these substrates focused on the reversibility to dialysis and the effect of the mild oxidant potassium ferricyanide on activity (Figure 2.9). For reference, two known mechanism-based inactivators furafylline (Kunze and Trager, 1993) and clorgyline (Polasek et al., 2006) were employed as positive controls for inactivation by protein alkylation and MI complex formation of CYP1A2, respectively. Inactivation caused by furafylline was not reversed by dialysis or ferricyanide treatment. However, full restoration of CYP1A2 activity after treatment with clorgyline followed by potassium ferricyanide was observed. Incubation of CYP1A2 with ENX (500 μM) and NADPH for 30 minutes resulted in the loss of 59% of enzyme activity relative to a vehicle control. The loss of activity was not restored by dialysis or treatment with water. Treatment of the inactivated and dialyzed enzyme with a potassium ferricyanide solution led to a statistically-significant ($p<0.05$) increase in CYP1A2 activity. The extent of recovery of activity due to ferricyanide treatment suggests that MI complex formation accounts for the majority of the inhibition. Loss of activity caused by N-OH-ENX was also reversed by treatment with ferricyanide but not by dialysis. Interestingly, the CYP1A2 activity observed after incubation with N-OH-ENX and reversal with ferricyanide was significantly greater ($p<0.05$) than the activities of both ENX- and vehicle-treated CYP1A2 that had been exposed to ferricyanide.

To further link the loss of CYP1A2 activity and appearance of an MI complex, phenacetin o-deethylase activity was measured from aliquots drawn directly from sample and reference cuvettes while concurrently assaying for MI complex formation in the spectrophotometer (Figure 2.10). This experiment was performed under the same conditions as were used in the earlier example of MI complex formation from ENX, except that the reference cuvette lacked NADPH instead of ENX. Thus, the NADPH-dependence of both MI complex formation and activity loss

was captured and determined to proceed at similar rates. The time point at which MI complex formation reached half-maximal nearly intersected with the time point for 50% loss of enzyme activity. As MI complex formation plateaued, the loss of enzyme activity also appeared to level off. Notably, the final yield of MI complex (~250 nM) was once again lower than expected based upon the nominal quantity of CYP1A2 present (initial [CYP1A2] = 500 nM). The final activity measure indicated that roughly 75% of the initial CYP1A2 activity was lost. This level of activity loss is somewhat greater than can be accounted for by MI complex formation alone. An activity loss of 60% would be a reasonable estimate if both MI complex formation and innate CYP1A2 degradation are taken into account. These results again suggest that MI complex formation accounts for the majority of CYP1A2 inactivation by ENX, but that there may be a secondary process that leads to inactivation as well.

2.3.7 High-Resolution Mass Spectrometry Metabolite Identification Studies Support the Existence of a Cyclic Nitrone Metabolite.

Based upon the aforegoing, a working hypothesis for the mechanism of MI complex was developed (Figure 2.11). This scheme features sequential formation of a cyclic nitrone (NITRONE-ENX) followed by a ring opened nitroso aldehyde (NITROSO-ENX). Initially, evidence for the existence of NITRONE-ENX as a metabolite of ENX was sought.

Incubations of ENX with CYP1A2 were examined for metabolites by LC/MS/MS. NADPH-dependent formation of N-OH-ENX, DES-ENX, and aniline ENX (structures 2, 3, and 4 in Figure 2.1) was confirmed (Figure 2.12, top panel) by comparison with authentic synthetic standards. In addition, it was noted that N-OH-ENX and DES-ENX were the most intense and observable metabolite peaks in the BPI (base peak intensity) chromatogram, suggesting that N-OH-ENX is a major metabolite of CYP1A2-mediated oxidation of ENX.

The data set was further processed by extracting out the exact monoisotopic masses of MH+ ions for NITRONE-ENX (335.115 Da) and NITRONE-ENX + H_2O (353.126 Da) within a ±0.010 Da window (Figure 2.12, middle and bottom panels) to filter out irrelevant signals. NADPH-dependent peaks were observed at both masses as shown. In the 335 m/z window, two prominent peaks were observed the peak at 3.55 minutes co-eluted with a peak observed in the 353 m/z window (t = 3.55 minutes). This suggested that the peak at 3.55 minutes is NITRONE-ENX since the reversible addition of water to a cyclic nitrone moiety might be expected. Further, the observed masses for the peaks assigned as NITRONE-ENX and NITRONE-ENX + H_2O matched the theoretical MH+ monoisotopic masses within 1 mDa unit.

A synthetic standard of NITRONE-ENX was not available. Further evidence was sought via chemical oxidation of N-OH-ENX with ferricyanide. The oxidation of N-hydroxy-piperidine by potassium ferricyanide to a cyclic nitrone has been reported in the literature (Thesing and Mayer, 1957). N-OH-ENX was first incubated in phosphate buffer alone prior to analysis by HPLC-MS to demonstrate the stability of N-OH-ENX under the incubation conditions (Figure 2.13, top panel). A parallel incubation with potassium ferricyanide was then assayed. The signal for N-OH-ENX decreased and two new major product peaks were observed (Figure 2.13, middle panel) in the TIC. The first eluting peak was shown to be DES-ENX by comparison of retention time and mass to a synthetic standard. The second product peak matched the exact mass and retention time of the putative NITRONE-ENX metabolite peak observed in incubations of ENX with CYP1A2 and NADPH. Subsequent addition of potassium cyanide (KCN) to the N-OH-ENX / potassium ferricyanide mixture resulted in complete loss of the peak assigned as NITRONE-ENX with little to no effect on the peaks corresponding to DES-ENX and N-OH-ENX. In addition, a new product was observed at 4.98 minutes with an m/z value that matched the expected addition of HCN to NITRONE-ENX [362.127 m/z (observed) vs. 362.126 m/z

(theoretical) for MH+]. The observation of the expected cyanide derivative of the putative NITRONE-ENX generated by ferricyanide reaction provided strong evidence of structure.

Accordingly we sought to trap the putative NITRONE-ENX generated by incubation of ENX with CYP1A2 with cyanide. A 1:1 mixture of KCN and isotopically-labeled KCN (^{13}C, ^{15}N) was added to an incubation mixture assayed for the formation of the expected NADPH-dependent peaks at 362 m/z and 364 m/z. Both peaks were observed in the chromatogram of equal intensity and were dependent upon the presence of NADPH and KCN (Figure 2.14). Further, the retention time for the cyanide-trapped NITRONE-ENX from metabolic incubations matched the retention time of that observed in the chemical oxidation and trapping study (4.98 minutes). These data support the assignment of NITRONE-ENX as a CYP1A2-generated metabolite of ENX.

The structures of N-OH-ENX, NITRONE-ENX, and the HCN-adduct of NITRONE-ENX metabolites were further characterized by analysis of the high-resolution fragmentation spectra. A comparison of the fragmentation patterns for N-OH-ENX and NITRONE-ENX at equivalent collision energies (30 eV) is shown in Figure 2.15. Assignment of the specific atoms lost at each stage of fragmentation and the most likely sites of bond-cleavage for N-OH-ENX, NITRONE-ENX, and HCN-NITRONE-ENX are provided in Figures 2.16, 2.17, and 2.18, respectively. The fragmentation patterns are consistent with the assigned structures. In particular, two consecutive water losses occur from N-OH-ENX while only a single water loss is observed from NITRONE-ENX consistent with the number of –OH groups present in those structures. Loss of C_3H_5NO is specific to NITRONE-ENX and consistent with the nitrone moiety. Furthermore, the fragments of the HCN adduct of NITRONE-ENX match those of NITRONE-ENX as expected upon neutral loss of HCN.

Further characterization of NITRONE-ENX was sought via preparative scale synthesis. Unfortunately this compound was found to be unstable in the solid form as will be detailed later.

However, we were able to obtain a concentrated solution of this compound in D_2O of sufficient purity for NMR analysis (see Sections 2.2.3 and 2.3.2 for details). The proton NMR spectrum revealed a new broad singlet at 7.60 ppm. This chemical shift is consistent with that of the vinylic proton of a nitrone moiety. We also observed a doublet (J=12.9 Hz) at 7.84 ppm characteristic of the J_{HF} coupling of ~13 Hz of the aromatic proton split by the neighboring fluorine atom. As expected from the structure, integration of these signals provided a peak area ratio of 1:1, confirming that the signal at 7.60 is a single proton as expected for the vinylic proton of a nitrone. The balance of the 1-dimensional proton NMR spectrum contained additional NMR signals in agreement with the structure of NITRONE-ENX, but also indicated that a substantial quantity of DES-ENX was present. A comparison of peak integrations suggested that the purity of NITRONE-ENX was 77%. The major impurity was DES-ENX, verified by LCMS, and perhaps very low levels of unidentified impurities. NMR signals were found for only 2 of the 3 methylene groups on the 2,3,4,5-tetrahydropyrazine-1-oxide moiety of the cyclic nitrone. Two-dimensional ^{1}H-^{1}H COSY NMR (Figure 2.19) revealed a proton signal present slightly upfield from the large HDO signal. Clear proton proton couplings of the vinylic nitrone proton at 7.60 ppm to the signal for the methylene protons of C5 at 4.08 ppm were seen in the 2D spectrum. The HDO signal was suppressed post-acquisition in Figure 2.19 which allowed us to observe the hidden proton signal slightly upfield and resolved from HDO (4.79 ppm). That this proton signal was coupled to the vinylic proton and to the C3 methylene protons confirmed that it could account for the missing methylene group at C5 of the proposed 2,3,4,5-tetrahydropyrazine-1-oxide moiety. Hence, NITRONE-ENX was structurally confirmed by proton NMR.

This concentrated stock solution of NITRONE-ENX was subjected to a range of chemical tests monitored by high-resolution LC-MS analysis (Figure 2.20). The NITRONE-ENX eluted at 3.67 minutes with the expected 335.115 m/z value (Figure 2.20, A). Reduction of a 1 μM solution of the NITRONE-ENX in water by sodium borohydride yielded N-OH-ENX as confirmed

by comparison with synthetic standard (Figure 2.20, B and C). Notably, the signal obtained for the N-OH-ENX formed via reduction of 1 μM NITRONE-ENX gave an equivalent peak height when compared to that of a 1 μM solution of authentic N-OH-ENX. Thus, NITRONE-ENX was quantitatively reduced to N-OH-ENX by sodium borohydride. Addition of KCN to an aqueous solution of NITRONE-ENX gave the expected HCN adduct (Figure 2.20, D). Finally, the stability of NITRONE-ENX to strong acid and strong base was tested by treatment with 1 M HCl and 1 M NaOH, respectively. We found that within minutes at room temperature, NITRONE-ENX is converted to DES-ENX by treatment with acid or base (Figure 2.20, E and F). The results of the chemical characterization of NITRONE-ENX are summarized in Figure 2.21.

The facile conversion of NITRONE-ENX to DES-ENX under a variety of conditions was surprising and suggested the possibility that DES-ENX found in incubations is a product of decomposition of the nitrone metabolite. In fact, we had observed formation of DES-ENX during the ferricyanide-mediated oxidation of N-OH-ENX in pH 7.4 phosphate buffer (Figure 2.13). Further study demonstrated that NITRONE-ENX undergoes slow (days) decomposition to DES-ENX in pH 7.4 phosphate buffer at room temperature. However, aqueous solutions of NITRONE-ENX were found to be stable for up to 2 weeks when stored at 4 °C. Hence, DES-ENX can arise from decomposition of NITRONE-ENX in ionic solutions as well as acid and base. The possible relevance of this process to the overall appearance of DES-ENX in CYP1A2 metabolic incubations and in vivo is unclear.

Synthetic NITRONE-ENX exhibited LC-MS and LC-MS/MS characteristics that agreed with those of the CYP1A2-generated metabolite (Figure 2.22, A and C). Further, both synthetic nitrone and metabolite reacted with cyanide to give HCN adducts with the same retention time (Figure 2.22, B and D). Fragmentation of synthetic nitrone and metabolite gave matching fragmentation patterns (Figure 2.23). The fragments could be rationalized as loss of water (335→317), C_3H_5NO (335→264), or both (335→246), followed by loss of C_2H_4 (246→218).

Proposed fragment structures are shown in Figure 2.23. Calculated m/z values for these fragments matched the observed m/z values within 1 mDa unit.

To support the fragment assignments further, a comparison was made between NITRONE-ENX and N-OH-ENX (Figure 2.24, Top Panels). NITRONE-ENX undergoes a single water loss (335 → 317) while N-OH-ENX undergoes a double water loss (337 → 319 → 301) as NITRONE-ENX contains 1 OH group in its structure while N-OH-ENX contains 2 OH groups. Fragmentation which resulted in the loss of the oxygen connected to the nitrogen could be pinpointed for both species by comparing fragmentation of ^{18}O-NITRONE-ENX and N-^{18}OH-ENX (Figure 2.24, Bottom Panels). The labeled analogue supports the indicated fragmentation as the ^{18}O label was lost in fragments 264 m/z and 246 m/z. Loss of ^{18}O to create either fragment involves cleavage of the tetrahydropyrazine N-oxide (-$C_3H_5N^{18}O$) either before or after water loss from the carboxylic acid. We find that the double water loss from N-^{18}OH-ENX occurs in a specific order where the first water loss comes from the carboxylic acid (339 → 321) and the second water loss is a specific loss of the N-^{18}OH oxygen (321 → 301). Thus, the critical structural differences between the tetrahydropyrazine N-oxide species and the N-hydroxy-piperazine species are highlighted here and the ^{18}O label provided useful information regarding the oxidation state of the attached nitrogen. Thus the structure of NITRONE-ENX has been rationalized by high-resolution LC-MS/MS in addition to proton NMR.

A second NADPH-dependent metabolite of ENX was observed in the 335.115 m/z extracted high-resolution ion chromatogram (XIC) at 4.19 minutes (Figure 2.22, A). This peak co-eluted with N-OH-ENX and was mislabeled by the software as a mass of 337.131 and in some cases could be chromatographically resolved from N-OH-ENX (see Figure 2.12). This same unidentified metabolite is also observed with N-OH-ENX as the substrate (NADPH-dependent) and, unlike NITRONE-ENX, was unaffected by the presence of KCN in the incubation. Therefore, the unknown metabolite peak at 4.19 minutes is a metabolite of both ENX

and N-OH-ENX that is isobaric with synthetic NITRONE-ENX but elutes at a later retention time and is not reactive with cyanide. One possible structure consistent with this mass would be a hydroxylamine bearing a C=C double bond on the piperazine. Another possible structure is the lactam (Oxo-enoxacin, structure 7, Figure 2.1). The structure of this metabolite remains unconfirmed.

2.3.8 HPLC-MS/MS Characterization of the Released MI Complex Ligand.

Ferricyanide treatment of the CYP1A2 ENX MI complex led to reversal of the complex and restoration of activity and CO binding properties of the ferrous enzyme. We sought to determine the structure of the ligand released by ferricyanide treatment utilizing substrates N-OH-ENX and N-^{18}OH-ENX to generate the MI complex followed by ferricyanide reversal and metabolite profiling by high-resolution HPLC-MS. Our proposed mechanism postulates that the nitroso ligand is the ring-opened NITROSO-ENX species (Figure 2.11). The mass of this ligand after release is 351.1105 m/z (theoretical MH+). Comparison of the high-resolution LC-MS XICs (351.110 ± 0.005) obtained from incubations of the MI complex formation of N-OH-ENX ±ferricyanide led to the discovery of a peak at 3.08 minutes which was increased by treatment with ferricyanide (Figure 2.25). The mass of this species was 351.1104 amu in agreement with the expected m/z value for NITROSO-ENX. Ferricyanide treatment increased the intensity of this peak by a statistically-significant ~2.4-fold in comparison to treatment with water. Two other well-defined metabolite peaks were observed in the XIC at 3.60 and 4.55 minutes (Figure 2.25), however, only the intensity of the peak at 3.08 minutes was altered by ferricyanide treatment. To confirm that this peak was derived from N-OH-ENX incubations were also conducted with N-^{18}OH-ENX (77% ^{18}O) and analyzed by high-resolution LC-MS. The major ion in the XIC of 353.115 exhibited approximately a 2-fold increase following ferricyanide treatment (data not shown). The observed m/z value of 353.1157 is in good agreement (within 1 mDa) of the

calculated mass for ^{18}O-labeled NITROSO-ENX (353.1148, theoretical MH+) demonstrating that the ^{18}O label was retained in the released ligand. However, the ^{18}O content could not be calculated accurately due to inadequate signal intensity of the ^{16}O signal of the less abundant ^{16}O isotope-containing NITROSO-ENX (expected 22.6%). A rough integration of the peaks provided an estimated ^{18}O content of 88% rather than the 77% expected value. Nonetheless, it was determined that the observed metabolite, which is consistent with NITROSO-ENX based upon accurate mass and responsiveness to ferricyanide treatment, retains the original ^{18}O atom on the nitrogen from the N-^{18}OH-ENX substrate.

High-resolution MS/MS experiments were conducted to further study the released ligand. The ions at 351 m/z and 353 m/z were fragmented at low (Figure 2.26) and high (Figure 2.27) collision energies. Comparison of the fragmentation patterns for the ^{18}O-labeled and unlabeled ions at low collision energy revealed a double water loss which was similar to that seen previously with N-OH-ENX. Specifically, the first water loss largely arises (~80%) from the carboxylic acid (compare 335 and 333 ion intensities in Figure 2.26, B) while the second water loss results in the predominant loss of ^{18}O indicating that an –OH group is present on the nitrogen bearing the ^{18}O atom. It is most likely, therefore, that the parent ion is the oxime tautomer of NITROSO-ENX. The oxime is favored under the nitroso/oxime equilibrium (H_2C-N=O vs HC=N-OH). After the second water loss, the fragments for both the ^{18}O-labeled and unlabeled metabolite were equivalent. Proposed structures for the major fragments consistent with the proposed oxime-ENX metabolite are provided in Figures 2.26 and 2.27.

We then performed further MS/MS experiments using the key fragments of the oxime-ENX identified above by high-resolution TOF MS. By a multiple-reaction monitoring (MRM) method on a triple-quadrupole mass spectrometer we monitored 4 channels corresponding to fragments of the parent ion mass (351 m/z) fragmenting to give product ion masses of 333, 315, 246, and 218 m/z. Analysis of an incubation of NADPH-fortified CYP1A2 with N-OH-ENX

provided a single peak for each of the four transitions at 3.72 minutes. We also observed an additional peak at 4.25 minutes in what is arguably the least unique MS/MS channel (351 → 333; loss of water). This peak is likely due to the same species seen in Figure 2.25 which eluted at 3.60 minutes since the relative intensities of the peaks at 3.72 and 4.25 minutes (under the current method) were similar to the relative intensities of the peaks at 3.08 and 3.60 minutes (under the TOF method) and this species eluted approximately 0.5 minutes later in both instances (the same column, mobile phases, and LC conditions were used albeit on a different instrument). Hence, the peak at 3.72 minutes was assigned as oxime-ENX and the peak at 4.25 minutes was utilized as a control peak to compare against in further analysis. The control peak represents a metabolite which is not associated with the released MI complex ligand and, therefore, should not substantially increase upon ferricyanide treatment. A series of experiments were then conducted by incubation with N-OH-ENX to generate the MI complex followed by cold dialysis and then treatment with either water vehicle or potassium ferricyanide. The levels of oxime-ENX (measured by all four transitions) and the isobaric control metabolite (measured in the water loss channel, 351 → 333) observed following "dialysis + water" or "dialysis + ferricyanide" were first normalized to an internal standard (enrofloxacin) which was added upon quenching with organic and then normalized again to the metabolite level present prior to dialysis. Therefore, the results of this experiment are presented in Figure 2.28 as the metabolite level relative to the level present "Before Dialysis".

The results of this experiment show that approximately 85% of the oxime-ENX present before dialysis could be removed by dialysis across all four MRM transitions. The isobaric control metabolite fell to 26% of control. When the dialyzed aliquots were treated with ferricyanide rather than water, a large statistically-significant increase was observed in the oxime channels. A small but significant increase was also seen in the control metabolite. Overall, the control metabolite increased 1.21-fold while the oxime-ENX increased 5.34-fold

when the increases for the four MRM transitions were averaged. For oxime-ENX, following the removal of ~85% of this metabolite by dialysis, the metabolite level returned to ~70% of the amount originally present. Quantitatively, this suggests that the amount of oxime-ENX observed following ferricyanide-mediated oxidation of the MI complex is similar to the amount already present in solution at the end of the incubation. That these two quantities might be similar was also captured in Figure 2.25 where treatment with ferricyanide led to an approximate doubling of the peak area for the ferricyanide-responsive peak which has now been assigned as oxime-ENX. Note also that in Figure 2.25, the control peak at retention time 3.60 minutes did not increase when ferricyanide was added to the incubation further subduing any interpretation of the modest, but statistically significant, increase in the level of the isobaric control metabolite in Figure 2.28. Overall, this experiment further supports oxime-ENX as the identity of the metabolite present following release of the coordinating ligand from the MI complex. The dialyzed MI complex was treated with ferricyanide and the peak assigned as oxime-ENX increased by over 5-fold when compared to treatment with water.

2.3.9 Partition Ratio Analysis of the Sequential CYP1A2 Inactivation by ENX.

The efficiency of inactivation of CYP1A2 by ENX was evaluated by determination of the partition ratios that reflect ENX consumption and metabolite production as ratios to enzyme inactivation. First we sought to estimate how many molecules of ENX are consumed per each CYP1A2 inactivation event, a substrate depletion partition ratio. The slow rate of inactivation at low concentrations of ENX required to measure ENX consumption complicated the analysis. Incubations of ENX (50 μM) with CYP1A2 at a nominal 100:1 ratio for 45 min led to a 51% reduction in active CYP1A2 (Table 2.4). An upper limit of the partition ratio was estimated from the standard error data. The maximal quantity of ENX that would have been consumed to provide a significant resulted consumed with 90% confidence (+1.3 standard deviations) was

determined and that amount divided by a conservative estimate of the amount of inactivated enzyme. The upper limit of the substrate depletion partition ratio for ENX was estimated at approximately 49 (Table 2.4). The same experimental design was used to calculate the depletion partition ratio for NOH-ENX where inactivation was more rapid. In this case a significant drop in substrate concentration was observed and, after propagation of errors, the depletion ratio was found to be 10 or less.

Partition ratios that reflected the amount of one of more known metabolites that accumulated in solution per inactivating event were determined by LC-MS/MS analysis. ENX was incubated with CYP1A2 (500 nM) under conditions that matched those used for spectral scanning studies. In this case the incubations were performed in tubes in a heated water bath as opposed to cuvettes in a scanning spectrophotometer. Time- and NADPH-dependent loss of CYP1A2 activity was observed in this experiment over 70 minutes (Figure 30, A) along with an accumulation of NOH-ENX over the first 16 minutes (Figure 30, B). Note that the progress curve in this experiment is consistent with the time-course for MI complex formation determined spectrally (Figure 2.2, B). The accumulation curve for N-OH-ENX is shown in Figure 2.29 (Panel B). This curve exhibited a rapid burst followed by a more gradual accumulation of N-OH-ENX to a concentration of 400 nM at 16 minutes. The N-OH-ENX depletion partition ratio in this experiment was calculated at 16 minutes of incubation as 400 nM NOH-ENX produced per 225 nM CYP1A2 lost or 1.8. Since N-OH-ENX can be produced and consumed during the incubation there is no assurance that this partition ratio is a constant. Overall this comparison indicates that very low levels of N-OH-ENX are actually produced during of enzyme inactivation.

The concentrations of other metabolites for which we had synthetic standards were also determined at a time point beyond 1 hour and once loss of CYP1A2 activity had ceased to estimate a final partition ratio to all metabolites of ENX (Table 2.5). By this analysis approximately 3 molecules of N-OH-ENX, 1 molecule of NITRONE-ENX, and 2 molecules of

DES-ENX are released to solution for every molecule of CYP1A2 inactivated. Earlier metabolite identification studies suggested that N-OH-ENX and DES-ENX are the major CYP1A2-generated metabolites of ENX. For the other minor metabolites, N-formyl ENX and aniline ENX, the ratio was much less than 1. The total of all quantifiable metabolites per inactivated enzyme is 6.5 ± 0.6. Overall, the results of the above partition ratio analysis reveal a relatively low degree of metabolite formation and release over the course of enzyme inactivation.

A set of CYP1A2 inactivation experiments was designed to assess the potential contribution of released ENX metabolites to the rate of inactivation observed (Figure 2.30). In panel A, the NADPH-dependent loss of CYP1A2 (40 nM) activity by ENX (50 μM) was shown to follow first order kinetics (rate of 0.015 min^{-1}) with time. No evidence for a lag at the early time points or accelerated inactivation at the later time points that might be expected if a metabolite contributed to inactivation was observed. Incubation with N-OH-ENX (50 μM) drastically increases the rate of loss of activity (rate of 0.124 min^{-1}) and also appears to be first order. The ratio of these rates (0.124 min^{-1}:0.015 min^{-1}) indicates an over 8-fold faster rate for N-OH-ENX at the same concentration of inhibitor (50 μM) suggesting a substantial acceleration of activity loss would be observed if N-OH-ENX contributed to enzyme inactivation at later time points. We did not observe any such acceleration. In panel B, the 8 minute time-course for N-OH-ENX accumulation upon incubation of 100 nM CYP1A2 with 50 μM ENX is shown. N-OH-ENX rose in a linear fashion to a final concentration of 100 nM at a maximum rate of 0.1 nM N-OH-ENX / nM CYP1A2 / min (0.1 min^{-1}). Inactivation by N-OH-ENX was unaffected by KCN (1 mM) which is an efficient trap of the nitrone metabolite (Panel C). Finally, a set of experiments where the concentration of CYP1A2 was varied or N-OH-ENX was spiked were performed to evaluate any effects on the initial rate of CYP1A2 inactivation. Panel D (left) shows that the rate of inactivation by 50 μM ENX is not significantly affected by a 10-fold change in enzyme concentration (10 nM, 40 nM and 100 nM CYP1A2, respective initial rates of 0.012 ± 0.002,

0.013 ± 0.001, and 0.014 ± 0.002 min^{-1}). Panel D (center) shows the rate of inactivation observed due to co-incubation of a mixture of 49.9 μM ENX and 0.1 μM N-OH-ENX. The rate of inactivation (0.012 ± 0.002 min^{-1}) for the spiked incubation was not significantly different than that with ENX (50 μM) alone at the same enzyme concentration (0.013 ± 0.001 min^{-1}) where the concentration of N-OH-ENX free in solution will take approximately 25 minutes to equal the spiked level of 100 nM (based upon a rate of 0.1 min^{-1}). Thus no enhancement of the initial inactivation rate is observed when N-OH-ENX is spiked in at a level equivalent to what is observed near the end of an inactivation experiment. Finally, as a control the right portion of panel D shows that spiking in N-OH-ENX at 5 μM (50-fold higher than what is observed under ENX incubation conditions) in the presence of 45 μM ENX increased the initial inactivation rate from 0.013 ± 0.001 min^{-1} (50 μM ENX) to 0.026 ± 0.002 min^{-1} (45 μM ENX, 5 N-OH-ENX μM) and this increase was statistically-significant. The rate increased by 2-fold as a result of spiking in N-OH-ENX to a level 50-fold higher than what is observed at later time points in ENX incubations. This illustrates that N-OH-ENX will compete with ENX for the enzyme active site at sufficiently high concentrations. However, the levels of N-OH-ENX that must be reached for this metabolite to effectively compete cannot realistically be reached in a typical incubation.

2.3.10 Prediction of the In Vivo Effect of ENX on CYP1A2 Activity.

The predicted effect of ENX on CYP1A2 activity in vivo was estimated using standard equations for a static, steady-state prediction of effect. Studies where enoxacin was administered orally and measured in plasma at therapeutic doses provided C_{max} values that ranged from 8 to 16 μM (Yamaguchi et al., 1984; Marchbanks et al., 1990; Mizuki et al., 1996a; Hamel et al., 2000). The *in vivo* degradation rate for CYP1A2 was set at 0.00030 min^{-1} which corresponds to an enzyme half-life of 38.6 hours (Faber and Fuhr, 2004). The CYP1A2 inactivation parameters obtained in bactosomes (Figure 2.7) and equations 4 through 6 (see

Experimental) were used to predict the effect of 7.5 μM circulating enoxacin on CYP1A2 *in vivo*. The amount of active CYP1A2 in the liver was predicted to decrease by 85% during multiple dosing of ENX (Figure 2.31, open circle). This level of CYP1A2 impairment may cause a maximal AUC change of 10-fold for a hypothetical victim drug with $f_{m,CYP1A2}$ = 1. Estimates of the effect of ENX on the pharmacokinetics of two known in vivo substrates of CYP1A2, theophylline ($f_{m,CYP1A2}$ = 0.80; Venkatakrishnan et al. (2007)) and caffeine ($f_{m,CYP1A2}$ = 0.95; Venkatakrishnan et al. (2007)) were calculated. The fold-increases in exposure to theophylline and caffeine were predicted and compared to literature studies (Table 2.6). The predicted interaction with theophylline (AUC'/AUC = 3.5) agreed favorably with the literature value of 3.7 (Wijnands et al., 1986). Our predicted interaction with caffeine (AUC'/AUC = 6.7) was also within 1.25-fold of the observed interaction, AUC'/AUC = 5.7 (Kinzig-Schippers et al., 1999).

2.4 Discussion

2.4.1 Chapter Overview and Hypothesis.

The drug-drug interaction between ENX and theophylline is severely underpredicted when reversible inhibition by the parent drug is the only considered mechanism (Obach et al., 2006). Coadministration of ENX with caffeine, a more sensitive *in vivo* probe of CYP1A2 activity than theophylline based upon fraction metabolized in vivo, results in an accordingly greater interaction magnitude. While there has been a long-standing consensus that the increase in exposure to theophylline and caffeine is due to inhibition of CYP1A2 by ENX *in vivo*, no plausible mechanism which can account for the magnitude of the interaction has been identified.

The interaction between ENX and theophylline was first reported and studied by Wijnands et al. (1984). At a therapeutic dose, ENX raised the plasma concentration of theophylline 3.5-fold without affecting renal clearance or plasma protein binding. We note here that the full increase in theophylline exposure developed gradually over five days. The plasma concentration of theophylline was also measured on day three of this study, at which point theophylline concentration had only increased 2.0-fold. A similar time-dependence for inhibition of theophylline clearance was captured in another study two years later (Wijnands et al., 1986). The time-scale for reaching the full inhibitory effect on theophylline metabolic clearance is consistent with, albeit not exclusive to, a mechanism whereby metabolites of ENX with greater inhibitory potential than the parent drug must be generated. Furthermore, since ENX is a substrate of CYP1A2, an investigation into whether a metabolite of ENX may serve as a mechanism-based inhibitor was warranted.

The possibility that inhibition of CYP1A2 by ENX involves mechanism-based inactivation has been raised in the literature (Spaldin et al., 1994). However, a detailed mechanism for this process has never been described. To fill this knowledge gap, our lab has sought to expose any linkage between the metabolism of ENX and its inhibitory effect upon CYP1A2. Previous work

performed in this laboratory uncovered a potential role for the secondary hydroxylamine metabolite, N-OH-ENX, in mediating inactivation of CYP1A2 (Smith, 2007). Specifically, the formation of an MI complex was suspected via sequential metabolism of ENX to a ring-opened nitroso metabolite which coordinates to the ferrous heme-iron. However, formation of the MI complex could only be demonstrated in liver microsomes with N-OH-ENX as the substrate and with poor reproducibility. Evidence for MI complex formation from the parent drug, ENX, was lacking. Further assessment of these initial findings was needed to confirm whether or not MI complex formation is relevant to inhibition of CYP1A2 by ENX.

In this chapter, time-dependent inhibition of CYP1A2 by ENX was more thoroughly examined and evidence was provided to support our hypothesis that metabolism of ENX enhances inhibition of CYP1A2. Ultimately, mechanism-based inactivation of CYP1A2 by a metabolite of ENX was confirmed. MI complex formation was observed from both the parent drug and the N-hydroxylated metabolite, N-OH-ENX. The inactivation of CYP1A2 was highly efficient as evidenced by minimal consumption of ENX and low levels of metabolites produced while extensive enzyme inactivation took place. This led to the prediction that a therapeutic dose regimen provides an adequate quantity of ENX to inactivate the majority of the CYP1A2 in a human liver. Mechanistically, the inactivation process requires three oxidations and a ring-opening to convert ENX to a nitroso metabolite capable of coordinating to the ferrous heme iron. Interestingly, we observed no lags when monitoring MI complex formation or loss of CYP1A2 activity despite this requirement for multiple metabolic steps. A lag would be expected if the inactivation process involved release and rebinding of intermediates to the enzyme. Rather, it appeared that MI complex formation occurred both rapidly and efficiently in a process whereby intermediate species were not readily released from the CYP1A2 active site. Our proposed mechanism for MI complex formation from ENX (Figure 2.32) details these metabolic steps and specifies that a metabolite of N-OH-ENX, either NITRONE-ENX or α-hydroxy-N-OH-ENX, is the

true mechanism-based inhibitor of CYP1A2. Since the final metabolic step must involve oxidation and ring-opening that occurs within the CYP1A2 active site, mechanistic alternatives for oxidative ring-opening of this metabolite to NITROSO-ENX will be considered (Figures 2.33, 2.34, and 2.35).

This work seeks to clarify the mechanism of the DDI between ENX and CYP1A2-substrates while also, in a larger context, supporting the area of research dedicated to rationalizing metabolite-mediated DDI via sequential oxidative reactions (VandenBrink and Isoherranen, 2010). It is important to note that two distinct scenarios are possible when assessing a metabolite-mediated enzyme inactivation. Scenario 1 (*dissociative mechanism*): Intermediate metabolites which are on-path to enzyme inactivation are frequently released from the active site and these intermediates must reach sufficient levels in order to compete with their precursor and proceed towards enzyme inactivation. The kinetics of inactivation for the dissociative situation will be highly complex and heavily influenced by incubation variables such as enzyme concentration, thus hampering DDI prediction efforts. Scenario 2 (*non-dissociative mechanism*): Intermediates on-path to inactivation are rarely released from the enzyme active site and multiple consecutive catalytic steps following initial substrate binding leads directly to enzyme inactivation. As MI complex formation from ENX appears to follow a non-dissociative mechanism, it is appropriate to treat the multiple enzymatic steps involved in the inactivation of CYP1A2 by ENX as a single step for prediction purposes. A major finding of this study is the ability to predict a metabolite-mediated DDI using inactivation parameters obtained from the parent drug.

2.4.2 Inactivation of CYP1A2 by MI Complex Formation.

The results of our studies indicate that ENX is sequentially metabolized to an MI complex within a recombinant CYP1A2 enzyme system (Bactosomes®). Given the structure of ENX

(Figure 2.1, structure 1), a nitroso metabolite is the only logical MI complex ligand. Sequential oxidation and ring-opening of the piperazine ring is therefore implicated in this process. Of all the known in vivo metabolites of ENX, DES-ENX (Figure 2.1, structure 3) is the only metabolite which appears to be on-path to a nitroso metabolite. DES-ENX is not detected in circulation, but it is found in the urine as approximately 1% of the dose (Yamaguchi et al., 1984). The major metabolite of ENX (and the only detectable circulating metabolite) is the lactam, oxo-enoxacin (Figure 2.1, structure 7). The lactam structure should be stable and it would not be expected to undergo ring-opening. In addition, multiple studies have reported that oxo-enoxacin is a weaker inhibitor than ENX (Mulder et al., 1988; Sarkar et al., 1990; Fuhr et al., 1993; Mizuki et al., 1996a; Mizuki et al., 1996b). DES-ENX, on the other hand, has inhibitory potency similar to ENX (Fuhr et al., 1993) and contains a sterically-accessible terminal nitrogen which has been liberated from the ring-structure of the piperazine. On this basis, we chose DES-ENX as the most likely in vivo metabolite which may be on-path to MI complex formation.

Conversely, MI complex formation may proceed through the secondary hydroxylamine metabolite, N-OH-ENX (Figure 2.1, structure 2). N-OH-ENX is not a known in vivo metabolite. However, it is formed in a NADPH-dependent manner within recombinant CYP1A2 and CYP3A4 systems as well as in human liver microsomes (Smith, 2007). That N-OH-ENX is a NADPH-dependent metabolite of ENX was also confirmed in this study using recombinant CYP1A2 (Figure 2.12). Prior to this dissertation, the only evidence that ENX might be metabolized to an MI complex came from incubations with N-OH-ENX in human liver microsomes so enzyme identity was circumstantial (Smith, 2007). MI complex formation from ENX had not been documented previously. Thus evidence for a positive link between N-OH-ENX and ENX was inferred and whether or not MI complex formation could proceed from DES-ENX had not been evaluated. In the present study, by scanning spectrally for MI complex

formation from N-OH-ENX and DES-ENX, we could determine whether MI complex formation is initiated by N-hydroxylation or removal of the ethylene bridge of the piperazine moiety on ENX.

Spectral studies did not support MI complex formation from incubation with DES-ENX (Figure 2.3). A species absorbing maximally at 425-nm was generated when incubating CYP1A2 with DES-ENX. This same wavelength has been documented previously for ENX and related analogues in ligand binding studies performed in rat liver microsomes prepared from rats pre-treated with 3-methylcholanthrene to induce CYP1A (Mizuki et al., 1989). Since our spectral experiment was initiated by adding DES-ENX to the sample cuvette and vehicle to the reference cuvette, the spectral species observed at 425-nm may have been a simple ligand binding spectrum and was not necessarily NADPH-dependent. We found no evidence for MI complex formation from DES-ENX which argues against a role for this primary amine metabolite in the generation of an MI complex from ENX.

Incubation of CYP1A2 with ENX or N-OH-ENX resulted in MI complex formation from both substrates suggesting that N-hydroxylation is the first step in the mechanism. The faster MI complex formation rate for N-OH-ENX as compared to ENX was consistent with our hypothesis that N-OH-ENX is on-path to MI complex formation and one step closer to the final ligand. We proposed that both ENX and N-OH-ENX were metabolized to a common nitroso-bearing ligand which coordinates to the ferrous heme-iron of CYP1A2. The MI complex was apparently stable to dithionite and prevented a portion of the P450 molecules from binding CO. The spectral species formed from both ENX and N-OH-ENX absorbed maximally at 452-nm suggesting the same complex had formed from either substrate. This wavelength is red-shifted by 4-nm from the CYP1A2-CO complex (note, CYP1A2 was previously known as P448) confirming MI complex formation had occurred as opposed to generation of a CO complex in situ. The commonly used molar extinction coefficients of 65 $mM^{-1}cm^{-1}$ (Pershing and Franklin, 1982) and 91 $mM^{-1}cm^{-1}$ (Omura and Sato, 1964) were then employed to estimate the quantities of MI

complex and CO complex, respectively, at the end of each incubation. For unknown reasons, MI complex formation did not go to completion when incubating with either substrate. After MI complex formation had ceased, we assayed for uncomplexed CYP1A2 by reducing the cuvette contents with dithionite and bubbling CO gas into each cuvette individually to scan for the presence of P450-CO complex in sample and reference cuvettes (Omura and Sato, 1964). The higher CO complex was observed in the reference cuvette relative to the sample cuvette, strongly implying the presence of MI complex in the sample cuvette. The difference in CO complex quantity between the sample and reference cuvettes could be accurately accounted for by the quantity of MI complex formed in the sample cuvette (Table 2.1). Note that in the case of DES-ENX, approximately no difference was found in CO-complex formation between the vehicle- and inhibitor-containing cuvettes supporting our conclusion that DES-ENX is not metabolized to an MI complex. Incubation with either ENX or N-OH-ENX gave rise to a spectral species consistent with MI complex formation and the portion of the enzyme that existed as MI complex was unable to bind CO presumably because the ferrous heme iron was occupied by a nitroso metabolite.

While it is not clear why MI complex formation did not go to completion when incubating with ENX or N-OH-ENX, one possibility is that a portion of the CYP1A2 in our enzyme system (Bactosomes®) is catalytically-incompetent or isolated from cytochrome-P450 reductase. Alternative hypotheses include protection by downstream metabolites or a second mechanism of inactivation. If there is more than one mechanism of inactivation operating, then it must not involve heme-destruction or prevent CO-binding as the remaining portion of CYP1A2 was able to form a CO-complex.

To further assess the contribution of MI complex formation to CYP1A2 inhibition, we tested the reversibility of CYP1A2 inhibition to dialysis and potassium ferricyanide by using phenacetin o-deethylation as an activity marker (Figure 2.9). The results of these experiments

confirmed that incubation with ENX or N-OH-ENX leads to irreversible inhibition of CYP1A2 as activity did not return following dialysis. When the dialyzed enzyme was also treated with potassium ferricyanide, the inhibition was reversed, albeit to differing degrees depending upon whether ENX or N-OH-ENX served as the inhibitor. The overall results indicated that inhibition N-OH-ENX was due entirely to MI complex formation. Since we obtained greater than 100% activity (relative to a vehicle control) after ferricyanide reversal of enzyme incubated with N-OH-ENX, we can only speculate that CYP1A2 was stabilized in the MI complex state relative to the normal degradation rate present in the vehicle control. Notably, the inactivation caused by incubation with ENX was only partially reversible upon treatment with potassium ferricyanide. This is particularly striking since incubation with either ENX or N-OH-ENX led to similar yields of MI complex when the reaction was monitored by repetitive scanning in the spectrophotometer. In contrast, the results presented in Figure 2.9 suggest that incubation with N-OH-ENX leads to a higher yield of MI complex as compared to incubation with ENX. Ferricyanide reversal of the MI complex, measured spectrally, (Table 2.2) captured a quantitatively similar discrepancy between ENX and N-OH-ENX as a higher amount of MI complex was revealed following ferricyanide reversal of incubations with N-OH-ENX. These results further suggest metabolites of ENX produced by CYP1A2 may cause enzyme inactivation by two mechanisms: MI complex formation and possibly a second mechanism which is not reversible by potassium ferricyanide.

How can we account for differing extents of MI complex formation from ENX and N-OH-ENX when CYP1A2 is probed by ferricyanide reversal methods, but approximately equal MI complex yields when direct spectral scanning of complex formation is performed? One possible explanation is a sensitivity of the MI complex to blue light in the spectrophotometer. It is well established that cytochrome P450 CO and MI complexes undergo photolysis when treated with high-intensity blue light (Cooper et al., 1965; Diehl et al., 1969; Ullrich and Schnabel, 1973; Okuda et al., 1977). It is therefore conceivable that some degree of photolysis was occurring in

our spectral experiments, where the continuous scanning method causes excitation and scission of the Fe(II)-nitroso bond. Arguably, the results shown in Figure 2.9 are more relevant to MI complex formation in the liver. Overall, we believe incubation with ENX does, in fact, lead to a lower yield of MI complex than incubation with N-OH-ENX when the confounding factor of light excitation is removed. This again highlights a major finding; ENX inactivates CYP1A2 substantially through MI complex formation, but may also inactivate through a second mechanism. N-OH-ENX, however, appears to inactivate exclusively through MI complex formation.

Demonstration of the MI complex through spectral ferricyanide reversal supported the above reasoning that photoexcitation may complicate comparisons of MI complex yield from ENX and N-OH-ENX. By using a published procedure (Larrey et al., 1983) with some modifications (see Experimental), we once again demonstrated that MI complex formation proceeds from N-OH-ENX, but not from DES-ENX. The incubation conditions matched those used for spectral scanning experiments, with the important exception that the incubation phase was conducted in a water bath (to protect against photoexcitation). The incubation mixture was then divided into sample and reference cuvettes and the MI complex spectrum was recorded upon addition of ferricyanide to the reference cuvette. The CO-binding spectra were also recorded for ferricyanide- and water-treated CYP1A2 and the amounts of P448-CO complex were quantified (Figure 2.4). While the abbreviated exposure to blue light in this experimental design may have still caused some photolysis, we were able to observe a higher yield of the MI complex from incubation with N-OH-ENX in this experiment as compared to experiments which involved continuous spectral scanning and blue light exposure. These results also agree well with those of Figure 2.9, where restoration of enzyme activity upon treatment with ferricyanide appears to match the ferricyanide-mediated restoration of CO-binding capacity for CYP1A2 that was pre-incubated with N-OH-ENX. In other words, the return of enzyme activity and the

restored ability to bind CO to form the P448-CO complex following treatment with ferricyanide point to the same conclusion. Both results indicate that CYP1A2 was being restored to its native state and the magnitude of this restoration, by both measures, agreed reasonably well. In fact, while N-OH-ENX and ENX displayed similar MI complex yields in the continuous scanning experiment, both the spectral-based and activity-based ferricyanide reversals suggested that MI complex formation was more complete and greater in extent when N-OH-ENX served as the substrate. Following incubation of CYP1A2 with ENX, both the magnitude of enzyme activity restored and the quantity of MI complex revealed by ferricyanide treatment was roughly half of that seen following incubation with N-OH-ENX, Therefore, it must be true that MI complex formation is more complete when N-OH-ENX serves as the substrate. The only other possibility is that ENX is forming a similar quantity of MI complex, but for unknown reasons is not as susceptible to ferricyanide-mediated reversal. However, since incubation with both species leads to MI complexes with the same λ_{max} of 452-nm, we have generally assumed that the same final complex is being reached. There should be no difference in the susceptibility to ferricyanide if the same complex is being reached from either ENX or N-OH-ENX. It seems likely that the discrepancy between ENX and N-OH-ENX can be resolved if additional mechanisms of enzyme inactivation and protein damage are operative during ENX incubations.

The data presented support partial but significant conversion of CYP1A2 to an MI complex from ENX incubations (accounting for ~60-70% of the inactivation) as well as rapid and nearly-complete MI complex formation from N-OH-ENX incubations. It was confirmed that ENX and N-OH-ENX both cause NADPH-dependent loss of CYP1A2 activity while DES-ENX does not (Figure 2.5). The increased rate of MI complex formation for N-OH-ENX versus ENX was also reflected in the time-dependent inhibition results. MI complex formation is, therefore, a major contributor to CYP1A2 inhibition by ENX in vitro and MI complex formation likely proceeds through N-OH-ENX as an intermediate (Figure 2.11). To our knowledge, this is the first report of

a piperazine moiety being metabolized to an MI complex with a cytochrome P450 and may provide the basis for a new structural alert for MI complex formation.

2.4.3 Intermediates in the Mechanism for MI Complex Formation.

As discussed above, N-hydroxylation of the piperazine ring of ENX is the first step in the proposed pathway leading to MI complex formation. Incubating CYP1A2 with N-OH-ENX, a metabolite which we confirmed (Figure 2.12), led to drastically faster inactivation rates compared with ENX (Table 2.3). We made the critical distinction that MI complex formation goes through N-OH-ENX and not DES-ENX, suggesting that sequential N-oxidation and eventual ring-opening of the piperazine ring results in a nitroso metabolite coordinated to the ferrous heme iron (Figure 2.11). In this pathway, the step following N-hydroxylation is further oxidation to a cyclic nitrone (Figure 2.1, structure 11). The cyclic nitrone of ENX (NITRONE-ENX) was identified and confirmed as a NADPH-dependent metabolite of ENX by leveraging the chemical oxidation of N-OH-ENX by alkaline ferricyanide.

Incubation of ENX with CYP1A2 and NADPH gives two chromatographic peaks with accurate mass corresponding to that of NITRONE-ENX (Figure 2.12). We supported the assignment of the earlier eluting peak as NITRONE-ENX by a variety of means, ultimately culminating with confirmation of the structure of NITRONE-ENX by proton NMR experiments conducted on an impure solution of NITRONE-ENX in deuterium oxide. However, the first piece of evidence that led us to suspect that the earlier eluting peak was NITRONE-ENX was co-elution with a mass that equated to addition of water, consistent with the expected hydrated form of the nitrone. The peak of later retention time did not undergo this same water addition. This simple difference suggested that the earlier eluting peak is the cyclic nitrone metabolite and formed a basis for further investigation.

At the first stage of our investigation into the structure of the tentatively-assigned NITRONE-ENX, we incubated N-OH-ENX with the chemical oxidant potassium ferricyanide in an attempt to generate NITRONE-ENX "in situ." Chemical oxidation of N-hydroxy-piperidine by ferricyanide to a cyclic nitrone is a known reaction (Thesing and Mayer, 1957). As expected from the ferricyanide-based oxidative chemistry, the peak assigned as NITRONE-ENX from metabolic incubation could also be observed as one of the products of the chemical oxidation of N-OH-ENX (Figure 2.13) and the high-resolution fragmentation was consistent with a cyclic nitrone moiety (Figure 2.17). NITRONE-ENX generated both metabolically (ENX + NADPH-fortified CYP1A2) and chemically (N-OH-ENX + $K_3Fe(CN)_6$) reacted with cyanide to give HCN addition products of matching retention times (Figures 2.13 and 2.14). By fragmentation, the HCN-adduct of NITRONE-ENX gave the same fragments as NITRONE-ENX following neutral loss of HCN (Figure 2.18). Taken together, these preliminary findings strongly supported that N-OH-ENX is further oxidized to NITRONE-ENX by CYP1A2.

In order to confirm the structure of NITRONE-ENX, we modified the chemical oxidation reaction to generate a concentrated solution of this product and then partially purified the product by solid-phase extraction. Importantly, the solid phase extraction step allowed for isolation of NITRONE-ENX as a concentrated solution in deuterium oxide which facilitated characterization by proton NMR. Due to the interfering proton signals of impurity and solvent peaks, we turned to two-dimensional ^1H-^1H COSY NMR to structurally confirm NITRONE-ENX (Figure 2.19). Signals from water, trace methanol (used in the SPE elution), and DES-ENX could be observed in the 1D proton NMR. The methylene protons from the ethylene bridge of DES-ENX were upfield from the analogous protons of the ethylene bridge of the tetrahydropyridine N-oxide moiety (H_a and H_b) of NITRONE-ENX. This confirmed that the methylene protons (N-CH_2-CH_2-N) experienced greater electron-withdrawing in NITRONE-ENX due to the proximity of the nitrone moiety. Protons from the methylene group (H_c) vicinal to the

nitrone sp^2-carbon were concealed in the 1D proton NMR due to water, but could be seen by COSY NMR due to clear couplings to both the vinylic nitrone proton (H_n) and protons from the closest methylene group (H_a). That this proton signal was coupled to H_n and H_a, but not H_b, and was downfield from H_a and H_b was also consistent with the position of this methylene group in the molecule due to its close proximity to the electron-withdrawing nitrone. The nitrone proton (H_n of the sp^2-carbon) integrated appropriately as a single proton and was highly deshielded. That this highly deshielded proton was coupled to protons H_c of a methylene group of the tetrahydropyridine ring ultimately confirmed the structure of NITRONE-ENX.

Having obtained a solution of authentic NITRONE-ENX, we moved forward to chemically characterize the cyclic nitrone (Figures 2.20 and 2.21). The reduction of NITRONE-ENX to N-OH-ENX with sodium borohydride was facile and complete within minutes at room temperature. We confirmed that the reduction of an estimated 1 μM solution of NITRONE-ENX yielded an approximate 1 μM solution of N-OH-ENX as the signal intensity of the product matched the signal intensity of a 1 μM solution of authentic N-OH-ENX (in addition to the matching retention time and accurate mass). Our authentic NITRONE-ENX also reacted with cyanide to form the HCN-adduct. Out of interest in the stability of NITRONE-ENX, we treated it with strong acid or base and, surprisingly, observed rapid degradation of NITRONE-ENX to DES-ENX. While it is possible that the DES-ENX seen in metabolic incubations is formed by CYP1A2 directly, i.e. DES-ENX is a true metabolite, the degradation route to DES-ENX seen here raises the possibility that DES-ENX is actually a metabonate formed through chemical breakdown of NITRONE-ENX. If this were the case, the observation of DES-ENX as an in vivo metabolite would indirectly demonstrate that both N-OH-ENX (the precursor to NITRONE-ENX) and NITRONE-ENX itself are made in vivo. The possibility that DES-ENX is actually a metabonate would also coincide with its lack of a role in the inactivation process since it cannot, by definition, be associated with a non-dissociative process leading up to mechanism-based

inactivation of CYP1A2 if DES-ENX is the result of a chemical degradation that takes place outside the CYP1A2 active site.

We also confirmed that our authentic NITRONE-ENX matched the tentatively assigned NITRONE-ENX metabolite seen in metabolic incubation with ENX by HPLC-MS (Figures 2.22 and 2.23) as suggested by our preliminary experiments utilizing ferricyanide chemistry. We once again captured that there are two metabolite peaks with a matching m/z for ENX +O -2H (the biotransformation required for formation of NITRONE-ENX). The retention time of the authentic standard matched the earlier eluting peak and only this peak substantially decreased upon addition of KCN to the incubation. The corresponding HCN adducts of authentic and metabolically-formed NITRONE-ENX also matched as did their high-resolution fragmentation patterns. Hence, the CYP1A2-generated metabolite of ENX eluting at 3.65 minutes with m/z of 335.115 was confirmed as NITRONE-ENX. Interestingly, we find that incubation of NADPH-fortified CYP1A2 with N-^{18}OH-ENX led to formation of ^{18}O-labeled NITRONE-ENX with roughly the same ^{18}O content as the substrate. This further confirmed NITRONE-ENX as a metabolite which still contains an oxygen atom on the terminal nitrogen and, specifically, that NITRONE-ENX retains the original oxygen atom from the N-OH-ENX substrate.

It was informative to compare the fragmentation of the newly-identified NITRONE-ENX metabolite and N-OH-ENX as the former undergoes a single water loss while the later undergoes two (Figure 2.24). Initial water loss during fragmentation is consistently observed across the metabolites of ENX (and ENX itself) due to the conserved carboxylic acid moiety. The double water loss observed from N-OH-ENX suggested the presence of an additional OH group in the molecule in agreement with the hydroxylamine structure. That NITRONE-ENX does not undergo this second water loss highlights the oxidation state of the nitrogen atom (N-OH vs N^+-O^-). We also supported this reasoning by comparing the fragmentation of N-^{18}OH-ENX and the corresponding ^{18}O-labeled NITRONE-ENX. It could be seen with N-^{18}OH-ENX that the first

water loss is a loss of $H_2{}^{16}O$ and the second water loss is a loss of $H_2{}^{18}O$, clearly indicating the second water loss is from the hydroxylamine moiety. We sought to understand the fragmentation at this level because of its potential future utility in identifying the final species in our mechanism for MI complex formation from ENX.

In conclusion, these data support the proposed pathway to MI complex formation (Figure 2.11) as the identity of the cyclic nitrone metabolite was confirmed. We found that NITRONE-ENX is a NADPH-dependent metabolite of both ENX and N-OH-ENX. When the ^{18}O-labeled hydroxylamine, N-^{18}OH-ENX, served the substrate we detected the ^{18}O-labeled NITRONE-ENX metabolite with approximately unchanged ^{18}O content (74.7%) relative to the ^{18}O-labeled substrate (77.4%). Therefore, the CYP1A2-mediated enzymatic oxidation of N-OH-ENX to NITRONE-ENX retains the original oxygen atom on the nitrogen. It was also interesting to note that both the unlabeled NITRONE-ENX (335.115 m/z) and the ^{18}O-labeled NITRONE-ENX (337.120 m/z) co-eluted with a species matching the addition of +18.010 m/z (353.125 m/z and 355.130 m/z, respectively) suggesting a propensity for NITRONE-ENX to add water. The addition of H_2O parallels the addition of HCN to NITRONE-ENX upon addition of KCN where an alpha-hydroxy hydroxylamine results from water addition rather than the alpha-cyano hydroxylamine resulting from addition of HCN. Since the water adduct co-elutes with NITRONE-ENX, it appears that the hydrated and dehydrated species are in rapid equilibrium during chromatography. The possible implications of the equilibrium process between NITRONE-ENX and α-hydroxy-N-OH-ENX for the CYP1A2 inactivation process was noted and may be mechanistically important.

In addition to the HCN adduct of NITRONE-ENX, multiple other NADPH-dependent HCN adducts were detected upon addition of KCN:$K^{13}C^{15}N$ (1:1) to the incubation mixture. One of these adducts corresponded to reaction of cyanide anion with a dehydrogenated metabolite of ENX, potentially an iminium ion. While these electrophilic species may play an additive role in

mediating CYP1A2 inactivation, we simply note their presence and suspect that these reactive species are off-path from MI complex formation. These results demonstrate that multiple oxidations occur on the piperazine ring of ENX including N-oxidation, dehydrogenation, and N-dealkylation. The intermediate NITRONE-ENX results from dehydrogenation of the metabolite N-OH-ENX. MI complex formation will ultimately require one additional oxidation (and ring-opening) to afford the proposed nitroso metabolite (Figure 2.11). Having established that NITRONE-ENX is an NADPH-dependent metabolite of ENX, further experiments explored whether the final ligand complexed to CYP1A2 is consistent with NITROSO-ENX (structure 12 in Figure 2.1).

Our strategy to identify and structurally-elucidate the MI complex ligand was analogous to that used by Barbara et al. (2013). Essentially, ferricyanide treatment of the MI complex to release the coordinating ligand should result in an increased abundance of that specific metabolite as detected by HPLC-MS. In the case of ENX, we suspect that an oxidative ring-opening of NITRONE-ENX to NITROSO-ENX is the final step in MI complex formation. Our finding that a metabolite peak consistent with the mass of NITROSO-ENX more than doubled following ferricyanide treatment of inactivated CYP1A2 suggested this metabolite peak was due to release of the MI complex ligand (Figure 2.25). The presence of this metabolite peak without ferricyanide treatment indicates that a fraction of the time NITROSO-ENX is made in the active site and released before it can bind to the ferrous heme iron. Alternatively, quenching the incubation with acetonitrile may cause the MI complex ligand to release into solution to a small degree. In either case, the low level of this metabolite without ferricyanide treatment suggested that little release of NITROSO-ENX occurs relative to the successful binding of NITROSO-ENX to the ferrous heme iron to form the MI complex. The apparent doubling of this metabolite peak upon ferricyanide treatment quantitatively points to an approximate 50:50 chance that NITROSO-ENX generated in the CYP1A2 active site will bind to the ferrous heme iron before it

is released into solution. The final step in MI complex formation is, therefore, reasonably efficient by this approximation.

Incubation of N-^{18}OH-ENX with CYP1A2 gave the NITRONE-ENX metabolite with the ^{18}O label retained and we found that the newly-identified NITROSO-ENX peak also retains this ^{18}O label following incubation with the N-^{18}OH-ENX substrate. We fragmented this species both with and without the ^{18}O label in an attempt to structurally elucidate the molecule and determine if the fragmentation is consistent with a ring-opened nitroso metabolite (Figures 2.26 and 2.27). It was immediately apparent that the species being analyzed could not be NITROSO-ENX but rather was completely consistent with the oxime tautomer, oxime-ENX. The preference for the oxime tautomer over the nitroso is well-established as early efforts to form MI complexes directly from the nitroso ligand were thwarted by the rapid conversion of nitroso to oxime in water (Mansuy et al., 1977). Fragmentation of oxime-ENX gave a double water loss consistent with the presence of the N-OH group of the oxime and analogous to the double water loss seen from N-OH-ENX. The ^{18}O label again confirmed, as with N-^{18}OH-ENX, that the first water loss occurs preferentially from the carboxylic acid and the second water loss from the N-^{18}OH group. We find that oxime-ENX is the only logical structure that one can draw given the constraints of the observed fragments and the observation of a double water loss, where the second water loss includes loss of the ^{18}O atom. The oxime is also the most logical choice for this metabolite peak given the increased abundance following ferricyanide treatment of inactivated CYP1A2, suggestive of the release of a nitroso ligand from an MI complex, and the literature precedence for tautomerization of nitroso to oxime in water (Beckett et al., 1976).

The ferricyanide-dependent increase in the metabolite peak assigned as oxime-ENX was further investigated by evaluating the responsiveness of this peak to ferricyanide following dialysis of inactivated CYP1A2. Because ferricyanide is a chemical oxidant which can act upon various chemical species present in an incubation mixture and may therefore alter metabolite

profiles in unpredictable ways, it is important to interpret changes in the metabolite levels carefully. By dialyzing the MI complex prior to the use of ferricyanide, we sought to minimize the degree to which ferricyanide induced side-reactions with metabolites may create false-positive results. In this regard, note that we observed a greater fold-increase (~5.3-fold) in the assigned oxime-ENX metabolite level after dialysis (Figure 2.28) than the fold-increase (~2.4-fold) obtained from incubations that were not dialyzed (Figure 2.25). Since the dialyzed incubations should be “cleaner” with respective to potential side-reactions with ferricyanide, it would be reasonable to expect that metabolite level increases which are due to side-reactions would attenuate following dialysis. Therefore, the robust increase in the oxime-ENX peak area following ferricyanide treatment even after dialysis strongly suggests that the source of this increase is lysis of the MI complex. These data agree with the ferricyanide-mediated restoration of CYP1A2 activity following dialysis of CYP1A2 inactivated by N-OH-ENX (Figure 2.9) and once again demonstrate the stability of the MI complex to dialysis.

2.4.4 The Mechanism of the Final Catalytic Step in MI Complex Formation.

Our initially proposed mechanism for MI complex formation is summarized in Figure 2.11. As discussed above, we confirmed that ENX undergoes sequential metabolism to NITRONE-ENX. NITRONE-ENX was reactive with cyanide leading to the HCN-adduct, but also added water. The addition of water to NITRONE-ENX may initiate a ring-opening reaction to the primary hydroxylamine. Further oxidation of the primary hydroxylamine would yield NITROSO-ENX, the ultimate ligand which binds quasi-irreversibly to the ferrous heme iron (Figure 2.11). However, there are compelling reasons to believe that this description is incorrect and that a primary hydroxylamine is not involved in MI complex formation. The non-dissociative nature of enzyme inactivation observed here necessitates that NITRONE-ENX be converted to NITROSO-ENX within the CYP1A2 active site. There are relatively few water molecules

available within the active site, particularly when a substrate is bound. The CYP1A2 active site is especially small and rigid (Hendrychova et al., 2011). Therefore, the addition of water to NITRONE-ENX to drive a hydrolytic ring-opening is not likely to occur within the small, rigid, and sparsely hydrated space of the CYP1A2 active site.

An updated mechanism was proposed to suggest alternative metabolic routes to NITROSO-ENX and MI complex formation (Figure 2.32). Three possibilities (paths a, b, and c) are presented utilizing both the different states of the active CYP1A2 oxidant (Fe^{III}-OO^{-} or Fe^{V}=O) and the different substrates which may serve as the immediate precursor to NITROSO-ENX (NITRONE-ENX or α-hydroxy-N-OH-ENX). All of these mechanisms entail oxidative ring-opening via carbon-nitrogen bond cleavage. We favor an oxidative ring-opening over a primary hydroxylamine intermediate due to the compatibility of this process with non-dissociative enzyme inactivation. Each of the proposed paths (a, b, and c) was given equal consideration as to their likelihood and viability since our present dataset cannot exclude any of the three mechanisms. Each path is described and discussed individually below.

Path a - NITRONE-ENX and Fe^{III}-OO^{-}

As one alternative route to NITROSO-ENX, we propose that a ferric peroxy-anion species can mediate ring-opening and oxidation to a nitroso simultaneously (Figure 2.32, path a). The ferric peroxy-anion is a catalytic intermediate on-path to generation of Compound I, the principal active oxidizing species of cytochrome P450. Coon et al. (1998) have suggested that the iron-peroxy intermediates (Fe^{III}-OO^{-} and Fe^{III}-OOH) are active oxidants in P450 catalysis stemming from their work on P450-catalyzed deformylation reactions (Roberts et al., 1991; Vaz et al., 1991; Vaz et al., 1996). The peroxy-anion is nucleophilic in nature and we propose that it may react with the electrophilic sp^2-carbon of NITRONE-ENX. Interestingly, the delivery of a proton to facilitate formation of a six-membered ring transition state (Figure 2.33) may be accomplished

through the proton delivery expected via the normal catalytic mechanism. In this instance, it is conceivable that the N^{+}-O^{-} oxygen anion of NITRONE-ENX is able to intercept the proton originally intended for protonation of the distal oxygen either following or simultaneous with nucleophilic attack by the ferric peroxy-anion. This mechanism has the advantage of requiring minimal movements outside of those already required for normal catalysis. Ultimately, the transition state might be expected to collapse through either hetero- or homolytic C-N and O-O bond cleavages to form NITROSO-ENX. A potential downside to this mechanism is that a hydroxide anion is left coordinated to the ferric heme iron immediately following generation of the nitroso ligand. Rapid delivery of one proton and displacement of the resulting water molecule will then be in competition with release of NITROSO-ENX. Single electron reduction of the unoccupied ferric heme-iron is further required to allow for the nitroso moiety to coordinate to the ferrous heme-iron. The viability of this mechanism thus depends on (i) the reactivity and lifetime of the ferric peroxy anion with NITRONE-ENX and (ii) the rates of subsequent water displacement and reduction of the ferric heme-iron relative to the rate of NITROSO-ENX release from the active site.

Direct oxidative conversion of a nitrone to a nitroso was invoked by Cerny and Hanzlik (2005) in an attempt to explain why a nitrone substrate which was stable to hydrolysis could still be turned over to an MI complex at an appreciable rate. Hydrolysis to the primary hydroxylamine did not occur in their incubations over the course of 2-hours while MI complex formation proceeded in minutes suggesting direct oxidation of the nitrone substrate to a nitroso metabolite. The direct oxidative cleavage of nitrone to yield a nitroso and an aldehyde was originally conceived by Lindeke (1982). Lindeke described the decomposition of N,N-dibenzylhydroxylamine bearing a hydroperoxy group on the benzyl carbon (α to the nitrogen) via an intramolecular rearrangement to yield benzaldehyde, water, and α-nitrosotoluene. The hydroperoxy adduct originated from addition of peroxide to the nitrone and rearrangement to the

nitroso proceeds in a fashion that is strikingly similar to our proposed mechanism in Figure 2.33. Thus, we find some literature precedent to support the direct conversion of nitrones to nitroso species and this process may be operative in the conversion of NITRONE-ENX to NITROSO-ENX.

Path b – NITRONE-ENX and Fe^{V}=O

If a reaction between NITRONE-ENX and the ferric peroxy anion, Fe^{III}-OO^{-}, is not operative it is expected that the chemistry with the nitrone substrate will be due to Compound I, the Fe^{V}=O species. Oxygen insertion into the nitrone C=N bond (an "epoxidation") to yield an oxaziridinium N-oxide is a logical possibility (Figure 2.34). Opening of the strained three-membered ring and subsequent C-N bond cleavage would unveil the nitroso-bearing ligand directly above the ferric heme iron. Compared with path a, this current mechanism has the advantage of exposing the nitroso species to the heme-iron and does not require removal of hydroxide or water. A disadvantage of this mechanism is a lack literature precedent for the chemistry of oxaziridinium N-oxides. Sang et al. (1996) postulated that the peracid mCPBA could react with the well-known spin-trap reagent phenyl-N-tert-butyl nitrone (PBN) to form an oxaziridinium N-oxide and rearrange to yield the nitroso compound 2-methyl-2-nitrosopropane and benzaldehyde. Their suggestion matches our proposed mechanism although this chemistry has not been confirmed. It has been proposed that epoxidations can be mediated by the iron(III)-hydroperoxo state of P450 (Coon et al., 1998), however, density functional theory (DFT) calculations support Compound I as the superior epoxidant (Ogliaro et al., 2002). Hence, reaction of NITRONE-ENX with the electrophilic Compound I species can be considered a possibility for which the chemistry is not well understood.

Path c – α-hydroxy-N-OH-ENX and Fe^{V}=O

As an alternative to NITRONE-ENX, α-hydroxy-N-OH-ENX may serve as the immediate precursor to NITROSO-ENX. Addition of water to NITRONE-ENX and α-carbon hydroxylation of N-OH-ENX are both possible routes to this intermediate with the latter route being more direct (Figure 2.32, dashed line). Ultimately, cleavage of the C-N bond in HO-C-N-OH must occur in a $2e^-$ oxidation to yield a carbonyl and a nitroso (O=C and N=O) with production of 1 equivalent of water. This transformation is strikingly similar to the P450 side-chain cleavage (CYP11A1) reaction where the C-C bond of a 1,2-diol (HO-C-C-OH) is cleaved to produce two carbonyls (O=C and C=O) and 1 equivalent of water. Through electron paramagnetic resonance and electron nuclear double resonance, it has been demonstrated that Compound I is the active oxidizing species of CYP11A1 which performs the C-C cleavage (Davydov et al., 2015). Yoshimoto et al. (2016) further supported a role for Compound I in the C-C cleavage step where either hydroxyl group of the 1,2-diol may serve as a nucleophile to attack the electrophilic Compound I. The resulting complex (Fe-OO-C-C-OH) breaks down to form two carbonyls and water. In our proposed mechanism (Figure 2.35), oxygen from either of the hydroxyl groups in α-hydroxy-N-OH-ENX may potentially initiate nucleophilic attack on Compound I to initiate the reaction. Another possible mechanism is hydrogen atom abstractions from both hydroxyl groups to initiate a chain reaction of homolytic bond cleavages. In either case, the resulting product is the desired aldehyde-nitroso ligand. We know from incubations with N-^{18}OH-ENX that the ^{18}O label is retained in the final MI complex ligand. As such, the mechanism as drawn retains the original oxygen atoms from the substrate and the oxygen in Compound I (Fe^{V}=O) leaves as water. Following single electron reduction, the exposed ferrous heme-iron is left susceptible to the nitrogen lone pair of NITROSO-ENX. Note that dehydration of the α-hydroxy-N-OH-ENX substrate to form NITRONE-ENX in the active site is a competing process. If α-hydroxy-N-OH-ENX is the true mechanism-based inhibitor, then dehydration to the cyclic nitrone may be off-

path for MI complex formation. Of the three paths presented, path c is the most closely aligned with the literature due to its similarity to the mechanism of C-C cleavage of the 1,2-diol substrate in the cholesterol side-chain cleavage reaction.

2.4.5 Non-Dissociative Nature of ENX Metabolism and MI Complex Formation.

At this point, it is worth noting that all of the metabolites of ENX involve modification of the piperazine ring and that CYP1A2 can perform multiple oxidations directed at this ring. The orientation of ENX in the active site of rat CYP1A2 was elucidated by Mizuki et al. (1996c) and it was suggested that the terminal nitrogen of the piperazine ring lies closest to the heme-iron. In agreement, we find that N-OH-ENX is the most abundant of the CYP1A2-generated metabolites of ENX. The fact that we observe DES-ENX and aniline ENX as metabolites of ENX further highlights the accessibility of the piperazine ring to the active oxidizing species of CYP1A2 and perhaps a propensity to perform multiple oxidations at this site on the molecule. ENX fits the classical description of a CYP1A2 substrate due to an overall planar structure with the exception of the piperazine ring. Interestingly, Mizuki et al. (1996b) drew a link between the structural conformation of fluoroquinolones and their inhibitory potency. Specifically, they highlighted that the piperazine ring of ENX, the most potent fluoroquinolone inhibitor of CYP1A2, is oriented nearly in-plane with the quinolone (naphthyridone) core whereas less potent inhibitors have a piperazine ring that is increasingly rotated out of the plane defined by the quinolone core (Mizuki et al., 1996b). In the context of our results, this interpretation sheds some light on why ENX is an effective inhibitor. ENX exists in a planar conformation and orients the piperazine ring, a metabolic soft spot, towards the catalytic center of the enzyme. Thus, the effectiveness of ENX as an inhibitor is likely due to its suitability as a substrate as this characteristic is essential to a sequential mechanism-based inactivation process. This argument is further grounded by the requirement for at least three metabolic steps to generate an MI complex from ENX where these

metabolic steps appear to be performed consecutively and without release from the active site; i.e. the process is non-dissociative.

Multiple lines of evidence support the notion that inactivation of CYP1A2 involves non-dissociative sequential metabolism of ENX. Despite the requirement for multiple metabolic steps to inactivate CYP1A2 from ENX, we have consistently observed inactivation without an initial lag phase. In Figure 2.30 (Panel A), comparison of the enzyme inactivation slopes for ENX and N-OH-ENX (both at 50 μM) argues against a scenario where substantial conversion to N-OH-ENX is occurring. If this were the case, the latter time points would deviate from log-linearity as N-OH-ENX could hypothetically compete with ENX for access to the CYP1A2 active site and accelerate the rate of activity loss. We do not observe a lag, acceleration, or deviation from log-linearity when monitoring CYP1A2 inactivation from ENX. In addition, we found that inactivation rates do not increase upon increasing the concentration of CYP1A2 (across a 10-fold range) even though elevated enzyme levels should raise metabolite concentrations to levels better supporting enzyme inactivation (Figure 2.30, Panel D). In fact, the levels of N-OH-ENX are exceedingly low at early incubation times (Panel B) and the N-OH-ENX free in solution likely has minimal impact on enzyme inactivation. Accordingly, spiking N-OH-ENX into a ENX (49.9 μM) incubation to a level equal to N-OH-ENX observed at the end of a typical incubation (0.1 μM) had no significant effect on the inactivation rate (Figure 2.30, Panel D, middle gray bar) relative to a comparable ENX (50 μM) incubation where N-OH-ENX was not spiked (Panel D, left gray bar). In fact, the calculated inactivation rate for 0.1 μM N-OH-ENX using the apparent inactivation parameters (K_I=211 μM, k_{inact}=0.44 min^{-1}) and Equation 3 is 0.0002 min^{-1}. The calculated inactivation rate for 50 μM ENX (K_I=132 μM, k_{inact}=0.048 min^{-1}) matched the inactivation rate obtained in our experiment at 0.013 min^{-1}. In agreement with our results, this calculation predicts that the spiked N-OH-ENX will have no appreciable effect on inactivation and that the inactivation due to this concentration of N-OH-ENX would be impossible to detect in

vitro (CYP1A2 $t_{1/2}$ = ~58 hours). As a positive control, spiking in a 50-fold higher concentration (5 μM) of N-OH-ENX into a 45 μM ENX incubation doubled the inactivation rate (Panel D, right gray bar) relative to a comparable 50 μM ENX incubation from 0.013 min^{-1} to 0.026 min^{-1} demonstrating that if a high enough level of N-OH-ENX is reached (due to substantial conversion of ENX to N-OH-ENX) in an ENX incubation, then N-OH-ENX will begin to effectively compete with ENX for the CYP1A2 active site and contribute to the inactivation rate. Since both ENX and N-OH-ENX were well below their respective K_I values in these experiments, the majority of the CYP1A2 was unoccupied and free to bind substrate. The calculated inactivation rate for 5 μM N-OH-ENX from the above inactivation parameters (0.010 min^{-1}) is approximately equal to the increase in inactivation rate upon spiking of N-OH-ENX (0.013 min^{-1} increase) suggesting that inactivation from ENX and N-OH-ENX were additive. The easy conclusion to draw from this data is that N-OH-ENX can compete with ENX and contribute to inactivation. However, it further reveals that the observed inactivation in ENX incubations cannot be due to the free concentration of N-OH-ENX produced. If this were true, then hypothetically the inactivation observed during ENX incubation (50 μM) is being supported by ~0.1 μM N-OH-ENX which is more than three orders of magnitude below its apparent K_I value of 211 μM. Therefore, increasing the concentration (by spiking, in our case) of N-OH-ENX by 50-fold within this concentration range (from 0.1 to 5 μM) should have resulted in a nearly linear increase (~50-fold) in the inactivation rate *if inactivation were driven by the free concentration of N-OH-ENX*. Our result, which was a 2-fold increase in inactivation rate, dismisses any argument based on the level of free hydroxylamine and clearly implicates a non-dissociative process. While it is clear that N-OH-ENX is an intermediate to MI complex formation, it is also clear that MI complex formation would never have occurred in our incubations if this process relied upon the levels of N-OH-ENX free in solution. The final step in MI complex formation (conversion of NITRONE-ENX to NITROSO-ENX, Figure 2.1, structure 12) is also likely to be non-dissociative as

inactivation from N-OH-ENX incubations exhibited no lag and was insensitive to addition of the trapping agent potassium cyanide (Figure 2.30, Panel C) even though this agent effectively traps NITRONE-ENX (Figure 2.13).

All of our evidence points to a non-dissociative mechanism of enzyme inactivation while displaying none of the features characteristic of a dissociative mechanism. MI complex formation from benzphetamine (which requires multiple metabolic steps) gives rise to lags and attenuated rates of inactivation at high concentrations of substrate as is characteristic of a dissociative mechanism of enzyme inactivation (Werringloer and Estabrook, 1973). Those characteristics were not observed here. We found that relatively few metabolites were released per each inactivation event (Table 2.5) which, in conjunction with the minimal consumption of ENX per inactivation event (Table 2.4), confirms that inactivation is an efficient process whereby intermediate species are not readily released from the CYP1A2 active site. Interestingly, when incubating with a high concentration of ENX and CYP1A2 we observed evidence for a burst in N-OH-ENX formation (Figure 2.29). A burst is indicative of a fast catalytic rate followed by slow product release. Since we believe MI complex formation results from multiple catalytic steps without release, the notion that release of N-OH-ENX may be partially rate limiting following its formation in the CYP1A2 active site ties in well. Despite the presence of an apparent burst in N-OH-ENX formation, the concentrations of free N-OH-ENX present throughout the time course of enzyme inactivation are miniscule compared to the level required for this metabolite to compete with ENX. Given the evidence presented, we conclude that ENX is sequentially metabolized to an MI complex with CYP1A2 without depending upon the concentration of intermediates free in solution. Three CYP1A2-mediated oxidations of ENX to a ring-opened nitroso metabolite are performed within the active site and without release.

2.4.6 Efficiency of CYP1A2 Inactivation and Prediction of the DDI Magnitude.

Our substrate depletion partition ratio (Table 2.4) indicated that a therapeutic dose of ENX could substantially impact the levels of active hepatic CYP1A2. A typical daily dose of ENX (800 mg, 2.5 mmol) constitutes an approximate 1000:1 dosing stoichiometry of ENX molecules per each hepatic CYP1A2. By determining the maximum number of ENX molecules consumed per CYP1A2 inactivation event at 50 or less, we concluded that a daily dose of ENX provides more than 20-times the quantity of drug necessary to inactivate all of the CYP1A2 in a human liver provided that no other clearance pathways exist for ENX. Therefore, inactivation of hepatic CYP1A2 by ENX based on efficiency alone predicts a serious risk of DDI. Since ENX exhibits high bioavailability (Marchbanks et al., 1990) and is taken up into hepatocytes by active transport (Yamano et al., 1999; Maeda et al., 2007), we do not expect that drug absorption or distribution would limit hepatic exposure to ENX. Most of the dose is excreted as unchanged drug into urine with half-lives generally ranging from 4-6 hours (Yamaguchi et al., 1984). Thus, the metabolic stability of ENX in vivo is high with μM concentrations of ENX being maintained in circulation throughout a typical therapeutic course of treatment (days to weeks). The available data on the pharmacokinetics and hepatic uptake of ENX suggests that the liver receives adequate exposure to ENX to cause significant CYP1A2 inactivation according to our depletion-based partition ratio.

A partition ratio analysis of the number of metabolites released per CYP1A2 inactivation event also highlighted the efficiency of the inactivation process. We found that approximately 3 molecules of N-OH-ENX, 1 molecule if NITRONE-ENX, and 2 molecules of DES-ENX are produced during the inactivation of 1 molecule of CYP1A2 (Table 2.5). N-OH-ENX and DES-ENX are the two major metabolites observed in incubations with ENX. N-formyl and aniline ENX, two minor metabolites, give inactivation partition ratios much less than 1. These five metabolites likely constitute a major fraction of total metabolites and across these five we

calculate that less than 7 metabolites are produced per each CYP1A2 inactivation. These results (from a single enzyme system) indicate that the metabolism of ENX is highly coupled to MI complex formation in agreement with our evidence for the non-dissociative nature of the enzyme inactivation process.

Since hepatic exposure to ENX is likely significant and enzyme inactivation appears to proceed non-dissociatively from the parent drug, we ran static predictions which treat ENX as a one-step enzyme inactivator. Inactivation parameters (in bactosomes) of the parent drug were used to estimate the effect of circulating concentrations of ENX on CYP1A2 activity (Figure 2.31). At steady-state, more than 90% of hepatic CYP1A2 is predicted to be inactive assuming an in vivo CYP1A2 half-life of 38.6 hours (Faber and Fuhr, 2004). These predictions, using the apparent inactivation parameters K_I and k_{inact}, forecasted severe DDIs with CYP1A2 substrates. Accordingly, we predicted clinically-significant DDIs with theophylline and caffeine quantitatively similar to in vivo values found in the literature (Table 2.6). We included in our analysis a hypothetical "worse-case scenario" in which a victim drug is entirely reliant upon CYP1A2-mediated clearance. While the maximum possible AUC increase for a victim drug ($f_{m,CYP1A2} = 1$) is 160-fold at an infinite concentration of ENX, our predicted "worse-case scenario" DDI employed realistic circulating levels of ENX (7.5 μM in blood) to arrive at an AUC increase of ~10-fold (Table 2.6). In fact, more severe DDIs are possible for drugs subject to significant CYP1A2-mediated hepatic first pass metabolism. Bioavailability of tizanidine, for example, is limited by pre-systemic CYP1A2-mediated metabolism. Ciprofloxacin caused an average AUC increase of 10-fold for tizanidine in healthy volunteers with the AUC increases ranging from 6- to 24-fold (Granfors et al., 2004). The increase in tizanidine exposure was attributed entirely to an increase in bioavailability through inhibition of pre-systemic CYP1A2-mediated clearance. Notably, ciprofloxacin is a weaker inhibitor of CYP1A2 than ENX. We were unable to find a

study on the interaction between ENX and tizanidine. However, we suspect the DDI between ENX and tizanidine would be even greater than that observed with ciprofloxacin.

It is interesting and perhaps revealing that we accurately predicted the interaction of ENX with CYP1A2 substrates using apparent inactivation parameters from the parent drug. We expect that inhibition of CYP1A2 by ENX is predominantly due to MI complex formation and that, mechanistically, this process requires multiple metabolic steps. Translating enzyme inactivation parameters from in vitro to in vivo is particularly precarious when intermediate metabolites are required for inactivation. These intermediates may be subject to a myriad of in vivo metabolic processes which are not encountered in vitro thus altering inactivation rates. Poor predictivity would be expected in these situations. Our success with ENX leads us to believe that the inactivation of CYP1A2 by ENX may circumvent this problem and the most likely and simplest explanation is that ENX can be sequentially metabolized within the CYP1A2 active site to generate the MI complex without release and rebinding of intermediates. In this scenario, an inactivation process which requires multiple metabolic steps can justifiably be treated as a single step for the purpose of predicting enzyme inactivation in vivo. We believe that the non-dissociative nature of MI complex formation from ENX is a critical component of the mechanism and a major reason for the potent inhibition seen in vivo.

2.4.7 Conclusions.

In summary, we characterized the time-dependent inhibition of CYP1A2 by ENX and further explored the CYP1A2-generated metabolites of ENX. These results show that an MI complex is formed between a metabolite of ENX and CYP1A2 and that N-OH-ENX is a plausible intermediate in this process. Note that our proposed mechanism does not strictly require a piperazine ring and suggests that MI complexation to P450 may occur from any alicyclic amine substrate given a sufficient degree of sequential N-oxidation and eventual ring-

opening. Multiple reports confirm that N-hydroxylation and further oxidation to a cyclic nitrone is a relatively common occurrence for alicyclic amine substrates, particularly piperazines (Edlund and Baranczewski, 2004; Miller et al., 2004; Kalgutkar et al., 2007; Kalgutkar et al., 2009; Tong et al., 2010). The non-dissociative nature of enzyme inactivation seen here further emphasizes that an inactivation mechanism may be operative even when the intermediates are not abundant as multiple catalytic steps can occur in the P450 active site without release.

MI complex formation contributed substantially to inhibition from incubations with ENX. However, we found evidence that ENX may also cause enzyme inactivation through a second mechanism. We also found that ENX undergoes CYP1A2 catalyzed dehydrogenation to a metabolite which reacts with cyanide (Figure 2.32). This HCN-adduct could not be formed from incubations with N-OH-ENX (data not shown), perhaps accounting for an inactivation mechanism accessible from ENX but not N-OH-ENX.

The first step in our proposed pathway to MI complex formation begins with N-hydroxylation of the piperazine of ENX to a secondary hydroxylamine (Figure 2.32). Recent reports have also demonstrated that MI complex formation commonly proceeds through a secondary hydroxylamine as opposed to a primary amine (Cerny and Hanzlik, 2005; Hanson et al., 2010; Barbara et al., 2013) and our results suggest this trend may also hold true for MI complex formation from alicyclic amines. The secondary hydroxylamine, N-OH-ENX, may be dehydrogenated to the cyclic nitrone metabolite, NITRONE-ENX, or hydroxylated to yield α-hydroxy-N-OH-ENX. These two species are in equilibrium with one another by the addition or loss of water and both species are viable precursors to NITROSO-ENX. We have proposed three potential paths for the generation of the nitroso ligand and discussed the merits of each. While our dataset does not exclude or favor one of the three possibilities over the others, path c (oxidation of α-hydroxy-N-OH-ENX by Compound I) is perhaps the most plausible with regard to

literature precedent as the proposed reaction mechanism (Figure 2.35) parallels the well-studied cholesterol side-chain cleavage reaction (Yoshimoto et al., 2016).

Future studies will be aimed at clarifying the importance of non-dissociative sequential metabolism to inactivation of CYP1A2 by ENX. In more complex metabolic systems, such as human liver microsomes and hepatocytes, released metabolites will be subject to additional metabolic processes. If additional metabolic routes effectively capture released intermediates, then dissociative sequential metabolism of ENX to an MI complex would not be viable. That MI complex formation appears to proceed primarily through non-dissociative sequential metabolism of ENX suggests that our current results, generated with recombinant CYP1A2, can be effectively translated through more complicated metabolic systems, such as microsomes and hepatocytes, all the way to in vivo.

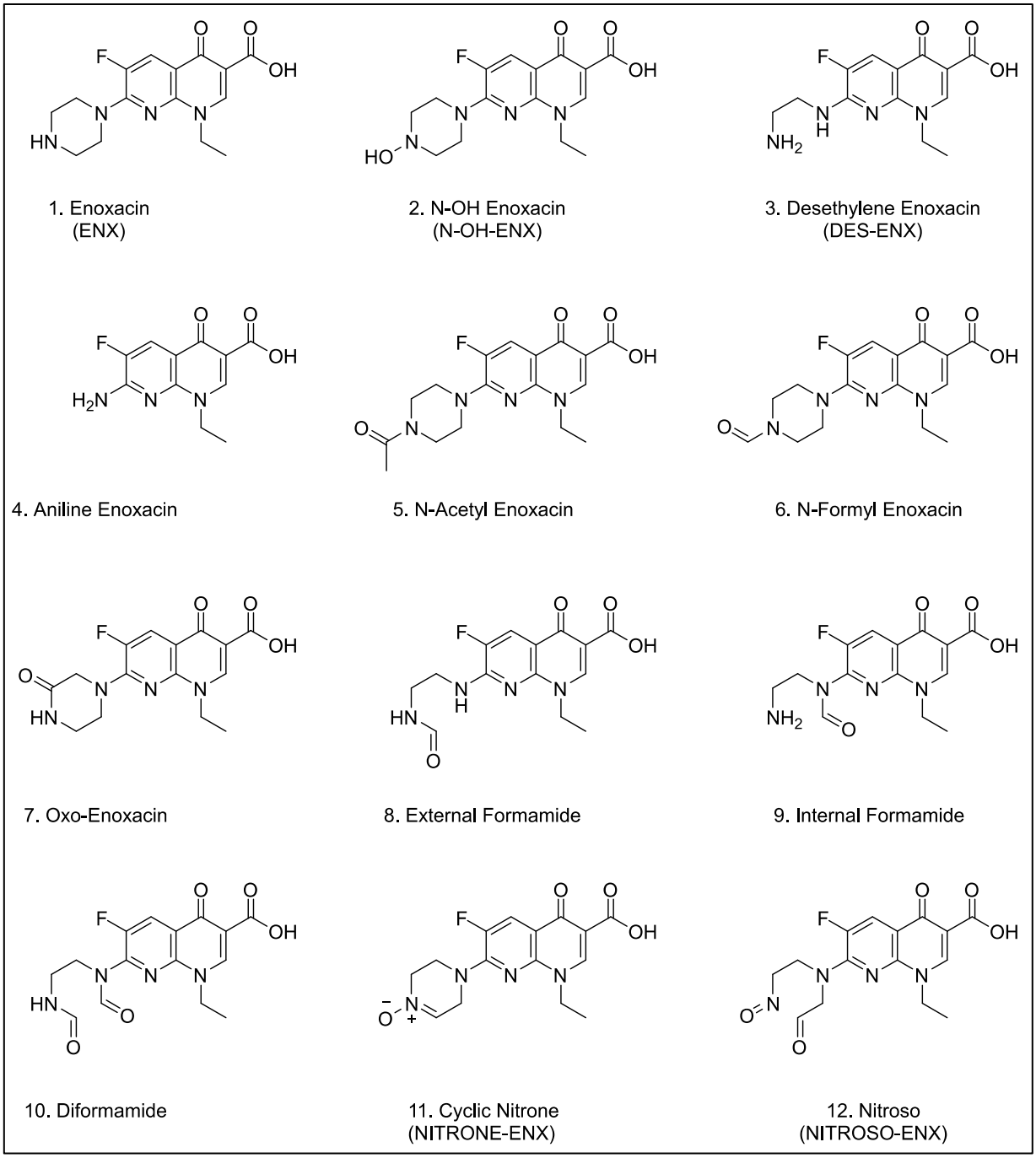

Figure 2.1 – Structures of enoxacin and metabolites
Chemical structures of enoxacin (1), metabolites of enoxacin (2 – 10), and proposed metabolites on-path to MI complex formation with CYP1A2 (11,12).

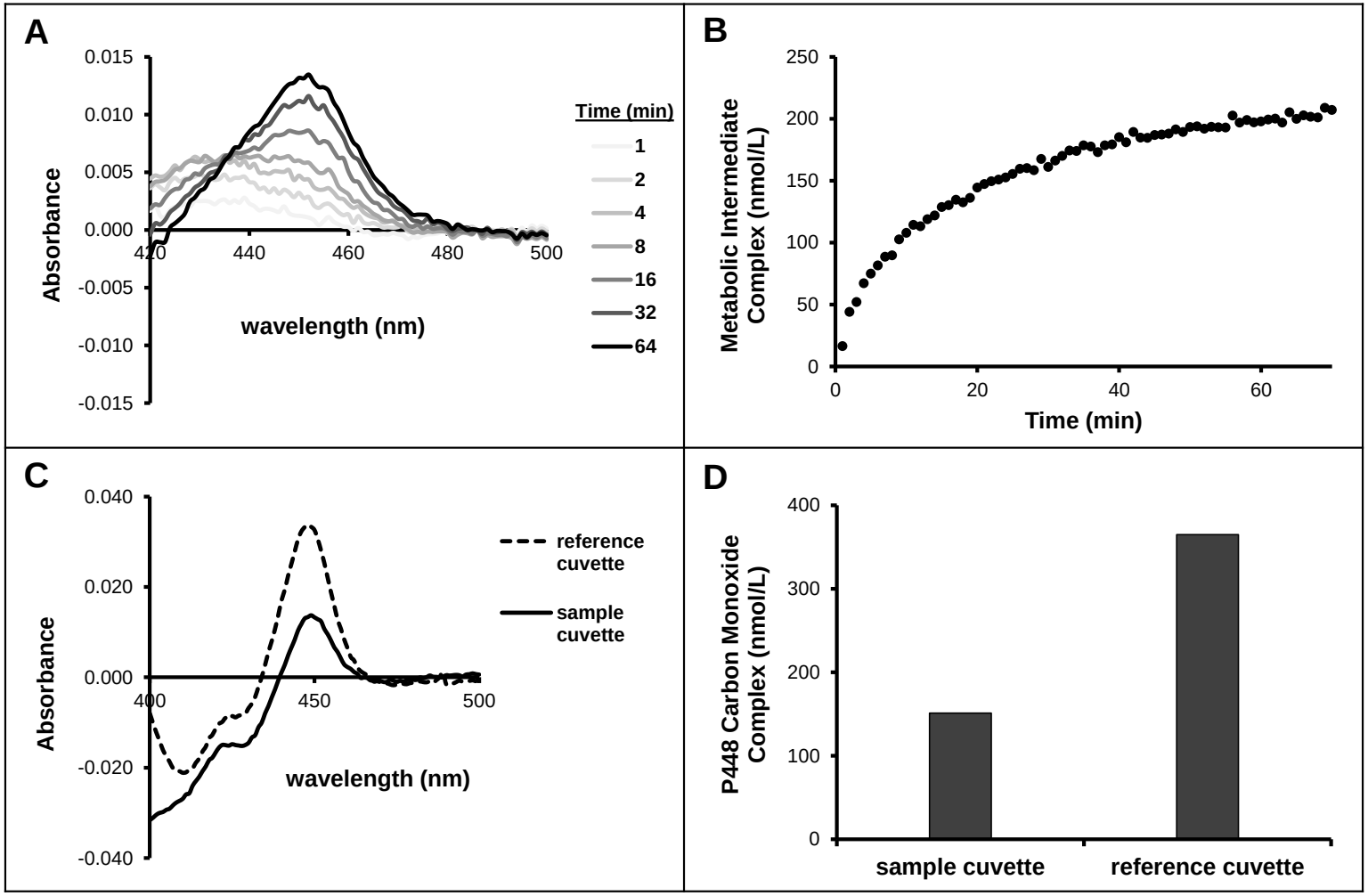

Figure 2.2 – MI complex formation from ENX in CYP1A2 bactosomes

MI complex formation with CYP1A2 bactosomes (0.5 μM) from incubation with ENX (640 μM) and NADPH (1.5 mM). The sample cuvette contained the complete incubation mixture while the reference cuvette lacked enoxacin. The reaction was initiated by addition of NADPH to both cuvettes. Spectral scanning of the reaction (A), the time-course of MI complex accumulation (B), carbon-monoxide binding spectra following the reaction (C), and quantitation of carbon-monoxide binding (D) are shown.

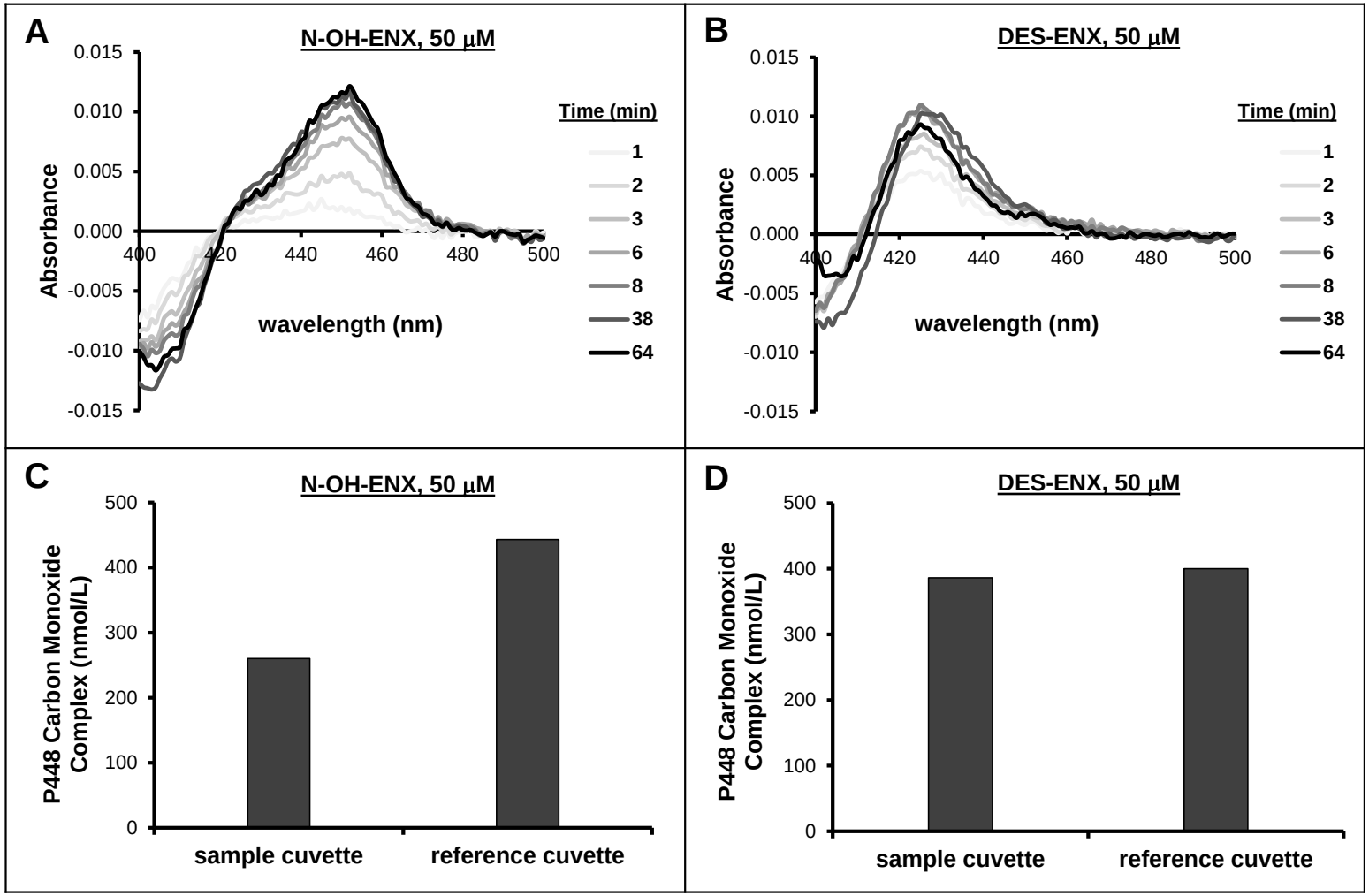

Figure 2.3 – MI complex formation from N-OH-ENX but not DES-ENX
MI complex formation with CYP1A2 bactosomes from incubation with N-OH-ENX (50 μM), but not DES-ENX (50 μM). Both cuvettes contained CYP1A2 (0.5 μM) and NADPH (1.5 mM). Addition of substrate to the sample cuvette and vehicle to the reference cuvette initiated the reaction. Spectral scanning of the reactions (A and B) and quantitation of carbon-monoxide binding following the reactions (C and D) with N-OH-ENX and DES-ENX, respectively, are shown.

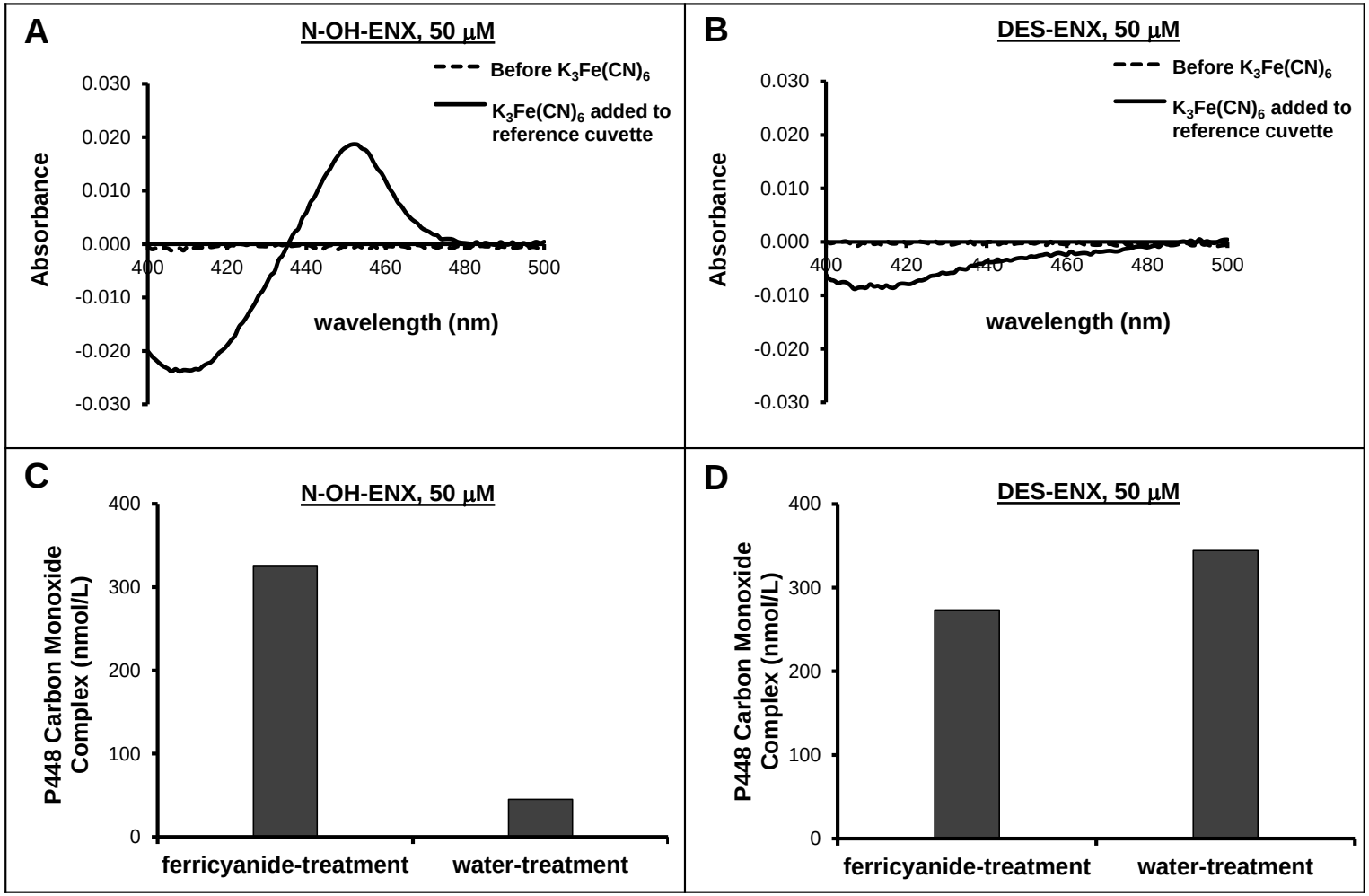

Figure 2.4 – Spectral ferricyanide reversal from N-OH-ENX but not DES-ENX
After incubation of CYP1A2 (0.5 μM) and NADPH (1.5 mM) with either N-OH-ENX (50 μM) or DES-ENX (50 μM) for 70 minutes, the incubation was split into sample and reference cuvettes and the spectrum was zeroed. Addition of water to the sample cuvette and $K_3Fe(CN)_6$ in water to the reference cuvette initiated the reaction. Spectral scans of the reactions (A and B) and quantitation of carbon-monoxide binding following the reactions (C and D) for N-OH-ENX and DES-ENX incubations, respectively, are shown.

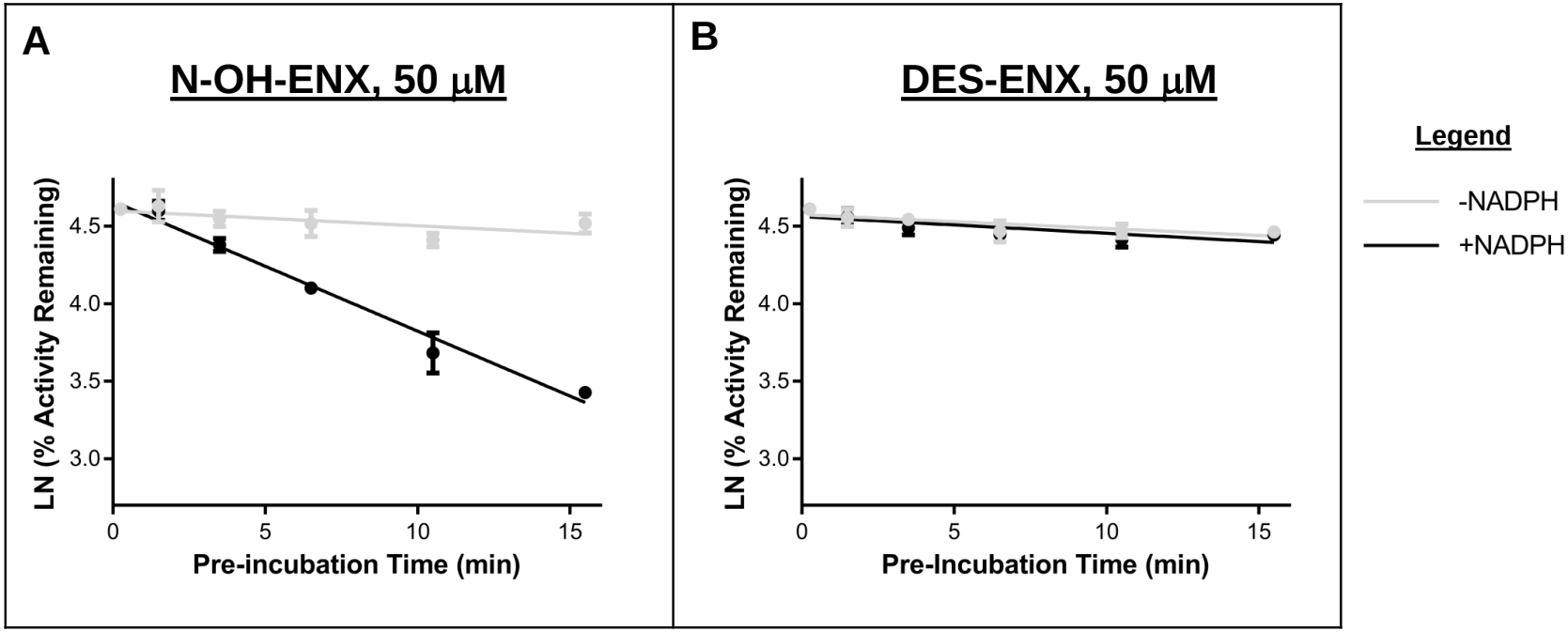

Figure 2.5 – Time-dependent inhibition of CYP1A2 by N-OH-ENX but not DES-ENX
Time- and NADPH-dependent loss of CYP1A2 activity from incubation with N-OH-ENX (Panel A), but not DES-ENX (Panel B). CYP1A2 bactosomes (50 nM) were pre-incubated with either N-OH-ENX (50 μM) or DES-ENX (50 μM) and NADPH (1 mM). At specified time-points, an aliquot of pre-incubation mixture was diluted into an activity assay containing phenacetin (300 μM) and NADPH (1 mM). CYP1A2 incubated in the presence of inhibitor but absence of NADPH served as controls. All time points are in triplicate ± SD.

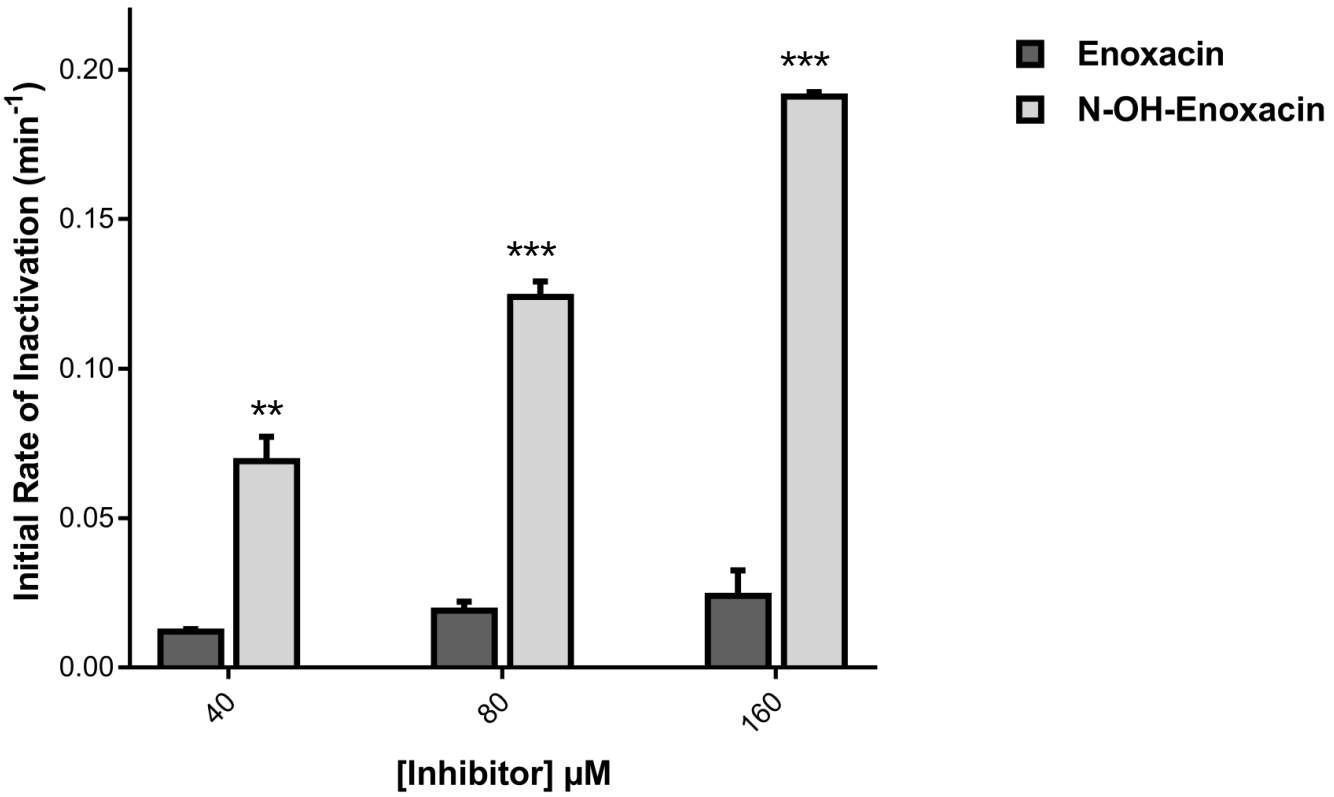

Figure 2.6 – Initial rates of CYP1A2 inactivation by ENX and N-OH-ENX
Comparisons of the initial rate of CYP1A2 inactivation from incubation with either ENX or N-OH-ENX at three concentrations of inhibitor. CYP1A2 bactosomes (50 nM) and NADPH (1mM) were pre-incubated with either ENX or N-OH-ENX. The loss of phenacetin O-deethylase activity was measured over time and compared to vehicle controls. Plots of activity loss over time were natural log transformed and the slope of the linear portion calculated by linear regression. Inactivation rates are reported in triplicate ± SD.

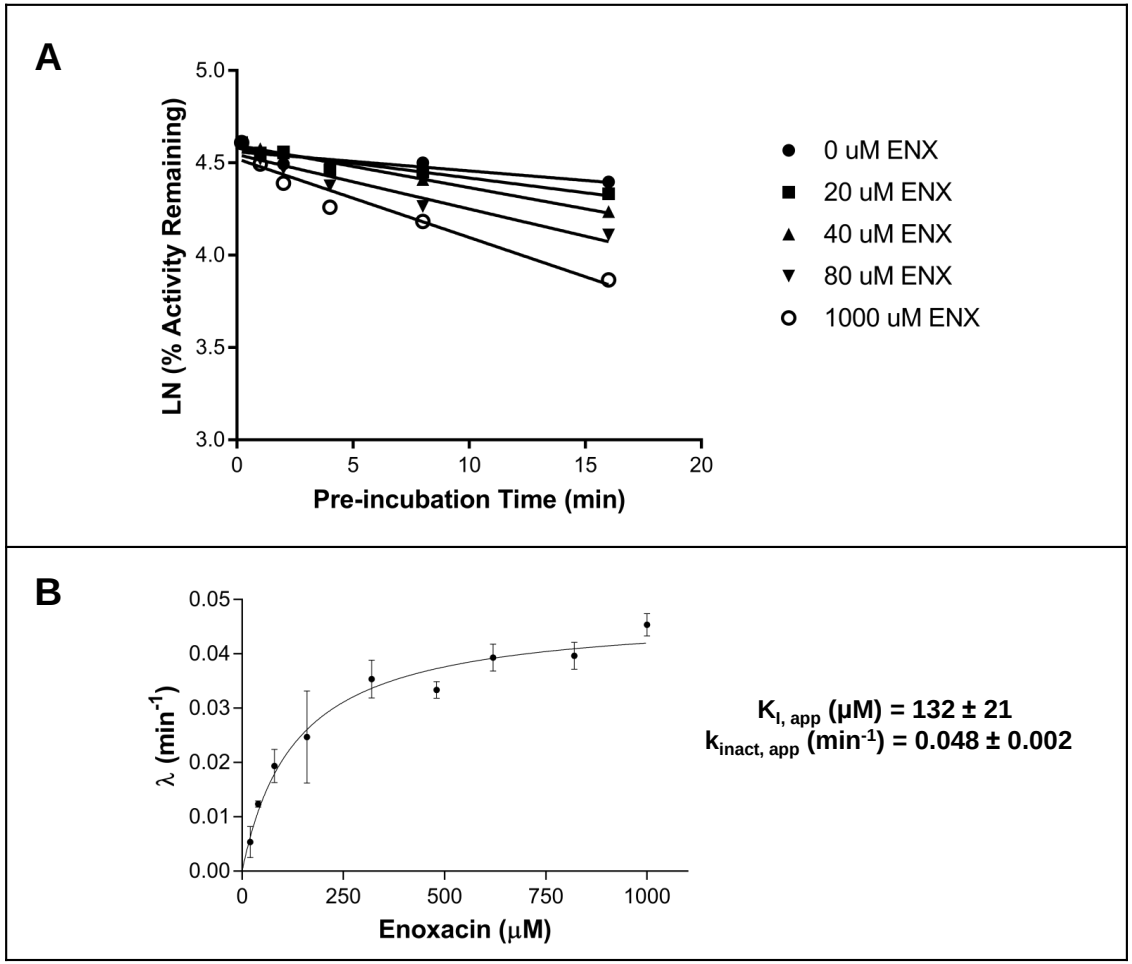

Figure 2.7 – Apparent inactivation parameters for ENX in CYP1A2 bactosomes
CYP1A2 bactosomes (50 nM) and NADPH (1mM) were pre-incubated in the presence of vehicle or increasing concentrations of ENX (20 μM, 40 μM, 80 μM, 160 μM, 320 μM, 480 μM, 640 μM, 820 μM, and 1000 μM). Loss of phenacetin O-deethylase activity was measured over time. Plots of activity loss over time were natural log transformed and the slope of the linear portion calculated by linear regression. All time points were performed in triplicate (In Panel A, error bars were omitted for clarity). Inactivation rates are reported in triplicate ± SD.

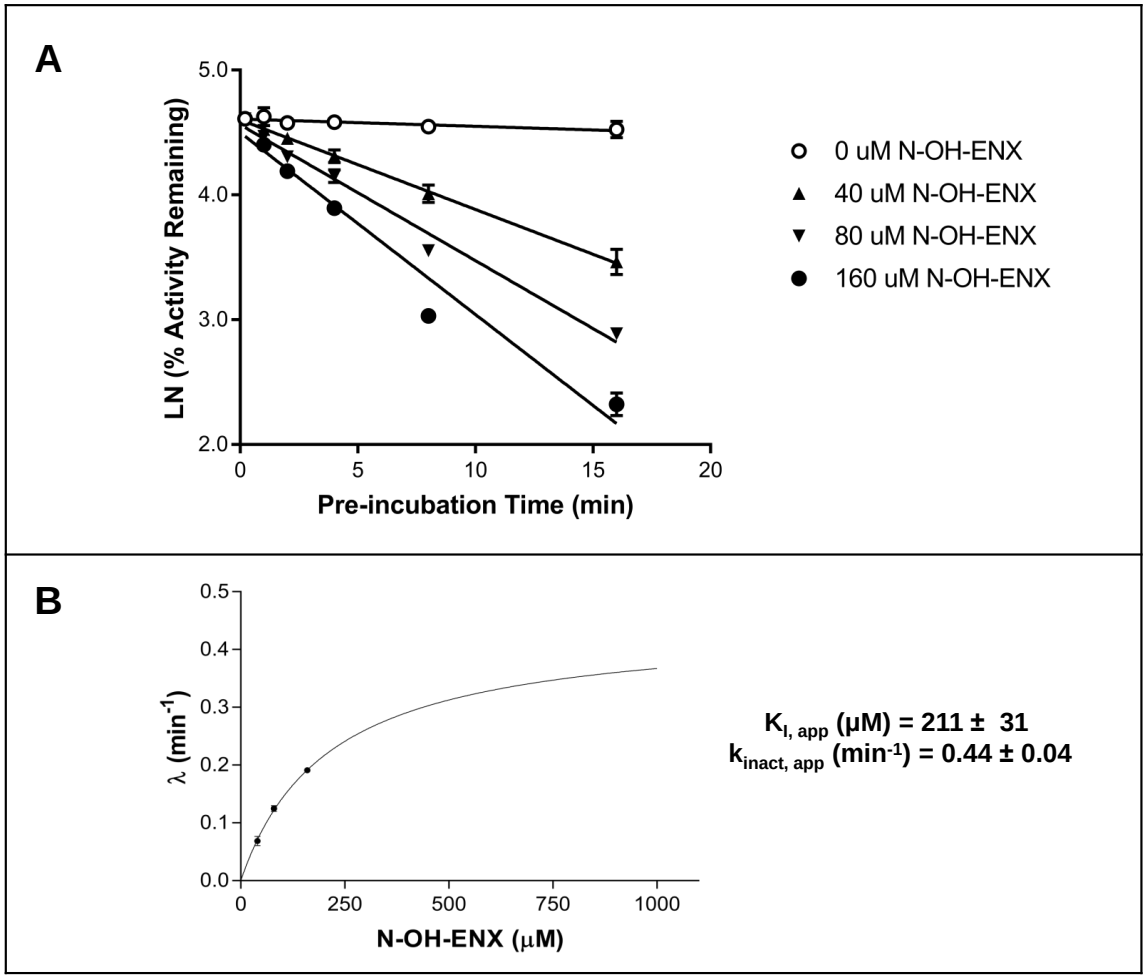

Figure 2.8 – Apparent inactivation parameters for N-OH-ENX in CYP1A2 bactosomes

CYP1A2 bactosomes (50 nM) and NADPH (1mM) were pre-incubated in the presence of vehicle or N-OH-ENX (40 μM, 80 μM, and 160 μM). Loss of phenacetin O-deethylase activity was measured over time. Plots of activity loss over time were natural log transformed and the slope of the linear portion calculated by linear regression. All time points were performed in triplicate. Inactivation rates are reported in triplicate ± SD. The final time point (16 min, Panel A) was removed when calculating the inactivation rates for N-OH-ENX (Panel B).

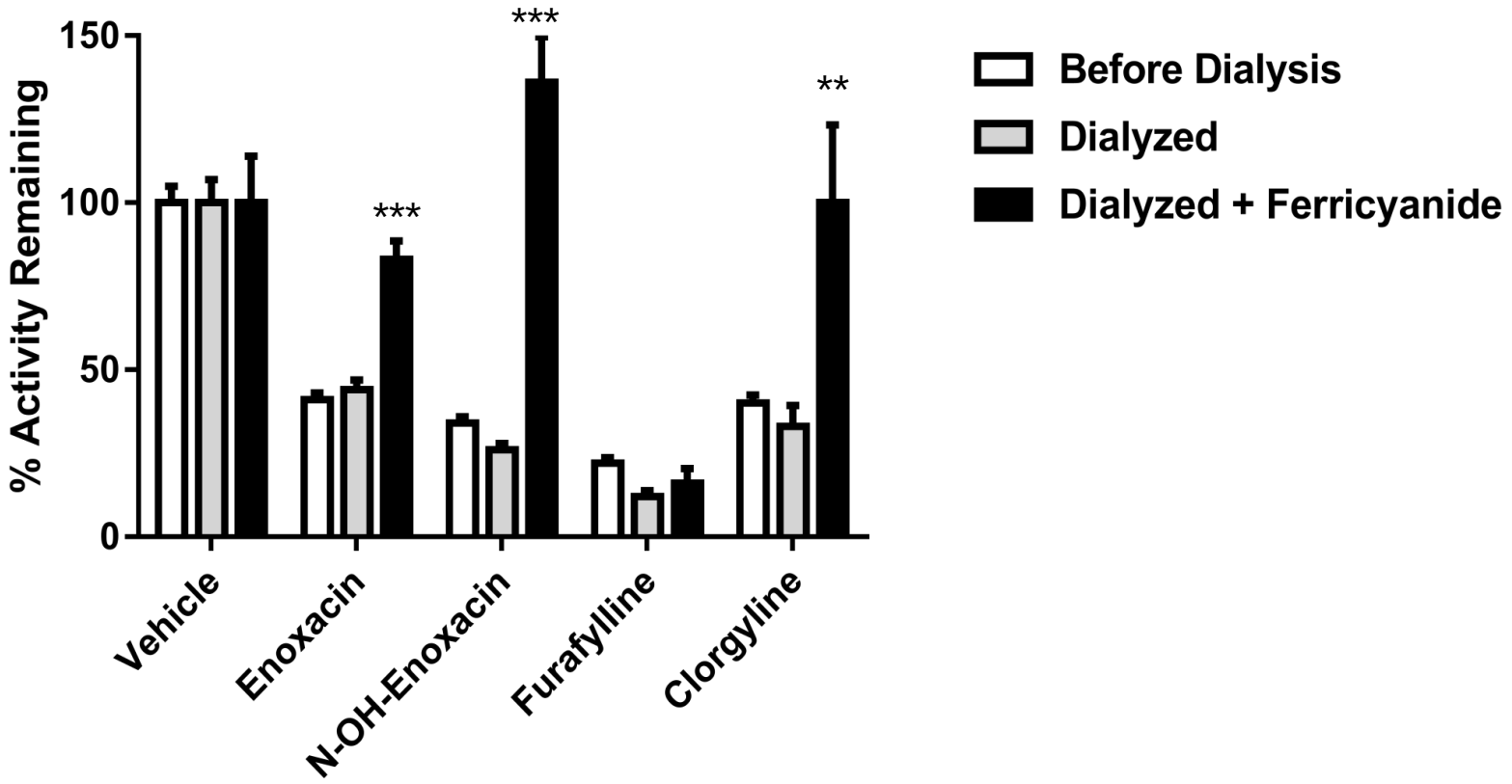

Figure 2.9 – Reversibility of inhibition to dialysis and ferricyanide treatments
CYP1A2 bactosomes (100 nM) and NADPH (1 mM) were pre-incubated in the presence of vehicle or inhibitor [ENX (500 μM), N-OH-ENX (50 μM), furafylline (10 μM), or clorgyline (10 μM)]. The remaining CYP1A2 activity was then measured both before and after cold dialysis (3.5 kDa MWCO). Dialyzed samples were treated with either water (gray bars) or $K_3Fe(CN)_6$ at a concentration of 1 mM (black bars) for 5 minutes before measurement of residual CYP1A2 activity. Remaining activities were normalized to their respective vehicle controls and are reported as the mean ± SD (N=4).

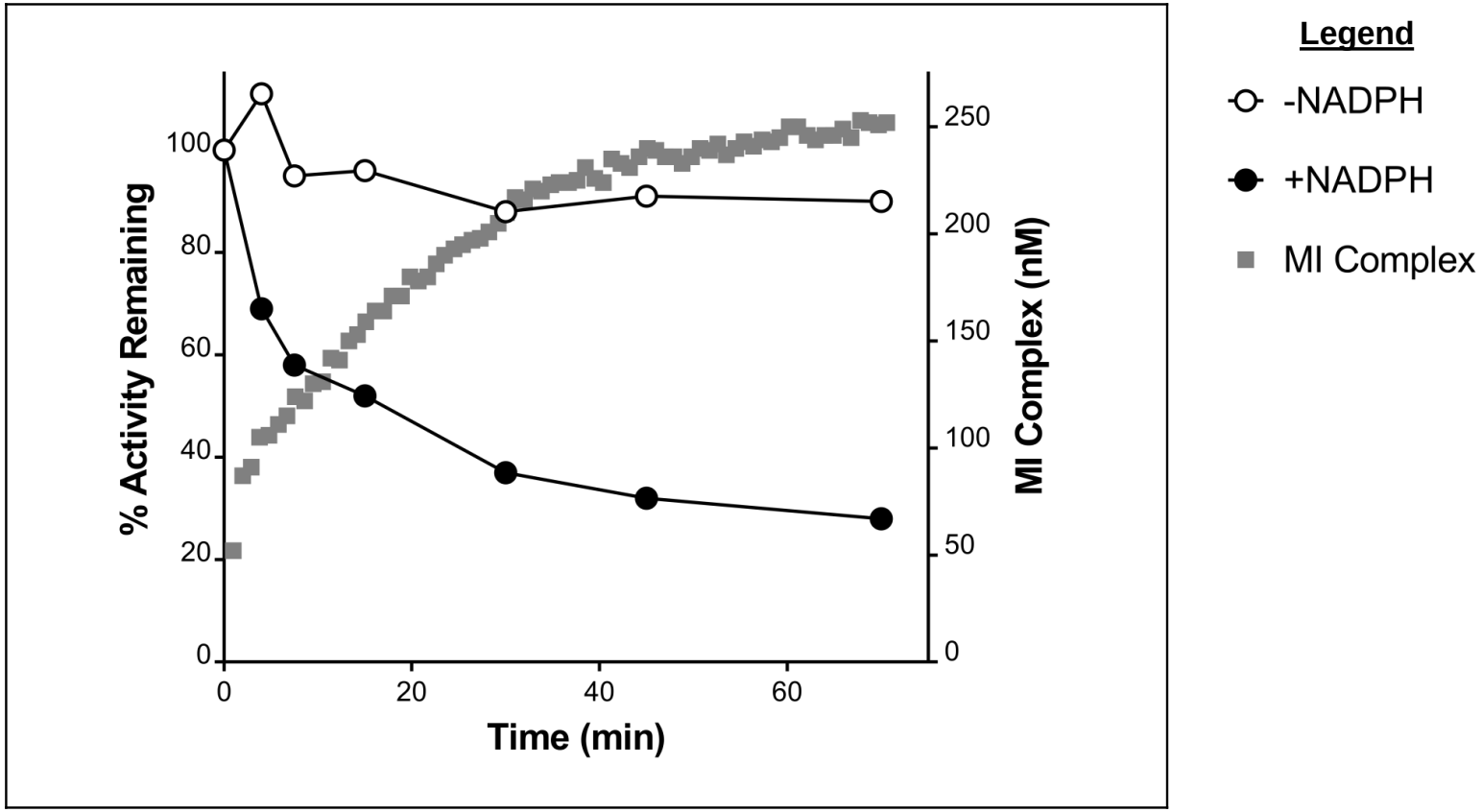

Figure 2.10 – Time-course of CYP1A2 activity loss compared with MI complex formation by ENX
While spectrally scanning an incubation with CYP1A2 bactosomes (0.5 μM), ENX (640 μM) and NADPH (1.5 mM) for MI complex formation, aliquots were removed directly from the sample and reference cuvettes and diluted into phenacetin o-deethylase activity assay. The sample cuvette (closed circles) contained the complete incubation mixture while the reference cuvette (open circles) lacked NADPH. For comparison, enzyme activity in both cuvettes at various time points (t = 0, 4, 7.5, 15, 30, 45 and 70 min) is plotted on top of the time-course of MI complex accumulation.

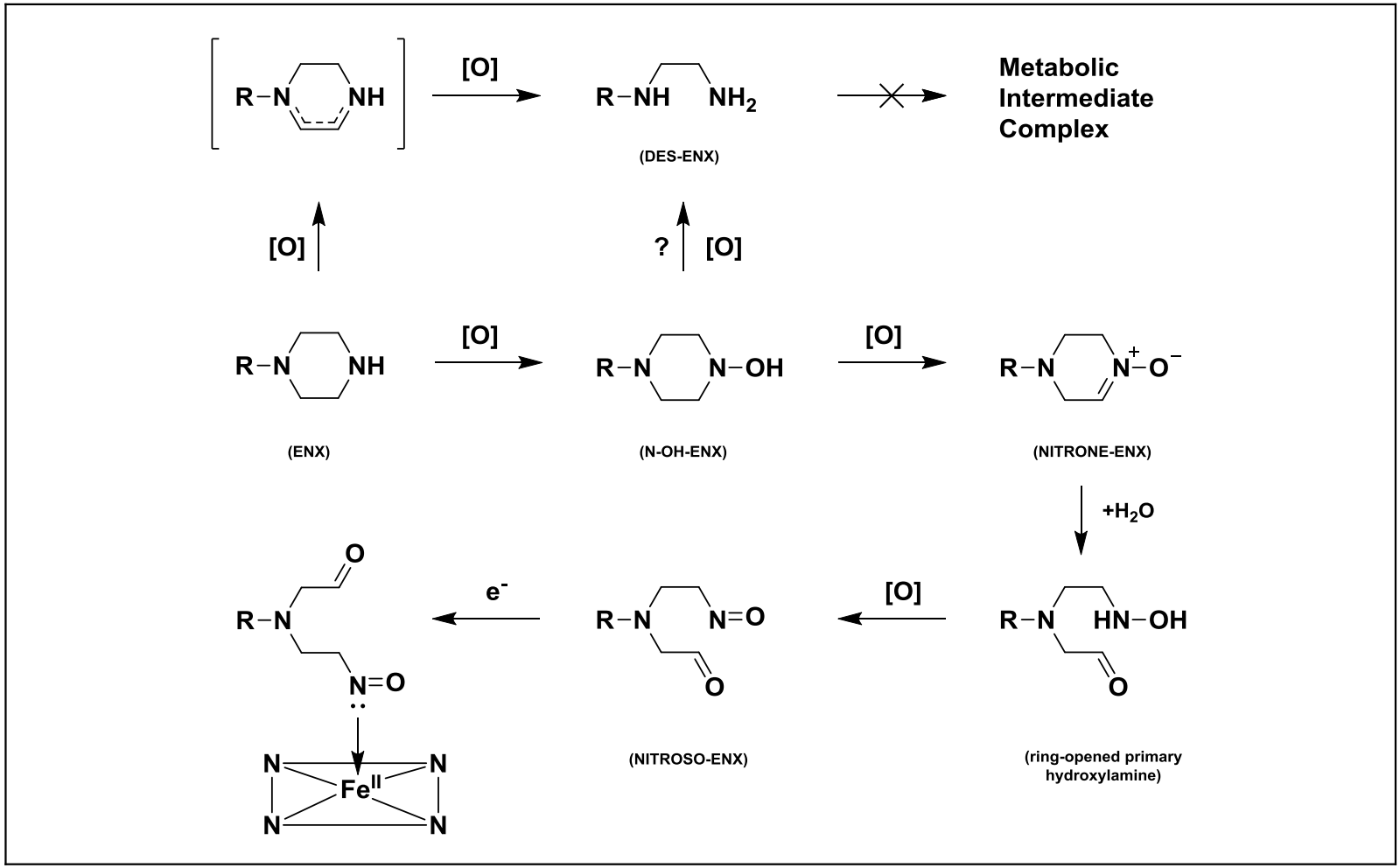

Figure 2.11 – Metabolic scheme suggesting a possible route to MI complex formation
A proposed mechanism for MI complex formation from CYP1A2-catalyzed oxidation of enoxacin. The primary amine metabolite, DES-ENX, is off-path from MI complex formation. The secondary hydroxylamine, N-OH-ENX, is further oxidized and ring-opened to yield a nitroso ligand which, upon single electron reduction of heme, coordinates tightly to the ferrous heme-iron of CYP1A2.

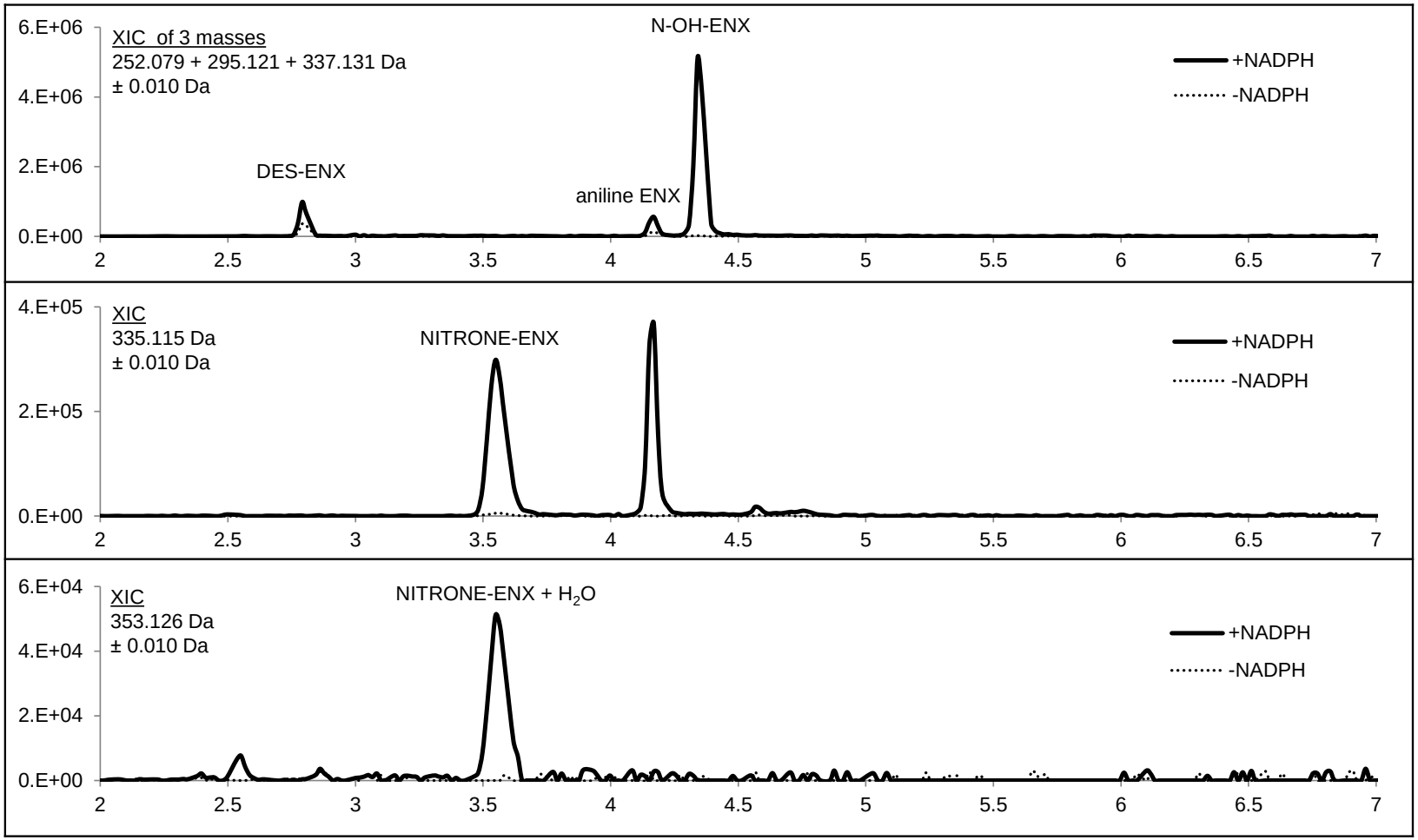

Figure 2.12 – LC-MS chromatograms of extracted masses for DES-ENX, aniline-ENX, N-OH-ENX, and NITRONE-ENX
Extraction ion chromatograms (XIC) of the accurate mass m/z values for CYP1A2-catalyzed N-dealkylation and N-oxidation products of enoxacin. At this stage of the study, DES-ENX, aniline-ENX, and N-OH-ENX were confirmed with authentic standards and NITRONE-ENX was a proposed metabolite.

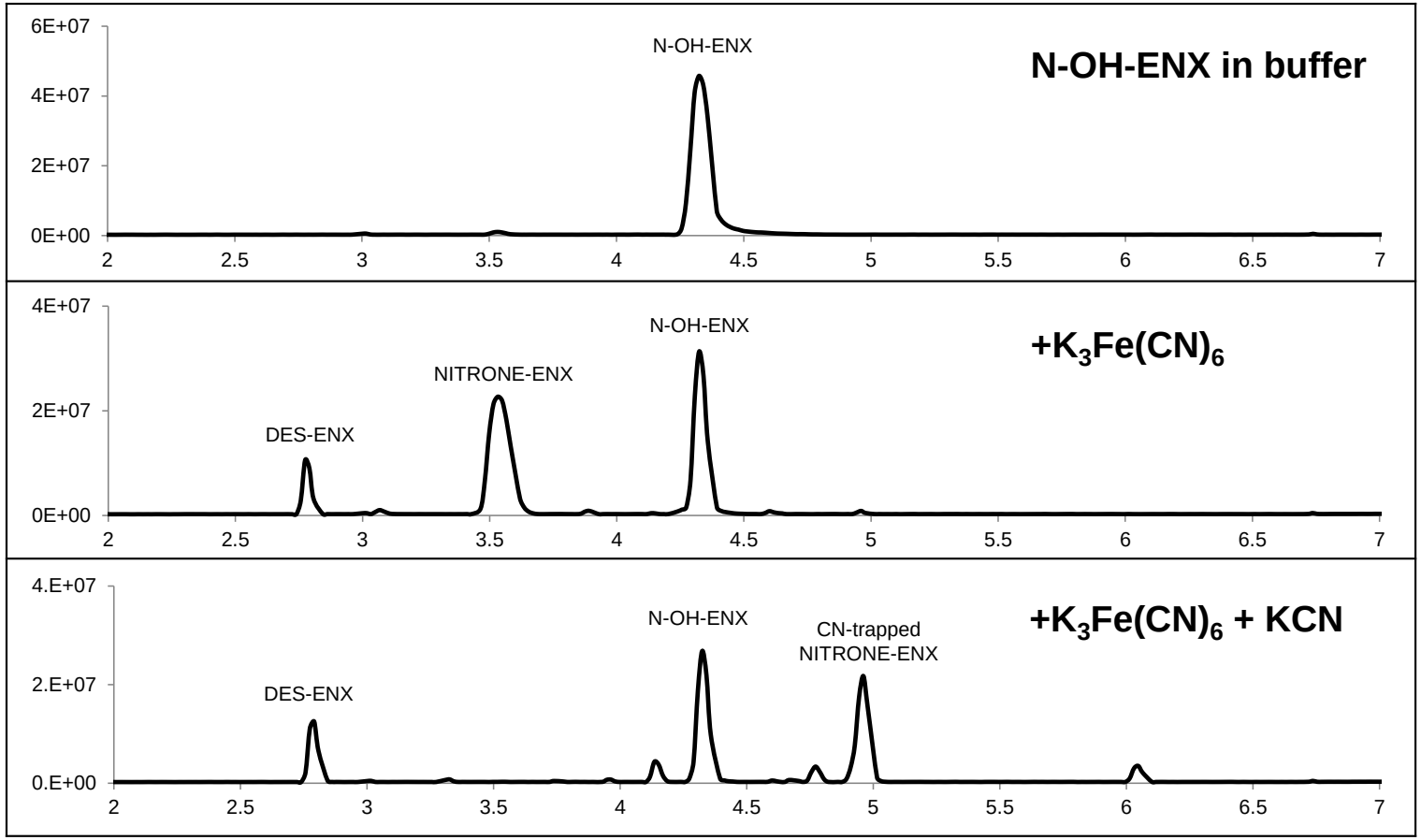

Figure 2.13 – LC-MS chromatograms to study the chemical oxidation of N-OH-ENX by potassium ferricyanide
HPLC-MS chromatograms of N-OH-ENX synthetic standard alone, after incubation with potassium ferricyanide, and after incubation with potassium ferricyanide and potassium cyanide. NITRONE-ENX was generated *in situ* by ferricyanide-mediated oxidation of N-OH-ENX and could be trapped with cyanide by addition of KCN. The traces shown are total ion currents (TIC).

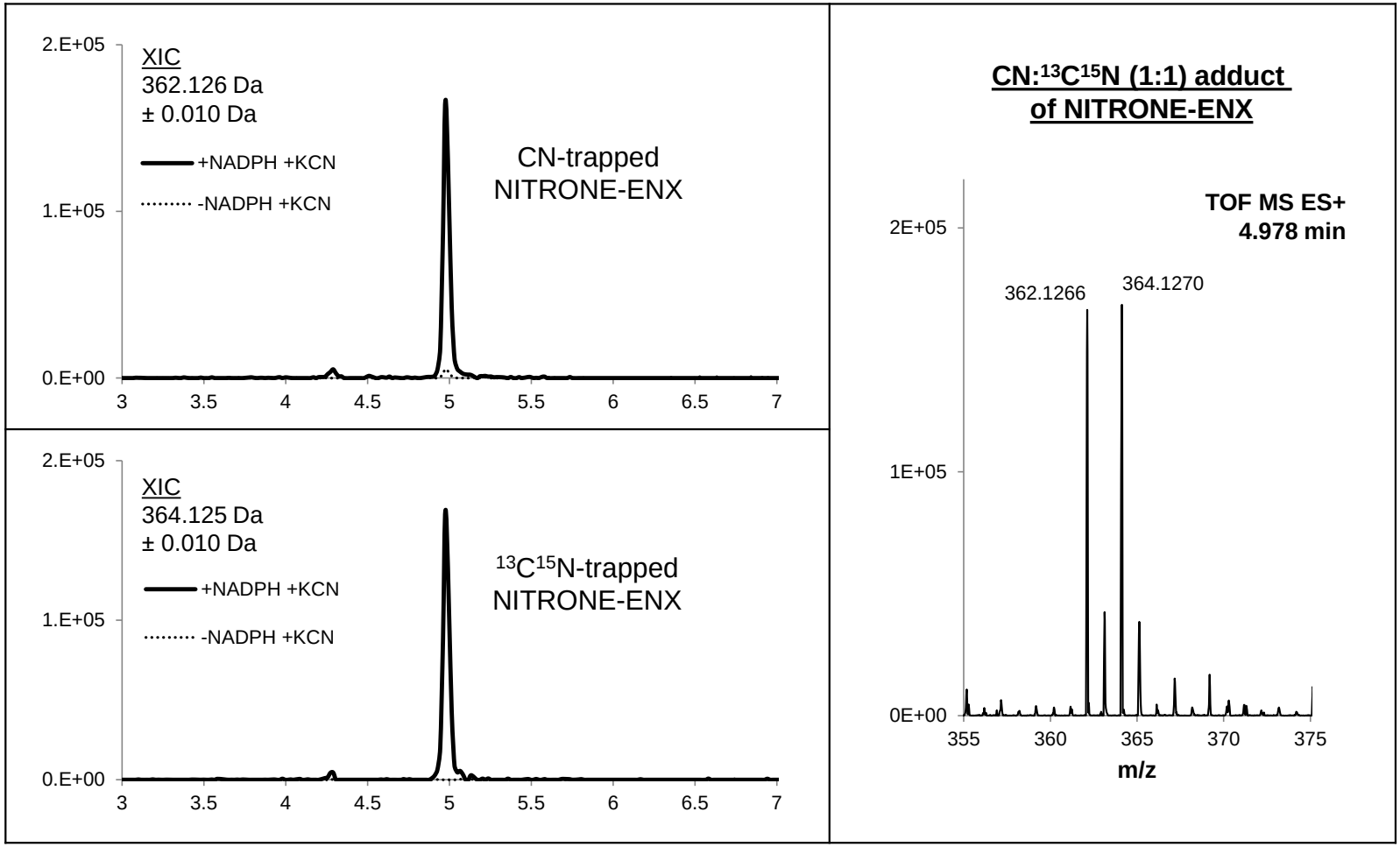

Figure 2.14 – Cyanide-trap of NITRONE-ENX generated metabolically by CYP1A2 with ENX
HPLC-MS of the cyanide-trapped NITRONE-ENX from metabolic incubation with CYP1A2. Enoxacin served as substrate. An equal mixture of KCN and isotopically-labeled $K^{13}C^{15}N$ was added to trap the cyclic nitrone. XIC (extracted ion chromatogram) for 362.126 m/z (top) and 364.125 m/z (bottom) are displayed alongside the mass spectrum (4.978 minutes, 355 to 375 m/z window).

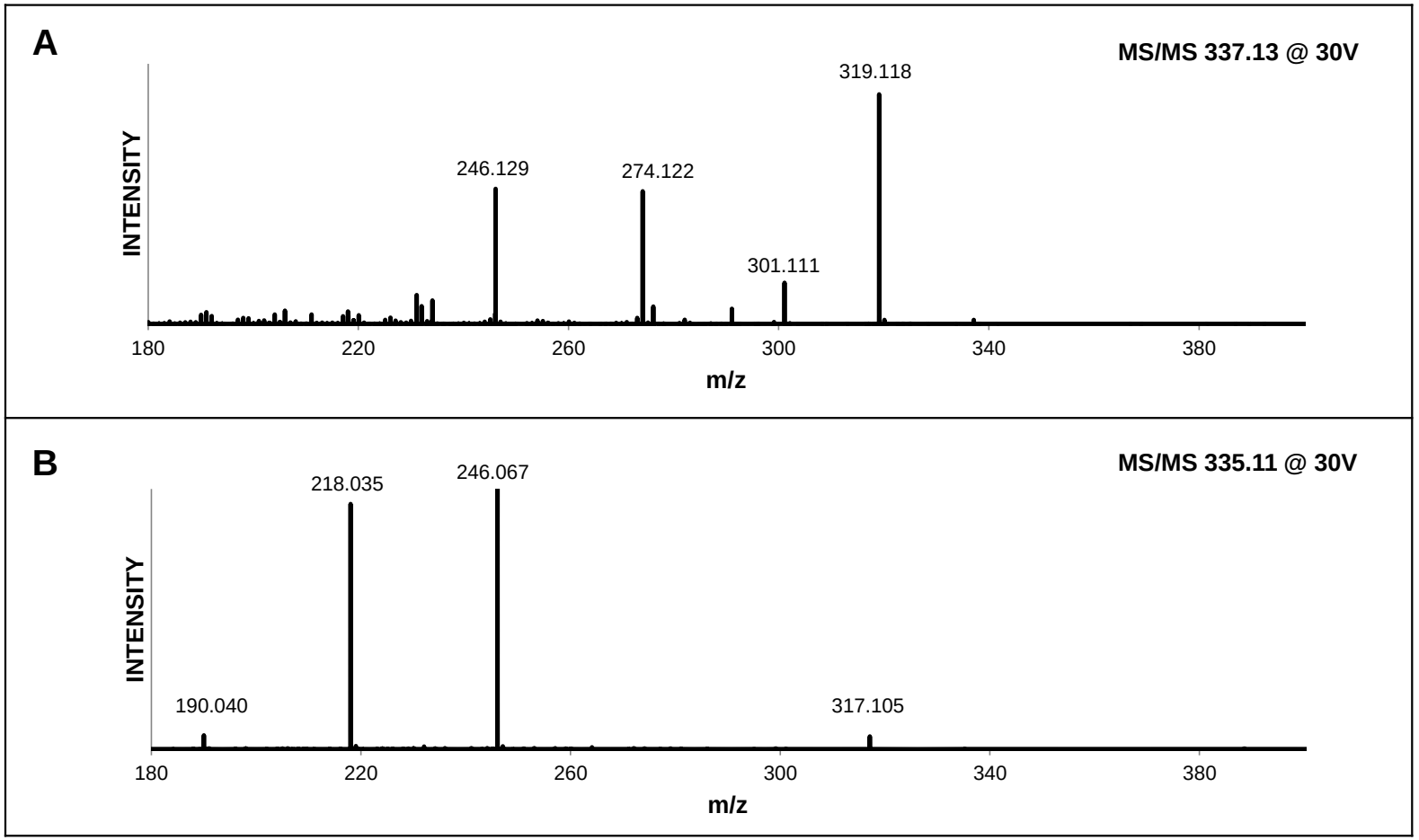

Figure 2.15 – High-resolution MS fragmentation patterns for N-OH-ENX and NITRONE-ENX
N-OH-ENX, 337 m/z (Panel A), and NITRONE-ENX, 335 m/z (Panel B), were fragmented at a collision energy of 30 eV.

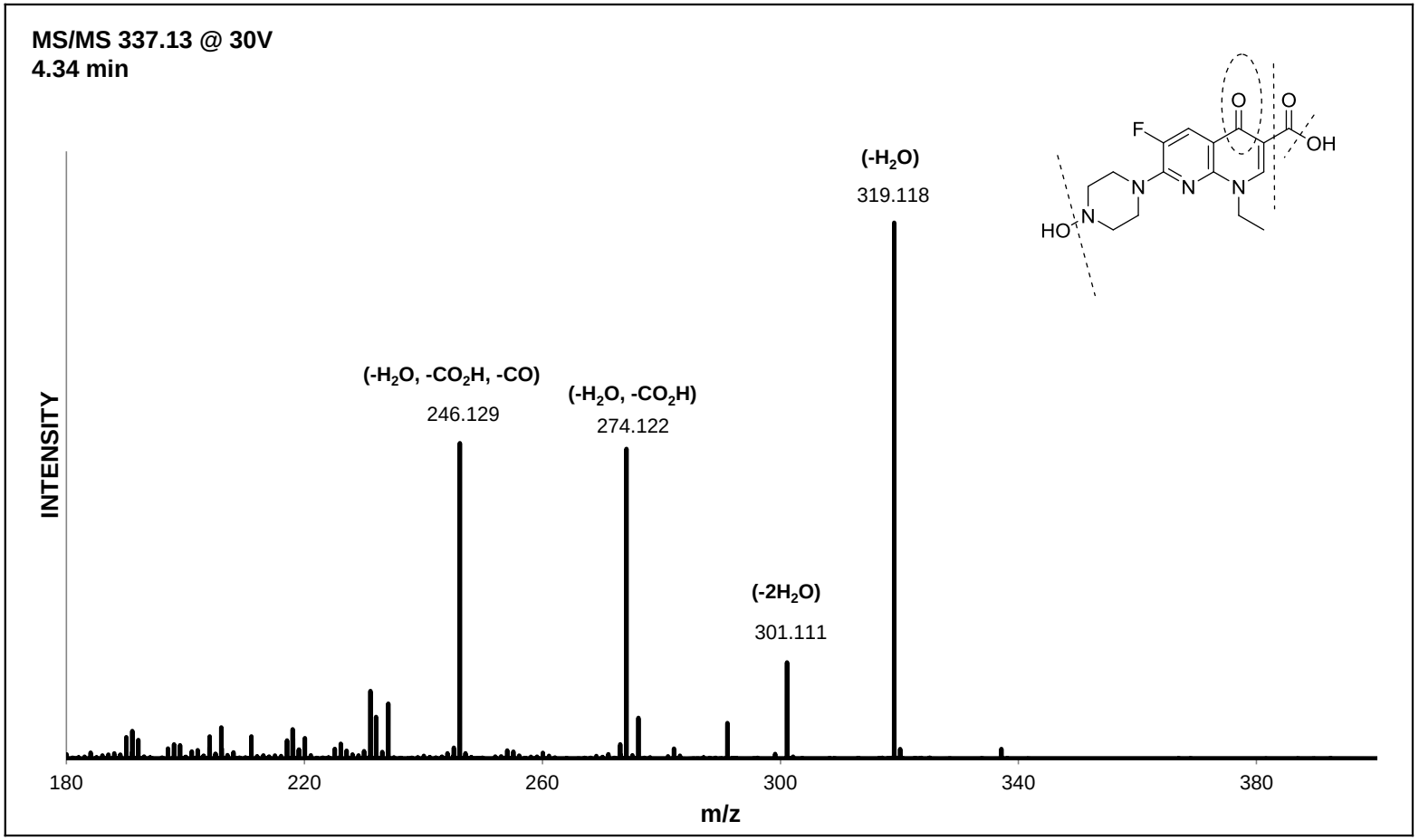

Figure 2.16 – High-resolution MS fragmentation pattern for N-OH-ENX with proposed cleavage sites
The necessary loss of atoms (supported by accurate mass) is indicated above each m/z ion value

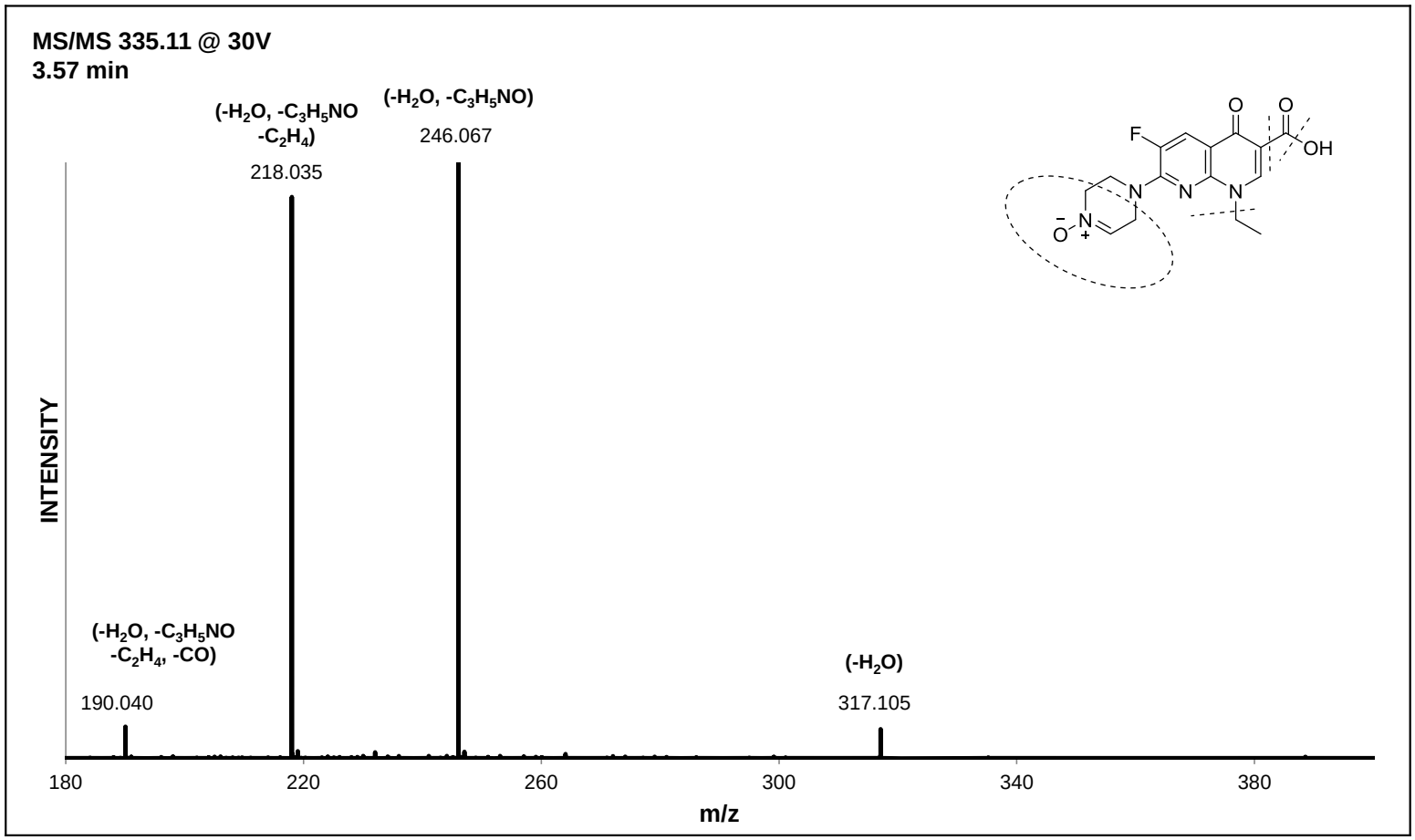

Figure 2.17 – High-resolution MS fragmentation pattern for NITRONE-ENX with proposed cleavage sites
The necessary loss of atoms (supported by accurate mass) is indicated above each m/z ion value

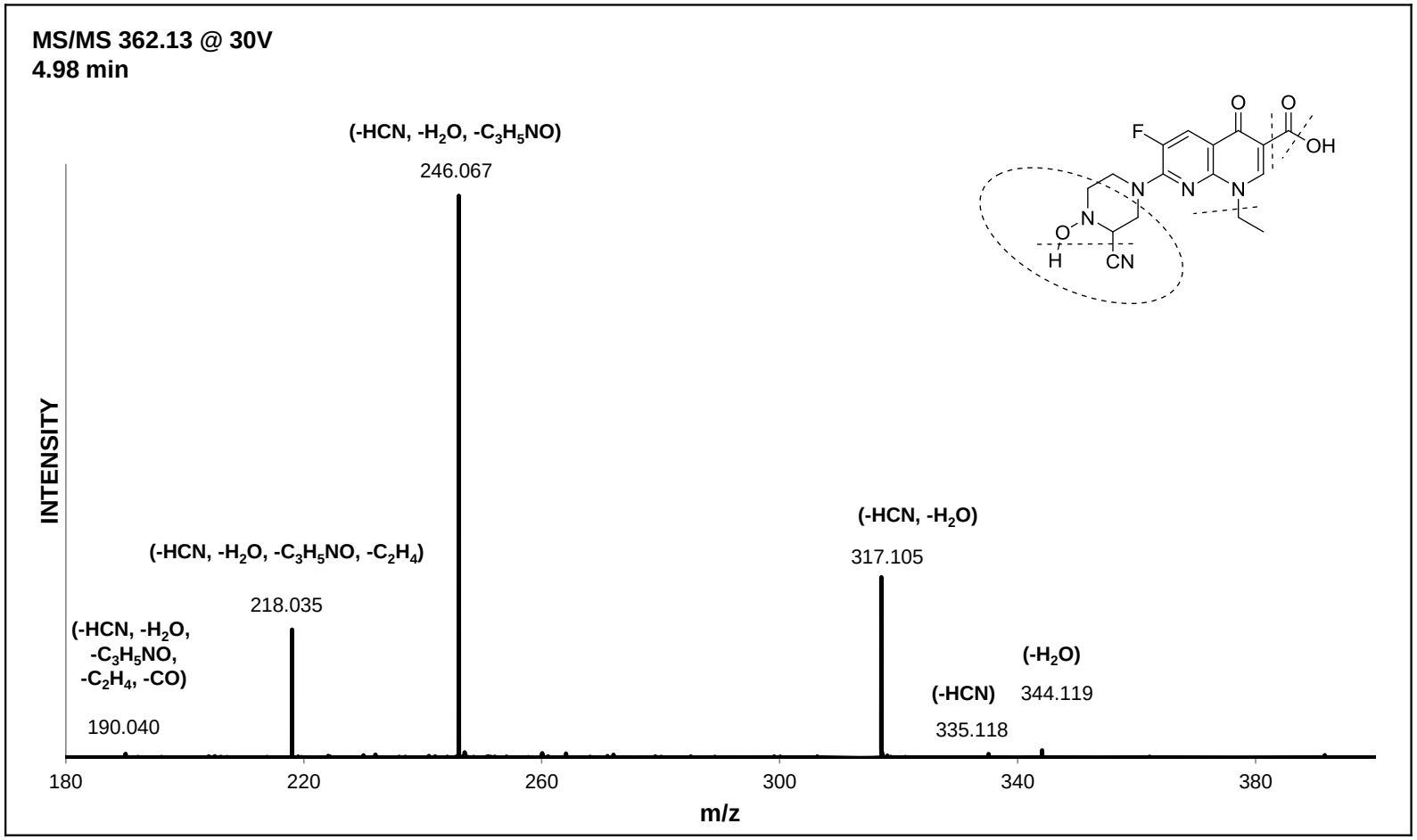

Figure 2.18 – High-resolution MS fragmentation of cyanide-trapped NITRONE-ENX with proposed cleavage sites
The necessary loss of atoms (supported by accurate mass) is indicated above each m/z ion value

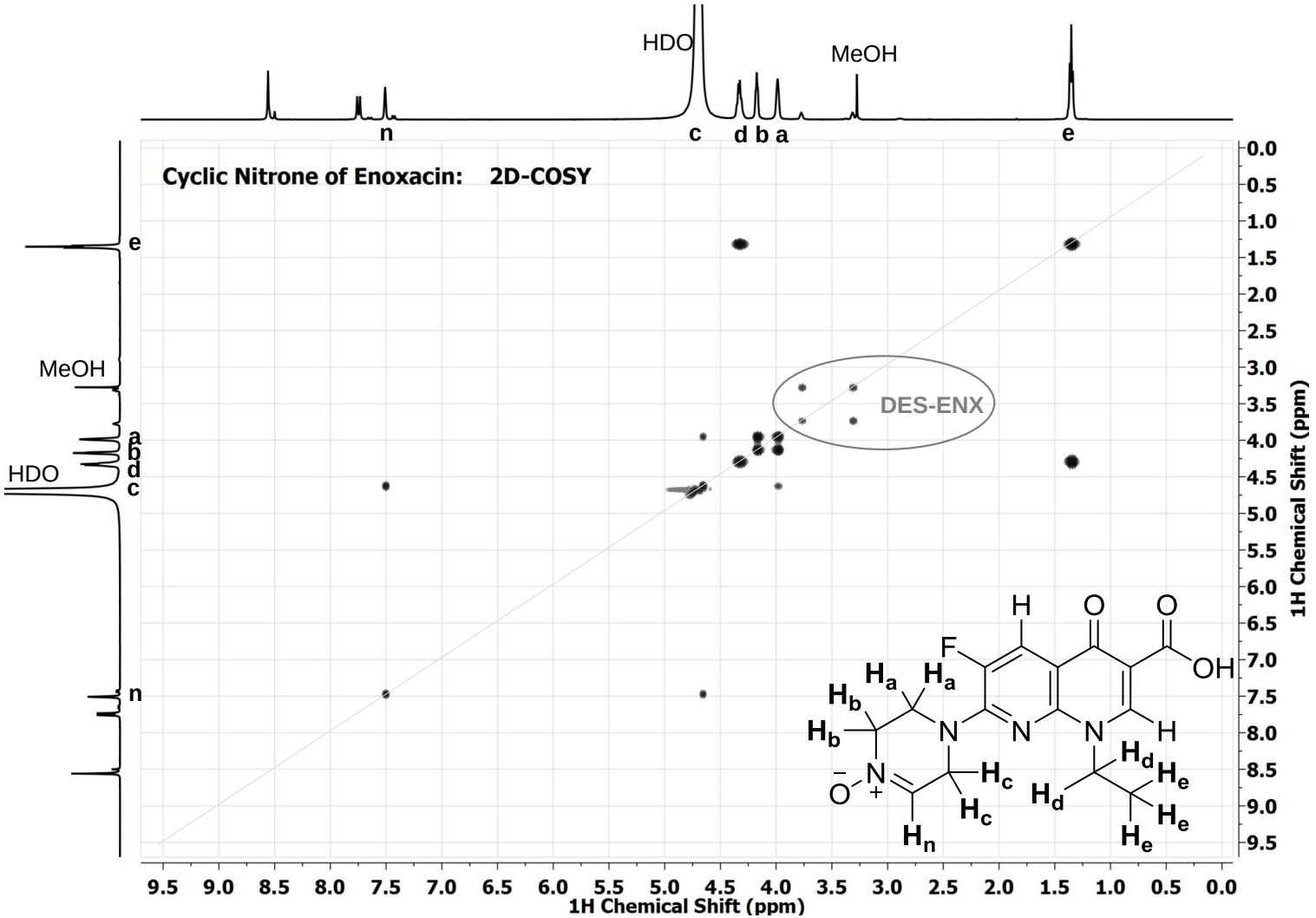

Figure 2.19 – Two-dimensional COSY NMR of synthesized and partially-purified NITRONE-ENX in D_2O
^1H-^1H COSY NMR analysis of isolated NITRONE-ENX (~77%) containing DES-ENX impurity (~23%) in deuterium oxide. The HDO water peak at 4.79 ppm was suppressed post-acquisition to reveal the proton signals from one of the CH_2-piperazine groups. Protons from the ethylene bridge of DES-ENX impurity are circled. Protons for which there are structurally diagnostic couplings are labeled with letters on both the chemical structure of NITRONE-ENX and the 1D proton spectrum.

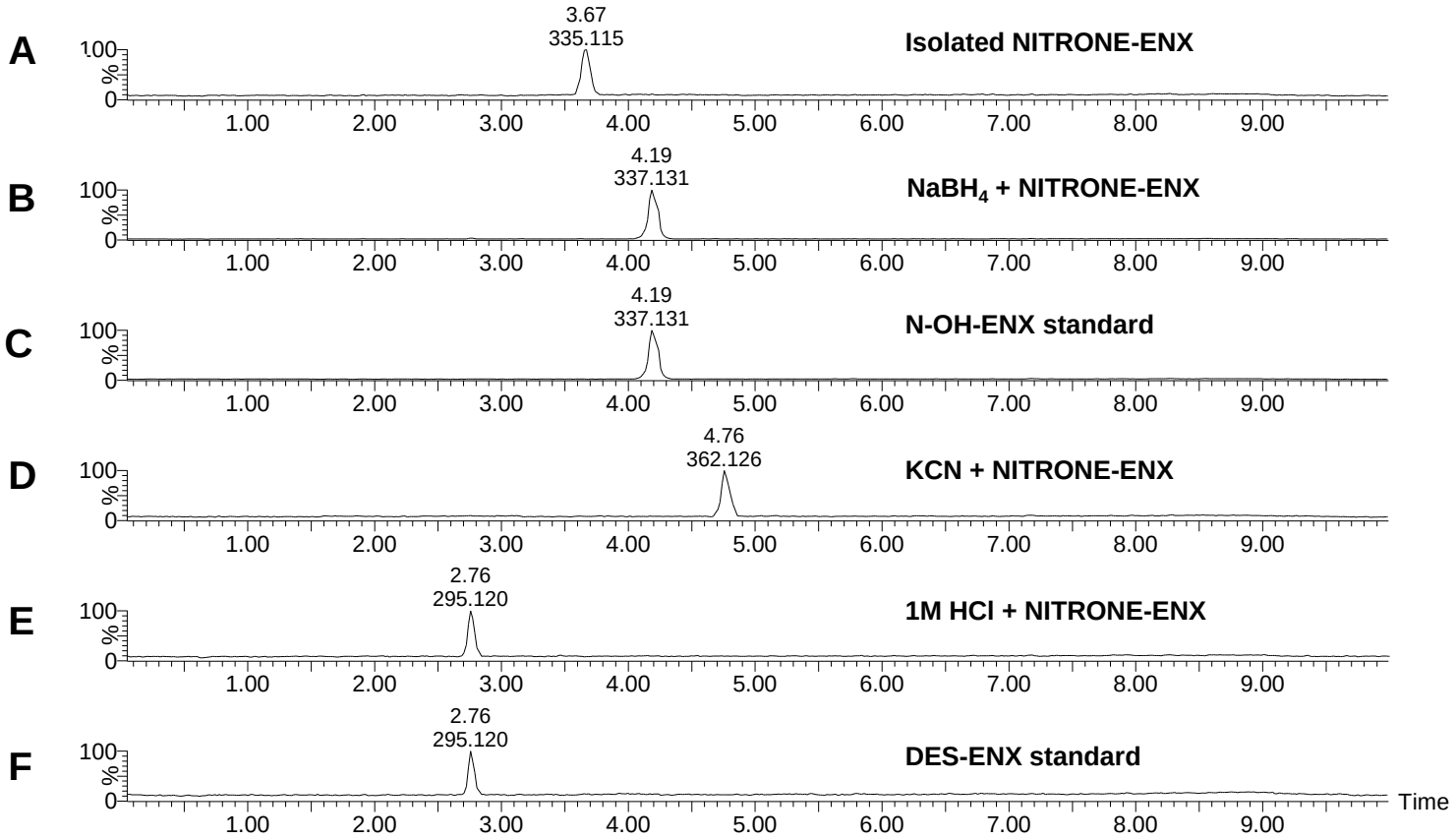

Figure 2.20 – LC-MS chromatograms for chemical characterization of synthesized NITRONE-ENX
1 μM isolated NITRONE ENX (trace A), product of the reaction of 1 μM NITRONE-ENX with $NaBH_4$ (trace B), 1 μM synthetic N-OH-ENX (trace C), product of the reaction of 1 μM NITRONE-ENX with KCN (trace D), product of the reaction of 1 μM NITRONE-ENX with acid (trace E), and 1 μM synthetic DES-ENX (trace F), are shown. Peak annotation represents the retention time (minutes) and the most abundant ion (m/z).

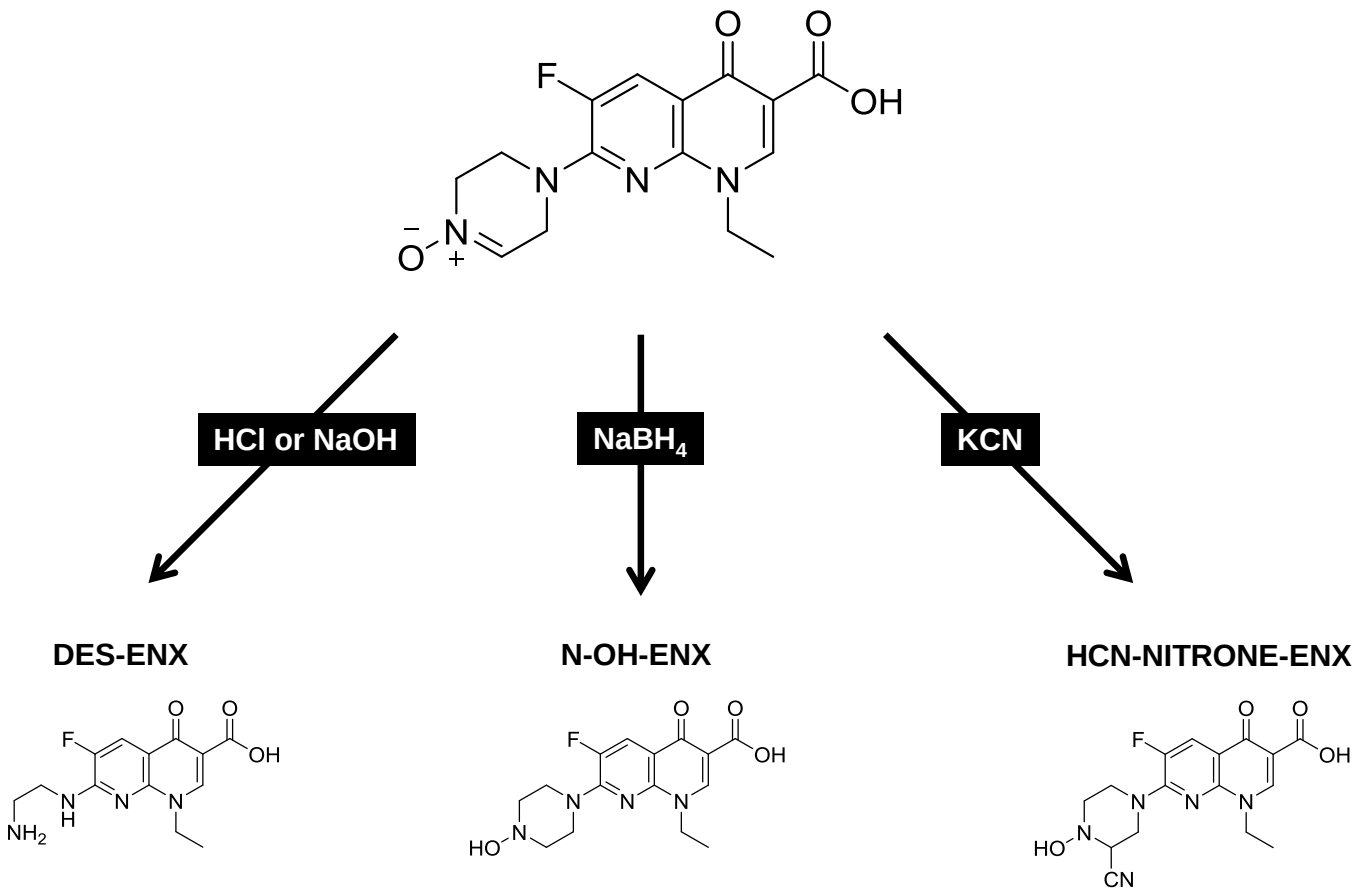

Figure 2.21 – Summary of the chemical characterization results for synthesized NITRONE-ENX
Treatment with either strong acid or strong base led to DES-ENX by an unknown mechanism. Reduction with sodium borohydride yielded N-OH-ENX. Nucleophilic trapping with cyanide anion formed the expected HCN adduct.

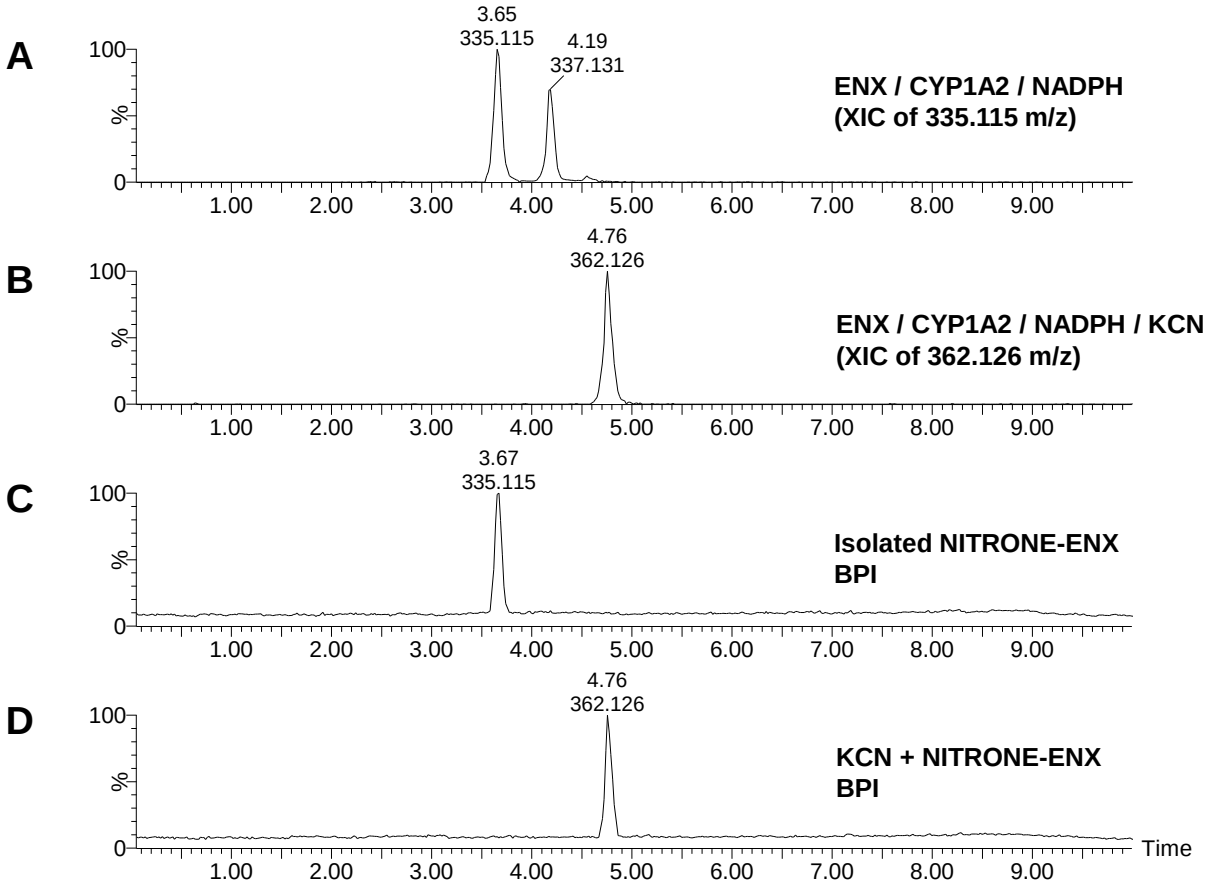

Figure 2.22 – LC-MS chromatograms of metabolite vs synthesized NITRONE-ENX and cyanide-trapping
1A2-generated metabolites (XIC of 335.115 m/z) of ENX (trace A), the same metabolic incubation (XIC of 362.126 m/z) supplemented with KCN (trace B), 1 mM isolated NITRONE ENX (trace C), and the product of the reaction of 1 mM NITRONE-ENX with KCN (trace D) are shown. Peak annotation represents the retention time (minutes) and the most abundant ion (m/z). The lower two traces are base peak intensity (BPI) chromatograms.

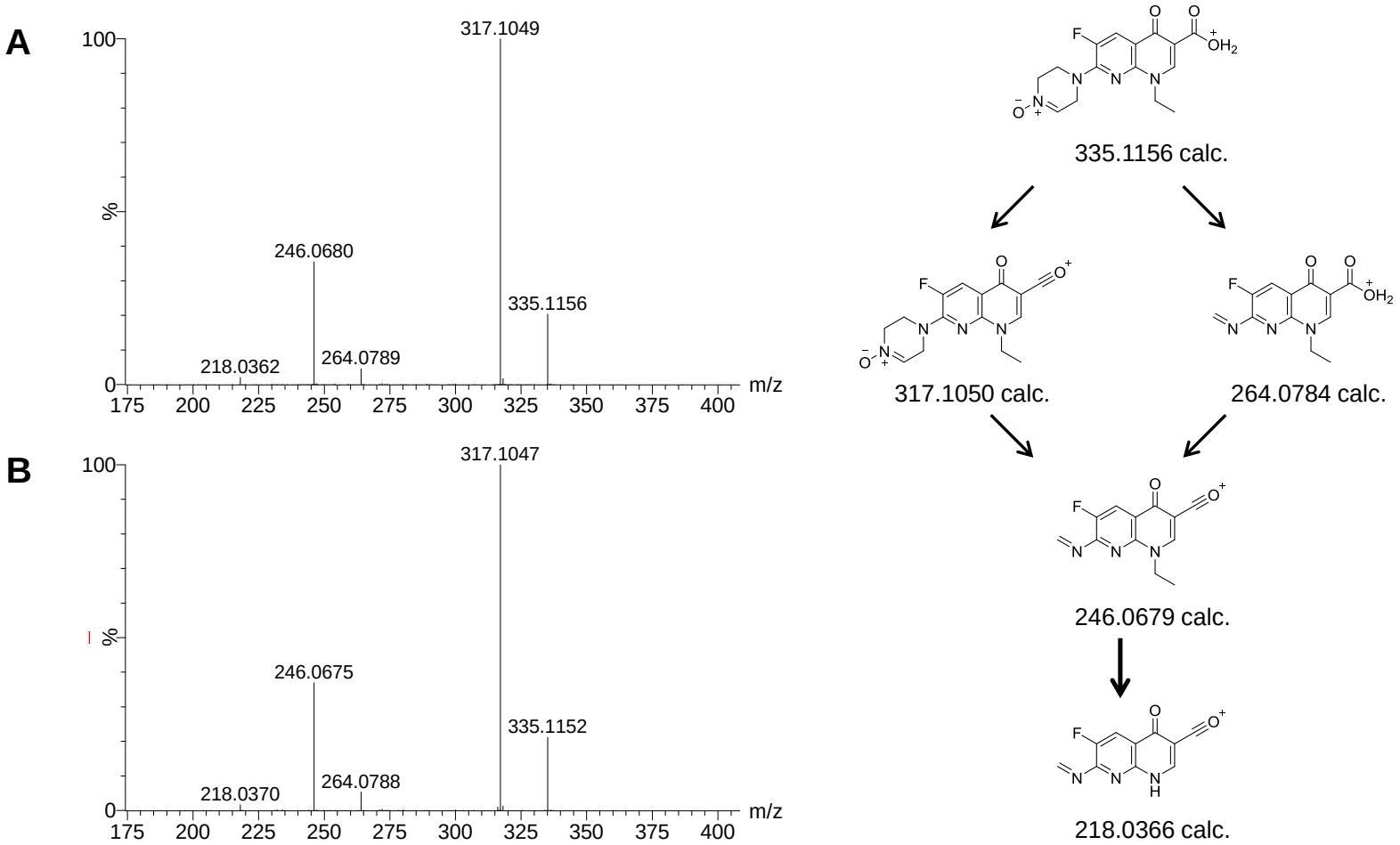

Figure 2.23 – High-resolution MS fragmentation patterns for synthesized vs metabolite NITRONE-ENX
Fragmentation patterns for the isolated NITRONE-ENX (Panel A) and the metabolite NITRONE-ENX from metabolic incubations with CYP1A2, ENX, and NADPH (Panel B) are shown. The retention times for both species matched at 3.65 min. The mass of NITRONE-ENX (335 m/z) was fragmented at 15 eV. Proposed fragments and calculated m/z values are shown.

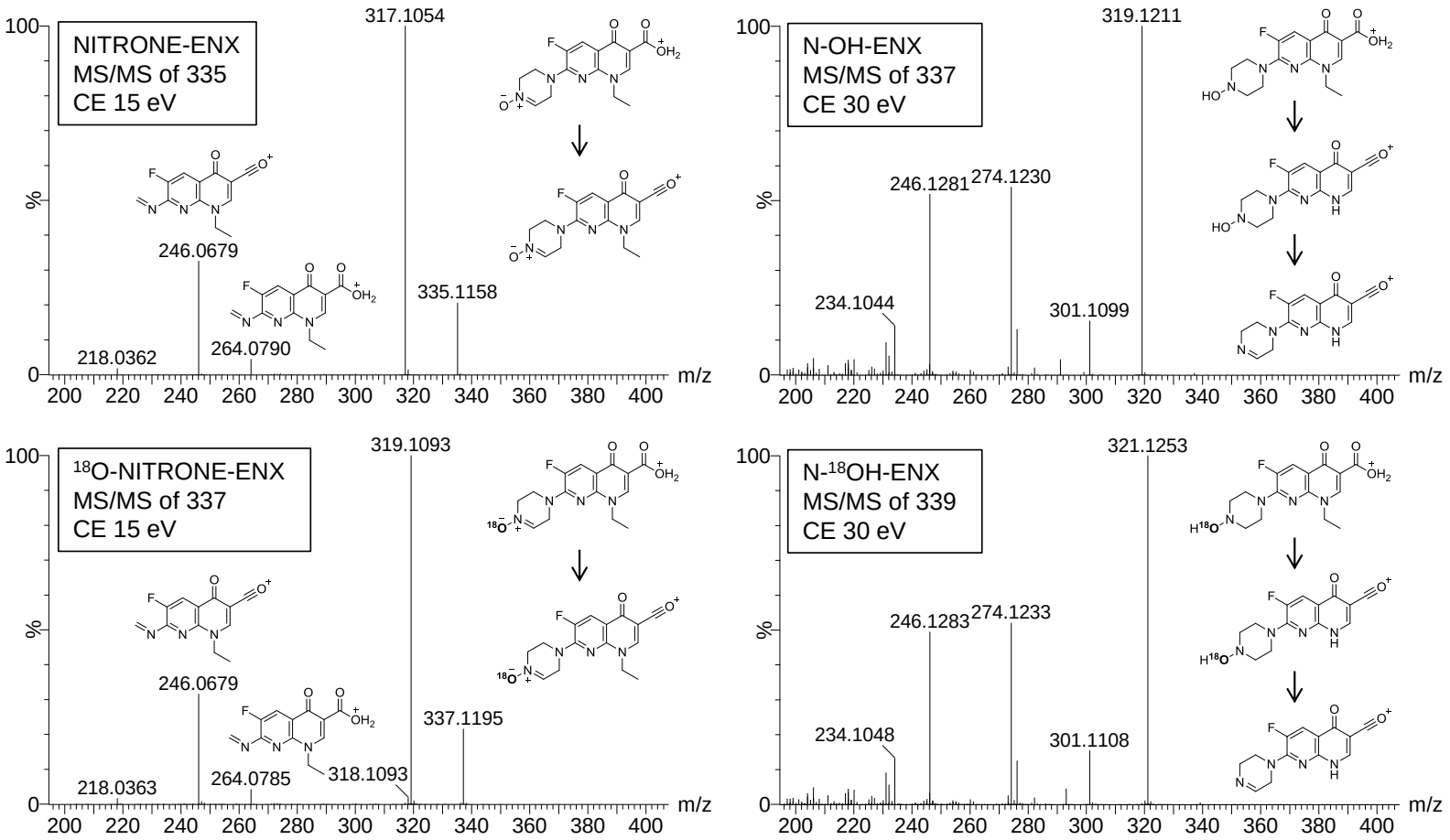

Figure 2.24 – Comparison of the ^{18}O-labeled and unlabeled NITRONE-ENX and N-OH-ENX fragmentation patterns
Fragments are provided to indicate the cleavages which result in loss of ^{18}O and to support the overall fragment assignments. NITRONE-ENX undergoes a single water loss from the carboxylic acid moiety. N-OH-ENX undergoes a double water loss in a specific order; water loss from the carboxylic acid moiety followed by water loss from the hydroxylamine moiety.

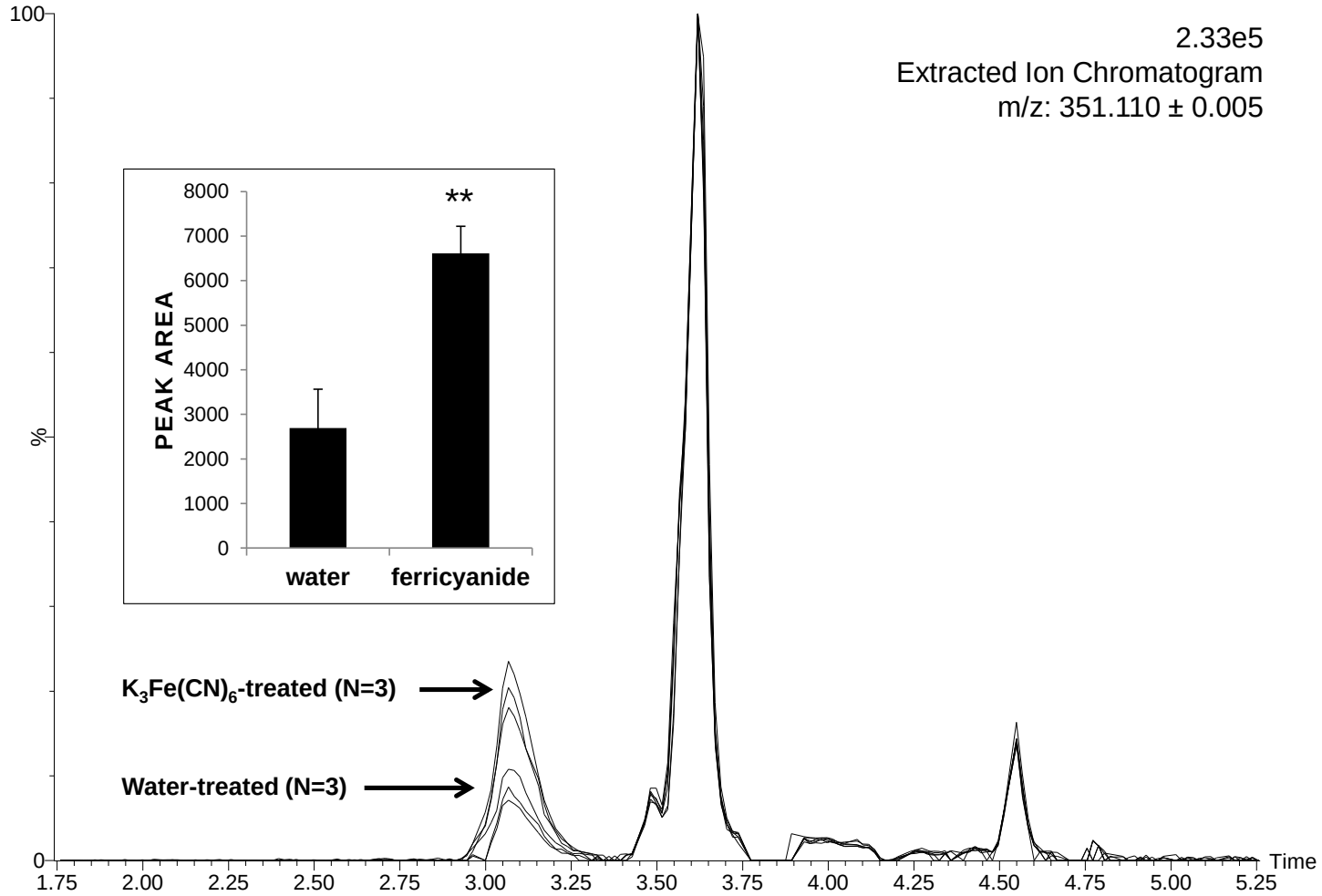

Figure 2.25 – LC-MS chromatogram demonstrating release of the MI complex ligand by potassium ferricyanide treatment
Overlaid LC-MS metabolite profiles (XIC of 351.110 m/z) following incubation of N-OH-ENX with NADPH-fortified CYP1A2 and treatment with either water or potassium ferricyanide in water (final concentration of 100 μM). Each condition was performed in triplicate and the mean peak areas ± SD for the ferricyanide responsive peak at 3.1 minutes are given for water- and ferricyanide-exposed incubations (inset).

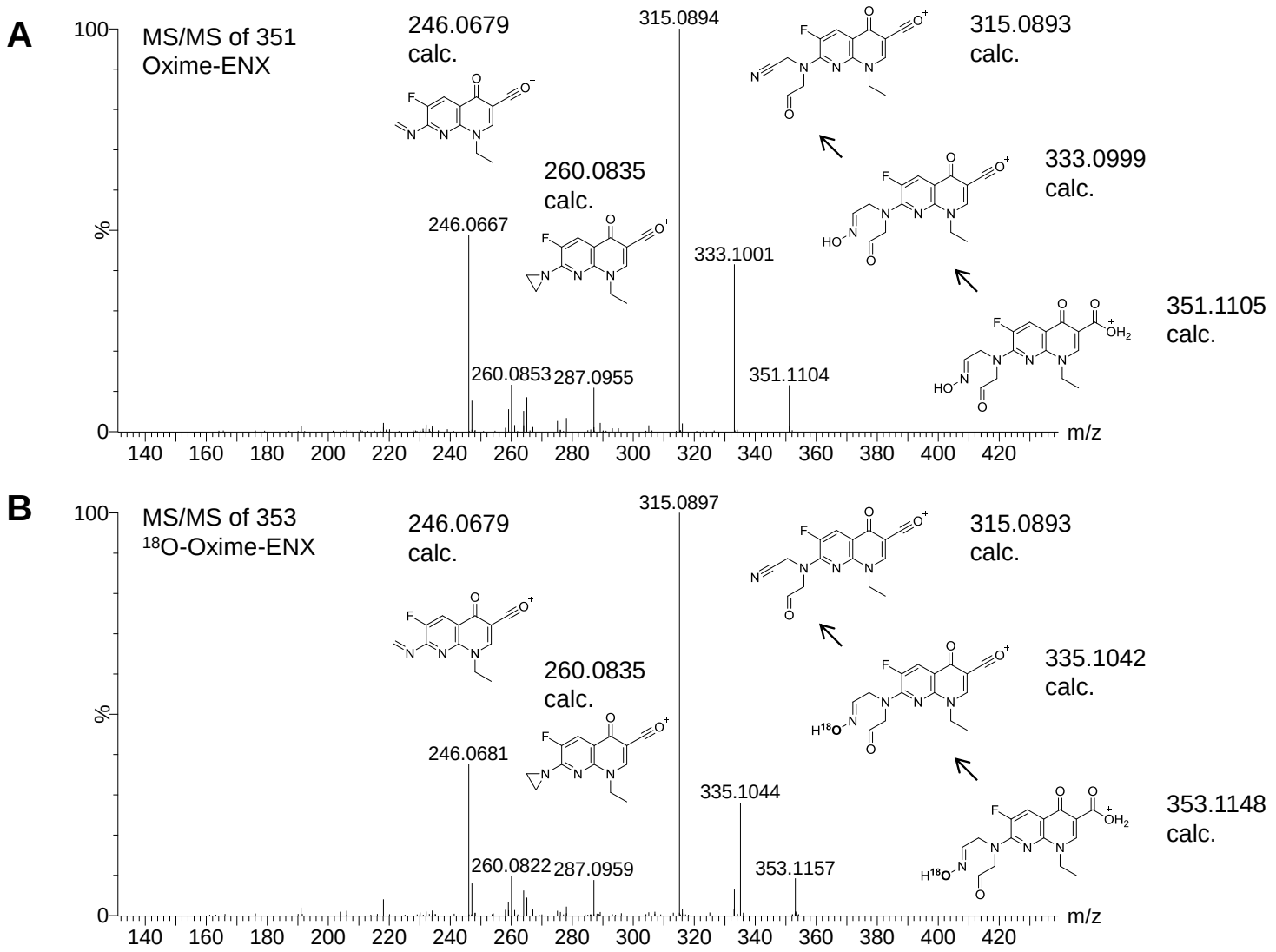

Figure 2.26 – High-resolution MS fragmentation of the released MI complex ligand at low collision energy
Fragmentation (15 eV collision energy) of the putative nitroso/oxime metabolite eluting at 3.1 minutes following incubation of NADPH-supplemented CYP1A2 with N-OH-ENX and fragmentation of 351 m/z (Panel A), or with N-^{18}OH-ENX and fragmentation of 353 m/z (Panel B). Proposed structures are presented alongside their calculated exact mass.

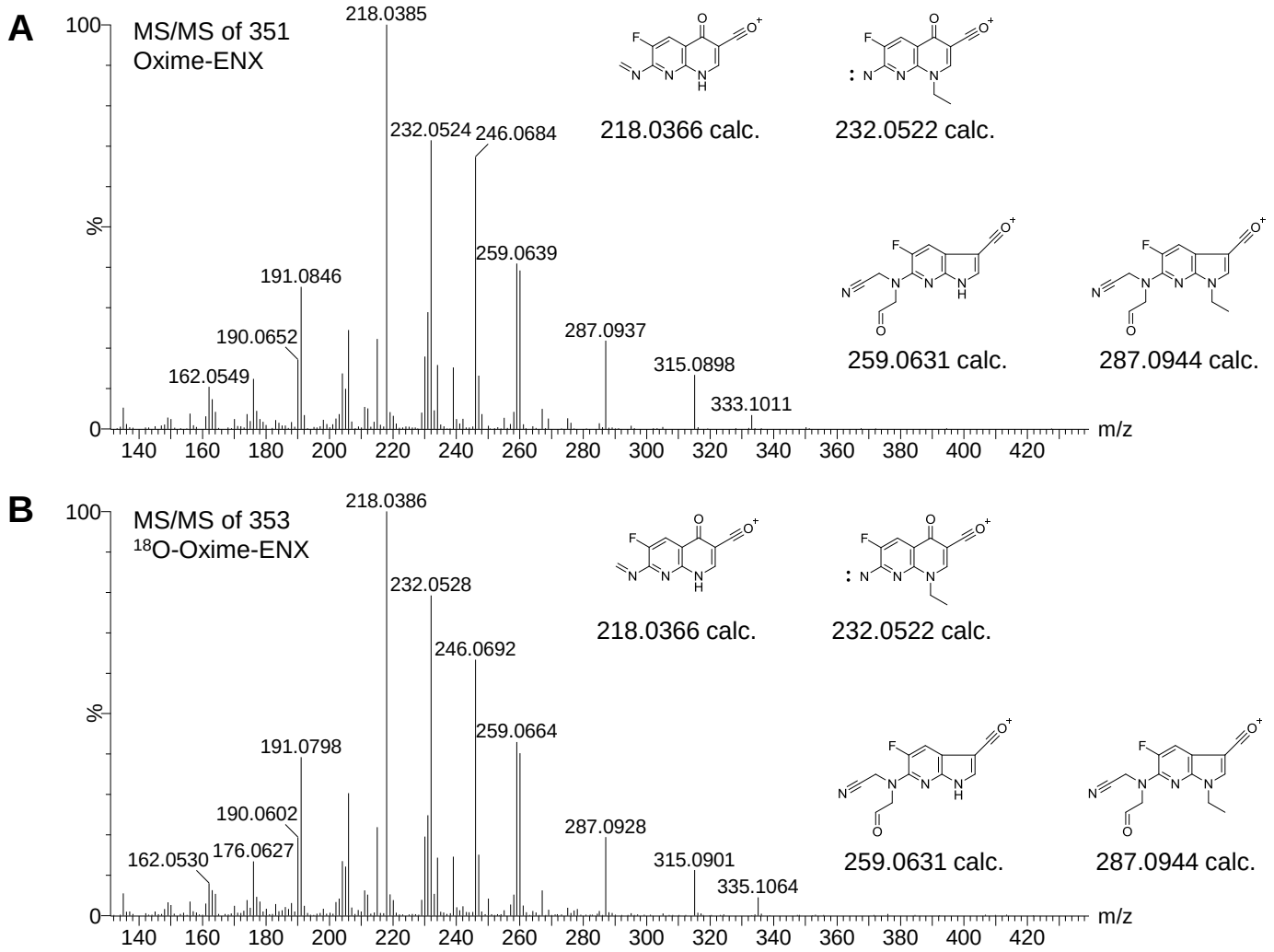

Figure 2.27 – High-resolution MS fragmentation of the released MI complex ligand at high collision energy
Fragmentation (30 eV collision energy) of the putative nitroso/oxime metabolite eluting at 3.1 minutes following incubation of NADPH-supplemented CYP1A2 with N-OH-ENX and fragmentation of 351 m/z (Panel A), or with N-^{18}OH-ENX and fragmentation of 353 m/z (Panel B). Proposed structures are presented alongside their calculated exact mass.

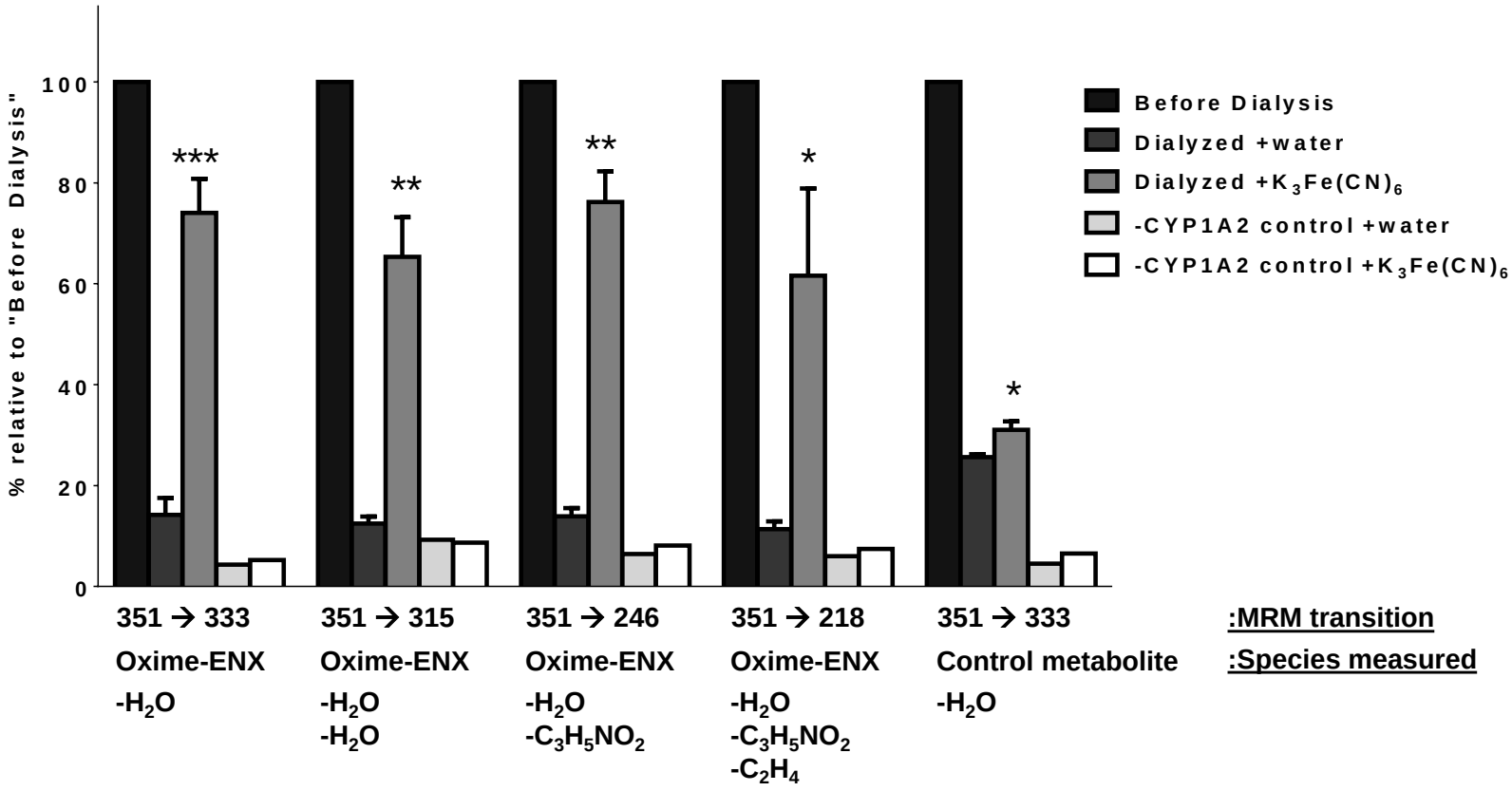

Figure 2.28 – Effect of dialysis and ferricyanide treatments on the peak area for the released MI complex ligand vs an isobaric control metabolite

Responsiveness of the putative nitroso/oxime-ENX peak to ferricyanide treatment following incubation of NADPH-fortified CYP1A2 with N-OH-ENX and dialysis of the incubation mixture (3.5 kDa MWCO) was evaluated. Four MS/MS transitions were monitored on a Triple-Quadrupole mass spectrometer corresponding to the major fragments of oxime/nitroso-ENX seen by MS/MS on the Synapt G2 Q-TOF. The LC chromatogram of the 351 to 333 m/z transition contained both the oxime/nitroso-ENX species (retention time: 3.72 min) and a separate “Control Metabolite” peak (retention time: 4.25 min) which was designated as a control peak for this analysis. All peak areas were normalized to the internal standard, enrofloxacin, during data work up. Mean ± SD (N=3) are reported for dialyzed samples while single measures were taken for “Before Dialysis” and the “-1A2” controls.

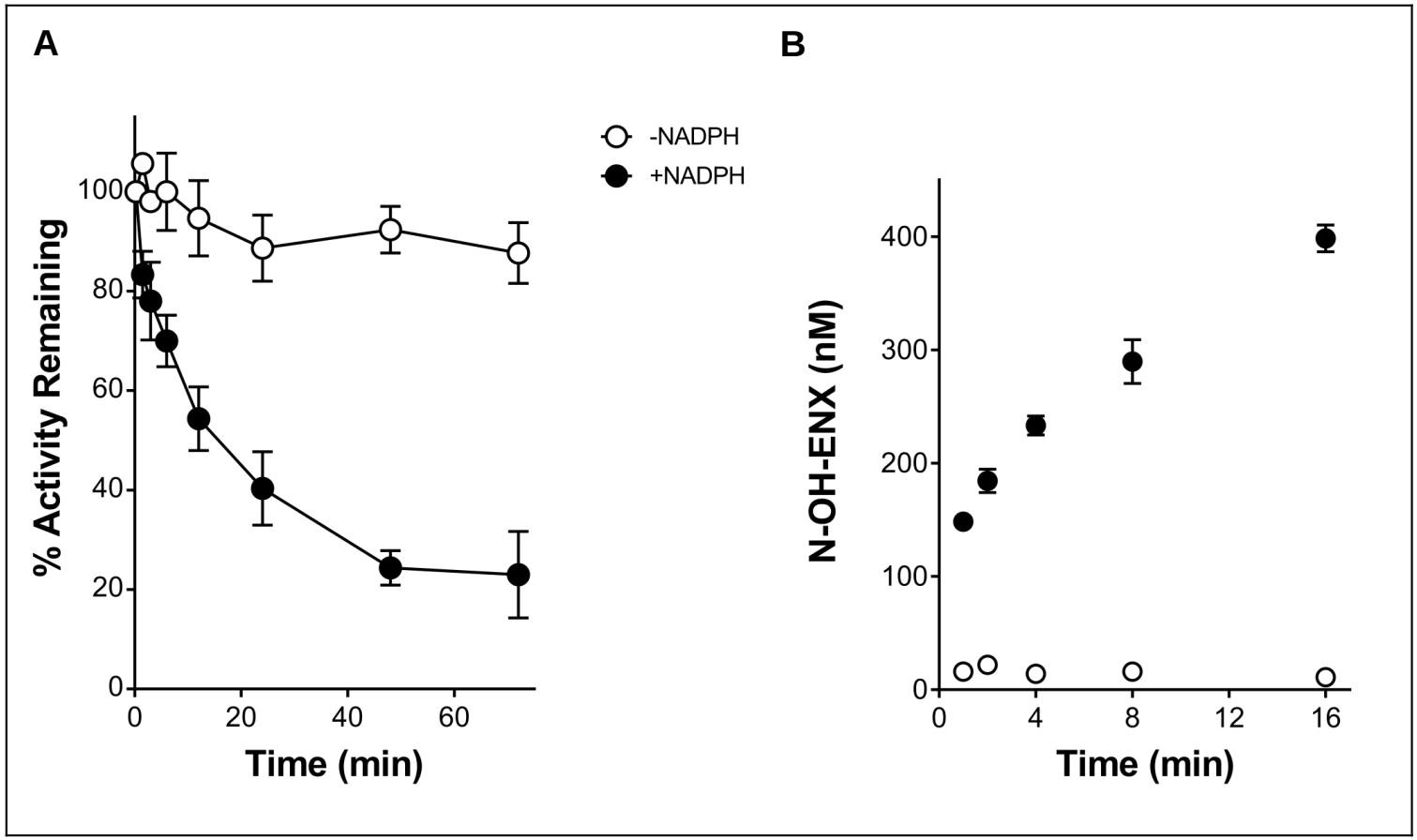

Figure 2.29 – Time-course of CYP1A2 activity loss compared with N-OH-ENX formation by incubation with ENX
The time-courses for CYP1A2 activity loss (A) and N-OH-ENX formation (B) from incubation conditions designed to match the experiment for MI complex formation from ENX: CYP1A2 bactosomes (0.5 μM), ENX (640 μM) and NADPH (1.5 mM). Incubations were performed in polypropylene tubes in a heated water bath as opposed to in cuvettes in a spectrophotometer. All data points are in triplicate ± SD, with the exception of the open circles in Panel B which are single measures.

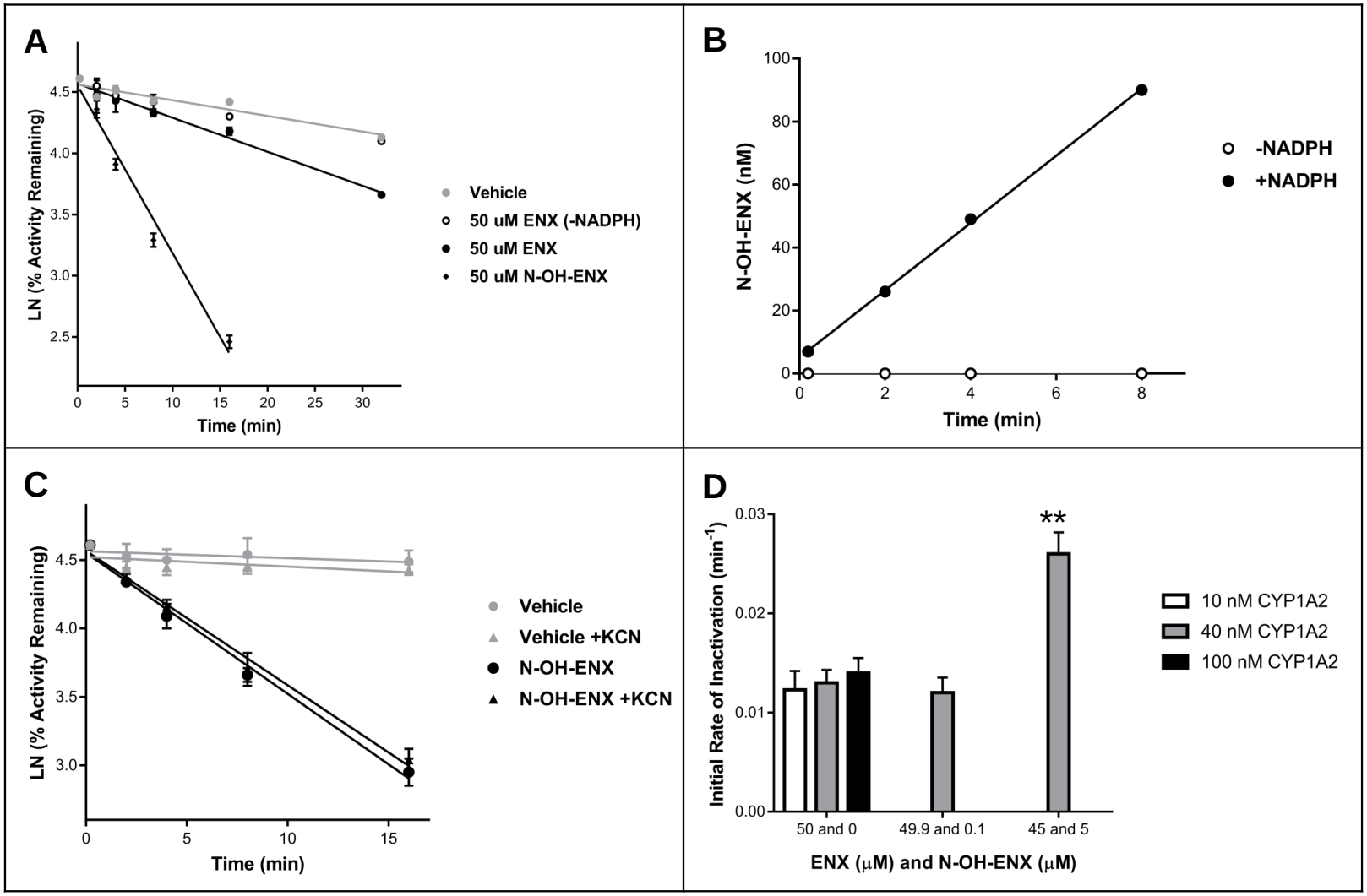

Figure 2.30 – Evidence that inactivation of CYP1A2 by ENX proceeds through non-dissociative metabolism
Comparison of time-dependent inhibition by ENX and N-OH-ENX at 40 nM CYP1A2 (A), time-course of N-OH-ENX formation from 50 μM ENX at 100 nM CYP1A2 (B), time-dependent inhibition by N-OH-ENX (50 μM) in the ±1 mM KCN (C), and the rate of enzyme inactivation at varying concentration of CYP1A2 in the presence of ENX and spiked N-OH-ENX (D) are shown.

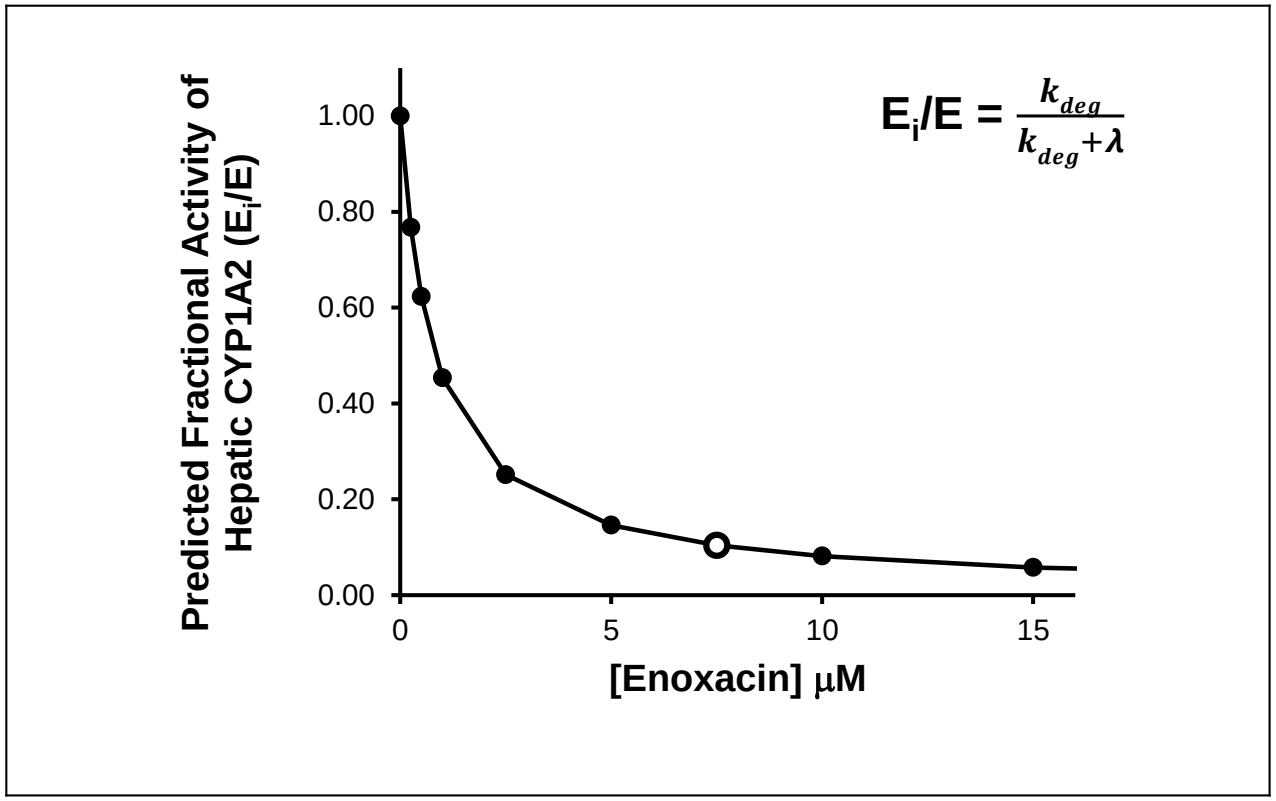

Figure 2.31 – Static prediction of the reduction in active hepatic CYP1A2 vs [ENX] in vivo
The effect of circulating enoxacin concentrations on the active levels of hepatic CYP1A2 in vivo was predicted. The apparent inactivation parameters K_I and k_{inact} from bactosomes were used to run a static prediction at each plotted enoxacin concentration. The in vivo half-life of CYP1A2 was assumed to be 38.6 hours (Faber and Fuhr, 2004). The open circle indicates the circulating plasma concentration of enoxacin at a therapeutic dose and the concentration used in further static predictions.

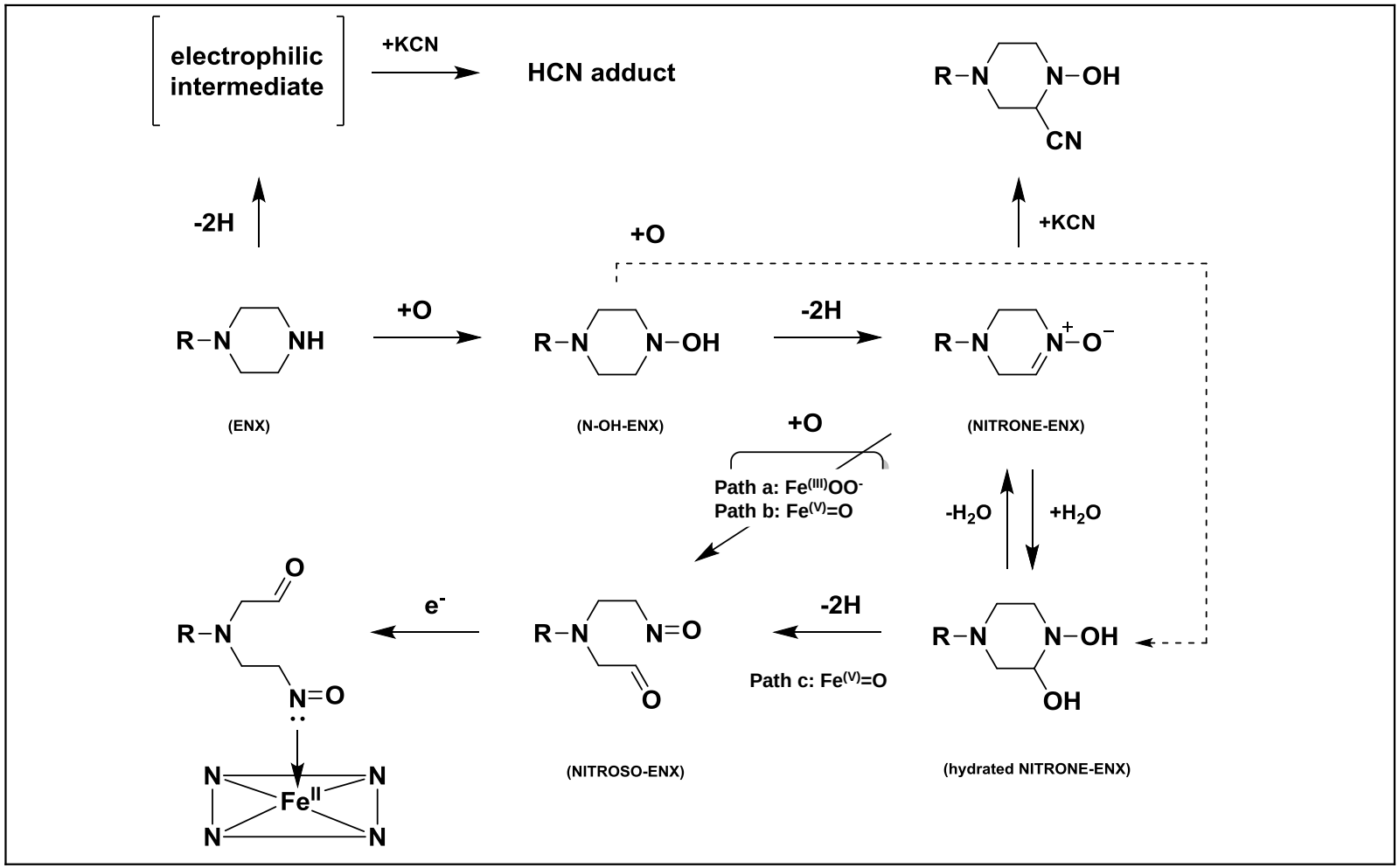

Figure 2.32 – Metabolic scheme with proposed paths to the MI complex with CYP1A2 and cyanide-trapped species
Conversion of the NITRONE-ENX to NITROSO-ENX may utilize the ferric peroxy anion (path a) or compound I (path b). Alternatively, NITROSO-ENX may be formed through hydrated NITRONE-ENX by Compound I (path c). Note that the hydrated NITRONE-ENX is also accessible by direct oxidation of N-OH-ENX. In addition to the MI complex pathway, we found evidence for a dehydrogenated metabolite of enoxacin which reacts with cyanide.

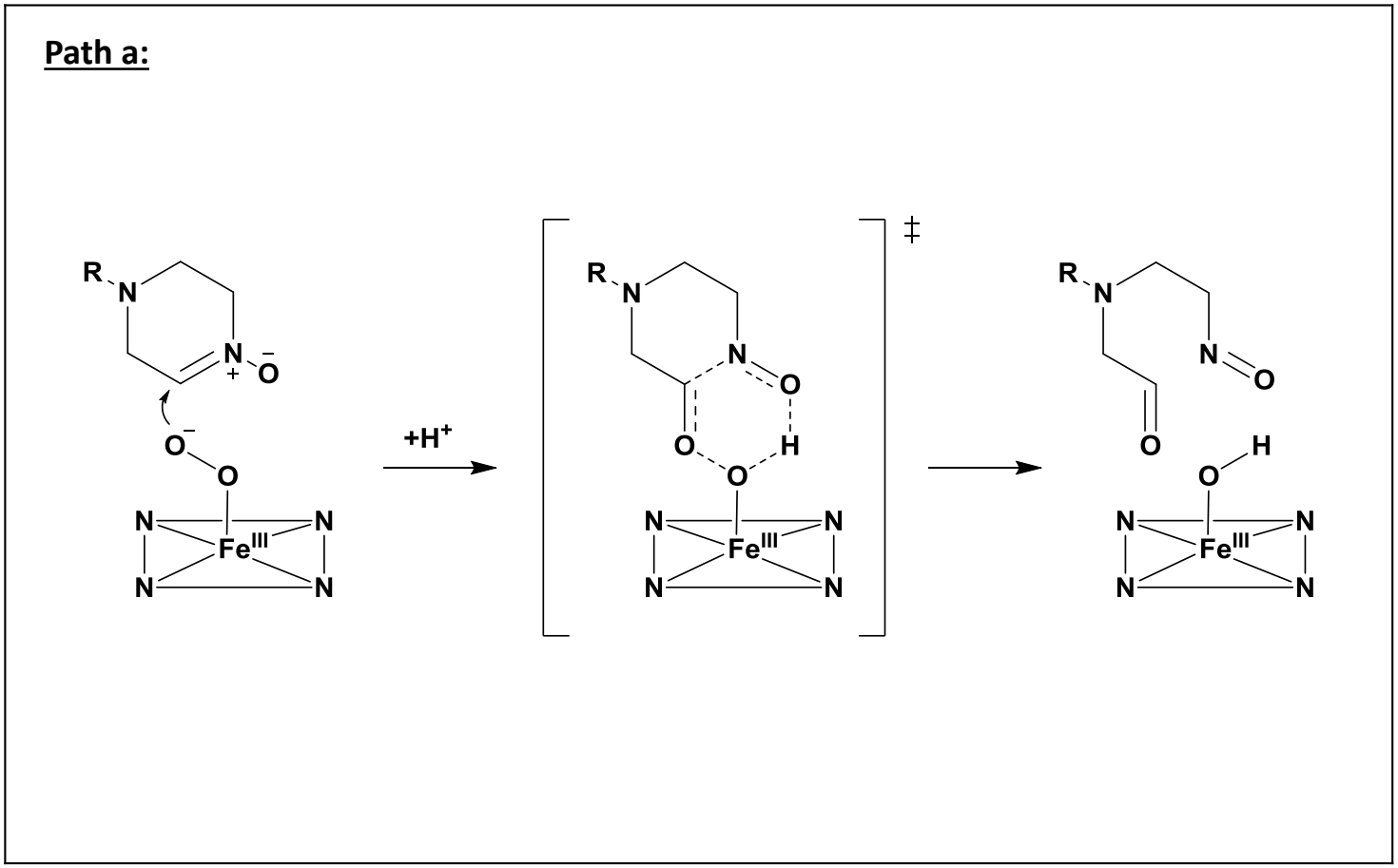

Figure 2.33 – Path (a) of the mechanistic alternatives for the final step in MI complex formation
A proposed mechanism for the conversion of NITRONE-ENX to NITROSO-ENX by the ferric peroxy anion state of CYP1A2. Delivery of a proton facilitates formation of a six-membered ring transition state. Bond formations and scissions are represented by dashed lines.

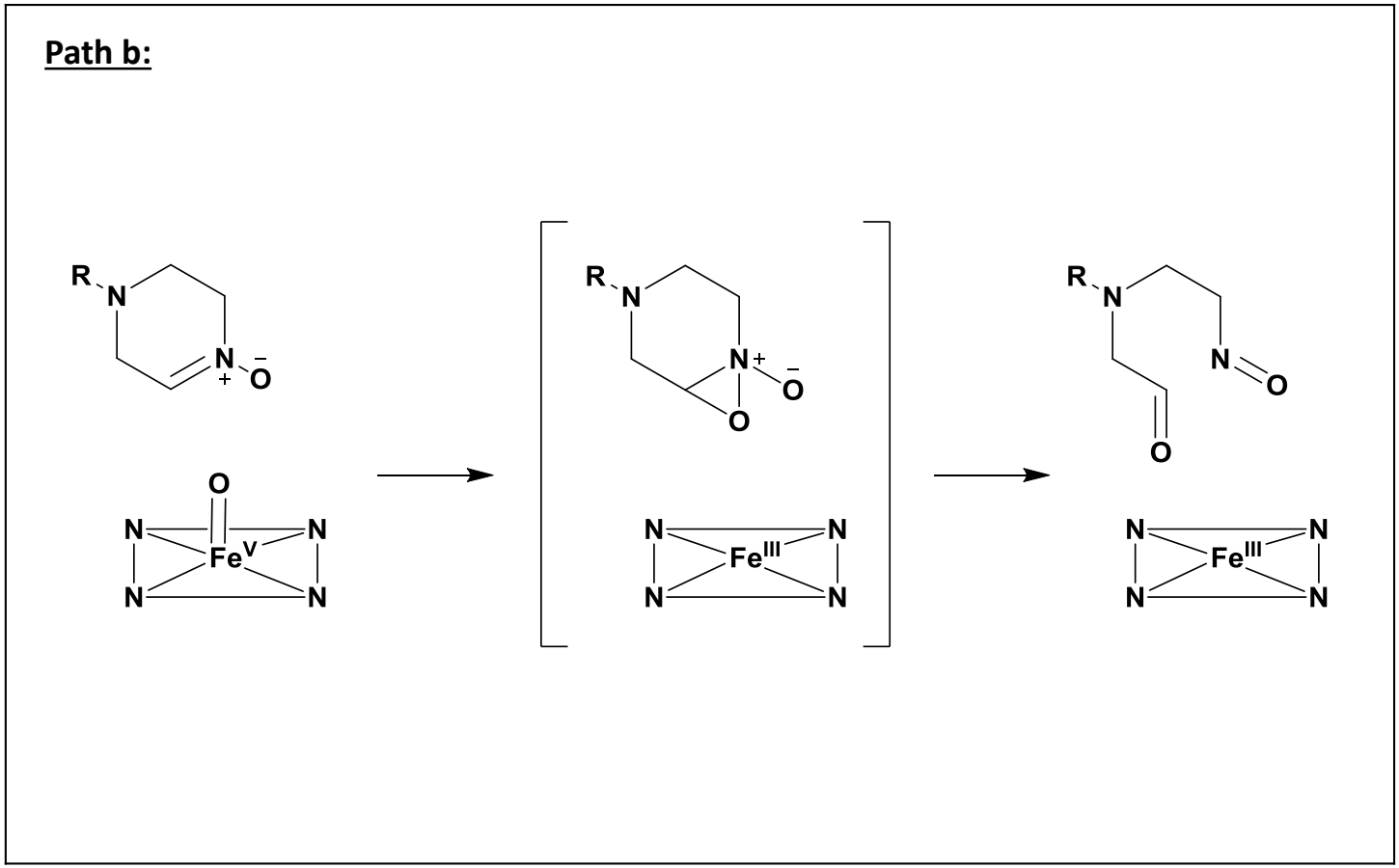

Figure 2.34 – Path (b) of the mechanistic alternatives for the final step in MI complex formation
A proposed mechanism for the conversion of NITRONE-ENX to NITROSO-ENX by the Compound I state of CYP1A2. Oxygen insertion produces an oxaziridinium N-oxide intermediate which ring-opens to NITROSO-ENX.

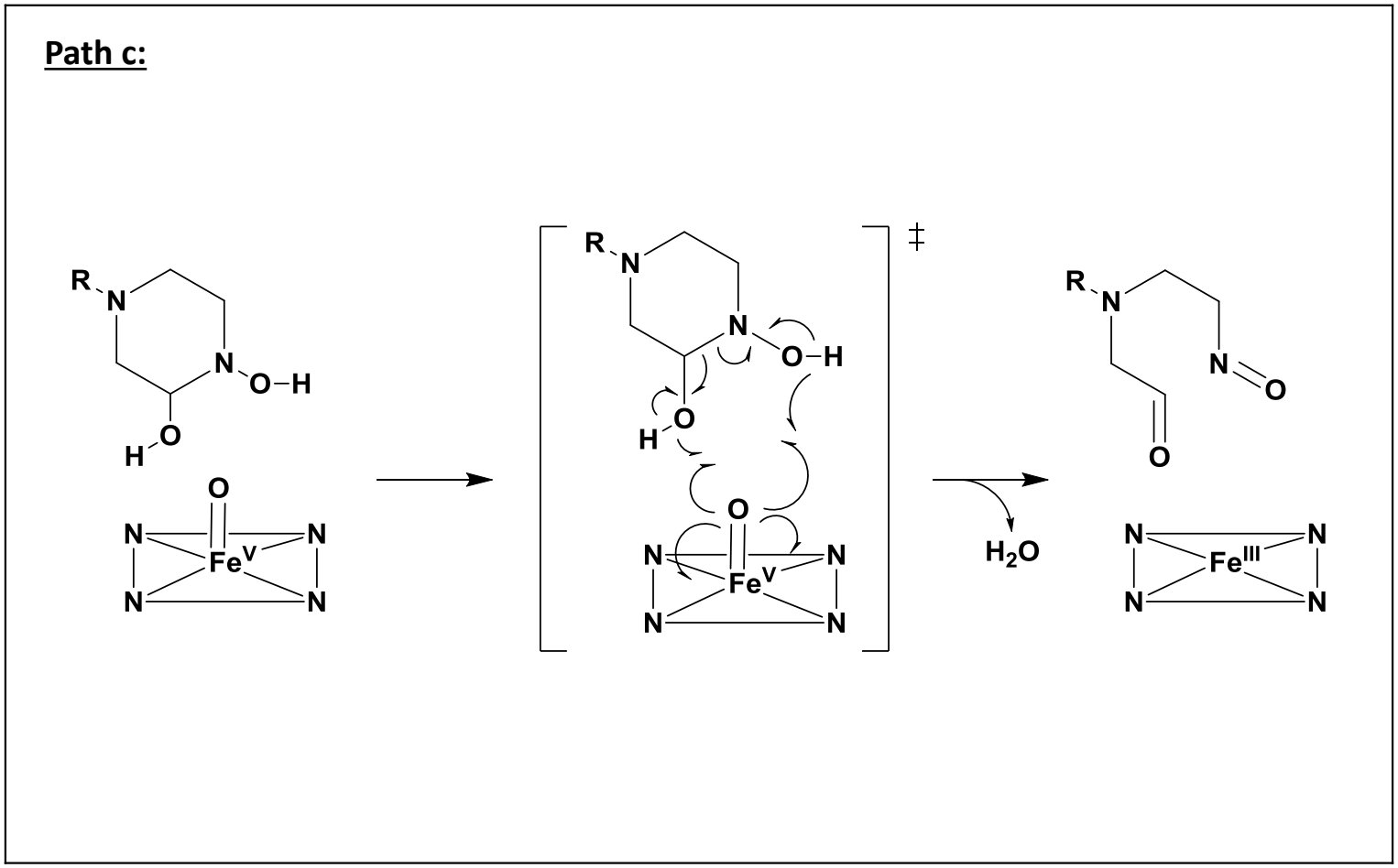

Figure 2.35 – Path (c) of the mechanistic alternatives for the final step in MI complex formation
A proposed mechanism for the conversion of hydrated NITRONE-ENX to NITROSO-ENX by the Compound I state of CYP1A2. This 2 electron oxidation is accomplished through two hydrogen atom abstractions to produce an equivalent of water. Bond cleavages are homolytic and concerted.

Table 2-1: Summary of MI complex formation and CO complex mass balance

Substrate	λ_{max}	Sample Cuvette			Reference Cuvette
		[MI complex]	[CO complex]	Total	[CO complex]
	nm	nmol/L	nmol/L	nmol/L	nmol/L
ENX	452	**205**	**151**	**356**	**365**
N-OH-ENX	452	**185**	**260**	**445**	**443**
DES-ENX	425	ND	**386**	-	**400**

N = 1 for each substrate
ND = not detected
The CO complex for CYP1A2 absorbs maximally at 448 nm

Table 2-2: Spectral ferricyanide reversal and CO binding summary

Substrate	MIC λ_{max}	Ferricyanide-treated cuvette		Water-treated cuvette
		[MIC] reversed	[CO complex]	[CO complex]
	nm	nmol/L	nmol/L	nmol/L
ENX	452	**128** ± 9	**204** ± 46	**156** ± 18
N-OH-ENX	452	**290** ± 16	**295** ± 35	**30** ± 17
DES-ENX	ND	ND	**219** ± 47	**267** ± 68

N = 3 for each substrate
Averages are given ±1 standard deviation
ND = not detected
The CO complex for CYP1A2 absorbs maximally at 448 nm

Table 2-3: Comparison of CYP1A2 inactivation results for ENX and N-OH-ENX

Measurement	ENX	N-OH-ENX	
NADPH-dependent enzyme inactivation?	**Yes**	**Yes**	
Reversible to dialysis?	**No**	**No**	
Reversible to $K_3Fe(CN)_6$?	**Partially**	**Completely**	
			Ratio of λ (N-OH-ENX:ENX)
λ at 40 μM (min^{-1})	**0.012** ± 0.001	**0.069** ± 0.008	**5.8** ± 0.8
λ at 80 μM (min^{-1})	**0.019** ± 0.003	**0.124** ± 0.005	**6.5** ± 1
λ at 160 μM (min^{-1})	**0.024** ± 0.008	**0.191** ± 0.001	**8.0** ± 3
$k_{inact,app}$ (min^{-1})	**0.048** ± 0.002	**0.44** ± 0.04	**9.2** ± 0.9

Table 2-4: Estimated depletion-based partition ratios for ENX and N-OH-ENX

	ENX	N-OH ENX
Incubated [Substrate:CYP1A2] ratio	**100:1**	**50:1**
%CYP1A2 Activity Remaining (t = 45 min)	**49** ± 1	**12** ± 1
%Substrate Remaining (t = 45 min)	**91** ± 12	**89** ± 4
Partition Ratio (90% confidence)	**< 50**	**< 10**
[ENX:CYP1A2] ratio in vivo at 800 mg dose	**1000:1**	

Table 2-5: Stoichiometry of enzyme inactivation:
Quantifying metabolites released per CYP1A2 inactivation event

Metabolite	[Metabolite:CYP1A2 Inactivated] Ratio
N-OH-ENX	**2.8** ± 0.5
NITRONE-ENX	**1.2** ± 0.1
DES-ENX	**2.0** ± 0.4
N-formyl ENX	**0.27** ± 0.08
aniline ENX	**0.22** ± 0.05
Above Total	**6.5** ± 0.6

Table 2-6: Observed vs predicted DDI values (using ENX apparent K_I & k_{inact})

Pharmaceutical	In Vivo DDI (AUC_i/AUC)	Predicted DDI
Theophylline ($f_{m,\ CYP1A2}$ = 0.80)[a]	**3.7** (Wijnands et al., 1986)	**3.5**
Caffeine ($f_{m,\ CYP1A2}$ = 0.95)[a]	**5.7** (Kinzig-Schippers et al., 1999)	**6.7**
Worst-case scenario ($f_{m,\ CYP1A2}$ = 1.00)	n/a	**9.6**

[a] Literature source for f_m was Venkatakrishnan et al. (2007)

Chapter 3: Characterization of the Inhibition of CYP1A2 by Enoxacin in Multiple Enzyme Systems

3.1 Introduction

In the previous chapter (Chapter 2), we demonstrated that enoxacin (ENX) is sequentially metabolized by CYP1A2 to a metabolic-intermediate (MI) complex in recombinantly-expressed CYP1A2. Thus, ENX was determined to be a time-dependent inhibitor of CYP1A2 where sequential metabolism generates a mechanism-based inactivator in the enzyme active site. We also provided strong evidence that the concentrations of the intermediate metabolites do not reach concentrations high enough to affect the rate of inactivation. Put another way, inactivation of CYP1A2 is a *non-dissociative* sequential process where released metabolites do not contribute to inactivation. Time-dependent inhibition (TDI) of CYP1A2 by ENX is important because the in vivo DDI magnitudes with theophylline [3.7-fold AUC increase; Wijnands et al. (1986)] and caffeine [5.7-fold; Kinzig-Schippers et al. (1999)] are severely underpredicted by reversible ENX-CYP1A2 affinity constants even when maximal hepatic inlet concentrations of ENX are applied in the prediction (Obach et al., 2006). We accurately (within 1.25-fold) predicted the DDI magnitude for both theophylline and caffeine in a static in vitro to in vivo prediction by applying apparent inactivation parameters [K_I(μM)=132±21, k_{inact}(min^{-1})=0.048±0.002] for ENX measured in recombinantly-expressed CYP1A2 Bactosomes® (Cypex). The theoretical underpinnings for the mathematical prediction is that the three step process can be kinetically treated as a single step. Thus, an understanding of the inhibition mechanism was critical for accurate prediction of the DDI.

Furthermore, since our DDI prediction relied upon in vitro data generated in bactosomes, it is interesting to note how successful our prediction was despite a number of physiologically-

irrelevant aspects of this system (e.g., lipid content and composition; the ratio of cytochrome P450 reductase to CYP1A2; absence of cytochrome b5, other cytochrome P450 isoforms, other hepatic redox proteins, or human hepatic conjugative “Phase II” enzymes; and the presence of membrane proteins from the *Escherichia coli* host strain, to name a few). Bactosomes, like human liver microsomes (HLM) or any other “broken-cell” preparation, are also non-physiological relative to a liver in that drugs, in vivo or in cultured hepatocytes, must cross the cell membrane (by diffusion or active transport) to access cytochrome P450. ENX can be transported by the hepatic uptake transporter OATP1A2 (Maeda et al., 2007). ENX has also been shown to be concentrated (by ~9-fold) in rat liver relative to blood and ~20-fold more concentrated in isolated rat hepatocytes (oil-spin method) relative to nominal ENX media concentrations (Yamano et al., 1999). Thus, the actual concentrations of the inhibitor and the metabolites produced that are available to CYP1A2 relative to the nominal concentrations of inhibitor and metabolites in incubations may be very different between broken-cell enzyme preparations and intact hepatocytes. This disparity may also exist in vivo where concentrations of inhibitor and metabolites in blood may differ substantially from the concentrations of inhibitor and metabolites available to CYP1A2 in the liver.

The “best” in vitro system to use for characterizing inhibition of cytochrome P450 has been continuously debated (Tucker et al., 2001; Brown et al., 2010; Parkinson et al., 2010) and the rationalization process addressing why data generated in one in vitro system better predicts an in vivo DDI than data generated in another in vitro system is also actively debated. A few illuminating examples of this so called “system-dependent” P450 inhibition have been reviewed by Parkinson et al. (2010) where the use of hepatocytes rather than HLM was essential for characterizing P450 inhibition in a way that accurately reflects in vivo.

For example, gemfibrozil is converted to an acyl glucuronide in hepatocytes and the glucuronide metabolite is a mechanism-based inhibitor of CYP2C8 via heme alkylation (Baer et

al., 2009). In HLM, the mechanism-based inhibition of CYP2C8 does not occur upon incubation with gemfibrozil and NADPH causing an underprediction of the DDI magnitude with CYP2C8 substrates. Indeed, gemfibrozil precipitates a severe DDI with cerivastatin in vivo (Backman et al., 2002). System-dependent P450 inhibition is also observed for ezetimibe when comparing inhibition of CYP3A4 in HLM and hepatocytes. In HLM, ezetimibe is a time-dependent inhibitor of CYP3A4 whereas in hepatocytes, ezetimibe is rapidly and extensively glucuronidated leading to depletion of the time-dependent inhibitor and, thus, protection of CYP3A4. Here again, use of hepatocytes to characterize the inhibition of CYP3A4 by ezetimibe was critical for the purpose of DDI prediction as ezetimibe does not cause an interaction in vivo with the CYP3A4 substrates midazolam, simvastatin, atorvastatin, or lovastatin (Kosoglou et al., 2005). Thus, as highlighted by Parkinson et al. (2010), it is particularly important to evaluate P450 inhibition in hepatocytes when the parent drug is susceptible to extensive non-CYP mediated metabolism. Under those circumstances, a substantial system-dependent effect on the outcome of P450 inhibition studies may be expected.

However, in some instances P450 inhibition is reasonably conserved across in vitro systems (e.g., recombinant P450, HLM, and hepatocytes) leading to system-*independent* outcomes. Omeprazole, for example, is a time-dependent inhibitor of CYP2C19 with similar inhibition potencies in recombinant CYP2C19, HLM, and hepatocytes (Parkinson et al., 2010). Zhao et al. (2005) evaluated TDI of CYP3A4 for six structurally-diverse drugs in both HLM and hepatocytes. For the drugs exhibiting TDI of CYP3A4 in HLM, TDI of CYP3A4 was also observed in hepatocytes. Discrepancies between the TDI characteristics in HLM and hepatocytes for these drugs could be partially explained by taking into account factors such as differing metabolic stability and nonspecific binding of the parent drug in either system as well as the effects of active transport of the drug across the cell membrane in hepatocytes (Zhao et al., 2005). There are many potential factors and complexities that can lead to discrepancies

between TDI of P450 in HLM and hepatocytes. Nonetheless, McGinnity et al. (2006) have shown that the inactivation parameters (K_I and k_{inact}) obtained from TDI experiments are sometimes similar across systems (recombinant P450, HLM, and hepatocytes). As there are many obvious experimental advantages to working with recombinant P450 and HLM (over hepatocytes), it is often more practical to conduct inhibition studies in these systems. Currently, it appears that the information gained from microsomal and recombinant P450 inhibition studies can be useful and the use of hepatocytes is another in vitro tool to augment the utility of in vitro data for prediction of DDIs and understanding inhibition mechanisms. More examples of inhibition studies and, in particular, time-dependent inhibition studies of P450 by various drugs with thoughtful experimental designs to compare inhibition across in vitro systems are needed.

Such a comparison has been conducted for ENX using liver microsomes and hepatocytes from rats (Brown et al., 2010). In this study, inhibition of rat CYP1A2 by ENX was characterized using theophylline (conversion to 1,3-dimethyluric acid) as a well-established activity probe. When characterized as a reversible inhibitor, ENX caused 24-fold more potent inhibition of CYP1A2 activity in rat hepatocytes (K_i=120 μM) compared with rat liver microsomes (K_i=2800 μM). Note that the fractions unbound for ENX were 0.99 in both microsomes (measured) and intracellularly in hepatocytes (calculated). Thus, the dramatic difference in inhibition potencies could not be rationalized by protein binding. The authors ultimately concluded that the difference must lie with a high rate of hepatic uptake paired with the low metabolic clearance of ENX. The inhibition of theophylline turnover is, therefore, thought to be due to accumulation of ENX in rat hepatocytes (Yamano et al., 1999). However, as we have noted throughout this dissertation and as calculated by Obach et al. (2006), the reversible affinity constants for inhibition of CYP1A2 by ENX are too high to explain the DDI with theophylline in vivo.

To that end, we further characterized the time-dependent inhibition of CYP1A2 by ENX in HLM and primary human hepatocytes as a follow-up to our mechanistic studies in recombinant

CYP1A2 bactosomes in order to test the hypothesis that no significant systems effects were operative. We compared the inhibition parameters obtained in HLM and hepatocytes with those obtained in CYP1A2 bactosomes where these inhibition parameters may or may not be susceptible to system-dependent effects depending upon the inhibition mechanism. Accordingly, we hypothesize that, despite the increased complexity of HLM and hepatocytes, ENX will still inactivate CYP1A2 by the same mechanism (i.e., sequential metabolism to an MI complex) due to the apparent non-dissociative nature of CYP1A2 inactivation observed in CYP1A2 bactosomes. More generally speaking, we hypothesized that a non-dissociative process within the P450 active site can be translated across in vitro systems.

3.2 Experimental

3.2.1 Materials.

All chemicals from commercial sources were of analytical grade. Acetonitrile and water used in liquid chromatography were of Optima LC-MS grade and purchased from Fisher-Scientific (Santa Clara, CA). Enoxacin (1) sesquihydrate, enrofloxacin (internal standard), phenacetin, acetaminophen, benzamidoxime, benzamidine hydrochloride, N-methylhydroxylamine hydrochloride, NADPH/NADH co-factors, potassium ferricyanide, potassium cyanide, superoxide dismutase (SOD), and catalase (CAT) were purchased from Sigma-Aldrich (St. Louis, MO). CAY10566 (CAS# 944808-88-2) was purchased from Cayman Chemical (Ann Arbor, MI). The internal standard, methyl-labeled acetaminophen-d_3, was purchased from TLC PharmaChem (Vaughan, ON, Canada). N-hydroxy enoxacin (2), desethylene enoxacin (3), aniline enoxacin (4), N-formyl enoxacin (6), and the internally and externally N-formylated analogues of desethylene enoxacin (8 and 9) were synthesized in house by Dr. Kantipudi N. Babu and their identities were confirmed by NMR and mass spectrometry. The cyclic nitrone of enoxacin (11) and labeled N-hydroxy enoxacin (2; oxygen-18 label in the N-hydroxy group) were synthesized as described previously (see previous chapter). Oxygen-18 gas (99%, Stohler Isotope Chemicals) was a gift from the laboratory of Dr. Sid Nelson. The numbers in parentheses correspond to the structures in Figure 2.1 (see Chapter 2). All other chemicals were from Sigma-Aldrich unless specified.

3.2.2 Preparation of Human Liver Microsomes.

Frozen liver pieces from four human livers (HL135, HL141, HL147, and HL149 from the University of Washington Human Liver Bank, 10 grams per donor) were combined and thawed over ice in homogenizing buffer [50 mM potassium phosphate, pH 7.4, 0.25 M sucrose] (10 g of

liver per 50 ml buffer) and homogenized briefly at low speed using a Waring blender followed by five strokes in a glass-Teflon homogenizer kept in ice-water. The homogenate was centrifuged at 10,000 g for 30 minutes at 4°C. The supernatant was decanted and centrifuged at 108,000 g for 70 minutes at 4°C. The supernatant was discarded and the microsomal pellet was carefully separated from the lower, translucent glycogen pellet by gentle vortexing until the microsomal pellet came free while the glycogen remained adhered to the side of the tube. The microsomal pellet was transferred to a glass homogenizer and, after a brief homogenization, resuspended in KCl wash buffer [0.15 M KCl, 50 mM potassium phosphate, pH 7.4] (25 ml of buffer per 10 g of original liver weight) and centrifuged at 108,000 g for 70 minutes at 4°C. The resulting supernatants were discarded and the pellets were resuspended in homogenizing buffer. The final protein concentration was 15 mg/mL (BCA assay) and the P450 content was 315 pmol/mg (carbon-monoxide binding spectrum). Aliquots of suspended microsomes were stored at -80°C until use.

3.2.3 HPLC-MS/MS (MRM) Method for Quantification of Acetaminophen (APAP).

After work-up, samples from phenacetin o-deethylase activity assays were injected onto a Thermo Hypersil GOLD C_{18} column (100 x 2.1 mm, 1.9- µm particle) attached to a Waters ACQUITY UPLC pump (Waters Corp., Milford, MA). Separation was performed at a flow rate of 0.4 mL/min with a mixture of mobile phases (A: 0.1% formic acid in water; B: 0.1% formic acid in acetonitrile). Initially, mobile phase composition consisted of 90% A / 10% B and the %B was linearly increased to 40% over 2 minutes. The %B was then increased to 80% for 0.7 minutes before returning to the initial conditions and re-equilibrating. The total run time for each injection was 4.7 minutes. Acetaminophen and acetaminophen-d_3 eluted at 1.5 minutes and were detected by tandem mass spectrometry on an API-4000 Q-Trap triple-quadrupole mass spectrometer (AB Sciex, Foster City, CA). The instrument was operated in ESI-(+) mode with a

source temperature of 550°C and an ion spray voltage of 5000 V. The declustering potential, collision energy and collision cell exit potential were 60 V, 23 eV and 6 V, respectively, with mass transitions being monitored at 152 > 110 (m/z) for acetaminophen and 155 > 111 (m/z) for acetaminophen-d_3. Peak areas were normalized to that of the deuterated internal standard during data work-up.

3.2.4 HPLC-MS/MS (MRM) Method for Quantification of Enoxacin and Metabolites.

After work-up, samples from incubations were injected onto a Thermo Hypersil GOLD C_{18} column (100 x 2.1 mm, 1.9- µm particle) attached to a Waters ACQUITY UPLC pump (Waters Corp., Milford, MA). Separation was performed at a flow rate of 0.4 mL/min with a mixture of mobile phases (A: 0.1% formic acid in water, pH adjusted to 3.0 with ammonium hydroxide; B: 0.1% formic acid in acetonitrile). Initially, mobile phase composition consisted of 95% A / 5 % B and the %B was linearly increased to 34% over 7.5 minutes. The %B was then increased to 80% for 2.4 minutes before returning to the initial conditions and re-equilibrating. The total run time for each injection was 11.9 minutes. Analytes were detected by tandem mass spectrometry on an API-4000 Q-Trap triple-quadrupole mass spectrometer (AB Sciex, Foster City, CA). The instrument was operated in ESI-(+) mode with a source temperature of 400°C and an ion spray voltage of 4200 V. Mass transitions for each analyte along with instrument parameters are listed below in order of increasing retention time (RT). DP, CE, and CXP stand for declustering potential, collision energy, and collision cell exit potential, respectively.

[ANALYTE, RT; (*m/z* mass transition); DP, CE, CXP]: [desethylene enoxacin, 3.36 min; (295→257); 61, 35, 10], [enoxacin, 3.73 min; (321→234); 86, 31, 16], [nitrone enoxacin, 4.52 min; (335→246); 60, 30, 20], [nitrone+water enoxacin, 4.52 min; (353→246); 60, 30, 20], [enrofloxacin, 4.58 min; (360→316); 66, 27, 22], [aniline enoxacin, 5.25 min; (252→123); 61, 61, 10], [N-hydroxy enoxacin, 5.74 min; (337→274); 71, 43, 24], [N-formyl enoxacin, 6.46 min;

(349→231); 61, 51, 12], [CN-nitrone enoxacin, 6.68 min; (362→246); 60, 30, 20]. The following channel was left open to search for the nitroso enoxacin metabolite (structure 12 in Figure 2.1): [nitroso enoxacin, retention time unknown; (351→333); 60, 30, 20]. Peak areas were normalized to that of the internal standard, enrofloxacin, during data work-up.

3.2.5 HPLC-MS/MS (MRM) Method for Quantification of Benzamidine.

After work-up, samples from benzamidoxime (BZAO) reductase activity assays were injected onto a Thermo Hypersil GOLD C_{18} column (100 x 2.1 mm, 1.9- µm particle) attached to a Waters ACQUITY UPLC pump (Waters Corp., Milford, MA). Separation was performed at a flow rate of 0.4 mL/min with a mixture of mobile phases (A: 0.1% formic acid in water, pH adjusted to 3.0 with ammonium hydroxide; B: 0.1% formic acid in acetonitrile). Initially, mobile phase composition consisted of 90% A / 10% B and the %B was linearly increased to 85% over 4 minutes. The %B was then returned to the initial conditions for column re-equilibration. The total run time for each injection was 7 minutes. Benzamidine (BZA) eluted at 0.9 minutes and enrofloxacin (internal standard) eluted at 2.4 minutes and were detected by tandem mass spectrometry on an API-4000 Q-Trap triple-quadrupole mass spectrometer (AB Sciex, Foster City, CA). The instrument was operated in ESI-(+) mode with a source temperature of 400°C and an ion spray voltage of 3500 V. The declustering potential, collision energy and collision cell exit potential were 66 V, 27 eV and 22 V, respectively, with mass transitions being monitored at 121 > 104 (m/z) for BZA and 360 > 316 (m/z) for enrofloxacin. Peak areas were normalized to that of the deuterated internal standard during data work-up.

3.2.6 Identification of Metabolites by High-Resolution Mass Spectrometry.

Samples for metabolite identification were prepared by incubating HLM (1 mg/mL) with substrates in 0.1 M potassium phosphate buffer (pH 7.4) in the presence or absence of NADPH (1 mM). DMSO was present at 0.5% (v/v). All incubations were performed at 37°C for 30 minutes and then quenched by addition of an equal volume of ice-cold acetonitrile. Samples were centrifuged and an aliquot of supernatant was diluted into 3 volume equivalents of water in an LC vial. The samples were injected onto a Waters Synapt G2 Q-TOF mass spectrometer coupled to a Waters ACQUITY UPLC system equipped with a Thermo Hypersil GOLD (100 x 2.1 mm, 1.9- µm particle) C_{18} column. The mobile phase flow rate was set at 0.4 mL/min. Initial conditions for the LC gradient were 95% A (0.1% formic acid in water, pH adjusted to 3.0 with ammonium hydroxide) and 5% B (0.1% formic acid in acetonitrile). The %B was linearly increased to 55% over 8 minutes. The %B was then returned to 5% and the column re-equilibrated. The total run time for each injection was 10 minutes. Samples were ionized by electrospray ionization in positive ion mode. The source conditions were as follows: capillary voltage of 3.5 kV, cone voltage of 30 V, source temperature at 120°C, and desolvation temperature at 350°C. Ion m/z values were recorded in the 50 – 1000 m/z range. The instrument was calibrated immediately prior to analysis by infusion of sodium formate solution. Leu-enkephalin lock mass (556.2771 m/z) solution was simultaneously infused during each data collection and automatically-applied as a mass correction reference. Note that the retention times for some analytes shifted (≤0.25 minutes) across datasets due to the purchasing of new columns and slight reconfigurations of the HPLC system which occurred over the course of this study.

3.2.7 General Description of Microsomal Incubation Procedures.

Incubations were performed in polypropylene tubes or 96-well plates in a heated water bath. HLM were thawed on ice and diluted into 0.1 M potassium phosphate buffer (pH 7.4), usually to a final concentration in the range of 0.25 to 1.00 mg/mL. Substrates or inhibitors were generally added from DMSO stock solutions and the %DMSO in incubations did not exceed 1% of the incubation volume (in most experiments, DMSO was present at 0.5% (v/v)). Superoxide dismutase (SOD) and catalase (CAT), where used, were added at 50 μg/mL and 2000 U/mL, respectively. Incubations were run at 37°C and a 3-minute temperature equilibration period preceded initiation of the experiment. Generally, experiments were initiated by addition of NADPH dissolved in phosphate buffer to a final concentration of 1 mM. Incubations were quenched by addition of an equal volume of ice-cold acetonitrile containing 200 nM enrofloxacin (internal standard). The quenched incubations were then centrifuged and an aliquot of supernatant was diluted 4-fold into water prior to analysis by LC-MS or LC-MS/MS.

3.2.8 Time-Dependent Inhibition in Human Liver Microsomes.

Assays were carried out in 96-well polypropylene plates in a 37°C water incubator. Each inhibitor concentration was carried out in triplicate. Pre-incubation wells containing inhibitor and HLM (1 mg/mL) in 0.1 M potassium phosphate buffer (pH 7.4) were warmed to 37°C for 3 minutes. The incubation was initiated by addition of 20 μL of 10 mM NADPH dissolved in phosphate buffer. The final pre-incubation volume was 200 μL per well and contained 0.5% DMSO (v/v). At specified time points (generally 0.2, 1, 2, 4, 8, and 16 minutes), an aliquot (20 μL) of the pre-incubation mixture was diluted 10-fold into a CYP1A2 activity assay. Activity assays consisted of 100 μM phenacetin and 1 mM NADPH in phosphate buffer in a final volume of 200 μL per well. After 5 minutes, an aliquot (150 μL) of activity assay was quenched into 75 μL of ice cold ACN containing 15 pmol of acetaminophen-d_3. The quenched samples were

centrifuged at 13,000 x g for 10 minutes at 4°C. An aliquot (60 µL) of supernatant was transferred to a clean 96-well plate containing 140 µL of water per well and the samples were analyzed for APAP and APAP-d_3 by HPLC-MS/MS as described above.

3.2.9 Ferricyanide-Reversal in Human Liver Microsomes.

The procedure for ferricyanide reversal was similar to the time-dependent inhibition experiment, but with an additional treatment phase of either water (control) or potassium ferricyanide (treatment) after the pre-incubation phase but before the CYP1A2 activity incubation. HLM (1 mg/mL) were pre-incubated in the presence of vehicle (0.5% DMSO) or inhibitor and 1 mM NADPH for 30 minutes at 37°C. Each incubation was performed in quadruplicate. An aliquot of pre-incubation mixture was then diluted 1:1 into either water or 2 mM potassium ferricyanide in water (final concentration 1 mM $K_3Fe(CN)_6$) and incubated for 5 minutes. Finally, the water-treated and ferricyanide-treated HLM solutions were diluted 10-fold into CYP1A2 activity assay containing 100 µM phenacetin and 1 mM NADPH. Activity incubations were quenched at 8 minutes with ice cold acetonitrile containing acetaminophen-d_3. Acetaminophen and acetaminophen-d_3 were quantified by LC-MS/MS as described above.

3.2.10 CYP1A2 Component of Michaelis-Menten Parameters in Human Liver Microsomes

Assays were carried out in 96-well polypropylene plates in a 37°C water incubator. ENX metabolite formation rates were measured after a pre-incubation phase with vehicle (V) or furafylline (V_{FF}) to isolate the CYP1A2-mediated component of metabolism by subtraction of the rates ($V-V_{FF}$) and error propagation. Pre-incubation wells containing furafylline (10 µM) or vehicle (0.1% DMSO (v/v)) and HLM (2 mg/mL) in 0.1 M potassium phosphate buffer (pH 7.4) were warmed to 37°C for 3 minutes. The pre-incubation was initiated by addition of 20 µL of 20

mM NADPH dissolved in phosphate buffer. The final pre-incubation volume was 200 µL per well and contained 0.1% DMSO (v/v) and 2 mM NADPH. After a 5-minute pre-incubation, aliquots of pre-incubation mixtures were diluted 1:1 into phosphate buffer containing ENX at 2x the desired final concentration and 1% DMSO (v/v). The resulting incubations contained 1 mM NADPH, 1 mg/mL HLM (vehicle- or FF-pre-incubated), 0.55% DMSO (v/v) and ENX at concentrations of 15.625, 31.25, 62.5, 125, 250, and 500 µM. Each enoxacin concentration was carried out in triplicate. After 5 minutes, the incubations were quenched with an equal volume of ice-cold acetonitrile containing 200 nM enrofloxacin (internal standard). The quenched incubations were then centrifuged and an aliquot of supernatant was diluted 4-fold into water prior to analysis by an LC-MS/MS (MRM) method to quantify ENX metabolites as described above.

3.2.11 Spectral Scanning for MI Complex Formation in Human Liver Microsomes.

UV-Vis spectroscopy was performed on an Olis-modernized Aminco DW-2 spectrophotometer (Olis, Bogart, GA) operated in split-beam mode. The sample temperature was maintained at 25°C by a Julabo F30-C compact refrigerated circulator (Julabo USA, Inc., Allentown, PA). HLM were thawed on ice and diluted into 0.1 M potassium phosphate buffer (pH 7.4) containing NADPH. The solution was split into two 1-cm pathlength quartz cuvettes which were loaded into the spectrophotometer and the temperature was allowed to equilibrate for 5 minutes. Meanwhile, scans were taken to ensure a stable baseline. Scans were performed from 500- to 400-nm wavelength light at 1-nm intervals at a scan rate of ~1 scan per minute. To initiate the reaction, vehicle was added to the reference cuvette and inhibitor stock was added to the sample cuvette. In all cases, the total volume in each cuvette was 0.4 mL. The final concentrations of HLM and NADPH were 2 mg/mL and 1 mM, respectively. DMSO was present at 0.5% (v/v). Spectra were recorded repetitively over the course of about 25 minutes for N-OH-ENX or about 50 minutes for ENX.

3.2.12 Cryopreserved Human Hepatocytes: Thawing, Plating, and Incubation Conditions.

Cryopreserved primary human hepatocytes were removed from liquid nitrogen storage and quickly thawed in a 37°C water bath. Immediately upon thawing, cells were added to hepatocyte recovery media (K8000; XenoTech, LLC), spun at 100x g for 5 minutes at room temperature, and the resulting cell pellet was re-suspended in hepatocyte plating media (K8200; XenoTech, LLC). The cells were then plated in collagen-coated 96-well plates (Thermo Scientific Nalgene 152036) at a density of ~55,000 cells / well and placed in a 37°C incubator (5% CO2 and 95% relative humidity) for a 5 to 6-hour attachment period. After cell attachment, the plating media was removed and replaced with Hank's Balanced Salt Solution (HBSS) to a final volume of 200 μL/well at which point the cells were ready to be dosed.

3.2.13 Time-Dependent Inhibition in Plated Primary Human Hepatocytes

Hepatocytes were plated on 96-well collagen-coated plates as described above. To initiate a time-dependent inhibition assay, 80% of the volume in the well (160 out 200 μL of HBSS) was removed and replaced with an equal volume of HBSS containing inhibitor at (5/4)-fold the desired final concentration. The final %DMSO was 0.5% (v/v). Cells were pre-incubated with inhibitor in a 37°C incubator (5% CO2 and 95% relative humidity) followed by measurement of phenacetin o-deethylase activity at the desired time point. At this point, 160 μL was removed from the well and, to the remaining 40 μL, 110 μL of HBSS containing 136 μM phenacetin was added resulting in a final concentration of 100 μM phenacetin (0.2% MeOH (v/v)). Phenacetin o-deethylation activity assay was run for 15 minutes at 37°C before the entire well was quenched by addition of 150 μL of ice-cold acetonitrile containing 0.5 μM APAP-d_3. Supernatants were

analyzed by an LC-MS/MS (MRM) assay for quantification of APAP and APAP-d_3 as described above.

In one experiment, an intermediate cell washing procedure was employed after the pre-incubation phase, but before the phenacetin o-deethylase activity assay. The procedure for cell washing was to remove 80% of the volume in the well (160 out of 200 μL) and replace this volume with fresh HBSS. This procedure was performed three times resulting in a 125-fold dilution of the nominal inhibitor concentration initially present. The cells were then allowed to incubate in a 37°C incubator (5% CO2 and 95% relative humidity) for 30 minutes to allow inhibitor concentrations inside the cells to equilibrate with the diluted inhibitor concentrations in the HBSS. The phenacetin o-deethylase activity assay was then performed as described above.

3.2.14 Data analysis.

Mass spectral data was processed using MassLynx 4.10 (Micromass Ltd., Milford, MA) for high-resolution TOF data (Synapt G2 mass spectrometer) or Analyst software (AB SCIEX, Framingham, MA) for multiple-reaction monitoring (MRM) data (API-4000 mass spectrometer). Spectrophotometric data was processed using Olis Globalworks (Bogart, GA) and the maximum smoothing setting was applied (Digital-Filter [Savitzky-Golay] = 25).

For time-dependent inhibition analysis, natural log of residual CYP1A2 activity remaining was plotted against pre-incubation time in the presence or absence of inhibitor. The slope of the linear portion of the resulting line was calculated in Microsoft Excel (Redmond, WA). As described by equations 1 and 2, this slope is equal to the enzyme inactivation rate, λ.

$$A_t = A_o * e^{-\lambda t} \qquad (1)$$

$$LN\left(\frac{A_t}{A_o}\right) = -\lambda * t \qquad (2)$$

The enzyme inactivation rate, after correcting for background inactivation in the absence of inhibitor, was plotted against concentration of inhibitor in GraphPad Prism (San Diego, CA). The apparent inactivation parameters, k_{inact} and K_I, were estimated by non-linear regression using equation 3:

$$\lambda = \frac{k_{inact}\,[I]}{K_I + [I]} \qquad (3)$$

Errors, where displayed, are the standard deviation of the mean (typically, N=3). Standard practices for propagation of error were applied. Tests for statistical significance were performed in Microsoft Excel using Student's t-test (two-tailed, unpaired). Statistical significance was assumed at $P<0.05$. The use of asterisks in figures follows the convention: * ($P<0.05$), ** ($P<0.01$), and *** ($P<0.001$).

3.2.15 Static Prediction of CYP1A2 MBI on Active Enzyme and AUC_i/AUC.

Inactivation parameters K_I and k_{inact} were used to calculate an estimate of active CYP1A2 levels in a human liver exposed to circulating concentrations of enoxacin at a therapeutic dose. The maximal effect on active CYP1A2 levels is described by Equation 4 (Mayhew et al., 2000):

$$\frac{E'}{E} = \frac{k_{deg}}{k_{deg} + \lambda} \qquad (4)$$

The corresponding maximal effect on the fold-increase in AUC of a victim drug is described by Equation 5 (Mayhew et al., 2000):

$$\frac{\mathrm{AUC}'}{\mathrm{AUC}} = 1 + \frac{\lambda}{k_{deg}} \qquad (5)$$

AUC' and AUC are the area under the plasma concentration vs time curve for a victim drug in the presence and absence of inhibitor, respectively. The predicted AUC increase of specific victim drugs was then calculated by using the corresponding literature value for fraction metabolized by CYP1A2, $f_{m,\,CYP1A2}$, and equation 6 (Grimm et al., 2009):

$$\frac{\mathrm{AUC}'}{\mathrm{AUC}} = \frac{1}{\left(\frac{fm}{1+\lambda/\mathrm{k_{deg}}}\right)+(1-\mathrm{f_m})} \qquad (6)$$

All predictions were carried out using the above equations in Microsoft Excel.

3.3 Results

3.3.1 Evidence for MI Complex Formation in Human Liver Microsomes.

Incubation of N-OH-ENX (50 μM) with NADPH-supplemented HLM (2 mg/mL) resulted in a time-dependent absorbance increase at 452 nm λ_{max} in the UV-Vis difference spectra (Figure 3.1). In control incubations where the potent CYP1A2 mechanism-based inhibitor furafylline (FF) (10 μM) was co-incubated with N-OH-ENX, no absorbance increase near 450 nm was observed (data not shown). The time to reach half-maximal absorbance increase was ~2 ½ minutes, indicating that the approximate rate of MI complex formation was about 0.28 min^{-1}. By application of an extinction coefficient (65 $mM^{-1}cM^{-1}$; Pershing and Franklin (1982)) to the maximal delta absorbance (452-490nm), the final concentration of MI complex was estimated across three runs yielding an average concentration of 66 ± 15 nM. For comparison, the cytochrome P450 content of the HLM used in this experiment is ~315 pmol per mg of protein and, therefore, the total [P450] in the cuvette was ~630 nM at 2 mg/mL. Thus, the concentration of MI complex formed from incubation with N-OH-ENX constitutes ~10% of the total P450 present. This estimate is within the range of the percent CYP1A2 composition of total human microsomal P450 (Achour et al., 2014) and, combined with the evidence that MI complex formation could be blocked by FF, suggests that MI complex formation was occurring with the CYP1A2 isoform.

Incubation of ENX (50 μM) with NADPH-supplemented HLM (2 mg/mL) resulted in a similar time-dependent absorbance increase at ~451 nm (450-452 nm λ_{max} range) in the UV-Vis difference spectra (Figure 3.2). As was seen with N-OH-ENX, the absorbance increase near 450 nm was blocked when FF (10 μM) was co-incubated with ENX in HLM (data not shown). The rate of MI complex accumulation with ENX was markedly slower compared to incubations with N-OH-ENX. The absorbance increase [dAbs(451-490nm)] developed gradually over 50 minutes. However, the rate of MI complex formation from ENX could not be determined due to

an apparent spectral perturbation occurring at approximately 30 minutes into the incubation. We observed a transient increase in absorbance at 413 nm and a transient decrease in absorbance at 449 with an isosbestic point occurring near 432 nm (scans not shown). This spectral perturbation may have been due to sensitivity of heme or flavin to blue light from the spectrophotometer and was unrelated to MI complex formation as we also observed this spectral event in control incubations containing FF where no MI complex formation occurs. Ultimately, this transient event prevented accurate recording of the time course for absorbance increase near 450 nm, but did not interfere with detection of the MI complex after the spectral perturbation had ceased. The final average yield of MI complex, calculated using the above extinction coefficient, was 68 ± 28 nM which, in agreement with the yield of MI complex from incubation with N-OH-ENX, indicates that ~11% of the total P450 present in the microsomes formed an MI complex. As with N-OH-ENX, this percentage compares favorably with the average CYP1A2 content in microsomes. Due to the quantity of MI complex formed and the lack of MI complex formation from incubations containing the CYP1A2 inhibitor FF, we suspect MI complex formation from ENX, like N-OH-ENX, occurs with the CYP1A2 isoform of microsomal P450.

To confirm that the absorbance increases seen spectrally from ENX and N-OH-ENX were due to MI complex formation, we utilized potassium ferricyanide as a chemical reagent to lyse the MI complex and restore enzyme activity. We specifically assayed for CYP1A2 activity in HLM via a phenacetin o-deethylation activity assay at a concentration of phenacetin (100 μM) at which the majority of o-deethylation to yield acetaminophen (APAP) is due to the CYP1A2 isoform. HLM pre-incubated with FF (10 μM) and clorgyline (10 μM) served as positive controls for CYP1A2 inactivation by covalent mechanism-based inactivation (Kunze and Trager, 1993) and MI complex formation (Polasek et al., 2006), respectively. HLM pre-incubated with FF for 30 minutes lost more than 90% of phenacetin o-deethylase activity (7±1 %activity remaining)

relative to the vehicle control (Figure 3.3). Inhibition by FF was unaffected by ferricyanide (1 mM) treatment (8±2 %activity). HLM pre-incubated with clorgyline for 30 minutes resulted in >80% inhibition of phenacetin o-deethylase activity (14±1 %activity remaining), however, the activity was fully restored by treatment with ferricyanide (115±8 %activity). These results validated our ability to discriminate between covalent mechanism-based inactivation and MI complex formation in HLM using the ferricyanide-based reversal assay. Pre-incubation of HLM with ENX (50 μM) for 30 minutes resulted in ~50% inhibition of phenacetin o-deethylase activity (51±2 %activity remaining) and activity was partially restored by ferricyanide treatment (82±3 %activity remaining). Hence, more than half of the activity loss was restored by ferricyanide treatment and the increase (51±2→82±3 %activity remaining) was statistically-significant. HLM pre-incubated with N-OH-ENX (50 μM) for 30 minutes lost >80% of phenacetin o-deethylase activity (13±1 %activity remaining). Activity was fully-restored by ferricyanide treatment (115±4 %activity remaining) and this increase was statistically-significant (Figure 3.3). These results suggest that the majority of the inhibition of phenacetin o-deethylase activity in HLM caused by pre-incubation with ENX or N-OH-ENX can be attributed to MI complex formation. The results are also consistent with our previous investigation into the reversibility of inhibition by ferricyanide treatment in CYP1A2 bactosomes pre-incubated with ENX or N-OH-ENX (see Chapter 2; Figure 2.9).

3.3.2 Time-Dependent Inhibition in Human Liver Microsomes.

Loss of phenacetin o-deethylase activity over time was measured following pre-incubation of HLM with ENX (50 μM) or N-OH-ENX (50 μM) and NADPH (1 mM). At the concentration of phenacetin used (100 μM), the majority of phenacetin o-deethylation can be attributed to the CYP1A2 isoform in HLM as verified by pre-incubation with FF (10 μM) for 30 minutes which resulted in loss of >90% phenacetin o-deethylase activity (Figure 3.3). Time-dependent loss of

phenacetin o-deethylase activity from pre-incubation with ENX or N-OH-ENX was NADPH-dependent and we observed no apparent lag phase (Figure 3.4, A). The initial rates of activity loss were 0.033±0.005 and 0.256±0.024 min^{-1} for ENX and N-OH-ENX, respectively, when pre-incubated in the presence of NADPH which roughly translates to CYP1A2 half-lives of 21 and 3 minutes (Figure 3.4, B). In the absence of NADPH, the rates were 0.008±0.002 and 0.006±0.003 min^{-1} (approximate half-life of 100 minutes) for ENX and N-OH-ENX, respectively. Hence, the increased rates in the presence of NADPH were statistically significant for both ENX and N-OH-ENX. Further, the rates of activity loss seen in the absence of NADPH are, from our experience, typical for CYP1A2 in HLM and matches rates we have document for vehicle controls. These results demonstrate time- and NADPH-dependent loss of phenacetin o-deethylase activity in HLM caused by pre-incubation with ENX or N-OH-ENX. The rate of activity loss caused by the secondary hydroxylamine metabolite, N-OH-ENX, compared to the parent drug, ENX, was approximately 8-fold faster.

The apparent inactivation parameters K_I and k_{inact} were estimated for ENX and N-OH-ENX in HLM by measuring the initial inactivation rates (λ) caused by pre-incubation of HLM with a range of inhibitor concentrations followed by non-linear regression analysis of λ vs [inhibitor] plots using Equation 3 (Figures 3.5 and 3.6). Pre-incubation with ENX over a wide range of inhibitor concentrations (20 – 1000 μM) resulted in saturable inactivation kinetics (Figure 3.5). The maximal inactivation rate, $k_{inact,\ app}$, was estimated at 0.038±0.001 min^{-1} and the concentration of ENX resulting in half-maximal inactivation rate, $K_{I,\ app}$, was 24±3 μM. For the secondary hydroxylamine metabolite, N-OH-ENX, we only measured inactivation rates at three inhibitor concentrations (40, 80, and 160 μM) due to solubility limitations (Figure 3.6). A plot of λ vs [inhibitor] showed a significant degree of saturation in the inactivation rate and non-linear regression analysis was performed to estimate the apparent inactivation parameters. The

maximal inactivation rate, $k_{inact, app}$, was estimated at 0.49±0.02 min^{-1} and the concentration of N-OH-ENX resulting in half-maximal inactivation rate, $K_{I, app}$, was 35±5 μM.

In Table 3.1, the inactivation parameters obtained for ENX and N-OH-ENX in HLM are compared with those obtained in CYP1A2 bactosomes (data obtained in Chapter 2). Maximal inactivation rates (min^{-1}) for both ENX and N-OH-ENX were similar in both enzyme systems at 0.048±0.002 (bactosomes) vs 0.038±0.001 (HLM) for ENX and 0.44±0.04 (bactosomes) vs 0.49±0.02 (HLM) for N-OH-ENX. In both systems, the estimated maximal inactivation rate is approximately 10-fold faster for the secondary hydroxylamine metabolite, N-OH-ENX. The K_I, however, decreased by approximately 6-fold when the enzyme system was changed from bactosomes to HLM. Therefore, the CYP1A2 inactivation efficiencies for ENX and N-OH-ENX are greater in HLM than in CYP1A2 bactosomes. Interestingly, since the apparent K_I values decreased by about the same fold for ENX and N-OH-ENX, the N-OH-ENX:ENX K_I value ratios were the same in both systems at 1.6±0.3 (bactosomes) and 1.5±0.3 (HLM). Overall, these results show that the inactivation parameters obtained from these two enzyme systems were comparable with the exception of a considerable 6-fold decrease in apparent K_I values when moving from bactosomes to HLM.

3.3.3 Time-Dependent Inhibition in Primary Human Hepatocytes.

The time-dependent inhibition of CYP1A2 by ENX and N-OH-ENX was investigated in plated primary human hepatocytes (single donor; HC1-29). FF served as a positive control for inactivation of CYP1A2 with time. After pre-incubation for 0.1, 0.5, and 1.5 hours with ENX (20 μM), N-OH-ENX (20 μM), or FF (10 μM), phenacetin (100 μM) o-deethylase activity was measured and compared to vehicle controls (Figure 3.7). The % activities remaining at 0.1, 0.5, and 1.5 hours, respectively, after pre-incubation with inhibitor were 98±8, 74±11, and 64±6 for ENX, 68±9, 46±10, and 47±5 for N-OH-ENX, and 54±7, 46±3, and 41±6 for FF. Thus,

phenacetin o-deethylase activity decreased with pre-incubation time of inhibitor and the decrease was statistically-significant for all three inhibitors relative to vehicle controls at both the 0.5 and 1.5 hour time points. Notably, the differences in % activity remaining following pre-incubation with N-OH-ENX and FF (a potent mechanism-based inactivator of CYP1A2) were not statistically-significant at all three time points, although FF did appear to cause marginally faster activity loss. Comparison of the % activities remaining for FF at 0.5 and 1.5 hours suggests that inactivation of the CYP1A2-mediated component of phenacetin o-deethylase activity had reached completion by 1.5 hours. This suggests a high degree of background phenacetin o-deethylation by other enzymes in this particular lot of hepatocytes (HC1-29; Caucasian female, 24 years of age). Overall, the inhibitory potencies and apparent rates of time-dependent activity loss followed the expected trend for the three inhibitors (i.e., FF > N-OH-ENX > ENX). However, further experiments were not performed with this lot of hepatocytes as the high background phenacetin o-deethylase activity would complicate our efforts to more accurately determine CYP1A2 inactivation rates.

The remaining time-dependent inhibition experiments were performed in a different hepatocyte lot (H835; Hispanic male, 23 years of age) from the same vendor (XenoTech, LLC) which we verified, using FF, to have a much lower background level of non-CYP1A2-mediated phenacetin o-deethylation than HC1-29. Time-dependent loss of CYP1A2 activity was measured for ENX (2 and 20 μM), N-OH-ENX (2 and 20 μM), and FF (10 μM) over the course of 1.6 hours (Figure 3.8). After pre-incubation, the inhibitor-containing media was removed and replaced with media containing phenacetin (100 μM). The cells were not washed prior to addition of phenacetin. FF pre-treatment inactivated 90% of phenacetin o-deethylase activity in this lot of cells with an apparent half-life of 6 minutes. ENX did not cause detectable loss of phenacetin o-deethylase activity at 2 μM, however, at 20 μM ENX time-dependent loss of enzyme activity was observed with an apparent half-life of 48 minutes. A similar time-course of

activity loss and the same apparent half-life were observed for N-OH-ENX at a 10-fold lower nominal inhibitor concentration (2 μM). When N-OH-ENX was incubated at 20 μM, more rapid activity loss resulted and the apparent half-life was 12 minutes. Thus, the approximate CYP1A2 inactivation rates for ENX and N-OH-ENX at 20 μM in these hepatocytes were ~0.014 min^{-1} and ~0.058 min^{-1}, respectively. These rates are based upon loss of phenacetin o-deethylase activity over time without correcting for the non-CYP1A2 phenacetin o-deethylase activity and, therefore, these rates are conservative estimates. The rate for 20 μM ENX could be accurately predicted from the inactivation parameters obtained in HLM using Equation 3 where the calculated inactivation rate at 20 μM is 0.017 min^{-1}. The rate for 20 μM N-OH-ENX, however, was ~3-fold slower in hepatocytes (0.058 min^{-1}) than the predicted rate from HLM (0.18 min^{-1}). Nonetheless, we found that N-OH-ENX causes faster inactivation of CYP1A2 activity than ENX when these two species are compared at the same concentration whether the system is HLM or primary human hepatocytes.

To obtain estimates of the apparent inactivation parameters for ENX in hepatocytes, we measured inactivation rates across a range of inhibitor concentrations (5 – 200 μM) followed by non-linear regression analysis of λ vs [ENX] using Equation 3 (Figure 3.9). At 200 μM ENX, we observed evidence for a slight degree of reversible inhibition (~10-15%) of CYP1A2 by ENX at the first time point (0.6 minutes). ENX caused detectable time-dependent loss of phenacetin o-deethylase activity over the course of 24 minutes of pre-incubation time at all concentrations tested (Figure 3.9, A). This included concentrations of 5 and 10 μM ENX which are both within the range of circulating concentrations of ENX in humans following a therapeutic dose. However, the time-dependent loss of phenacetin o-deethylase activity appeared to cease after 12 minutes of pre-incubation with ENX. Although the time-course for CYP1A2 activity loss had deviated from log-linearity by 12 minutes, we used the pre-incubation times points 0.6, 6, and 12 minutes in order to have 3 points when calculating the slope (after log transform) of the

phenacetin o-deethylase activity remaining by linear regression. The final pre-incubation time point (24 minutes) was excluded when calculating the inactivation rates. The plot of λ vs [ENX] showed saturable inactivation kinetics (Figure 3.9, B) with an apparent maximal inactivation rate of 0.058±0.008 min^{-1} and a concentration of ENX resulting in half-maximal inactivation rate of 18±8 μM. Thus, the apparent inactivation parameters for ENX in primary human hepatocytes are very similar to those estimated in HLM ($k_{inact, app}$ of 0.038±0.001 min^{-1} and $K_{I, app}$ of 24±3 μM).

Since there is evidence that ENX is taken up into hepatocytes by active transport (Yamano et al., 1999; Maeda et al., 2007), it is possible that time-dependent accumulation of high concentrations of ENX inside the cells caused increasing potent reversible inhibition. We sought to confirm that the inhibition in hepatocytes was irreversible. Plated hepatocytes that had been pre-incubated with vehicle, ENX (50 μM), or N-OH-ENX (50 μM) for 1.6 hours were subjected to a washing procedure prior to measurement of phenacetin o-deethylase activity. The activity measures (normalized to vehicle controls) of the washed cells were then compared to those from cells which underwent the same pre-incubation procedure but no washing step to determine if washing the cells could alleviate all, or a sizeable fraction, of the inhibition. The washing procedure included a 125-fold dilution of the nominal inhibitor concentration (50 μM → 0.4 μM) followed by a "wash period" where the cells were allowed to incubate at 37°C for 30 minutes. The purpose of this "wash period" was to allow inhibitor concentrations inside the cells to re-establish equilibrium with the now relatively dilute inhibitor concentrations outside the cells. For cells pre-incubated with ENX or N-OH-ENX, the washing procedure resulted in statistically significant increases in phenacetin o-deethylase activity relative to cells from the "not washed" group (Figure 3.10). However, the increases in %activity remaining afforded by the washing procedure were marginal (40±5→49±5 for ENX and 18±1→26±1 for N-OH-ENX). Thus, the majority of the inhibition caused by pre-incubation of hepatocytes with ENX or N-OH-ENX was

not reversible to our washing procedure suggesting that the majority of the inhibition observed is irreversible.

3.3.4 Metabolism of ENX in Human Liver Microsomes.

Incubations of ENX (20 μM) with HLM (1 mg/mL) where either NADPH was excluded or the potent CYP1A2 inhibitor FF (10 μM) was co-incubated revealed that N-OH-ENX is the major NADPH-dependent metabolite of ENX and its formation is highly-dependent on the CYP1A2 isoform (Figure 3.11, left). N-OH-ENX (confirmed by retention time and accurate mass of authentic standard) was the only metabolite of ENX detectable in the full scan LC-MS chromatogram from incubation with NADPH-fortified HLM. Detection of additional metabolites required filtering out the exact monoisotopic masses of those species. By filtering for metabolites of 335.115±0.005 m/z value (the exact monoisotopic mass of NITRONE-ENX) we were able to detect two NADPH-dependent metabolite peaks (retention times of 3.65 and 4.19 minutes) which were not present when FF was co-incubated (Figure 3.11, right). The peak at 3.65 minutes was confirmed as NITRONE-ENX by comparison with authentic standard.

When N-OH-ENX (20 μM) was incubated with HLM (1 mg/mL), two NADPH-dependent peaks were found (Figure 3.12). NITRONE-ENX and ENX are the two detectable NADPH-dependent products in the full scan LC-MS chromatogram from incubation of N-OH-ENX in HLM. Thus, N-OH-ENX is further oxidized to NITRONE-ENX or, alternatively, N-OH-ENX can be reduced to the parent drug, ENX, in NADPH-dependent processes in HLM. The metabolite of ENX which was isobaric with NITRONE-ENX, but eluted at a later retention time (4.19 minutes; Figure 3.11), was not observed in incubations with N-OH-ENX in NADPH-fortified HLM.

FF (10 μM) effectively inhibited the conversion of ENX (20 μM) to N-OH-ENX or NITRONE-ENX in NADPH-fortified HLM (Figure 3.11). We ran a follow-up study comparing the

rates of ENX→N-OH-ENX and ENX→NITRONE-ENX after a 5-minute pre-incubation of HLM with FF (10 μM) or vehicle (0.1% DMSO) to determine the CYP1A2-mediated contribution to formation of these metabolites in HLM (Figure 3.13). In our experience, a 5-minute pre-incubation with FF (10 μM) inactivates ~85% of phenacetin o-deethylase activity in our specific HLM preparation which corresponds to inactivation of >90% of microsomal CYP1A2 assuming that ~10% of phenacetin-odeethylase activity (at 100 μM phenacetin) is due to other enzymes. Based on this assumption, the rates of metabolite formation in the vehicle pre-incubated HLM (V) and FF pre-incubated HLM (V_{FF}) were measured across a range of ENX concentrations and by subtraction of the latter from the former ($V-V_{FF}$) the resulting rates of metabolite formation were assumed to be due to CYP1A2 alone. Non-linear regression analysis was performed on the resulting V vs S plots to obtain apparent Michaelis-Menten parameters K_m and V_{max}. This analysis yielded apparent V_{max} (pmol/min/mg) values of 16±1 for ENX→N-OH-ENX and 2.4±0.1 for ENX→NITRONE-ENX with respective K_m (μM) values of 25±8 and 49±9 for the CYP1A2-mediated component of metabolite formation. Overall, it appeared that N-OH-ENX formation rates were much higher than those of NITRONE-ENX and that metabolite formation was most sensitive to FF pre-incubation at the lower concentrations of ENX. At the lowest concentration of ENX tested (15.625 μM), FF pre-incubation strongly inhibited (by ~80%) both N-OH-ENX and NITRONE-ENX formation.

3.3.5 Microsomal Stability of ENX and N-OH-ENX.

The stability of ENX (2 μM) in HLM (1 mg/mL supplemented with superoxide dismutase (SOD) and catalase (CAT)) was measured in the presence or absence of NADPH (1 mM) over time (Figure 3.14, A). No significant depletion of ENX was detected over a 64-minute incubation. NADPH-dependent formation of N-OH-ENX was observed with the level of N-OH-ENX appearing to level off at approximately 30 nM between the 32 and 64 minute time points. As

shown below, NOH-ENX is metabolized in HLM (Panel B) which may explain the leveling of the metabolite observed in Panel A. Thus, N-OH-ENX (the major NADPH-dependent metabolite of ENX in HLM) only reached low nM levels over the course of a 1-hour incubation and ENX was metabolically stable in NADPH-fortified HLM over this time period.

The stability of N-OH-ENX (2 μM) in HLM (1 mg/mL supplemented with SOD/CAT) was measured in the presence or absence of NADPH (1 mM) or NADH (1 mM) over time (Figure 3.14, B). Significant depletion of N-OH-ENX was observed in both NADPH- and NADH-fortified HLM, but N-OH-ENX was stable in the absence of co-factor. N-OH-ENX fell to levels below 1 μM by the 64 minute time point. On the same timescale, ENX was produced and reached a level of ~1 μM (50% of the initial concentration of N-OH-ENX) by 64 minutes. The time-courses for depletion of N-OH-ENX and formation of ENX were very similar whether NADPH or NADH served as the co-factor. However, oxidation of N-OH-ENX to NITRONE-ENX depended on NADPH and this reaction was not supported by NADH. The levels of NITRONE-ENX in NADPH-fortified HLM initially rose and then appeared to level off at approximately 30 nM. Thus, N-OH-ENX is susceptible to depletion in NADPH- or NADH-fortified HLM primarily through reduction to ENX.

3.3.6 Hydroxylamine Reductase: Reduction of N-OH-ENX vs Benzamidoxime.

We chose to further characterize the NADPH/NADH-dependent reduction of N-OH-ENX to ENX in HLM as this process may significantly control the accumulation of N-OH-ENX in incubations with ENX. While reduction of N-hydroxylated species in HLM remains a poorly understood process, the most studied example is the reduction of benzamidoxime (BZAO) to benzamidine (BZA) (Clement et al., 2000). We designed the following experiments to compare the reduction of these two substrates (N-OH-ENX vs BZAO) in HLM and explore the possibility

that N-OH-ENX is reduced to ENX by the same enzyme system (termed the “benzamidoxime reductase”) that reduces BZAO to BZA.

Michaelis-Menten parameters were estimated for both the NADH- and NADPH-supported reductions of N-OH-ENX and BZAO in HLM by measuring the reaction rates over 5 minutes (Figure 3.15). We observed reduction of both substrates in HLM supplemented with either co-factor. The kinetics of reduction appeared saturable. The NADH-supported reaction rates were faster for both substrates by ~2-fold relative to the NADPH-supported rates. Apparent V_{max} (pmol/min/mg) values were 202±6 vs 106±6 (NADH vs NADPH) for reduction of N-OH-ENX and 297±10 vs 128±7 (NADH vs NADPH) for reduction of BZAO. Hence, the maximal reduction rates were highly similar for these two substrates. Apparent K_m values were (in μM) 14±1 vs 30±5 (NADH vs NADPH) for reduction of N-OH-ENX and (in mM) 0.4±0.04 vs 0.6±0.1 (NADH vs NADPH) for reduction of BZAO thus indicating that N-OH-ENX was a higher affinity substrate by more than an order of magnitude.

We next determined if these two substrates could mutually inhibit the reduction of each other in HLM by measuring IC_{50} values (Figure 3.16). The substrates, N-OH-ENX and BZAO, were incubated at concentrations near their respective K_m values in NADH-fortified HLM. Inhibition caused by co-incubation with increasing concentrations of the other substrate was then determined. BZAO inhibited the reduction of N-OH-ENX with an IC_{50} value of 210±19 μM. N-OH-ENX inhibited the reduction of BZAO with an IC_{50} value of 33±2 μM. The lower IC_{50} value for N-OH-ENX compared to BZAO is consistent with the fact that N-OH-ENX is a high affinity substrate as indicated by the above K_m value measurements. Thus, N-OH-ENX and BZAO mutually inhibited the reduction of one another in HLM suggesting that the same enzyme system mediates reduction of both substrates. Further, we found that N-methylhydroxylamine (NMHA), reported to be a potent inhibitor of hydroxylamine reduction in HLM (Andersson et al., 2005), potently inhibited the NADH-supported reduction of N-OH-ENX and BZAO in HLM

(Figure 3.17). The IC_{50} values for inhibition of reduction of N-OH-ENX and BZAO (both incubated near their respective K_m values) by NMHA were nearly identical at 0.62±0.05 μM and 0.65±0.06 μM, respectively. These results further confirmed that the same enzyme system, "Benzamidoxime Reductase" reduces both substrates in HLM.

We measured the stability of this enzyme system over time by pre-incubating HLM in a time-dependent inhibition assay format where aliquots of pre-incubation mixture were diluted (5-fold) into an activity assay containing N-OH-ENX (100 μM) and NADH (1 mM) at the indicated time-points over 16 minutes of pre-incubation (Figure 3.18). Pre-incubation of HLM was performed in buffer alone or with co-factor or with co-factor +SOD/CAT. The co-factor present during pre-incubation was either 1 mM NADPH (Figure 3.18, A) or 1 mM NADH (Figure 3.18, B) and, in both cases, supplementation with SOD/CAT was presumed to protect against accumulation of reactive oxygen species. We found that the N-OH-ENX reductase activity was reasonably stable over time in buffer alone. However, activity was lost rapidly in HLM pre-incubated NADPH (half-life of ~3 minutes) with nearly complete loss of activity by the final pre-incubation time point (16 min). Activity loss for HLM pre-incubated with NADH was less pronounced, but still substantial with about half of the activity lost by the final pre-incubation time point. The co-factor- and time-dependent loss of N-OH-ENX reductase activity was completely prevented by supplementation with SOD/CAT suggesting, perhaps, a role for reactive oxygen species in destabilizing, inhibiting, or inactivating the N-OH-ENX reductase enzyme system.

We next pre-incubated HLM with NADPH (1 mM) for 20 minutes in the absence of SOD/CAT. A parallel incubation in the absence of NADPH served as the control. After the pre-incubation phase, both sets of HLM were pelleted by ultracentrifugation and the pellets were washed by rinsing with buffer. Pellets were re-suspended and supplemented with NADH (1 mM) and SOD/CAT. Time-courses for the reduction of N-OH-ENX to ENX (Panel A) and BZAO to

BZA (Panel B) were then measured for both sets of HLM (Figure 3.19). The reduction of both substrates was severely attenuated in the NADPH pre-treated microsomes relative to buffer pre-treated microsomes. Thus, pre-incubation with NADPH irreversibly inactivates the reductase activity for both N-OH-ENX and BZAO in HLM.

A panel of chemical inhibitors was tested on the NADH-dependent reduction of N-OH-ENX (15 μM) in HLM (1 mg/mL +SOD/CAT). Inhibitors of the cytochrome P450 isoforms 1A2, 2A6, 2S1, 3A4, 2C8, 2C9, 2C19, 2D6, and 2E1 and an inhibitor of stearoyl-CoA desaturase 1 (SCD-1) were utilized (Figure 3.20; inhibitor names listed therein). At concentrations of inhibitor which should have potently inhibited each respective enzyme, none of the inhibitors caused substantial inhibition of the reduction of N-OH-ENX. Small but statistically significant inhibition was observed with itraconazole and ketoconazole (CYP3A4 inhibitors), sulfaphenazole (CYP2C9 inhibitor), and quinidine (CYP2D6 inhibitor).

Finally, as our last effort to characterize reduction of N-OH-ENX vs reduction of BZAO in HLM, we measured reduction rates across a range of incubation buffer pH values (from 5.8 to 8.0). The rate of reduction of hydroxylamines in HLM is reported to optimize near pH 6.0 (Andersson et al., 2005). We found that NADH-supported reduction rates for substrates N-OH-ENX and BZAO were both enhanced in HLM by lowering the incubation pH from 8.0 to 5.8 (Figure 3.21). The magnitude of effect was greater for the N-OH-ENX→ENX reaction, however, both reactions appeared to be approaching an optimal pH near 5.8. These results further link the microsomal reduction of N-OH-ENX and BZAO to the same enzyme system.

3.3.7 Metabolism of ENX in Primary Human Hepatocytes.

We performed some preliminary investigations of the metabolism of ENX in hepatocytes. Generally speaking, the levels of metabolites generated in hepatocyte incubations were at the

limits of detection with the exception of the reduction of N-OH-ENX to ENX, which was easily detectable (data not shown). However, we were able to confirm that the following metabolic events took place in hepatocytes on the basis of high-resolution LC-MS and comparison with authentic standards. ENX (at 20 μM) is converted to N-OH-ENX in primary human hepatocytes. Conversion of ENX to N-OH-ENX depends on the presence of cells and is strongly inhibited (>50% inhibition) by FF (10 μM) suggesting that CYP1A2 is the primary isoform that N-hydroxylates ENX in hepatocytes (when ENX is present in the media at a nominal concentration of 20 μM). When N-OH-ENX (20 μM) is dosed to cells, reduction to ENX is observed. Reduction of N-OH-ENX to ENX depends on the presence of cells and is completely inhibited by N-methylhydroxylamine (100 μM nominal media concentration and delivered as the HCl salt). We have demonstrated (see Section 3.3.6) that N-methylhydroxylamine is a potent (submicromolar IC_{50}) inhibitor of the reduction of both N-OH-ENX and benzamidoxime in HLM. Hence, we can confirm that ENX can be converted to N-OH-ENX in hepatocytes and subsequently reduced back to ENX in a futile cycling process. The further oxidized metabolite of N-OH-ENX, NITRONE-ENX, was below the limits of detection in hepatocytes incubations.

3.3.8 Evidence for Non-Dissociative Inactivation of CYP1A2 by ENX.

Inactivation of CYP1A2 in HLM by ENX presents with no observable lag (Figures 3.4 and 3.5). If the inactivation of CYP1A2 caused by ENX is due to sequential metabolism to an MI complex, then it is possible that on-path intermediates (such as N-OH-ENX) will accumulate and compete with ENX for access to the CYP1A2 active site. However, in that case an initial lag phase would be expected to occur during the initial accumulation of N-OH-ENX and the inactivation of CYP1A2 would accelerate as the concentration of N-OH-ENX rises. The following experiment was designed to evaluate whether free N-OH-ENX competes with ENX to

meaningfully contribute to CYP1A2 inactivation over the time-course of a typical time-dependent inhibition experiment with ENX in HLM.

The initial rate of CYP1A2 inactivation caused by pre-incubation with ENX (100 μM) in NADPH-fortified HLM was measured and compared to rates from parallel pre-incubations of ENX (100 μM) spiked with N-OH-ENX at 0.5 or 5 μM (Figure 3.22, A). We also measured the concentration of N-OH-ENX present in the pre-incubation mixtures at the beginning (1 min) and near the end (15 min) of the pre-incubation phase (Figure 3.22, B) and this same analysis was performed for NITRONE-ENX (Figure 3.22, C). The rates of inactivation (min^{-1}) were 0.028±0.003, 0.029±0.003, and 0.037±0.004 for pre-incubation with ENX (100 μM), ENX & N-OH-ENX (100 & 0.5 μM), and ENX & N-OH-ENX (100 & 5 μM), respectively. There was no statistically significant difference in rate between ENX alone and ENX spiked with 0.5 μM N-OH-ENX. The rate from ENX spiked with 5 μM N-OH-ENX was marginally higher and this increase was statistically significant. The concentrations of N-OH-ENX (nM) at 1 min and 15 min in the pre-incubation mixtures were 22±0.5 and 155±6, 563±11 and 613±37, and, 4906±103 and 4401±127 for pre-incubation mixtures containing ENX (100 μM), ENX & N-OH-ENX (100 & 0.5 μM), and ENX & N-OH-ENX (100 & 5 μM), respectively. Thus, the concentration of N-OH-ENX increased (statistically significant) between 1 and 15 minutes for pre-incubation mixtures containing ENX (100 μM) and ENX & N-OH-ENX (100 & 0.5 μM). However, for the pre-incubation mixture containing ENX & N-OH-ENX (100 & 5 μM), the concentration of N-OH-ENX decreased (statistically significant) between 1 and 15 minutes into the pre-incubation. The concentrations of NITRONE-ENX (nM) at 1 min and 15 min in the pre-incubation mixtures were 5±0.2 and 19±1, 5±0.3 and 23±2, and, 12±1 and 41±2 for pre-incubation mixtures containing ENX (100 μM), ENX & N-OH-ENX (100 & 0.5 μM), and ENX & N-OH-ENX (100 & 5 μM), respectively. Thus, the concentration of NITRONE-ENX in the pre-incubation mixtures increased (statistically significant) between 1 and 15 minutes. These results show that N-OH-

ENX at 0.5 μM or below cannot compete with ENX (100 μM) to meaningfully contribute to the observed inactivation rate observed with ENX alone. Further, it appears that there is a limit on the quantity of N-OH-ENX that can accumulate in HLM during the pre-incubation.

3.3.9 Static Prediction of the DDI with CYP1A2 Substrates.

The predicted effect of ENX on the fold AUC increases (AUC_i/AUC) of two known in vivo substrates of CYP1A2, theophylline and caffeine, was estimated using the standard equation for a static, steady-state prediction of effect (Equation 6). The circulating concentration of ENX was fixed at 7.5 μM as studies where enoxacin was administered orally and measured in plasma at therapeutic doses provided C_{max} values that ranged from 8 to 16 μM (Yamaguchi et al., 1984; Marchbanks et al., 1990; Mizuki et al., 1996a; Hamel et al., 2000). The *in vivo* degradation rate for CYP1A2 (k_{deg}) was set at 0.00030 min^{-1} which corresponds to an enzyme half-life of 38.6 hours (Faber and Fuhr, 2004). The apparent inactivation parameters for ENX obtained in bactosomes (see Chapter 2; Figure 2.7), HLM (Figure 3.5), and primary human hepatocytes (Figure 3.9) were used to calculate the inactivation rates (λ) of CYP1A2 caused by 7.5 μM ENX in each given in vitro system and these rates were applied to the in vivo predictions.

The predicted fold AUC increases for theophylline ($f_{m,CYP1A2}$ = 0.80; Venkatakrishnan et al. (2007)) were 3.5-, 4.4-, and 4.7-fold using inactivation parameters obtained from CYP1A2 bactosomes, HLM, and hepatocytes, respectively (Table 3-2). The predicted fold AUC increases for caffeine ($f_{m,CYP1A2}$ = 0.95; Venkatakrishnan et al. (2007)) were 6.7-, 12.4-, and 15.1-fold for those same systems, respectively (Table 3-2).

Thus, our predicted interactions with theophylline agreed well with the literature value of 3.7 (Wijnands et al., 1986) using the in vitro inactivation parameters from all three vitro systems. The interaction with caffeine (literature value AUC_i/AUC = 5.7; Kinzig-Schippers et al. (1999)),

however, was only well-predicted using inactivation parameters from CYP1A2 bactosomes. Use of the inactivation parameters from HLM or hepatocytes resulted in an over-prediction of the effect by more than 2-fold.

3.4 Discussion

3.4.1 Chapter Overview and Hypothesis.

The current chapter builds upon the previous chapter (Chapter 2) where we demonstrated that ENX is sequentially metabolized in the CYP1A2 active site to an MI complex and further invoked this time-dependent enzyme inactivation process to account for the DDIs observed between ENX and CYP1A2 substrates in vivo. As the mechanistic studies performed in Chapter 2 utilized a recombinant CYP1A2 enzyme system (Bactosomes®), here (in Chapter 3) we sought to further characterize the inhibition of CYP1A2 by ENX in the more physiologically-relevant in vitro systems HLM and hepatocytes. HLM were prepared in-house from a pool of four livers (see Experimental) while primary human hepatocytes were purchased (XenoTech, LLC) in the cryopreserved state. HLM and cryopreserved human hepatocytes are perhaps the two most commonly utilized in vitro systems to study the inhibition of cytochrome P450 by drug molecules, particularly in the pharmaceutical industry (Soars et al., 2007; Fowler and Zhang, 2008), and the P450 inhibition data generated in these systems is commonly applied to the in vitro to in vivo prediction of DDIs. Thus, as part of our effort to compare the inhibition of CYP1A2 by ENX in multiple enzyme systems, we evaluated ENX as a time-dependent inhibitor of CYP1A2 in HLM and hepatocytes following our observation of NADPH-dependent TDI by ENX in CYP1A2 bactosomes. Further, we sought to confirm that the mechanism of inhibition determined in CYP1A2 bactosomes (i.e., sequential metabolism of ENX to an MI complex) is still viable in HLM and that ENX causes irreversible time-dependent loss of CYP1A2 activity in hepatocytes. The additional complexities of HLM and hepatocytes (compared to bactosomes) with respect to additional metabolic pathways and, in hepatocyte incubations, the cellular drug (and metabolite(s)) transport processes raises the possibility that inhibition of CYP1A2 by ENX may differ across systems in the manifestation of so called “system-dependent” effects (Parkinson et al., 2010).

However, as we have described (see Chapter 2) the sequential metabolism of ENX to an MI complex with CYP1A2 is likely a *non-dissociative* process. To review the mechanism, we proposed that ENX is oxidized three times on the terminal nitrogen of the piperazine ring with the final CYP1A2-catalyzed step being an oxidative ring-opening to a nitroso metabolite capable of coordinating tightly and quasi-irreversibly to the ferrous heme iron of CYP1A2. Most importantly, we determined that MI complex formation must result from a process where all three catalytic steps occur inside the CYP1A2 active site without release of intermediate metabolites (i.e., *non-dissociative* sequential enzyme inactivation). The stoichiometry of enzyme inactivation was low indicating that very few metabolites were released per CYP1A2 inactivation event and, further, we determined that the released metabolites do not contribute to CYP1A2 inactivation. These mechanistic characteristics of the sequential metabolic inactivation process are, in our view, absolutely essential to understanding the inhibition of CYP1A2 by ENX in multiple enzyme systems. We hypothesized that, explicitly due to the non-dissociative nature of MI complex formation from ENX, the inhibition of CYP1A2 will be conserved across in vitro systems and likely in vivo. In other words, the non-dissociative sequential CYP1A2 inactivation process is likely insusceptible to changes in the in vitro incubation matrix as ENX, upon binding to the CYP1A2 active site, can be converted to an MI complex with CYP1A2 without any requirement for accumulating intermediate metabolites. Additionally, this eliminates any concern over the likelihood that intermediate metabolites can feasibly accumulate in a given in vitro matrix where opposing processes may deplete concentrations of these metabolites available to CYP1A2 (e.g., active efflux out of hepatocytes, reductive enzymes converting products back to substrates, or conjugative enzymes or other oxidative enzymes depleting intermediate metabolites). Ultimately, we hypothesized that, provided CYP1A2 is adequately exposed to ENX, CYP1A2 will be inactivated via the time-dependent sequestering of active CYP1A2 into the inactive MI complexed state, regardless of the in vitro system used or, importantly, whether in vitro or in vivo.

Therefore, perhaps the most critical determinant of whether a non-dissociative sequential inactivation process is viable in a given in vitro system is the requirement that the inhibitor (ENX, in our case) can access the cytochrome P450 and, further, that the inhibitor is metabolically-stable enough to persist over the time period necessary for P450 inactivation to occur. Note that this means only the most basic requirements must be met for the effective inhibition of CYP1A2 by ENX in any system: (1) ENX must be able to access CYP1A2, and, (2) ENX must not be rapidly depleted. ENX is relatively metabolically stable in CYP1A2 bactosomes, HLM, hepatocytes, and in vivo. Further, ENX is not highly protein bound in plasma or microsomal incubations and it is calculated to be mainly unbound as free drug intracellularly in hepatocytes (Brown et al., 2010). ENX is also actively transported by the hepatic uptake transporter OATP1A2 (Maeda et al., 2007) and ENX accumulates 10- to 20-fold in rat liver and hepatocytes (Yamano et al., 1999). In Chapter 2, we demonstrated that our apparent CYP1A2 inactivation parameters adequately predicted the approximate 4- and 6-fold increases in the AUC of theophylline (Wijnands et al., 1986) and caffeine (Kinzig-Schippers et al., 1999), respectively, in vivo by assuming an inactivation rate (λ) calculated off the circulating concentration of ENX observed in blood. This says that even the circulating concentration of ENX would be an adequate exposure level to cause substantial CYP1A2 inactivation however, as explained by Brown et al. (2010), the combination of low metabolic clearance and a high rate of hepatic uptake results in the accumulation of ENX in hepatocytes. Thus, whether in recombinant P450, HLM, hepatocytes, or in vivo, we can find no reason why adequate ENX concentrations would not be present and accessible to CYP1A2 and, it then follows that we see no reason why the non-dissociative sequential inactivation process would not be viable in any system, including in vivo.

Equipped with the above mechanistic understanding and the hypothesis that inhibition of CYP1A2 by ENX will be conserved across systems, in this chapter we characterized the

inhibition of CYP1A2 by ENX in HLM and hepatocytes. Importantly, we found that ENX is metabolized to N-OH-ENX in HLM and that, at pharmacologically-relevant concentrations of ENX, FF potently inhibits N-OH-ENX formation from ENX suggesting that N-OH-ENX is being formed in the CYP1A2 active site from ENX. Both ENX and N-OH-ENX caused NADPH- and time-dependent inhibition of CYP1A2, as assayed by phenacetin o-deethylase activity, in HLM with the latter species being the faster inactivator, as was seen in CYP1A2 bactosomes and as is expected from our mechanism for MI complex formation. Both ENX and N-OH-ENX were metabolized to MI complexes with CYP1A2 in HLM as evidenced by spectral scanning and activity-based ferricyanide-reversal experiments, with N-OH-ENX causing more rapid and extensive MI complex formation. We could not confirm whether MI complex formation occurs in hepatocytes, but we did observe time-dependent loss of CYP1A2 activity with ENX and, at a faster rate, with N-OH-ENX in support of the proposed mechanistic pathway to the MI complex. Further, the inhibition of CYP1A2 in hepatocytes was mostly irreversible as diluting out the inhibitor concentration in the incubation media failed to alleviate most of the inhibition. The inactivation of CYP1A2 by ENX in HLM was non-dissociative as spiking in N-OH-ENX above the levels typically observed in ENX incubations failed to affect the inactivation rate. Also, with regard to N-OH-ENX, we documented a potential system-dependent effect in that N-OH-ENX is reduced back to the parent drug in HLM as part of a futile cycling process. However, as inactivation of CYP1A2 is non-dissociative and the free levels of N-OH-ENX do not impact the inactivation rate, it appears that the reduction of N-OH-ENX to ENX carries little to no meaning in the overall context of CYP1A2 inactivation and DDI prediction. Finally, we utilized the apparent inactivation parameters for ENX in HLM and hepatocytes to predict DDI values for theophylline and caffeine that were comparable with literature DDI values and the DDI values predicted from apparent inactivation parameters generated in CYP1A2 bactosomes. The above findings and potential reasons for the relative success in predicting the DDIs will be further discussed.

3.4.2 Inactivation of CYP1A2 in Human Liver Microsomes vs Bactosomes.

ENX and N-OH-ENX caused NADPH- and time-dependent inhibition of CYP1A2 in bactosomes and HLM. The N-hydroxylated primary metabolite, N-OH-ENX, caused more rapid TDI than ENX in both systems. The estimated metabolite to parent k_{inact} ratios are 9.2±0.9 and 13±0.6 in CYP1A2 bactosomes and HLM (Table 3.1), respectively, suggesting that at saturating concentrations of substrate N-OH-ENX inactivates CYP1A2 approximately 10-fold faster than ENX in both systems. Further, the apparent k_{inact} values for ENX and N-OH-ENX did not change dramatically when moving from CYP1A2 bactosomes to HLM (Table 3.1). Thus, the kinetic relationship for k_{inact} between inactivation of CYP1A2 by ENX and N-OH-ENX was reasonably conserved across the two systems. These results suggest that the catalytic properties of CYP1A2 with respect to sequential metabolism are similar in HLM and bactosomes.

The K_I values estimated for ENX and N-OH-ENX, however, are clearly lower in HLM than in bactosomes. For other drug molecules, dramatic differences in reversible affinity constants for a P450 enzyme, such as K_i, K_s, and K_m, have been documented in microsomes vs recombinant enzyme even when the measurements are made in the same laboratory setting and after any differences in protein-binding have been corrected for (Kumar et al., 2006). Interestingly, the apparent K_I values for ENX and N-OH-ENX both fell by approximately 6-fold in HLM resulting in the same metabolite to parent K_I ratios in both CYP1A2 bactosomes (1.6±0.3) and HLM (1.5±0.3). Further, in either system, ENX exhibits slightly higher affinity for CYP1A2 than does the metabolite, N-OH-ENX. The reason for the apparent 6-fold drop in K_I values is not known and it is interesting that the same fold-decrease is seen for both ENX and N-OH-ENX when moving across systems. For example, if the decreases were due to the interactions of ENX and N-OH-ENX with the in vitro matrix, then it would be more likely that each molecule would be differentially affected by the matrix effect owing to the zwitterionic nature of ENX and the acidic nature of N-OH-ENX and associated effects on the charge distributions in these molecules. In

fact, in Chapter 2, we saw that inactivation rates of CYP1A2 by ENX did not change across a 10-fold range of protein concentration in CYP1A2 bactosomes (Chapter 2; Figure 2.30, Panel D). It therefore seems unlikely that ENX was significantly protein bound in bactosomes incubations and, as the apparent K_I value in HLM is 6-fold *lower* it then does not follow that protein-binding plays a role in HLM either, consistent with the fraction unbound for ENX (f_u=0.99) in 1 mg/mL rat liver microsomes (we used 1 mg/mL HLM in our TDI assays; see Experimental) measured by Brown et al. (2010). Rather, the lower K_I values probably reflect a difference in the conformation or dynamics of CYP1A2 in HLM compared to bactosomes. Note that, CYP1A2 Bactosomes® (Cypex) contain the full-length native sequence human CYP1A2 and human cytochrome P450 reductase. Thus, these two proteins should be the same in both systems although we cannot speak to the presence or absence of post-translational modifications. CYP1A2 in an HLM environment may behave differently than CYP1A2 in bactosomes due to differing lipid content and composition as well as the interaction of CYP1A2 with a different collection of proteins. Ultimately, we can only speculate that the lower K_I values for ENX and N-OH-ENX in HLM relative to bactosomes are due to environment-induced differences in CYP1A2 and the interactions of CYP1A2 with a differing set of surrounding proteins in HLM.

Having established that ENX and N-OH-ENX both still function as time-dependent inhibitors of CYP1A2 in HLM, we sought to confirm that MI complex formation is still the relevant mechanism of CYP1A2 inactivation. MI complex formation from incubation of NADPH-fortified HLM with ENX (50 μM) was confirmed spectrally (Figure 3.2). Due to the turbidity of the HLM (2 mg/mL) and the low signal to noise for the MI complex peak, it was necessary to apply a smoothing algorithm to the spectral scans collected. Therefore, it was difficult to determine the true λ_{max} for the MI complex in these incubations, but λ_{max} appeared to fall in the 450-452 nm range. MI complex formation was also observed from incubation of HLM with N-OH-ENX (50

μM) as a more rapid absorbance increase with a λ_{max} at 452 nm (Figure 3.1). Note that 452 nm is the λ_{max} observed for the MI complexes from ENX and N-OH-ENX in CYP1A2 bactosomes. Since multiple P450 isoforms are present in HLM, it was important that the quantity of MI complex formed (~10% of total P450 in HLM), estimated by use of an extinction coefficient (65 $mM^{-1}cm^{-1}$; Pershing and Franklin (1982)), approximated the amount of CYP1A2 protein in HLM. The potent mechanism-based inhibitor of CYP1A2, furafylline, blocked MI complex formation from ENX and N-OH-ENX in HLM. Thus, we provided evidence that MI complexation is occurring to CYP1A2 specifically and that the MI complex formed has a similar λ_{max} to what was seen in CYP1A2 bactosomes.

The activity-based ferricyanide reversal assay was also used to demonstrate that ENX and N-OH-ENX are metabolized to an MI complex with CYP1A2 in HLM. The phenacetin o-deethylase activity lost during pre-incubation of NADPH-fortified HLM with either ENX or N-OH-ENX could be restored (statistically-significant) by ferricyanide treatment (Figure 3.3). Again, as was true with bactosomes (Chapter 2; Figure 2.9), the ferricyanide-mediated restoration of CYP1A2 activity was complete for CYP1A2 inactivated in the N-OH-ENX pre-incubation but only partial for CYP1A2 inactivated in the ENX pre-incubation. This result suggests that, in both CYP1A2 bactosomes and HLM, ENX may cause inactivation of CYP1A2 through MI complex formation (major mechanism) and possibly a second unknown inactivation process (minor mechanism). N-OH-ENX, in both CYP1A2 bactosomes and HLM, appears to inactivate CYP1A2 exclusively via MI complex formation.

Finally, we showed that ENX inactivates CYP1A2 non-dissociatively in HLM using an experimental design similar to how we demonstrated non-dissociative inactivation of CYP1A2 in bactosomes. Spiking in N-OH-ENX (0.5 μM) into an ENX (100 μM) incubation to a level >2-fold higher than the amount of N-OH-ENX formed in typical ENX incubations has no effect on the CYP1A2 inactivation rate relative to a comparable ENX (100 μM) incubation where no N-OH-

ENX was spiked (Figure 3.22; Panel A). Thus, free N-OH-ENX formed in ENX incubations does not contribute to the CYP1A2 inactivation rate. When we spike in a large quantity of N-OH-ENX (5 μM) into an ENX (100 μM) incubation, the inactivation rate increases (statistically-significant), but only marginally (<1.5-fold). This confirmed that N-OH-ENX can compete with ENX, but not at the concentrations seen in a typical ENX incubation. Interestingly, in this spiked incubation (100 μM ENX, 5 μM N-OH-ENX), the concentration of N-OH-ENX actually decreased (statistically-significant) between the 1-min and 15-min pre-incubation times (Figure 3.22; Panel B). Since we know that N-OH-ENX is unstable in HLM, primarily through NADH- or NADPH-dependent reduction to ENX (Figure 3.14; Panel B), it appears that N-OH-ENX is unable to accumulate beyond a certain level in ENX incubations. If our inactivation process were dissociative, the reduction of N-OH-ENX to ENX may have had a significant impact on the CYP1A2 inactivation rate. However, since inactivation of CYP1A2 by ENX appears to proceed non-dissociatively in HLM, the reduction of N-OH-ENX in the incubation matrix should not interfere with the inactivation process. These results show that the non-dissociative nature of the sequential metabolic inactivation process is conserved across systems from CYP1A2 bactosomes to HLM.

3.4.3 N-OH-ENX Reduction by the Benzamidoxime Reductase.

We characterized the NADH- and NADPH-dependent reduction of N-OH-ENX to ENX in HLM as this process may modulate the levels of free N-OH-ENX that form in ENX incubations and, further, may be important for understanding why N-OH-ENX is not a known in vivo metabolite. In mice, a dose of N-hydroxy norfloxacin administered orally was shown to have been quantitatively reduced to norfloxacin less than 30 minutes after administration and mice dosed with N-hydroxy norfloxacin exhibited a higher AUC of norfloxacin than did mice given the same dose (mg/kg) of norfloxacin (Uno et al., 1990). Thus, rapid and extensive reduction of an

N-hydroxylated fluoroquinolone compound (with high structural similarity to N-OH-ENX) has been demonstrated in vivo. Enzymatic reduction of a number of aliphatic and aromatic N-hydroxy compounds has been documented in HLM (Clement et al., 2000; Trepanier and Miller, 2000; Kurian et al., 2004; Andersson et al., 2005), with these reduction reactions requiring supplementation with NADH or NADPH co-factor. The identities of the hydroxylamine reductases are still debated. N-hydroxy compounds can also be reduced in mitochondrial and microsomal preparations from multiple human tissues including liver, adipose, kidney, intestine, colon, and lung (Andersson et al., 2005) highlighting the ubiquity of hydroxylamine reductases. Importantly, these reduction reactions are operative in aerobic microsomal and mitochondrial incubations suggesting that enzymatic reduction processes may considerably alter the accumulation rate of N-hydroxylated metabolites in typical P450 inhibition assays.

Our approach to studying the microsomal reduction of N-OH-ENX to ENX was to compare it with the reduction of benzamidoxime (BZAO). BZAO is reduced in NADH- or NADPH-fortified HLM to benzamidine (BZA) and this process is attributed to an unidentified enzyme system known as the “benzamidoxime reductase” (Clement et al., 2000). In pig liver microsomes, the “benzamidoxime reductase” has been isolated and described as a cytochrome P450 enzyme of the CYP2D family (Clement et al., 1997). However, at the time of writing this dissertation, an analogous hydroxylamine-reducing P450 in HLM has not been identified and the identity of the human liver microsomal benzamidoxime reductase remains unknown. As reduction of BZAO to BZA is one of the most well-studied microsomal reduction reactions, we sought to determine if perhaps N-OH-ENX and BZAO are reduced by the same enzyme(s) in HLM.

Our finding that N-OH-ENX and BZAO mutually inhibit the reduction of each other in NADH-fortified HLM (Figure 3.16) strongly supports the notion these substrates compete for the same enzyme active site(s) and are, therefore, reduced by the same enzyme(s). N-methylhydroxylamine, a potent inhibitor of the benzamidoxime reductase (Andersson et al.,

2005), inhibited the reduction of both N-OH-ENX [IC_{50}(μM) 0.62±0.05] and BZAO [IC_{50}(μM) 0.65±0.06] with nearly identical IC_{50} values (Figure 3.17), further supporting a shared enzyme system. We also demonstrated that the reduction reactions for N-OH-ENX and BZAO in HLM share the same dependence on pH value (Figure 3.21) where lowering the pH from physiological (7.4) to pH 5.8 enhances the reaction rates (N-OH-ENX→ENX and BZAO→BZA). This enhancement of rates upon acidification with an approximate pH optimum near 6.0 is in agreement with results reported by Clement et al. for the benzamidoxime reductase and by Andersson et al. (2005) for reduction of N-hydroxy melagatran in HLM.

Since the benzamidoxime reductase from pig liver is known to be a P450 enzyme, we tested a panel of cytochrome P450 inhibitors to see if any of these molecules blocked reduction of N-OH-ENX (15 μM) in NADH-fortified HLM (Figure 3.20). One of these inhibitors, miconazole, was used at a high concentration (12 μM) to inhibit CYP2S1 (Fromel et al., 2013) as this P450 isoform is known to reduce aromatic hydroxylamines (Wang and Guengerich, 2013). The inhibitor CAY10566 (2 μM) was used to inhibit stearoyl-CoA desaturase (SCD) as SCD has been reported to reduce benzamidoxime (Reh et al., 2008). The remaining P450 inhibitors (2 μM) are commonly-used inhibitors of specific P450 isoforms (Lin and Lu, 1998) as noted in Figure 3.20. At the concentrations used, these inhibitors should have potently inhibited each respective enzyme. However, no such potent inhibition was observed for the reduction of N-OH-ENX when this substrate is incubated close to the apparent K_m value for reduction to ENX. Thus, we were unable to identify the hydroxylamine reductase as SCD, CYP2S1, or any of the common hepatic drug-metabolizing P450 enzymes.

Although we could not identify the hydroxylamine reductase, we made the startling discovery that a simple pre-incubation of HLM with NADPH, rapidly and irreversibly inactivates the hydroxylamine reductase activity (Figures 3.18 and 3.19) for both N-OH-ENX and BZAO. Interestingly, the time-dependent inactivation of the unknown reductase enzyme(s) could be

completely protected against by supplementing the NADPH-fortified HLM with superoxide dismutase and catalase. This is, to our knowledge, the first report of any kind of time-dependent inactivation for hydroxylamine reductase activity in HLM. However, the implied enzyme inactivation mechanism, which almost certainly involves enzyme degradation by reactive oxygen species, is consistent with observations made by Clement et al. (1997) where the activity of the benzamidoxime reductase isolated from pig liver microsomes could be enhanced by supplementation with superoxide dismutase. Thus, the NADPH-dependent inactivation of reductase activity, apparently due to generation of reactive oxygen species, further links the reduction of N-OH-ENX and BZAO to the same enzyme, the “benzamidoxime reductase”, and perhaps provides new information that may help in identifying the enzyme.

Thus, the enzymatic reduction of N-OH-ENX in HLM was characterized and linked to the benzamidoxime reductase. Ultimately, we concluded that the reduction of N-OH-ENX in HLM is unlikely to affect the CYP1A2 inactivation process as the sequential metabolic inactivation of CYP1A2 by ENX appears to be non-dissociative. Therefore, this portion of the dissertation can be considered an auxiliary study that we initiated due to interest in potential futile cycling between ENX and N-OH-ENX and, unbeknownst to us at the time, this process turns out to be unimportant in the overall context of CYP1A2 inactivation. However, this information may be useful in a larger context as our understanding of microsomal hydroxylamine reduction reactions continues to develop. The identity of the enzyme systems responsible for hydroxylamine reductions in HLM remains to be determined and the importance of hydroxylamine reduction reactions in vivo is perhaps not yet fully realized and appreciated.

3.4.4 Inactivation of CYP1A2 in Primary Human Hepatocytes vs Human Liver Microsomes.

As just discussed for the reduction of N-OH-ENX in HLM, each in vitro system will present with a unique set of system-dependent effects which may or may not be meaningful in the context of inhibition of CYP1A2 by ENX. The current section explores the time-dependent inhibition of CYP1A2 by ENX in human hepatocytes. We should begin this section by acknowledging that, as a field, our understanding of how to utilize hepatocytes in P450 inhibition studies and, in particular, in *time-dependent* inhibition studies is still in the early stages relative to our ability to perform such studies with recombinant P450 or HLM. Just as importantly, it is difficult to interpret data from hepatocytes due to the dynamic nature of cells and the dynamics of intracellular drug and metabolite concentrations. Wherever possible, we will attempt to warn the reader of any caveats in our interpretation of data generated in human hepatocytes.

Our initial efforts to characterize time-dependent inhibition of CYP1A2 in a particular lot of hepatocytes (HC1-29; Caucasian female, 24 years old) highlighted one of these caveats. We found that ENX and N-OH-ENX (each at 20 μM) caused time-dependent loss of phenacetin (100 μM) o-deethylase activity in this lot of hepatocytes over the course of 1.5 hours, with the latter species (N-OH-ENX) causing a more rapid time-dependent loss (Figure 3.7). These results are consistent with our mechanism for MI complex formation and with the results seen in HLM and bactosomes. However, between the 0.5 and 1.5 hour pre-incubation time points, it appeared that N-OH-ENX ceased to cause time-dependent loss of phenacetin o-deethylase activity even though a sizeable fraction (~40% relative to the vehicle control) of the activity remained. The same was true of our positive control mechanism-based inhibitor (of CYP1A2) furafylline (10 μM) which caused rapid time-dependent loss of phenacetin o-deethylase activity initially, but then failed to lower the activity much beyond ~40% activity remaining between 0.5 and 1.5 hours of pre-incubation. Note that in HLM, when phenacetin is used at the same

concentration (100 μM) in the activity assay, both furafylline and N-OH-ENX cause time-dependent loss of phenacetin o-deethylation to a level of ~10% activity remaining indicating that phenacetin (at 100 μM) is a reasonably specific probe substrate of CYP1A2. The large fraction of phenacetin o-deethylase activity remaining (~40%) after 1.5 hours of pre-incubation with furafylline confirms that hepatocyte lot HC1-29 (XenoTech, LLC), in our hands, exhibits a high degree of non-CYP1A2 mediated phenacetin o-deethylation. Thus, the dynamic range for evaluating loss of CYP1A2-specific phenacetin o-deethylase activity in these cells was severely compromised relative to what we observed in HLM. We chose not to perform further experiments in this lot of hepatocytes due to this limited dynamic range and associated complications this creates for interpreting the results.

Subsequently, in the next lot of hepatocytes used (H835; Hispanic male, 23 years old), we noted that furafylline (10 μM) caused a similarly rapid time-dependent loss of phenacetin o-deethylase activity (Figure 3.8), but this time the % activity remaining appeared to level off at ~10% indicating that the dynamic range for CYP1A2-specific phenacetin o-deethylation in these cells was superior to the previous lot of cells and similar to that seen in HLM. We further confirmed time-dependent loss caused by pre-incubation with ENX (20 μM) and N-OH-ENX (2 and 20 μM) and observed that in this lot of cells N-OH-ENX causes faster time-dependent inhibition than ENX (comparison made at 20 μM). Thus the rank order is preserved across systems; N-OH-ENX inactivates CYP1A2 faster than ENX in CYP1A2 bactosomes, in HLM, and, as confirmed in two separate donors, in primary human hepatocytes. This finding is particularly significant in human hepatocytes because (1) we have no means to confirm MI complex formation occurred in the cells, and (2) the relationship between nominal and intracellular concentrations of ENX and N-OH-ENX is not known. With respect to point (1), faster time-dependent loss of activity caused by N-OH-ENX supports MI complex formation as the mechanism of inactivation. With respect to point (2), since there is evidence for substantial

hepatic uptake of ENX (Yamano et al., 1999), it was not clear whether head-to-head comparisons of ENX vs N-OH-ENX would be confounded by preferential uptake of ENX over N-OH-ENX into hepatocytes.

In fact, while the relationship for faster inactivation by N-OH-ENX held up in hepatocytes, the ratio of the inactivation rates for N-OH-ENX:ENX at 20 μM was much lower (at ~4.1) than the calculated ratio of inactivation rates using apparent inactivation parameters from HLM (at 10.3). Therefore, it appears that even though N-OH-ENX causes faster time-dependent inhibition than ENX in hepatocytes, compared to what is predicted from HLM, ENX displays an advantage over N-OH-ENX in this system. In other words, N-OH-ENX was expected to inactivate CYP1A2 ~10-fold faster than ENX, but only did so at ~4-fold faster. One interpretation of this result is that ENX is being actively taken up into hepatocytes at a greater rate than N-OH-ENX, thus giving ENX the competitive (no pun intended) edge. It is interesting to note, however, that the rates of inactivation by ENX (20 μM) in HLM and hepatocytes both line up at approximately the same number (~0.015 min^{-1}). In light of this fact, the interpretation of what is happening almost certainly must shift as ENX, at a nominal concentration of 20 μM, exhibits the same inactivation rate in hepatocytes as it did in HLM thus displaying no advantage in hepatocytes. As must mathematically follow, it was the inactivation rate exhibited by N-OH-ENX that was actually slower in hepatocytes (by ~3-fold) than predicted from HLM. While the overall rate analysis argues against substantial uptake of ENX, an explanation where ENX can more effectively enter and remain in the hepatocytes than N-OH-ENX is still viable. However, due to our knowledge that N-OH-ENX is reduced to ENX in HLM (Figure 3.12) and mitochondria (data not shown), a more appealing explanation is that N-OH-ENX cannot persist (i.e. is rapidly reduced to ENX) within the small volume of the hepatocyte where this reduction could have a significant effect on the concentration of N-OH-ENX. We did, in fact, observe reduction of N-OH-ENX to ENX in hepatocyte incubations that could be inhibited by N-methyl hydroxylamine (data

not shown). If, upon entry into the hepatocyte, N-OH-ENX is reduced to ENX before it can bind to CYP1A2, then inactivation of CYP1A2 by N-OH-ENX will be significantly impeded in hepatocytes and the observed rate of inactivation will be brought effectively closer to that of ENX. That is to say, relative to HLM where the N-OH-ENX concentration is not severely affected by hydroxylamine reductase activity on the timescale of CYP1A2 inactivation, in a hepatocyte N-OH-ENX may be getting reduced on a timescale that competes with its timescale for entering the cell. In that situation, hydroxylamine reduction could greatly influence the intracellular concentration of N-OH-ENX and, as must follow in this scenario, ENX would then be present to competitively inhibit N-OH-ENX from binding to CYP1A2 (i.e. “protection” of CYP1A2 from a fast time-dependent inhibitor by a slower time-dependent inhibitor). Ultimately, we cannot confirm the true mechanism for the slower than expected rate of inactivation exhibited by N-OH-ENX. As highlighted at the beginning of this section, the interpretation of data generated in hepatocytes is extremely complicated due to the dynamics of the cells and, as now demonstrated, an uncertainty in the intracellular concentrations of inhibitor.

We attempted to address the issue of uptake into hepatocytes and whether or not this factor (a system-dependent effect not relevant to HLM or bactosomes) may have influenced the observed time-dependent inhibition of phenacetin o-deethylase activity. Our approach to this problem was to pre-incubate hepatocytes with inhibitor for 1.6 hours and then “wash” the hepatocytes to dilute the nominal inhibitor concentration down by ~125-fold followed by 30 minutes of further incubation at 37°C for the intracellular concentration of inhibitor to equilibrate with the (now 125-fold diluted) media concentration of inhibitor. The phenacetin o-deethylase activity remaining for “washed” cells was then compared with cells which had been pre-incubated with inhibitor but not washed to determine if the washing procedure could alleviate the inhibition. We would then interpret any alleviation of the inhibition as the reversible component of inhibition while any lack of alleviation would signify an irreversible component of inhibition.

Our result, following pre-incubation for 1.6 hours with ENX or N-OH-ENX (both at nominal concentrations of 50 μM) was that the cell washing procedure statistically-significantly alleviated a small amount of the inhibition caused by both inhibitors (i.e. there was a detectable reversible component), however the vast majority of the inhibition appeared to be irreversible for both inhibitors. Since we cannot directly verify that the above described washing procedure effectively reversed any accumulation of ENX or N-OH-ENX into hepatocytes, we say with caution and a degree of uncertainty that reversible inhibition of CYP1A2 by ENX or N-OH-ENX does not meaningfully contribute to the observed inhibition caused by pre-incubation with these species.

Finally, having established evidence for irreversible time-dependent inhibition of CYP1A2 by ENX in hepatocytes and having supported the proposed mechanism for MI complex formation (N-OH-ENX is still a faster inactivator), we moved forward to measure apparent inactivation parameters for ENX in hepatocytes (Figure 3.9). Unfortunately, the time-dependent inhibition plots presented with a plateau in the % activity remaining at ~50% suggesting a severely attenuated dynamic range of CYP1A2-specific phenacetin o-deethylase activity on the particular day this experiment was run even though on a prior day, the furafylline positive control had indicated that complete CYP1A2 inactivation could decrease the % remaining activity to ~10% in this same lot of cells (H835; XenoTech, LLC) (Figure 3.8). Furafylline was not present as a positive control in this specific experiment (Figure 3.9) and, in addition, we have never observed a % phenacetin o-deethylase activity remaining substantially below 50% caused by pre-incubation of hepatocytes with ENX. As a result, it was impossible to determine if the dynamic range for CYP1A2-specific phenacetin o-deethylation had actually narrowed on this day (perhaps due to variability associated with thawing and plating cryopreserved cells) or if a plateauing effect near 50% activity remaining is a characteristic of ENX as a time-dependent inhibitor in hepatocytes by an unknown mechanism. In addition to the pre-mature plateauing of

time-dependent activity loss, the standard deviations associated with the activity measures in this experiment were somewhat higher than desired. Nonetheless and despite some deviation from log-linearity by the third time point, we performed linear regression on the first three time points (0.6, 6, and 12 minutes) in the log-transformed % activities remaining plot (Figure 3.9, A) to estimate rates of inactivation. The rates were plotted vs [ENX] and nonlinear regression analysis corresponding to Equation 3 was carried out to estimate apparent inactivation parameters. While the errors on the rate estimates were high, we observed strong evidence for saturation of the inactivation rates over the range of 5 μM to 200 μM ENX and the nonlinear analysis provided a good fit to the rates. The apparent inactivation parameters for ENX in human hepatocytes, K_I(μM)=18±8 and k_{inact}(min^{-1})=0.058±0.008, are questionable estimates due to the above caveats. However, these estimated parameters are surprisingly similar to the apparent inactivation parameters for ENX in HLM, K_I(μM)=24±3 and k_{inact}(min^{-1})=0.038±0.001, suggesting that our poorly estimated inactivation parameters in hepatocytes may have at least landed within range of the correct values.

To reiterate, the data we have generated in hepatocytes may be justifiably questioned due to a variety of uncertainties surrounding the dynamics of the cells. We find the data in hepatocytes to be worth considering, but not necessarily relied upon. While hepatocytes are a more complete in vitro system for characterizing inhibition of P450 and possibly more reflective of in vivo, the limitations and the associated difficulties in measuring rates in hepatocytes juxtaposes with the reliability and ease of use for HLM and CYP1A2 bactosomes. However questionable the data, we were able to generate inactivation rates that were faster for N-OH-ENX than ENX, and observed saturation of inactivation rates at higher concentrations of ENX leading to estimation of the apparent inactivation parameters that can be used in the DDI prediction calculation.

3.4.5 DDI Prediction.

DDIs with the CYP1A2 substrates theophylline and caffeine were well-predicted using the apparent inactivation parameters for ENX in CYP1A2 bactosomes (Chapter 2). In the current chapter (Chapter 3), we obtained the inactivation parameters for the parent drug, ENX, in HLM and human hepatocytes and repeated the in vitro to in vivo static prediction process. The results of the DDI predictions for theophylline (f_m=0.80; Venkatakrishnan et al. (2007)) and caffeine (fm=0.95; Venkatakrishnan et al. (2007)) using inactivation parameters obtained in all three in vitro systems are presented in Table 3.2 for side-by-side comparison with the literature values for theophylline (3.7-fold AUC increase; Wijnands et al. (1986)) and caffeine (5.7-fold AUC increase; Kinzig-Schippers et al. (1999)). As described in the results, the interaction with theophylline was well-predicted from all three in vitro systems while the interaction with caffeine was well-predicted from CYP1A2 bactosomes, but over-predicted (by ~2-fold) from HLM and human hepatocytes. Overall, the predictions are reasonably accurate, even where off by 2-fold. It is perhaps better that we have over-predicted in a few instances rather than underpredicted because the in vivo DDI data with theophylline (Wijnands et al., 1984; Wijnands et al., 1986) seems to indicate a nearly complete “knock-out” of CYP1A2. The extent to which we over-predict the DDI may expose inaccuracy in other variables such as, for example, if the f_m values do not reflect the true CYP1A2 component of clearance in these studies. More useful to us is that over-prediction provides some degree of tolerance for other in vivo processes that may attenuate the CYP1A2 inactivation process. As the in vivo DDI seems to reflect a nearly complete “knock-out” of CYP1A2, it would seem advantageous that our inactivation parameters in conjugation with the circulating concentration of ENX predict a DDI as severe or more severe than the literature DDI. The reason that the over-prediction is fairly confined to caffeine is simply due to the high f_m value given for caffeine (0.95) by the literature reference above making caffeine more sensitive to changes in the inactivation parameters. In this regard it is important to

note that the fraction of CYP1A2 activity remaining does not depend upon f_m. Overall, we find the DDI predictions compare very favorably with the literature.

3.4.6 Conclusions.

The use of a variety of in vitro systems is commonly employed to study cytochrome P450 inhibition and the potential for such inhibition to elicit clinically-relevant DDI. In this chapter, we characterized inhibition of CYP1A2 in HLM and hepatocytes as a follow-up to our inhibition study conducted in recombinant CYP1A2 (Chapter 2). As just discussed in the previous section, the application of inactivation parameters obtained in these three in vitro systems performed exceptionally-well in the static in vitro to in vivo prediction of DDIs with theophylline and caffeine. Here we relied upon inactivation parameters from the parent drug, ENX, to predict CYP1A2 inactivation caused by a metabolite of ENX. In our view and supported by the evidence presented, this is only possible because ENX is sequentially metabolized to inactivate CYP1A2 in a non-dissociative process without release from the CYP1A2 active site meaning ENX can be treated, kinetically, as a one-step inactivator for predictive purposes. As hypothesized, we found evidence that ENX is sequentially metabolized to an MI complex with CYP1A2 and that this process was conserved across in vitro systems.

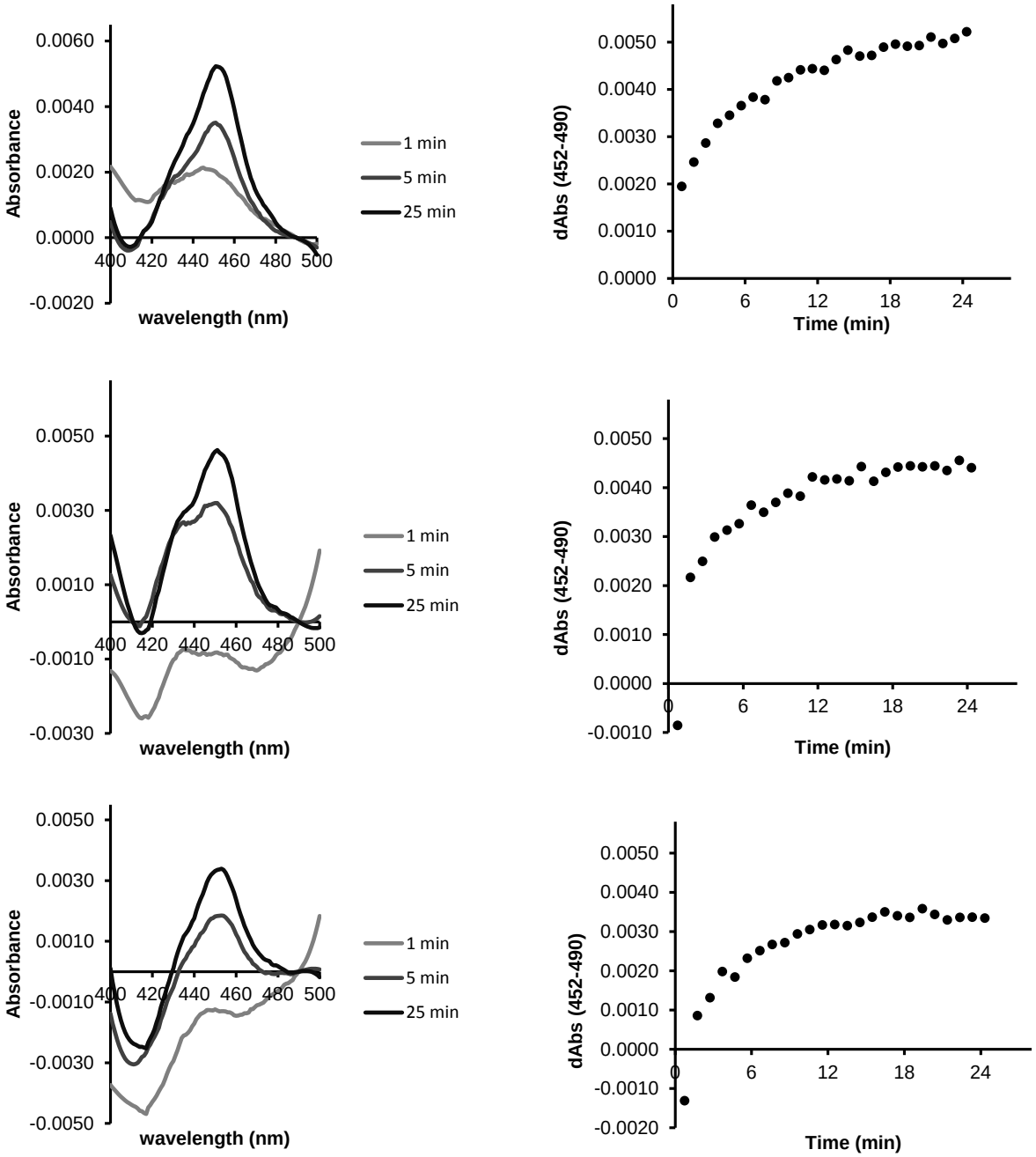

Figure 3.1 – MI complex formation from N-OH-ENX in human liver microsomes
MI complex formation with HLM (2 mg/mL) from incubation with N-OH-ENX (50 μM) and NADPH (1 mM) was tested. Cuvettes were balanced with HLM and NADPH. Addition of N-OH-ENX to the sample cuvette and vehicle to the reference cuvette initiated the reaction. The experiment was performed three times. Selected scans (1, 5, and 25 min) are shown alongside the time-course of the absorbance increase [dAbs(452-490nm)].

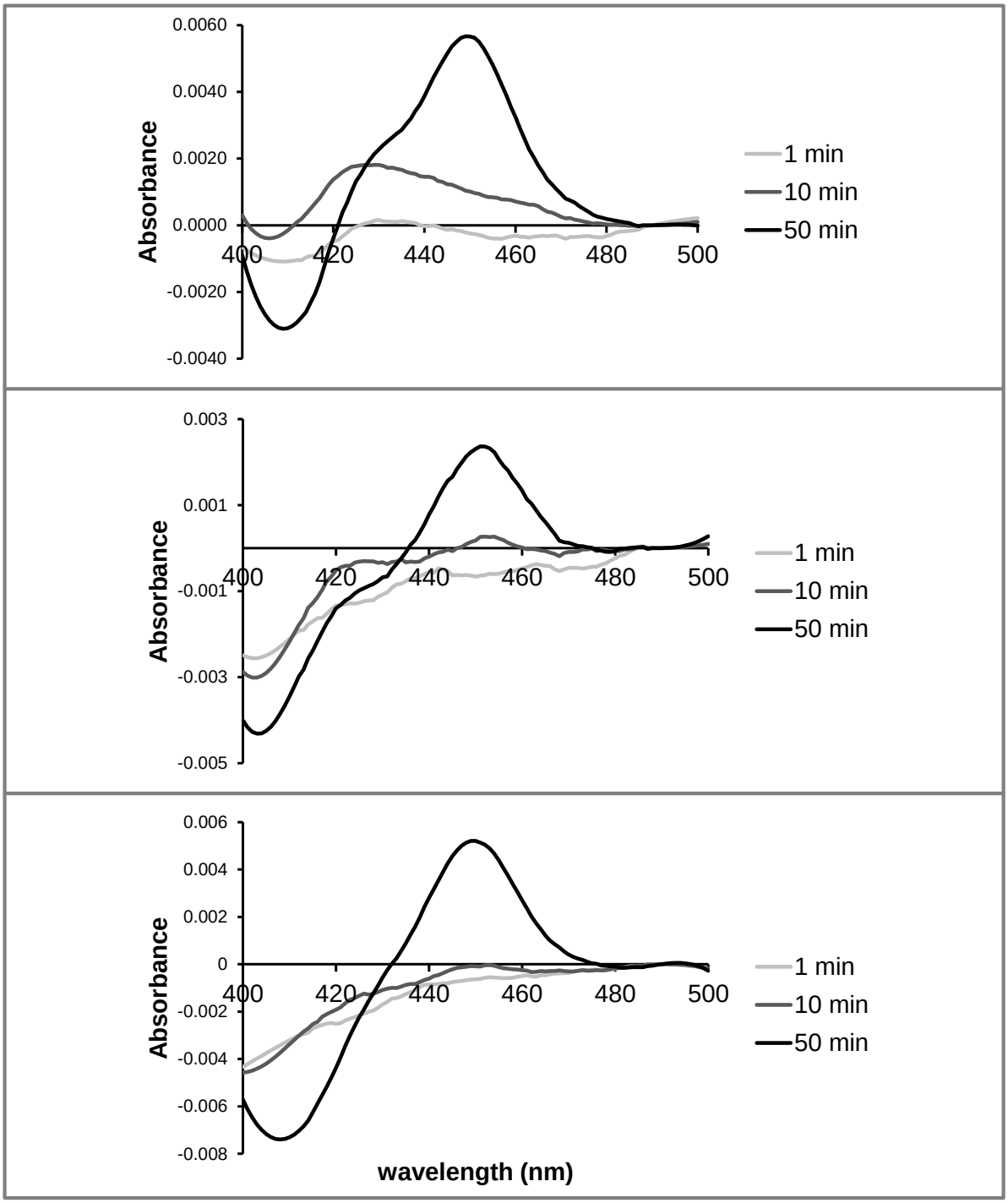

Figure 3.2 – MI complex formation from ENX in human liver microsomes
MI complex formation with HLM (2 mg/mL) from incubation with ENX (50 μM) and NADPH (1 mM) was tested. Cuvettes were balanced with HLM and NADPH. Addition of ENX to the sample cuvette and vehicle to the reference cuvette initiated the reaction. The experiment was performed three times. Selected scans (1, 10, and 50 min) are shown. A spectral perturbation occurring at ~30 minutes prevented accurate recording of the absorbance increase over time.

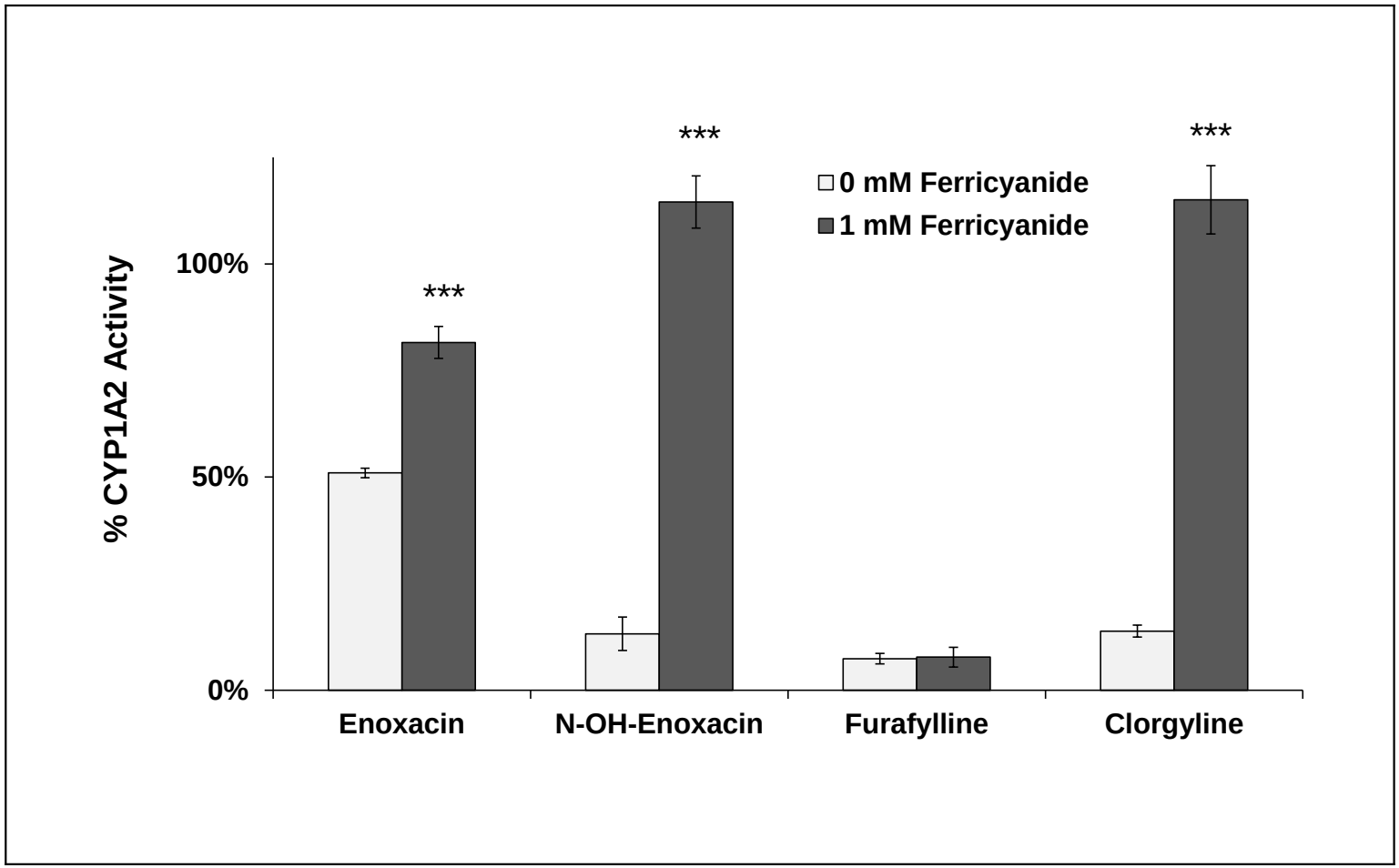

Figure 3.3 – Ferricyanide-mediated restoration of CYP1A2 activity in human liver microsomes
HLM (1 mg/mL) were pre-incubated with 1 mM NADPH and inhibitor (ENX, 50 μM; N-OH-ENX, 50 μM; furafylline, 10 μM; clorgyline, 10 μM) for 30 minutes. Recovery of CYP1A2 activity (phenacetin o-deethylase) upon treatment of inactivated enzyme with potassium ferricyanide (1 mM) was tested for. Values are reported in quadruplicate ± SD.

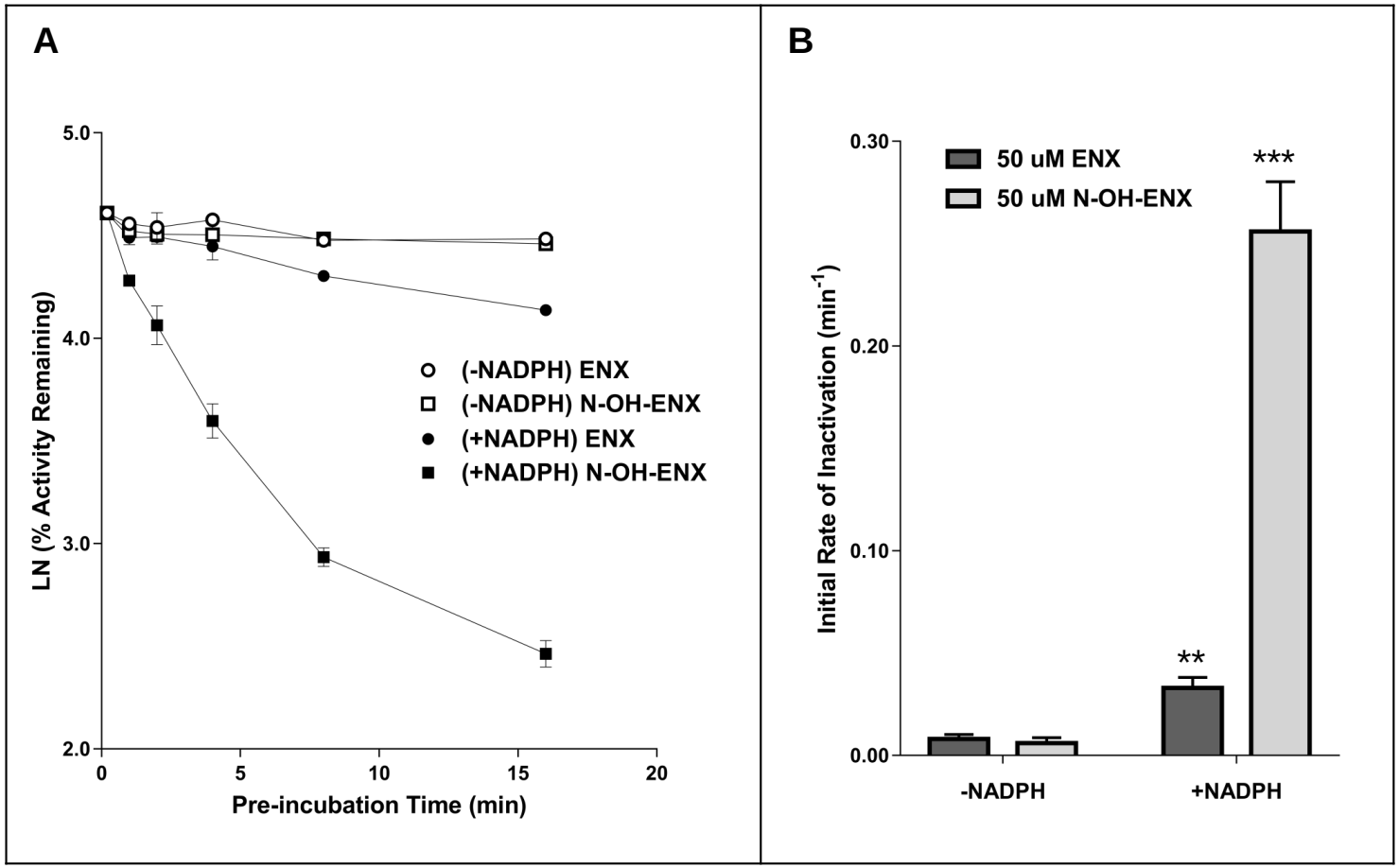

Figure 3.4 – Comparison of CYP1A2 time-dependent inhibition by 50 μM ENX vs N-OH-ENX
Time- and NADPH-dependent loss of CYP1A2 activity (phenacetin o-deethylase) was measured in pooled HLM (A) and the initial rates of inactivation were compared (B). The concentration of either ENX or N-OH-ENX used was 50 μM. Initial rates are defined as the slope of the linear portion of the log-transformed plot (A) All values are reported as the mean ± SD of determinations made in triplicate. Statistical significance for the rates in Panel B is relative to respective "-NADPH" controls for ENX and N-OH-ENX.

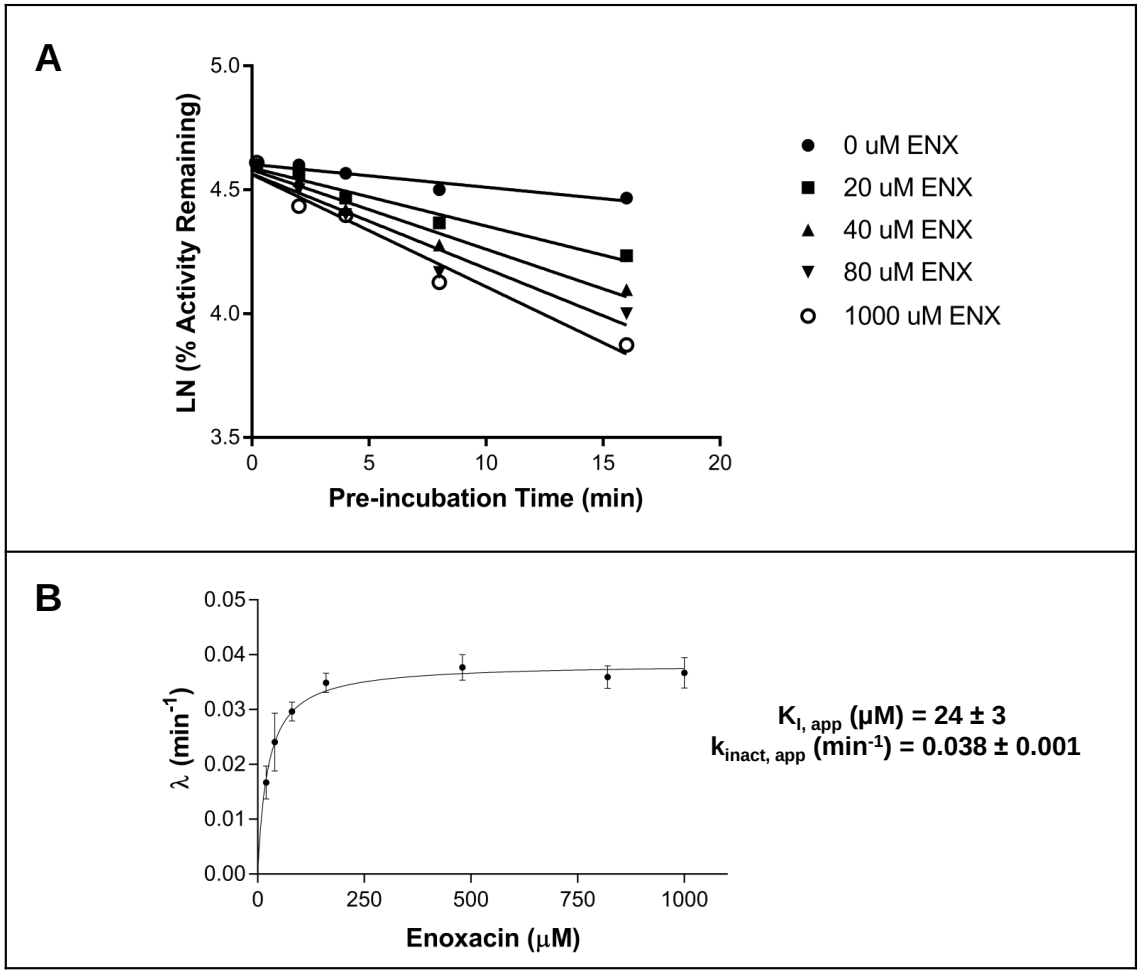

Figure 3.5 – Apparent inactivation parameters for ENX in human liver microsomes
Pooled HLM (1 mg/mL) and NADPH (1mM) were pre-incubated in the presence of vehicle or increasing concentrations of ENX (20 μM, 40 μM, 80 μM, 160 μM, 480 μM, 820 μM, and 1000 μM). Loss of phenacetin O-deethylase activity was measured over time and compared to vehicle controls. Plots of activity loss over time were natural log transformed and the slope of the linear portion calculated by linear regression. All time points were performed in triplicate (In Panel A, error bars were omitted for clarity). Inactivation rates are reported in triplicate ± SD.

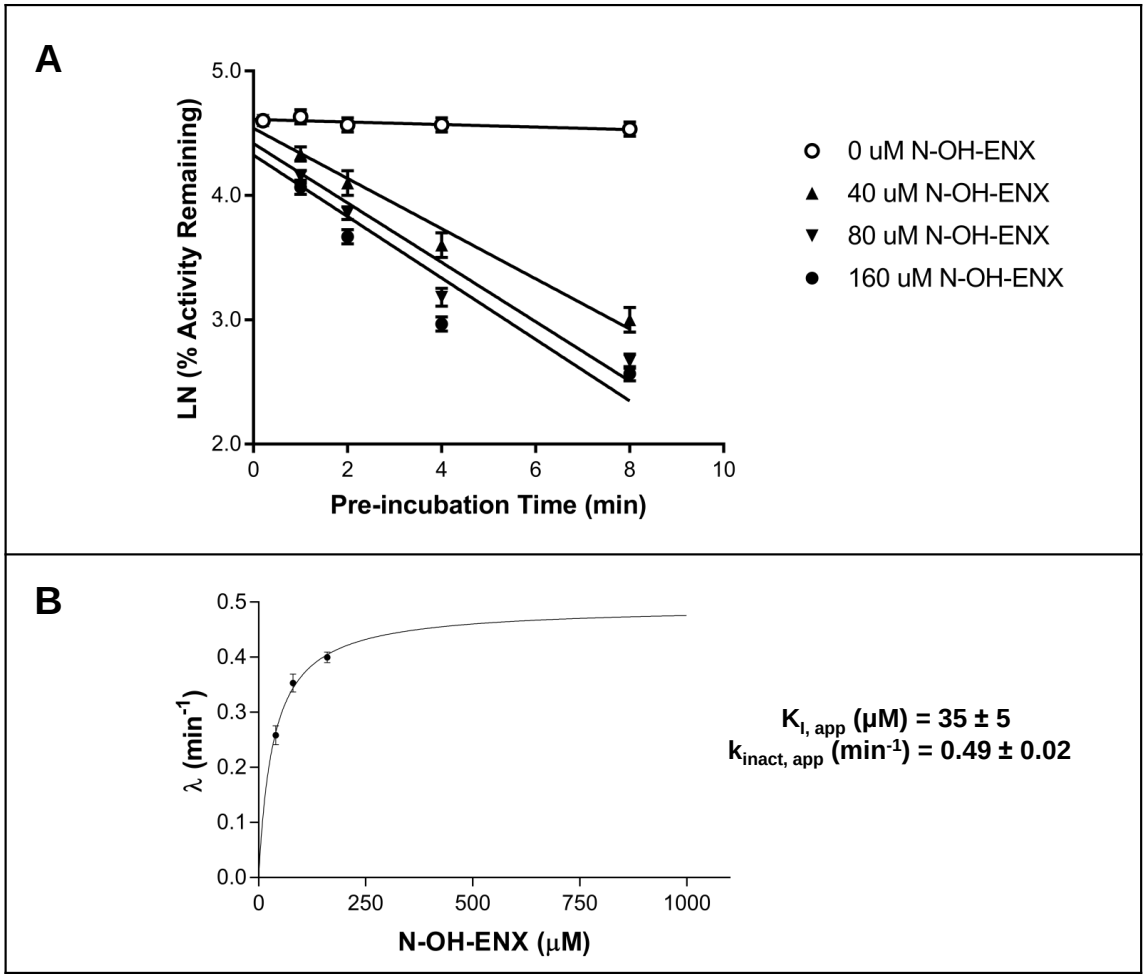

Figure 3.6 – Apparent inactivation parameters for N-OH-ENX in human liver microsomes
Pooled HLM (1 mg/mL) and NADPH (1mM) were pre-incubated in the presence of vehicle or increasing concentrations of N-OH-ENX (40 μM, 80 μM, and 160 μM). Loss of phenacetin O-deethylase activity was measured over time and compared to vehicle controls. Plots of activity loss over time were natural log transformed and the slope of the linear portion calculated by linear regression. All time points were performed in triplicate. Inactivation rates are reported in triplicate ± SD. The final time point (8 min, Panel A) was removed when calculating the inactivation rates for N-OH-ENX (Panel B).

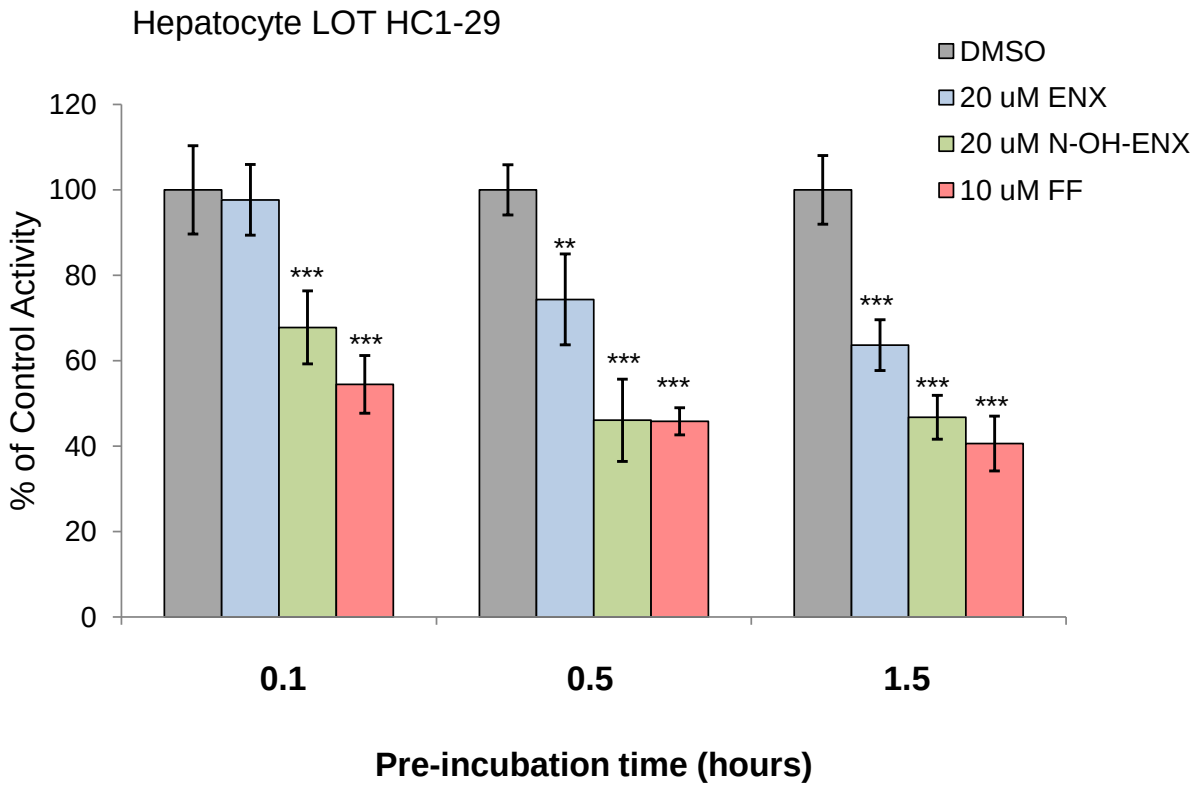

Figure 3.7 – Time-dependent loss of phenacetin o-deethylase activity in hepatocyte lot HC1-29
Phenacetin o-deethylase activity was measured after exposure of cells to vehicle, ENX (20 μM), N-OH-ENX (20 μM), or FF (10 μM) for the indicated period of time. Error bars are displayed as ±1 SD (N=5). Statistical significance is relative to vehicle controls.

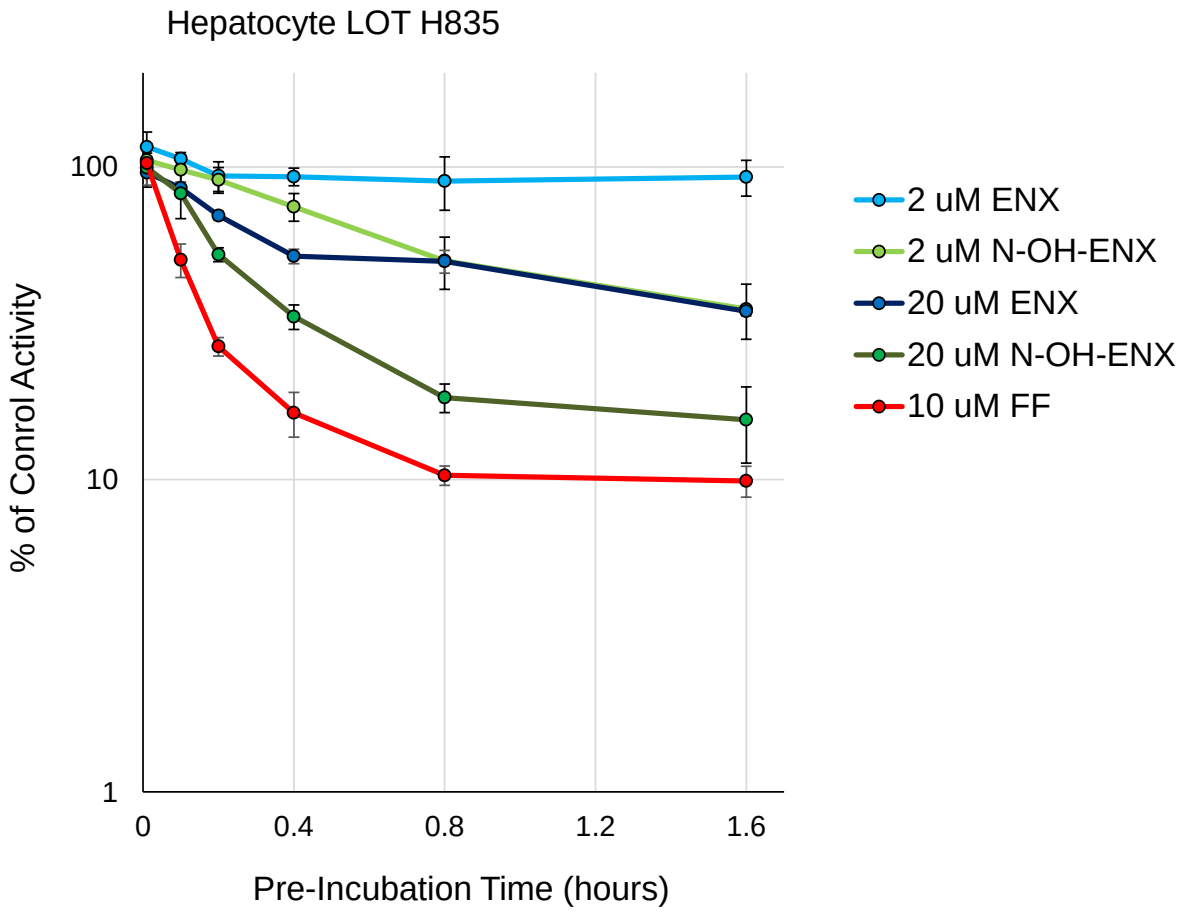

Figure 3.8 – Time-dependent loss of phenacetin o-deethylase activity in hepatocyte lot H835
Phenacetin o-deethylase activity was measured after exposure of cells to ENX (2 or 20 μM), N-OH-ENX (2 or 20 μM), or FF (10 μM) for the indicated period of time (0.01, 0.1, 0.2, 0.4, 0.8, or 1.6 hours) and the activities were then normalized to vehicle controls. Error bars are displayed as ±1 SD (N=5).

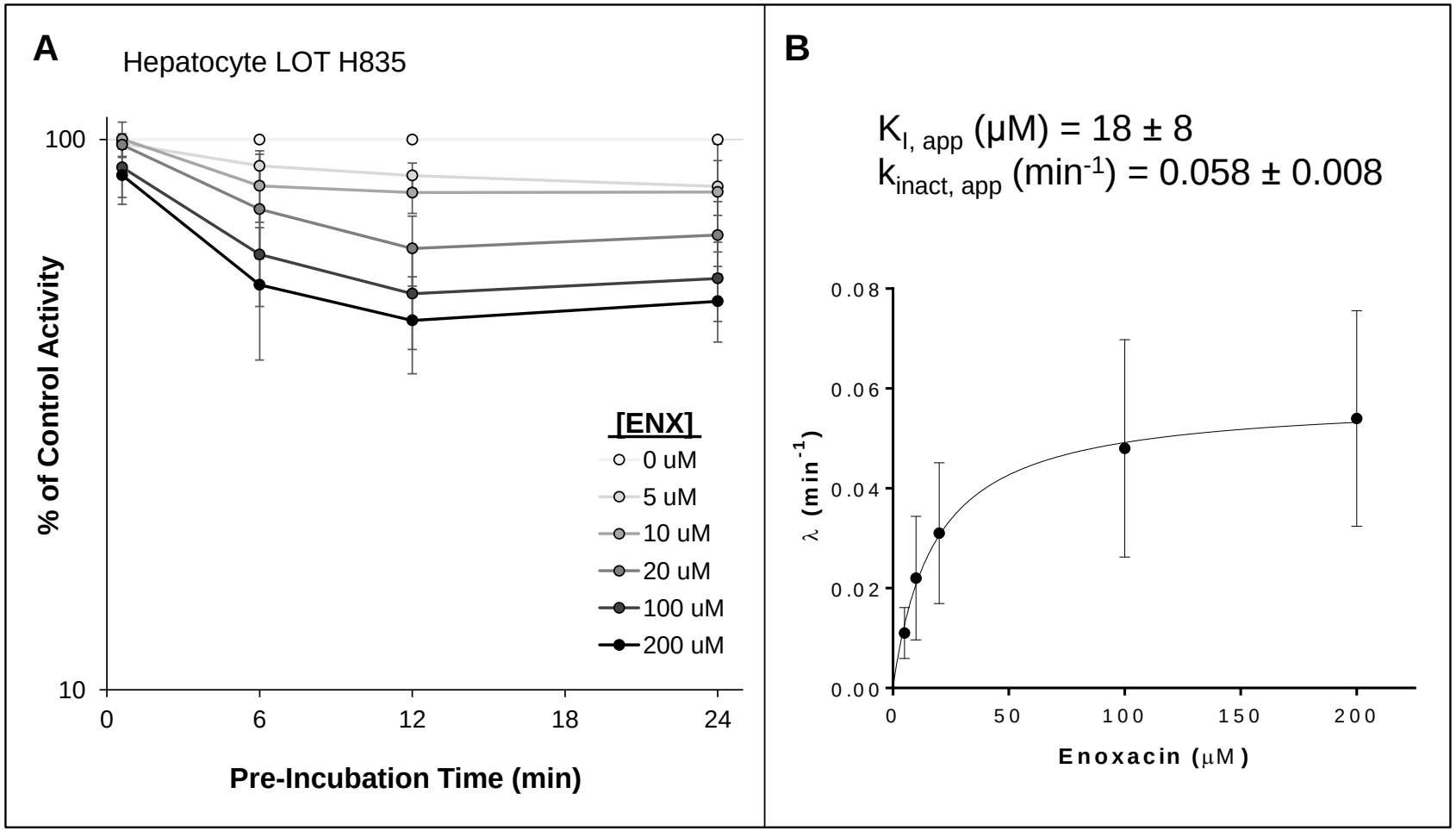

Figure 3.9 – Apparent inactivation parameters for ENX in plated primary human hepatocytes
Single donor cryopreserved human hepatocytes were thawed and plated. Phenacetin o-deethylase activity of cells exposed to vehicle or increasing concentrations of ENX (5 μM, 10 μM, 20 μM, 100 μM, and 200 μM) was measured after 0.6, 6, 12, or 24 minutes of pre-incubation exposure times. After log transform, the slope passing through the first 3 time points was calculated by linear regression. Inactivation rates are reported ±1 SD (N=4). Inactivation parameters were estimated by non-linear regression using Equation 3.

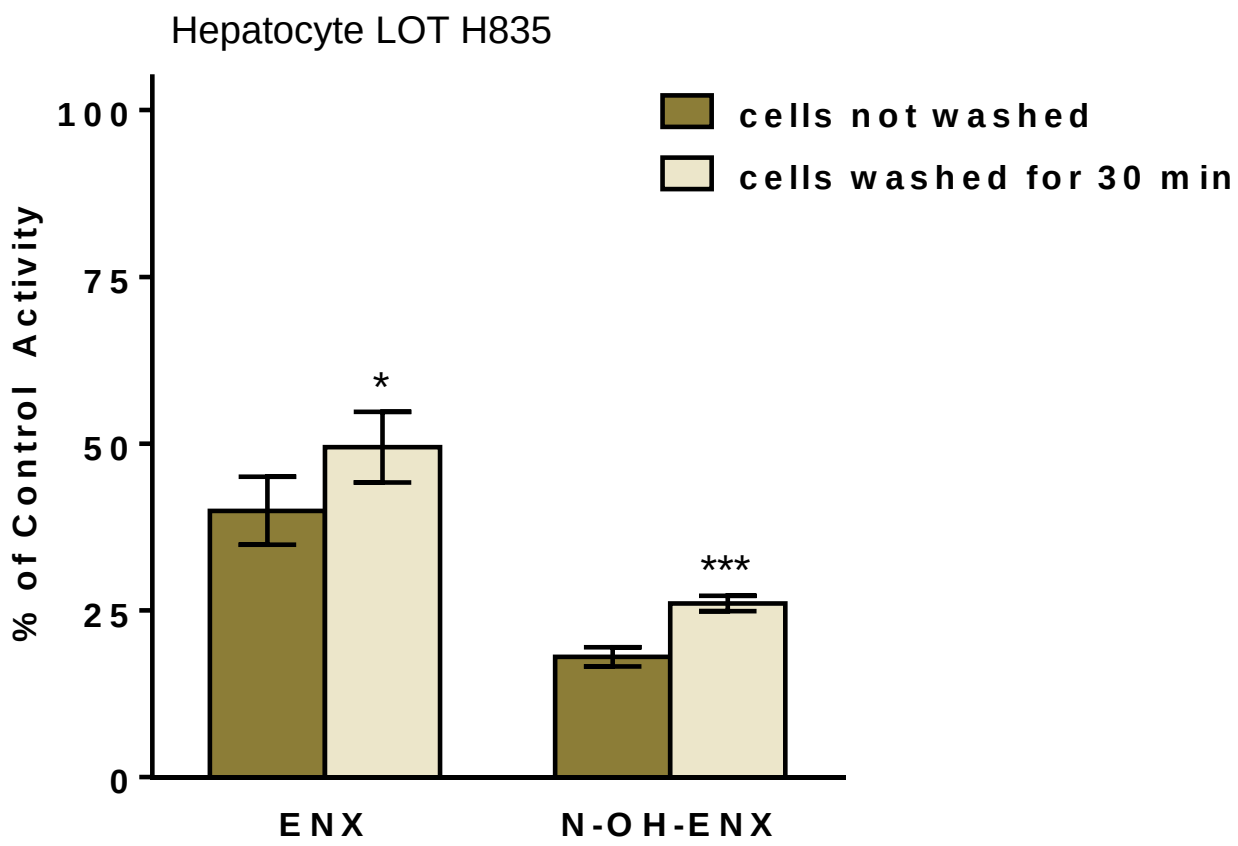

Figure 3.10 – Effect of washing cells on phenacetin o-deethylase activity following pre-incubation with ENX or N-OH-ENX
Plated hepatocytes were pre-incubated with vehicle, ENX (50 μM), or N-OH-ENX (50 μM) for 1.6 hours. Cells to be subjected to washing began the pre-incubation phase 30 min prior to cells not washed. After pre-incubation, the washing phase consisted of removing 80% of the volume in the well and replacing it with inhibitor-free Hank's Balanced Salt Solution (performed 3 times; overall dilution of 125-fold) followed by 30 min of further incubation at 37°C as a "wash" period. At the end of this 30 min wash period, the "not washed" group of cells had completed the 1.6 hour pre-incubation phase and phenacetin o-deethylase activity was measured for all cells. Activity measures were normalized to respective vehicle controls having undergone identical "washed" or "not washed" procedures. Error bars represent ±1 SD (N=4).

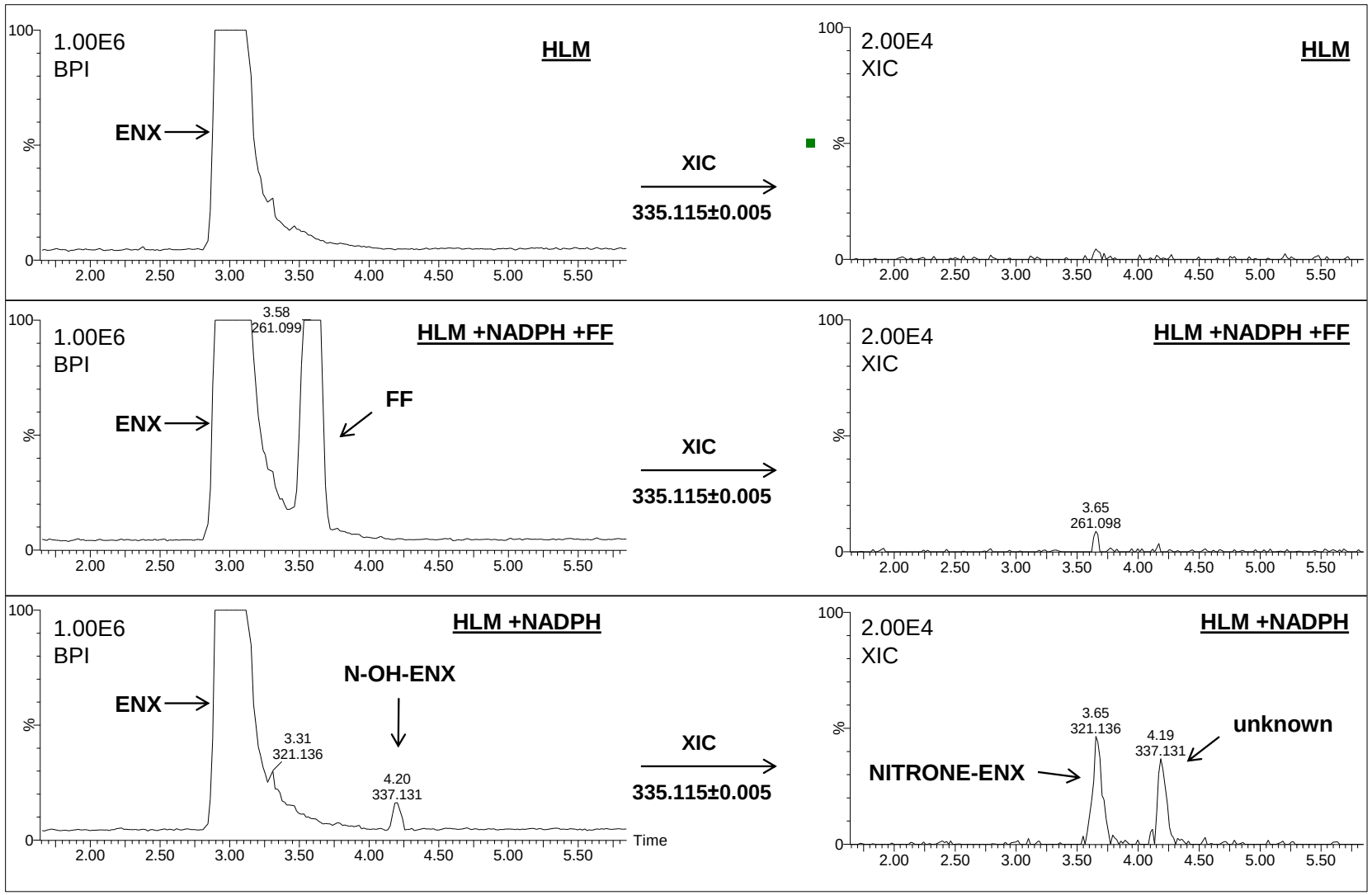

Figure 3.11 – High-resolution LC-MS of ENX metabolism in human liver microsomes
ENX (20 μM) was incubated in HLM (1 mg/mL) ±NADPH (1 mM) and ±FF (10 μM). The left side of the figure shows full scans of the metabolite profile. Moving to the right, each full scan was filtered for metabolites of mass 335.115±0.005 m/z. Peak annotations represent the retention time (min) and the mass (m/z value) of the most abundant ion.

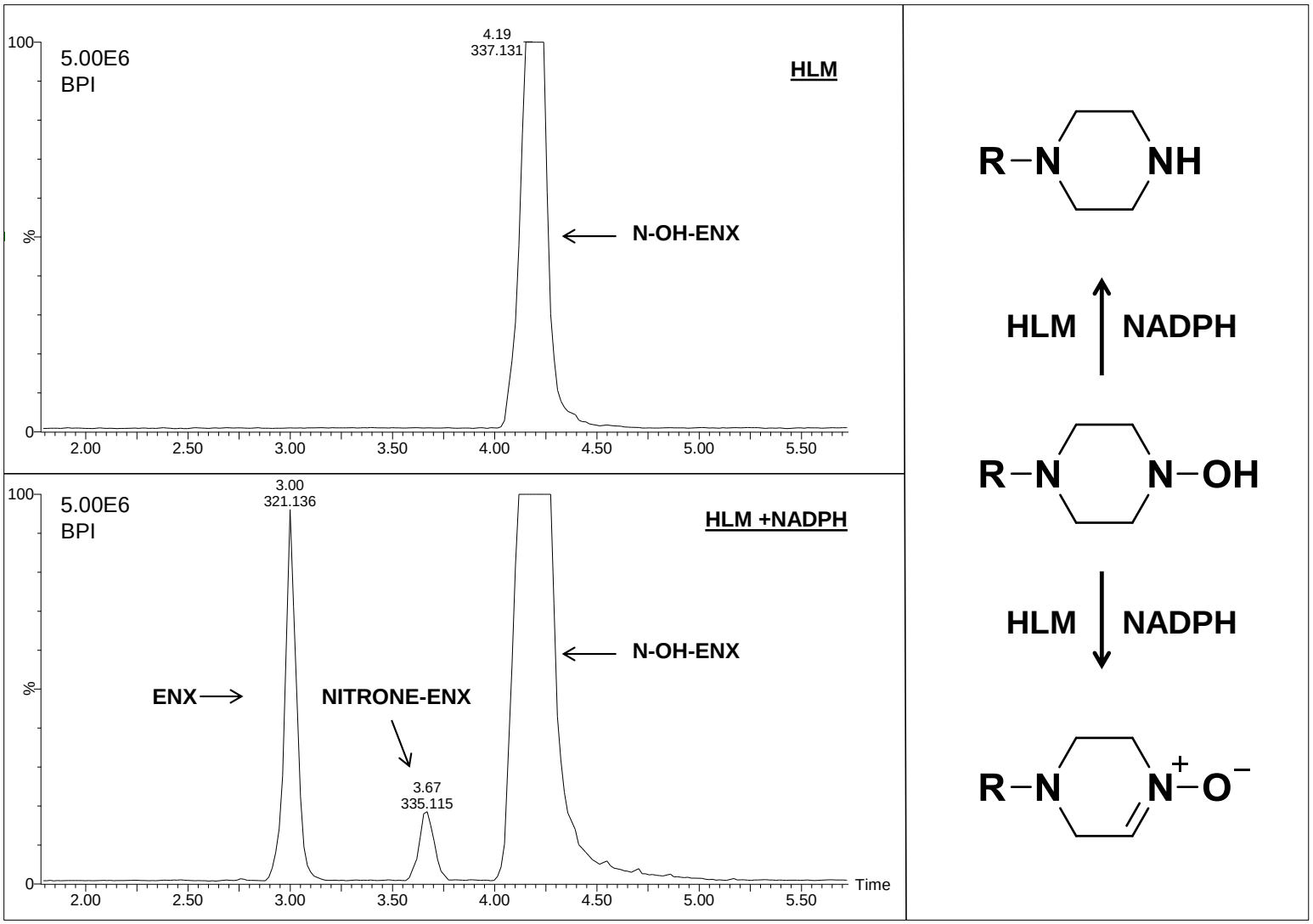

Figure 3.12 – High-resolution LC-MS of N-OH-ENX metabolism in human liver microsomes
N-OH-ENX (20 μM) was incubated in HLM (1 mg/mL) ±NADPH (1 mM). The left side of the figure shows full scans of the metabolite profile. The scheme on the right summarizes two metabolic fates of N-OH-ENX in HLM. Peak annotations represent the retention time (min) and the mass (m/z value) of the most abundant ion.

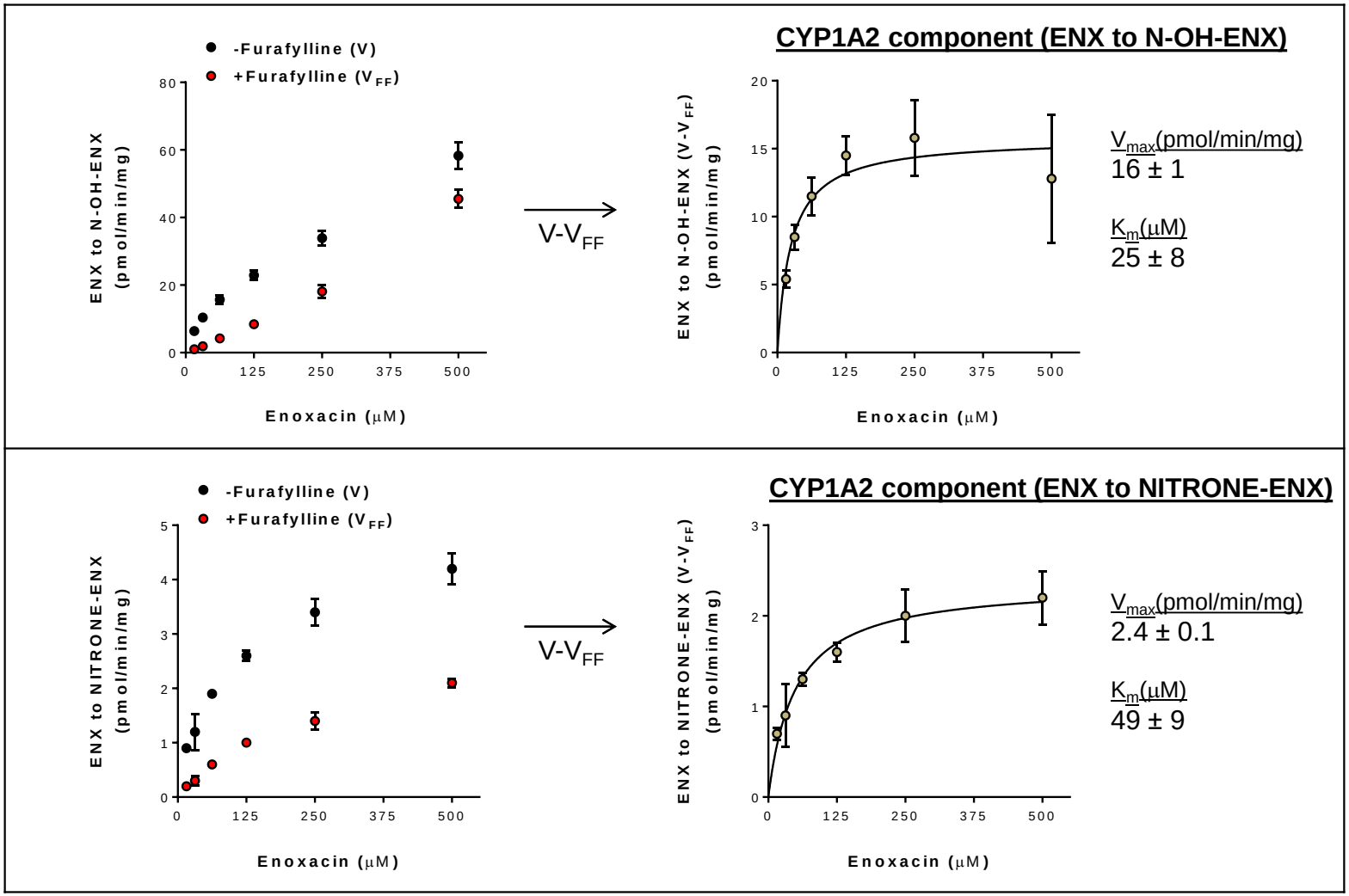

Figure 3.13 – CYP1A2-mediated N-OH-ENX and NITRONE-ENX formation from ENX in human liver microsomes
After a 5-minute pre-incubation phase ±FF (10 μM), ENX (from 15.625 to 500 μM) was incubated with NADPH(1 mM)-fortified HLM (1 mg/mL) and the rates of formation of N-OH-ENX and NITRONE-ENX were measured. By subtracting the rates determined after pre-incubation with FF (V_{FF}) from the rates determined after pre-incubation with vehicle (V), the CYP1A2-mediated component of product formation was estimated ($V-V_{FF}$). Michaelis-Menten parameters were estimated by non-linear regression (±1 SD).

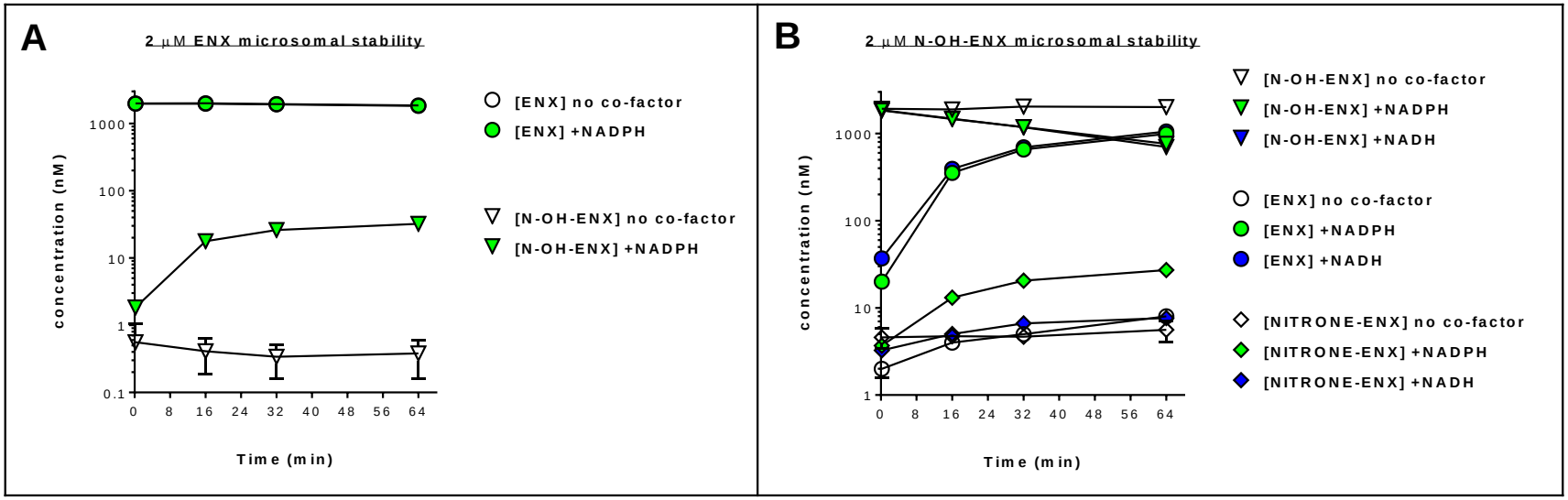

Figure 3.14 – Microsomal stability of ENX (±NADPH) and N-OH-ENX (±NADPH/±NADH)
ENX (2 μM) or N-OH-ENX (2 μM) was incubated with HLM (1 mg/mL) supplemented with superoxide dismutase (50 μg/mL) and catalase (2000 U/mL) at 37°C for 0.2, 16, 32, and 64 minutes. ENX incubations (Panel A) were performed in the absence or presence of NADPH (1 mM). N-OH-ENX incubations (Panel B) were performed in the absence or presence of NADPH (1 mM) or NADH (1 mM). Disappearance of the substrate and the formation of metabolites were quantified by an LC-MS/MS (MRM) assay. Note that the y-axes are log-transformed. Data points represent the average ±1 SD (N=8 in Panel A; N=6 in Panel B) and for most datum the error bars are contained within the data point.

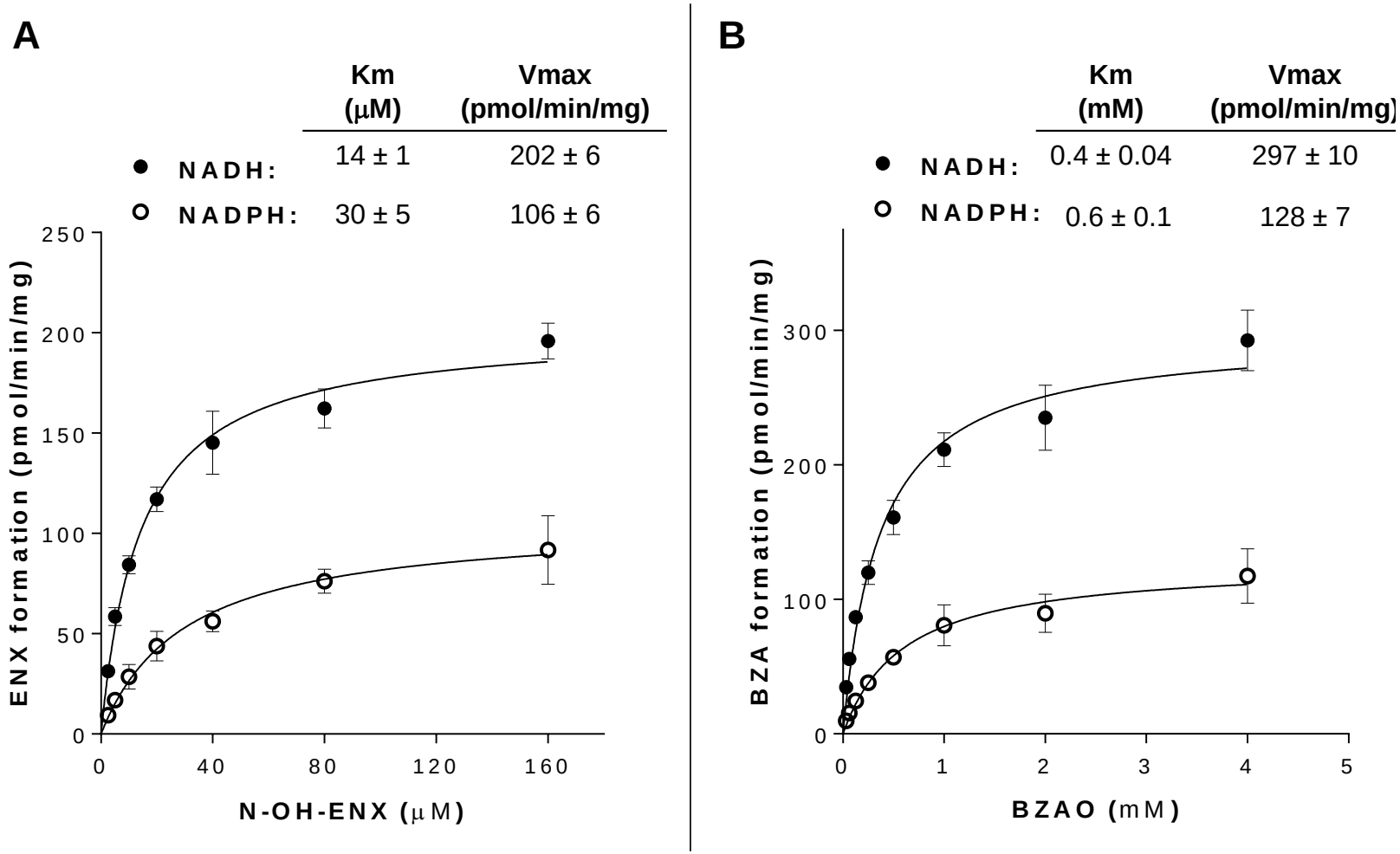

Figure 3.15 – Comparison of the reduction of N-OH-ENX vs benzamidoxime in human liver microsomes
Rates of NADH (1 mM)- and NADPH (1mM)-supported reduction of N-OH-ENX to ENX (Panel A) or benzamidoxime (BZAO) to benzamidine (BZA) (Panel B) were measured for a 5 minute incubation in pooled HLM across a range of substrate concentrations. Rates are reported as the average ±1 SD (N=3). Fitting by non-linear regression estimated the apparent Michaelis-Menten parameters K_m and V_{max} and the results are tabulated above each figure.

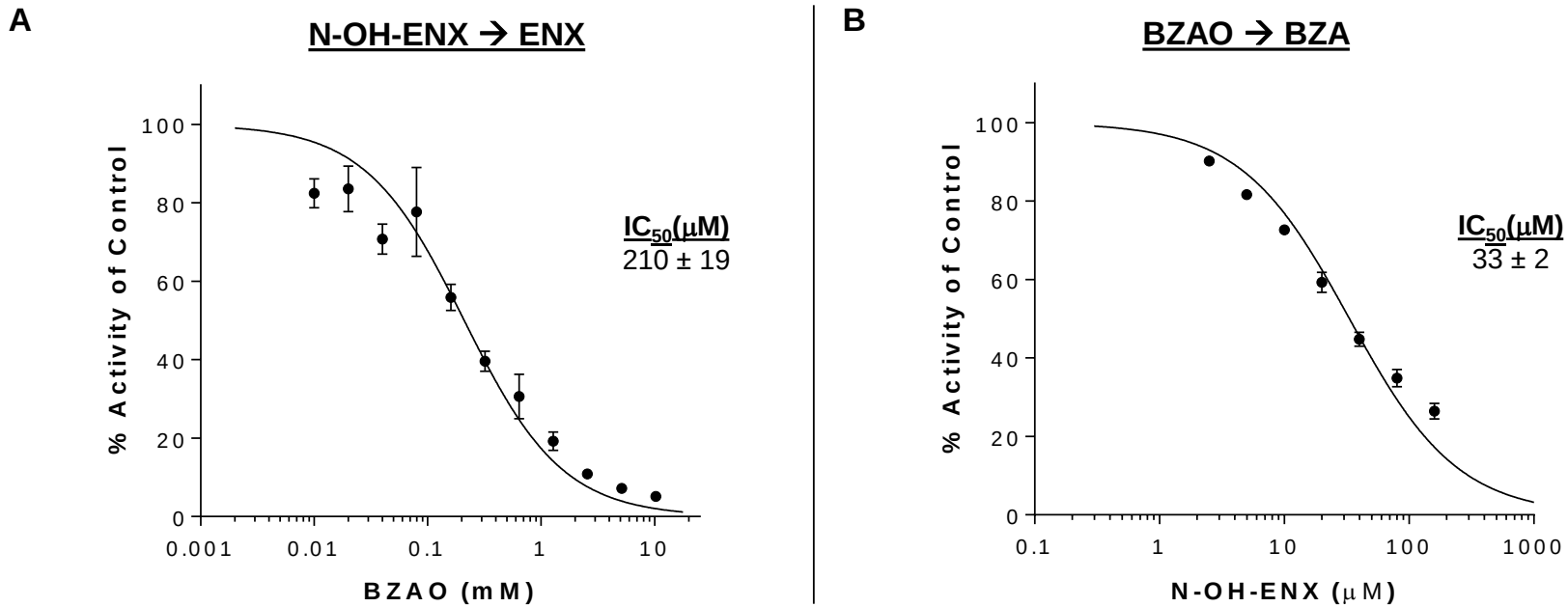

Figure 3.16 – Mutual inhibition of reduction in human liver microsomes by N-OH-ENX and benzamidoxime
The NADH (1mM)-dependent reduction of N-OH-ENX (15 μM) to ENX (Panel A) or BZAO (0.2 mM) to BZA (Panel B) was monitored in human liver microsomes (1 mg/mL) and the inhibitory effect of increasing concentrations of both of these substrates upon the respective reduction reaction of the other substrate was evaluated during a 5 minute co-incubation. IC_{50} curves were fit to the data and the resulting IC_{50} values are shown. Data are reported as the mean ±1 SD (N=3).

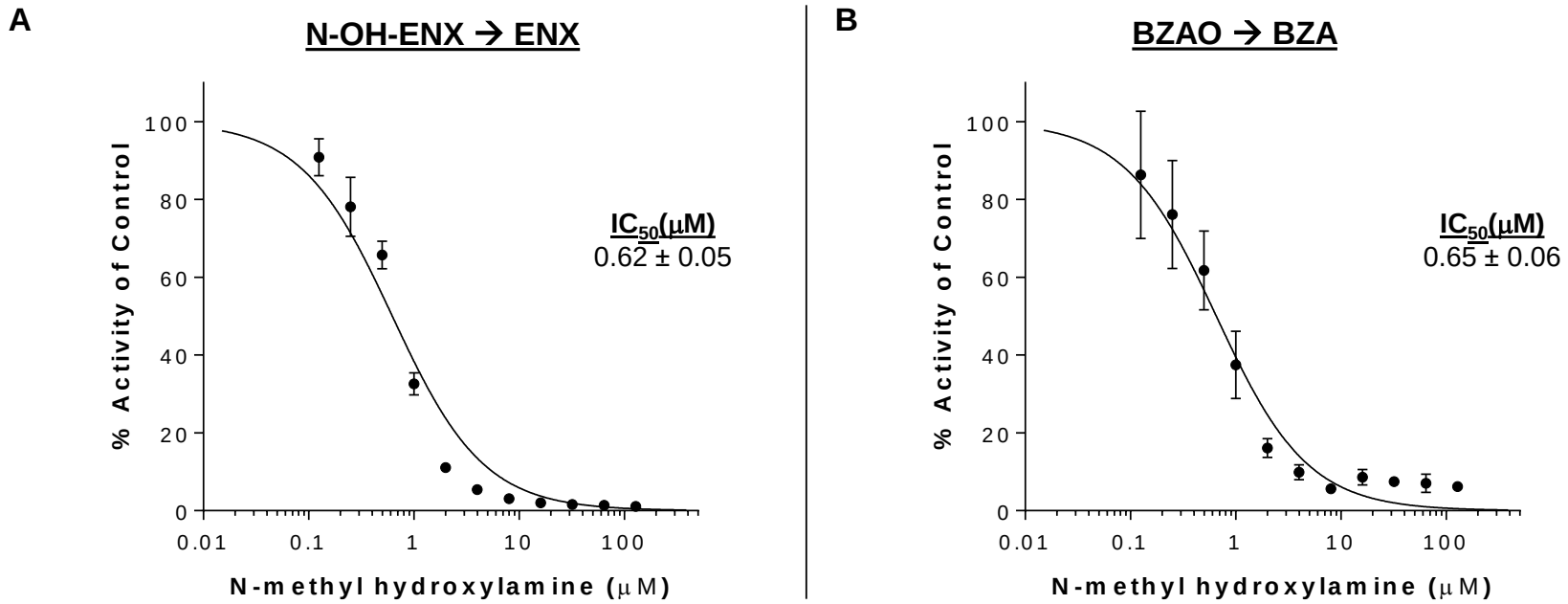

Figure 3.17 – Inhibition of N-OH-ENX and benzamidoxime reduction in human liver microsomes by N-methyl hydroxylamine
N-methyl hydroxylamine (delivered as the HCl salt) caused potent inhibition of the reduction of N-OH-ENX (15 μM) to ENX (Panel A) and BZAO (0.2 mM) to BZA (Panel B) in human liver microsomes during a 5 minute co-incubation. IC_{50} curves were fit to the data and the resulting IC_{50} values are shown. Data are reported as the mean ±1 SD (N=3).

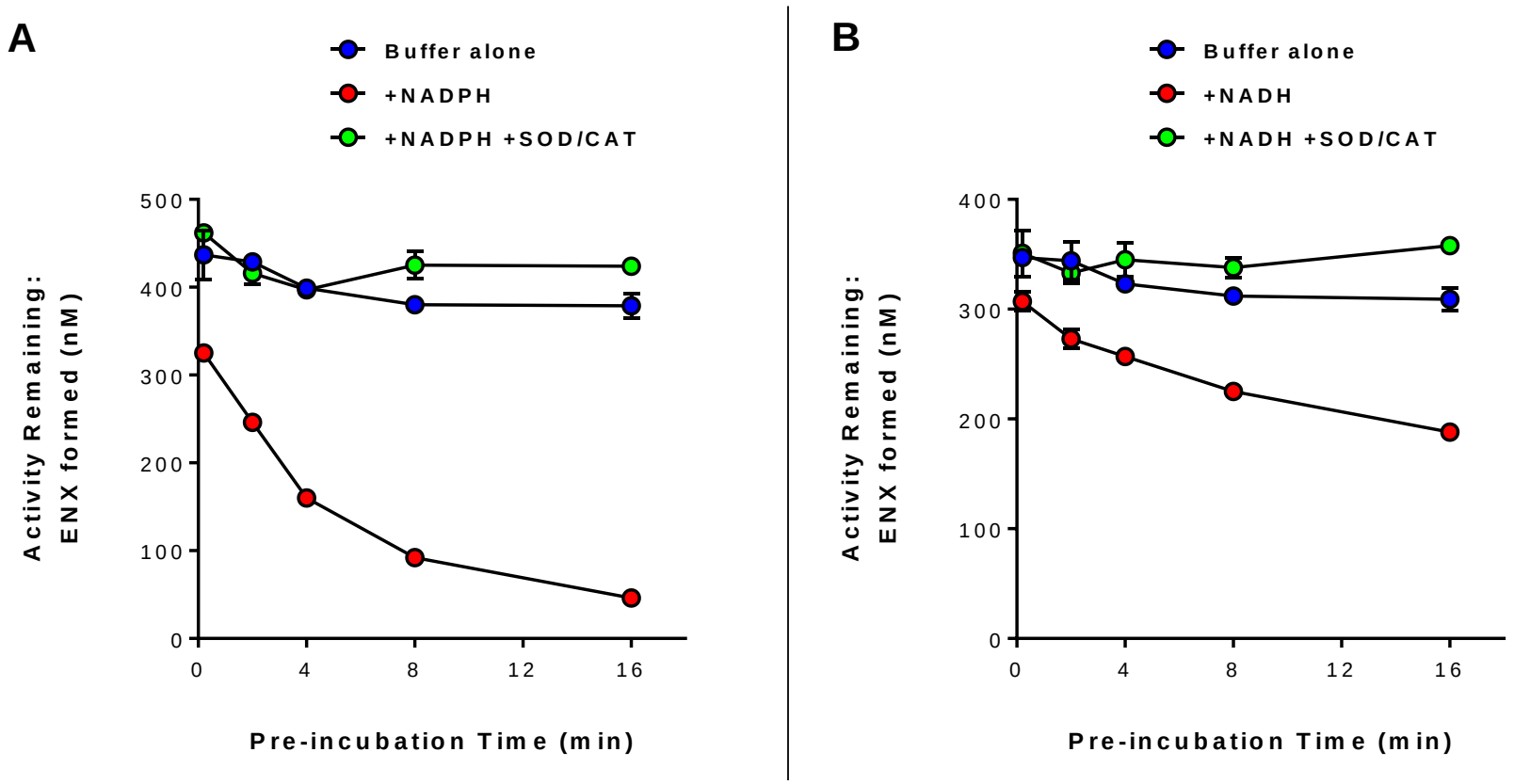

Figure 3.18 – Time-dependent loss of NADH-dependent N-OH-ENX reductase activity in the presence of NADPH/NADH is prevented by superoxide dismutase and catalase

HLM (2 mg/mL) were pre-incubated with buffer, NADPH (1 mM), or NADPH +SOD/CAT (50 μg/mL / 2000 U/mL) for the indicate periods of time (0.2, 2, 4, 8, or 16 minutes) before being diluted into an activity assay (Panel A). An identical experiment was also performed where pre-incubation took place with NADH (1 mM) instead of NADPH (Panel B). The activity assay consisted of N-OH-ENX (100 μM) and NADH (1 mM). The NADH-dependent formation of ENX from N-OH-ENX over 5 minutes served as an "activity remaining" measure following the pre-incubation phase. Data represent the mean ±1 SD (N=3) and for some datum the error bars are contained within the data point.

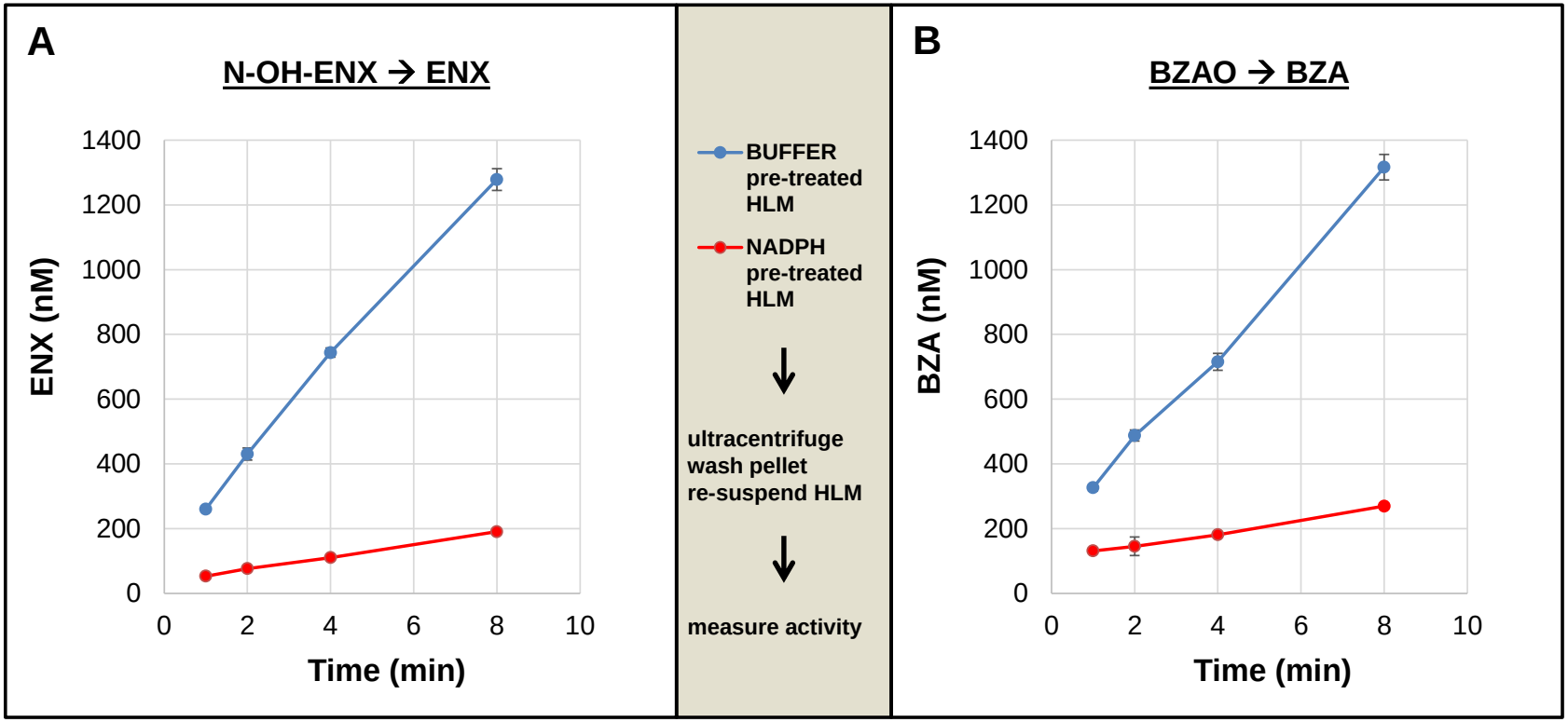

Figure 3.19 – Permanence of the NADPH-dependent inactivation of hydroxylamine reductase activity as demonstrated by ultracentrifugation and re-isolation of NADPH-treated microsomes
HLM (1 mg/mL) were incubated in phosphate buffer at 37°C for 20 minutes in the presence or absence of NADPH (1 mM). The microsomes were then pelleted by ultracentrifugation, washed with phosphate buffer, and re-suspended in phosphate buffer. The NADPH pre-treated and buffer(control) pre-treated microsomes were then tested for reductase activity (Panel A; N-OH-ENX(100 μM)→ENX, or, Panel B; BZAO(1 mM)→BZA) by measuring the time-courses for reduction of these substrates. Incubations were carried out with the re-isolated HLM (0.75 mg/mL) supplemented with NADH (1 mM)), superoxide dismutase (50 μg/mL), and catalase (2000 U/mL). Time points are the mean ±1 SD (N=3) and for some datum the error bars are contained within the data point.

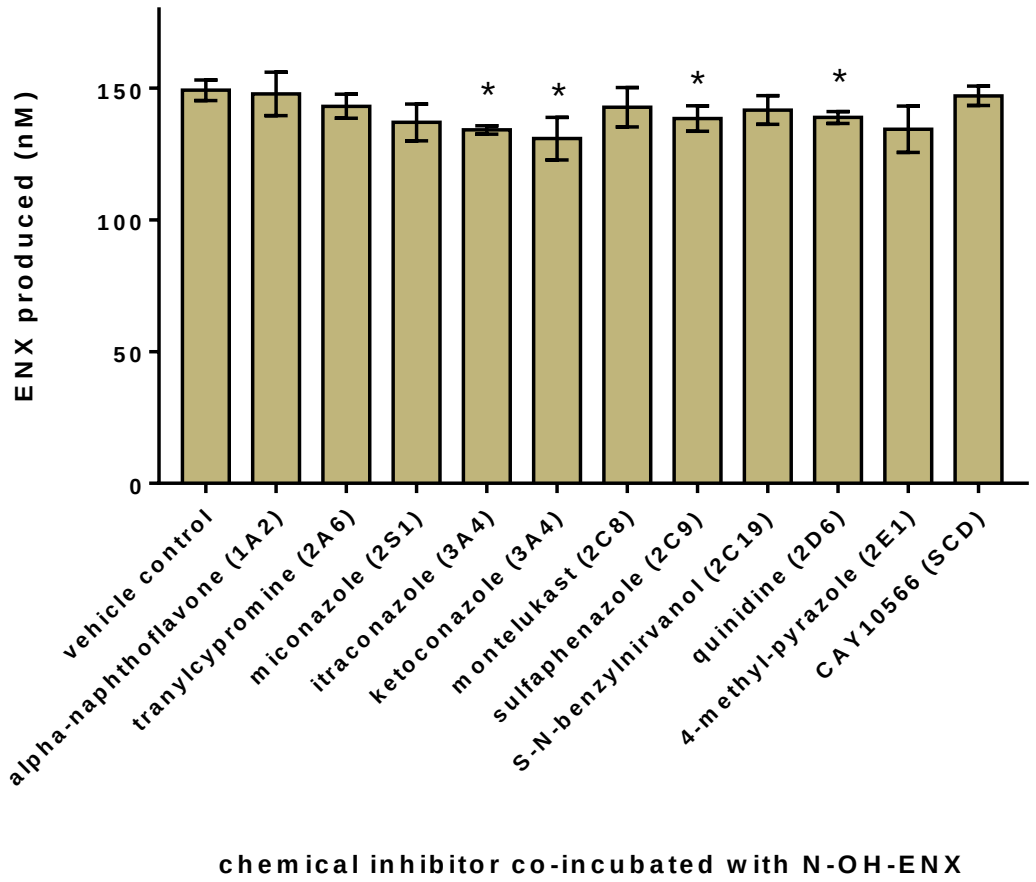

Figure 3.20 – Effect of a panel of chemical inhibitors on the NADH-dependent reduction of N-OH-ENX to ENX in human liver microsomes

N-OH-ENX (15 μM) was co-incubated with one of the above inhibitors (2 μM, except miconazole which was used at 12 μM) to inhibit a specific enzyme (CYP isoform indicated after inhibitor name, or, SCD = stearoyl-CoA desaturase) in HLM (0.5 mg/mL) supplemented with NADH (1 mM), superoxide dismutase (50 μg/mL), and catalase (2000 U/mL). After a 5 min co-incubation, the reaction was quenched and the amount of ENX product was quantified by LC-MS/MS. Average (N=3) values ±1 SD are displayed. Statistical significance is relative to the vehicle control.

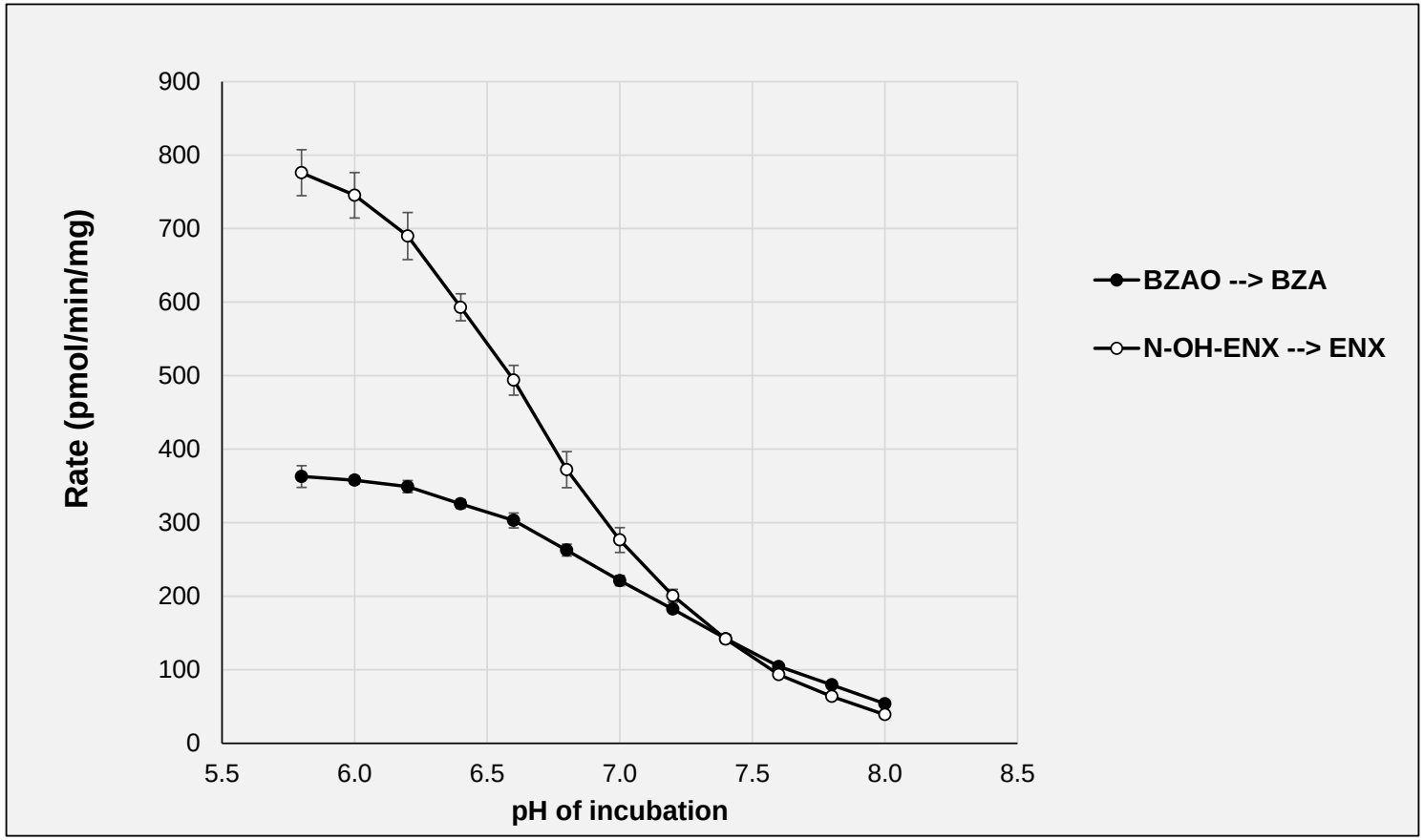

Figure 3.21 – Effect of pH on the NADH-dependent reduction of N-OH-ENX and BZAO in human liver microsomes
Reduction of N-OH-ENX (100 μM) or BZAO (1 mM) was measured in 1 mg/mL HLM incubations supplemented with 1 mM NADH. The incubations were run at pH values (0.1M potassium phosphate buffer) of 5.8, 6.0, 6.2, 6.4, 6.6, 6.8, 7.0, 7.2, 7.4, 7.6, 7.8, and 8.0 and the amount of reduced product formed (enoxacin or benzamidine) for a 5 minute incubation was measured by LC-MS/MS (MRM). Error bars of ±1 SD (N=3) are shown and, for some datum, are contained within the data point.

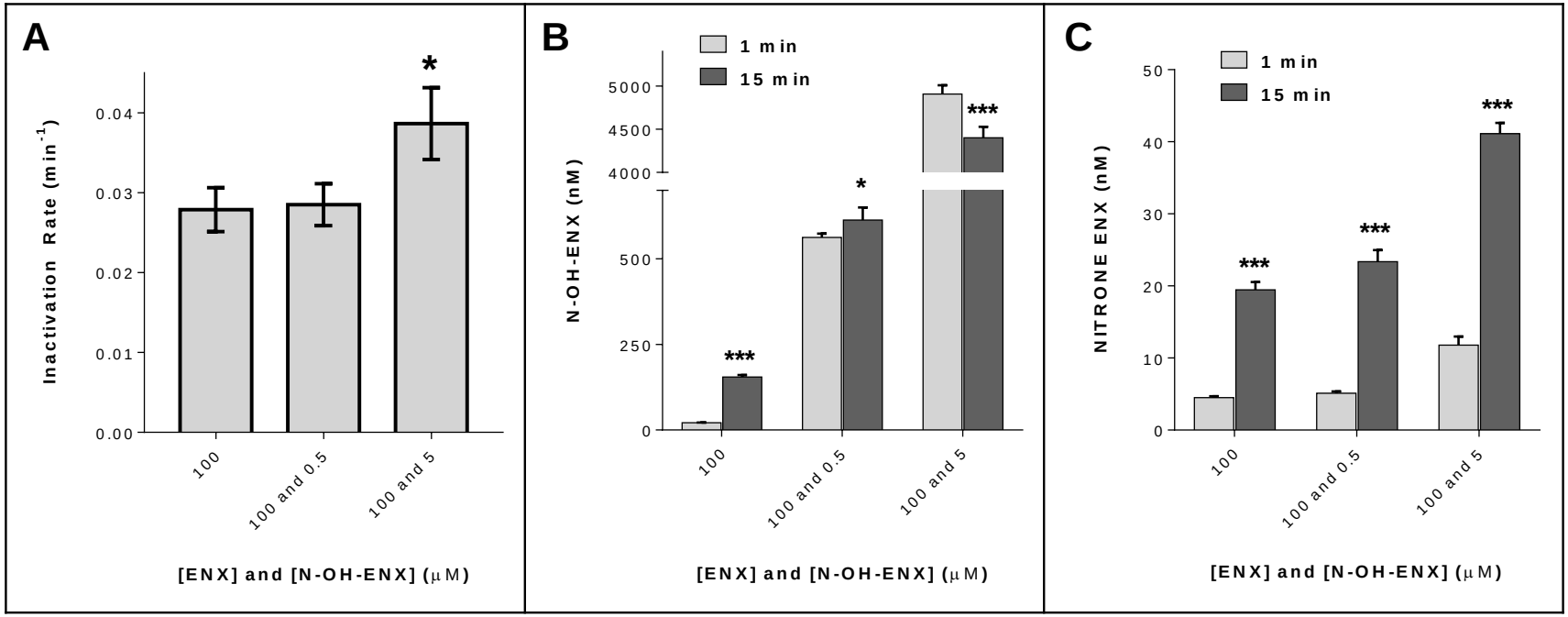

Figure 3.22 – Evidence for non-dissociative inactivation of CYP1A2 by ENX in human liver microsomes
ENX (100 μM) was pre-incubated in HLM (1 mg/mL) supplemented with NADPH (1 mM), superoxide dismutase (50 μg/mL), and catalase (2000 U/mL) with aliquots being removed and diluted into a phenacetin (100 μM) o-deethylase activity assay at 0.2, 2, 4, 8, and 16 minutes. Enzyme inactivation rates were measured from the time-dependent loss of phenacetin o-deethylase activity. Inactivation rates from pre-incubation with ENX alone (100 μM) and ENX spiked with N-OH-ENX (0.5 μM and 5 μM) are compared in Panel A. In addition to measuring the inactivation rate, aliquots taken from the pre-incubation mixtures at the beginning (1 minute into pre-incubation) and near the end (15 minutes into pre-incubation) of the assay were analyzed for metabolite levels. Panel B compares the levels of N-OH-ENX present at the beginning and end of the incubation. Panel C compares the levels of NITRONE-ENX present at the beginning and end of the incubation. Data are given as the average ±1 SD (N=3). In Panel A, statistical significance is given relative to without N-OH-ENX spiked. In Panels B and C, statistical significance is given relative to the amount of metabolite present at 1 minute.

Table 3-1: Comparison of inactivation parameters obtained in CYP1A2 bactosomes vs human liver microsomes

Enzyme system:	**CYP1A2 bactosomes***		**Pooled HLM**	
Parameter: Substrate	**K_I (μM)**	**k_{inact} (min^{-1})**	**K_I (μM)**	**k_{inact} (min^{-1})**
ENX	**132** ± 21	**0.048** ± 0.002	**24** ± 3	**0.038** ± 0.001
N-OH-ENX	**211** ± 31	**0.44** ± 0.04	**35** ± 5	**0.49** ± 0.02
parameter ratio (N-OH-ENX:ENX)	**1.6** ± 0.3	**9.2** ± 0.9	**1.5** ± 0.3	**13** ± 0.6

* bactosomes data obtained from Chapter 2

Table 3-2: DDI prediction using apparent inactivation parameters for ENX obtained from three in vitro systems

Pharmaceutical	In Vivo DDI (AUC_i/AUC)	Predicted DDI (AUC_i/AUC)		
		CYP1A2 Bactosomes*	Human Liver Microsomes	Human Hepatocytes
Theophylline ($f_{m,\ CYP1A2}$ = 0.80)[a]	3.7 (Wijnands et al., 1986)	3.5	4.4	4.7
Caffeine ($f_{m,\ CYP1A2}$ = 0.95)[a]	5.7 (Kinzig-Schippers et al., 1999)	6.7	12.4	15.1

[a] Literature source for f_m was Venkatakrishnan et al. (2007)
* bactosomes data obtained from Chapter 2

Chapter 4: Conclusions and Future Directions

4.1 Sequential Metabolism of a Piperazine to a Metabolic-Intermediate Complex

Alicyclic amines, such as piperidines and piperazines, are commonly used in drug design to add basicity and lipophilicity to chemical structures. From a drug metabolism perspective, alicyclic amines are a metabolic soft spot susceptible to oxidation by drug-metabolizing cytochrome P450 and flavin-containing monooxygenase enzymes. The metabolic lability of alicyclic amines is evident as examples of N-oxidized, N-dealkylated, dehydrogenated, and lactam metabolites are abundant in the literature where many of these metabolites result from more than one oxidation (Luffer-Atlas et al., 1997; Edlund and Baranczewski, 2004; Miller et al., 2004; Tong et al., 2010). Bioactivation of alicyclic amines to iminium ions, aldehydes, and cyclic nitrone species has been invoked to explain genotoxicity (Rodriguez et al., 1999; Kalgutkar et al., 2007; Kalgutkar et al., 2009) and the reaction of electrophilic metabolites with trapping agents such as cyanide (Argoti et al., 2005). Alicyclic amines are so notoriously metabolically unstable that medicinal chemists will attempt to block metabolism of alicyclic amines by introducing steric bulk and substitutions on the carbon atoms alpha to the nitrogen atom. Researchers at Merck investigated a series 2,2,6,6-tetramethylpiperidine analogues as part of a strategy to block metabolism that normally occurs at the α-carbons of the piperidine moiety. To their surprise, these analogues were still metabolized at the α-carbon via formation of a ring-contracted 2,2-dimethylpyrrolidine metabolite and the production of an equivalent of acetone (Yin et al., 2003; Yin et al., 2004). Thus, it appears that alicyclic amines are commonly targeted by oxidative drug metabolizing enzymes. Many of the metabolites found in the above literature examples require multiple oxidations suggesting that sequential metabolism of alicyclic amines may be common.

In this dissertation, sequential metabolism of the piperazine moiety of enoxacin (ENX) by cytochrome P450 1A2 (CYP1A2) was proposed to yield a ring-opened nitroso metabolite which binds the CYP1A2 ferrous heme iron (Figure 4.1; pink box). The resulting metabolite-enzyme complex, a metabolic-intermediate (MI) complex, is irreversible in vivo and we proposed that MI complex formation with CYP1A2 explains the drug-drug interactions (DDIs) precipitated by ENX with the CYP1A2 substrates theophylline and caffeine. Essentially, we described a sequential metabolic process that unveils a mechanism-based inhibitor in the CYP1A2 active site through multiple rounds of catalysis directed at the terminal nitrogen of the piperazine ring. The first two catalytic steps are likely N-hydroxylation and α-carbon hydroxylation (in either order) to yield a piperazine α-hydroxy secondary hydroxylamine, the true mechanism-based inhibitor of CYP1A2. We proposed that the third and final catalytic step is mediated by Compound I to lyse the C-N bond in an oxidative ring-opening to a nitroso-aldehyde metabolite. This C-N bond cleavage concomitant with C=O and N=O formation parallels the reaction of cytochrome P450 cholesterol side-chain cleavage where a 1,2-diol C-C bond is cleaved concomitant with formation of two carbonyls (Yoshimoto et al., 2016). Regardless of whether our mechanism is correct, the fact remains that we have captured evidence for MI complex formation with CYP1A2 through sequential metabolism of the piperazine ring of ENX.

This specific example raises an important question: can piperazines contained within the structures of other drugs be sequentially metabolized to form MI complexes with other P450 isoforms? Further, would our mechanism be viable with other alicyclic amines such as piperidines or pyrrolidines? In terms of the chemistry involved, we do not see any reason why our specific example cannot be generalized to all alicyclic amines. Sequential N-oxidation and ring-opening to a nitroso-aldehyde metabolite should be a viable chemical process with any alicyclic amine and would likely only be limited by the available binding orientations of the substrate in the P450 active site and the propensity of the P450 enzyme to perform multiple

oxidations on the substrate. We suggest that our specific example of an MI complex formed with CYP1A2 from ENX is generalizable and that, further, alicyclic amines should be designated as structural alerts for MI complex formation.

4.2 Non-Dissociative Sequential Inactivation is conserved across Enzyme Systems

We found evidence that the inactivation of CYP1A2 by (a metabolite of) ENX in bactosomes, HLM, and human hepatocytes is reasonably conserved across systems. Sequential metabolism of ENX to an MI complex with CYP1A2 was confirmed in bactosomes and HLM, and circumstantial evidence was provided in support of the MI complex mechanism in human hepatocytes. Importantly, the inactivation parameters in bactosomes and HLM (where MI complex formation was confirmed) predict the DDIs with theophylline and caffeine in vivo thus supporting the notion that MI complex formation also occurs in vivo.

We propose that the conservation of the inactivation process across enzyme systems to in vivo is specifically due to the sequential metabolism of ENX to an MI complex with CYP1A2 being a *non-dissociative* process. Figure 4.1 illustrates the importance of the fact that the entire metabolic sequence can take place inside the CYP1A2 active site (represented by the pink box). A non-dissociative process inside the enzyme active site is “insulated” from the effects of the in vitro incubation matrix, or, even the in vivo enzyme environment. Thus, such a process is expected to be conserved and viable across systems. We have emphasized that, for inactivation of CYP1A2 by ENX, the non-dissociative nature of the mechanism is a critical feature and a direct, causal factor for the potency of the inhibition and the DDI with CYP1A2 substrates observed in vivo.

4.3 Reduction of Hydroxylamines in Human Liver Microsomes and Hepatocytes

The secondary hydroxylamine, N-OH-ENX, is an intermediate metabolite in the sequence for metabolic inactivation of CYP1A2 caused by ENX and we find that N-OH-ENX is reduced back to ENX in HLM and human hepatocytes. In the specific scenario of the ENX-CYP1A2 DDI, it is difficult to tell whether the reduction of N-OH-ENX to ENX matters. Due to the non-dissociative nature of CYP1A2 inactivation, it is not necessary to accumulate free N-OH-ENX in order to inactivate CYP1A2. In HLM, we found that the hydroxylamine reduction reaction carries little to no meaning. However, in the confined space of a hepatocyte it is possible that hydroxylamine reduction competes with the rate of N-OH-ENX entry into the cell (in experiments where N-OH-ENX is dosed directly). In that case, both N-OH-ENX and ENX would be present at comparable levels inside the hepatocyte despite a high excess of N-OH-ENX outside the hepatocyte. The resulting CYP1A2 inactivation rate would reflect a mixture of N-OH-ENX and ENX inside the cell and not the nominal concentration of N-OH-ENX in the incubation media. Therefore, at the very least the hydroxylamine reduction could interfere with the interpretation of in vitro data.

While it is difficult to say definitively how hydroxylamine reductase activity affected our study of CYP1A2 inactivation caused by ENX, hydroxylamine reductases may more generally prevent the accumulation of hydroxylamine metabolites of numerous drugs in vivo. It is possible that a number of dissociative DDIs (through binding of hydroxylamine metabolites to P450 enzymes and further metabolism to MI complexes) are being prevented on a daily basis by the presence of hydroxylamine reductase activity. The importance of hydroxylamine reduction in vitro and in vivo remains an open question.

4.4 Future Directions

The extent to which other alicyclic amine substrates can be metabolized to MI complexes with cytochrome P450 remains to be determined and a general SAR study is needed. Beginning with ENX and CYP1A2, where we have confirmed MI complex formation occurs, it would be informative to design analogues of ENX where the piperazine ring is modified or replaced by a piperidine or pyrrolidine followed by testing for whether MI complex formation is still viable. Additional P450 isoforms and other alicyclic amines could then be tested as the SAR for MI complex formation from alicyclic amines develops and becomes better understood.

We noted in our study that ENX appears to inactivate CYP1A2 through MI complex formation and a second mechanism whereas N-OH-ENX inactivates CYP1A2 exclusively through MI complex formation. If the “second mechanism” of CYP1A2 inactivation also involves metabolism of the piperazine ring, then a branch point exists between N-hydroxylation leading to MI complex formation and oxidation at a different site leading into another inactivation mechanism. This second mechanism of inactivation remains to be described and, with respect to the above SAR study design, there may be a clear structural determinant that affects whether an alicyclic amine is metabolized exclusively towards MI complex formation or, instead, bifurcates into MI complex formation and a separate inactivation mechanism.

Finally, we detected reduction of N-OH-ENX to ENX in HLM, mitochondria, and hepatocytes. The importance of this reaction is not clear in the context of our study on the inactivation of CYP1A2 by ENX and the associated in vivo DDIs with CYP1A2 substrates. We suggested that the reduction reaction is not likely to matter in broken-cell enzyme preparations, such as HLM, but may strongly modulate the concentration of N-OH-ENX in hepatocytes and in vivo. The answer can likely be found in the complex interplay between the rates for ENX and N-OH-ENX transport into and out of hepatocytes, inactivation rates of CYP1A2 by ENX or N-OH-ENX where these two species compete for the active site, and the changes in the relative levels

of these two species due to the rate of reduction of N-OH-ENX to ENX. Thoughtful experimental designs are needed to tease apart these factors.

We suspect the most useful tool for dissecting the importance of the reduction reaction would be to evaluate the P450 inactivation kinetics in the absence of the reduction reaction. In other words, chemical tools should be developed to “turn off” hydroxylamine reduction such as development of specific mechanism-based inhibitors of hydroxylamine reductases. Such mechanism-based inhibitors would facilitate study of both dissociative and non-dissociative sequential enzyme inactivation processes where hydroxylamine metabolites are intermediates in the formation of MI complexes.

At the heart of this dissertation is the topic of metabolite-mediated enzyme inactivation and whether or not this metabolite, the true mechanism-based inhibitor of the enzyme, arises from dissociative or non-dissociative sequential metabolism of the parent drug. In the case of inactivation of CYP1A2 by (a metabolite of) ENX, the mechanism appears to be non-dissociative and a key point is that, given what we know, the DDIs between ENX and CYP1A2 substrates likely depend on the inactivation process being non-dissociative. Thus, when the inactivation of a P450 enzyme involves sequential metabolism of a substrate by the same P450 isoform, we would advise that the degree to which inactivation arises through non-dissociative vs dissociative sequential metabolism be considered a *critical* component of the mechanism and a *necessary* piece of information for predicting how the sequential metabolic inactivation process will translate across in vitro systems to in vivo (Figure 4.1).

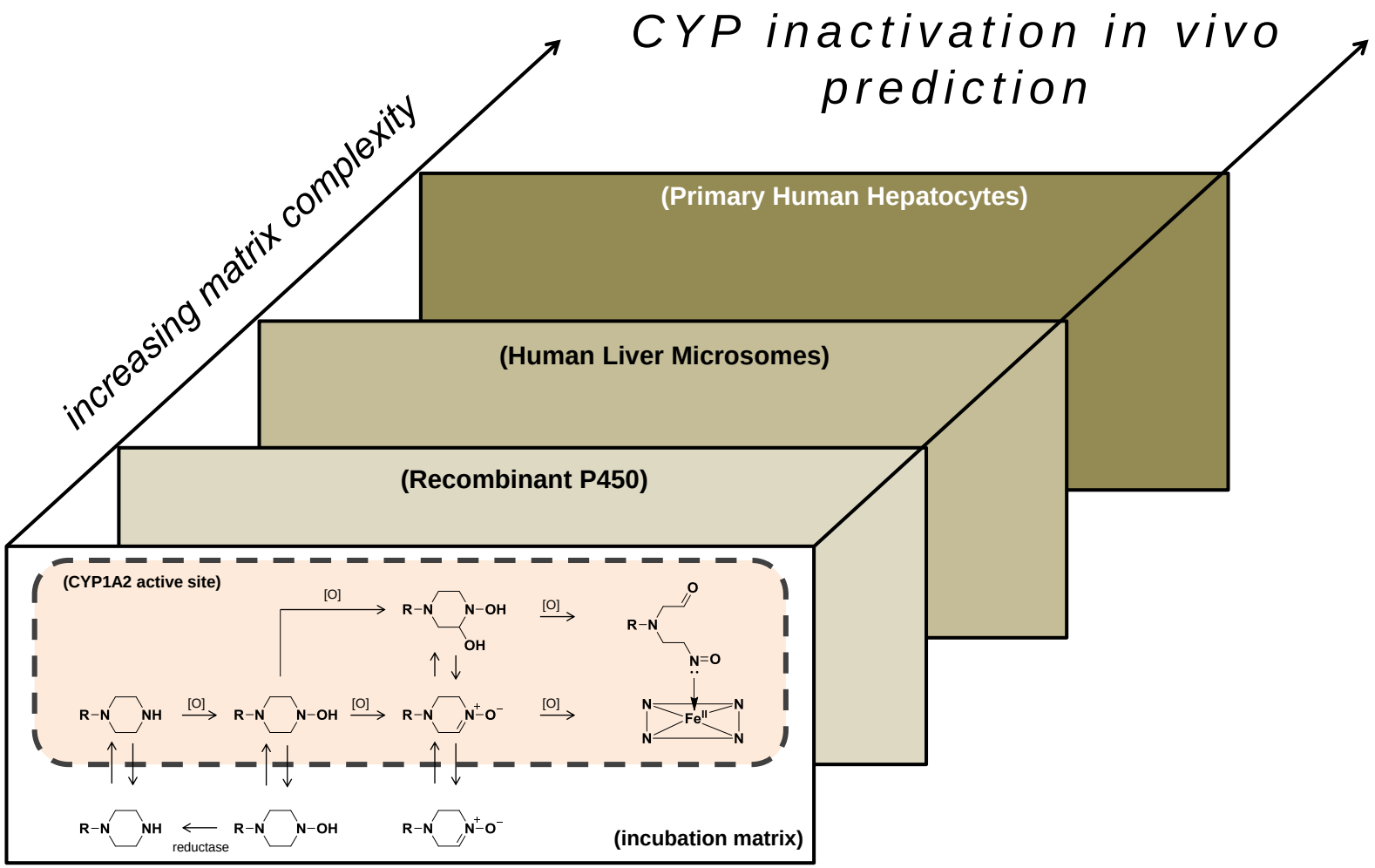

Figure 4.1 – Predicting from in vitro: translation of a sequential metabolic inactivation process across systems to in vivo
Non-dissociative sequential metabolism of a piperazine to a metabolic-intermediate complex within the CYP1A2 active site is conserved across systems.

References

Achour B, Russell MR, Barber J, and Rostami-Hodjegan A (2014) Simultaneous quantification of the abundance of several cytochrome P450 and uridine 5'-diphospho-glucuronosyltransferase enzymes in human liver microsomes using multiplexed targeted proteomics. *Drug Metab Dispos* **42:**500-510.

Andersson S, Hofmann Y, Nordling A, Li XQ, Nivelius S, Andersson TB, Ingelman-Sundberg M, and Johansson I (2005) Characterization and partial purification of the rat and human enzyme systems active in the reduction of N-hydroxymelagatran and benzamidoxime. *Drug Metab Dispos* **33:**570-578.

Argoti D, Liang L, Conteh A, Chen L, Bershas D, Yu CP, Vouros P, and Yang E (2005) Cyanide trapping of iminium ion reactive intermediates followed by detection and structure identification using liquid chromatography-tandem mass spectrometry (LC-MS/MS). *Chem Res Toxicol* **18:**1537-1544.

Backman JT, Kyrklund C, Neuvonen M, and Neuvonen PJ (2002) Gemfibrozil greatly increases plasma concentrations of cerivastatin. *Clinical pharmacology and therapeutics* **72:**685-691.

Baer BR, DeLisle RK, and Allen A (2009) Benzylic oxidation of gemfibrozil-1-O-beta-glucuronide by P450 2C8 leads to heme alkylation and irreversible inhibition. *Chem Res Toxicol* **22:**1298-1309.

Barbara JE, Kazmi F, Parkinson A, and Buckley DB (2013) Metabolism-dependent inhibition of CYP3A4 by lapatinib: evidence for formation of a metabolic intermediate complex with a nitroso/oxime metabolite formed via a nitrone intermediate. *Drug Metab Dispos* **41:**1012-1022.

Beckett AH, Jones GR, and Coutts RT (1976) Synthesis and properties of aralkylamine C-nitroso dimers. *Tetrahedron* **32:**1267-1276.

Brown HS, Wilby AJ, Alder J, and Houston JB (2010) Comparative use of isolated hepatocytes and hepatic microsomes for cytochrome P450 inhibition studies: transporter-enzyme interplay. *Drug Metab Dispos* **38:**2139-2146.

Burt HJ, Pertinez H, Sall C, Collins C, Hyland R, Houston JB, and Galetin A (2012) Progress curve mechanistic modeling approach for assessing time-dependent inhibition of CYP3A4. *Drug Metab Dispos* **40:**1658-1667.

Cerny MA and Hanzlik RP (2005) Cyclopropylamine inactivation of cytochromes P450: role of metabolic intermediate complexes. *Archives of biochemistry and biophysics* **436:**265-275.

Clement B, Behrens D, Moller W, and Cashman JR (2000) Reduction of amphetamine hydroxylamine and other aliphatic hydroxylamines by benzamidoxime reductase and human liver microsomes. *Chem Res Toxicol* **13:**1037-1045.

Clement B, Lomb R, and Moller W (1997) Isolation and characterization of the protein components of the liver microsomal O2-insensitive NADH-benzamidoxime reductase. *The Journal of biological chemistry* **272:**19615-19620.

Coon MJ, Vaz AD, McGinnity DF, and Peng HM (1998) Multiple activated oxygen species in P450 catalysis: contributions To specificity in drug metabolism. *Drug Metab Dispos* **26:**1190-1193.

Cooper DY, Levin S, Narasimhulu S, and Rosenthal O (1965) PHOTOCHEMICAL ACTION SPECTRUM OF THE TERMINAL OXIDASE OF MIXED FUNCTION OXIDASE SYSTEMS. *Science (New York, NY)* **147:**400-402.

Davydov DR (2001) Microsomal monooxygenase in apoptosis: another target for cytochrome c signaling? *Trends in Biochemical Sciences* **26:**155-160.

Davydov R, Strushkevich N, Smil D, Yantsevich A, Gilep A, Usanov S, and Hoffman BM (2015) Evidence That Compound I Is the Active Species in Both the Hydroxylase and Lyase Steps by Which P450scc Converts Cholesterol to Pregnenolone: EPR/ENDOR/Cryoreduction/Annealing Studies. *Biochemistry* **54:**7089-7097.

Delaforge M, Jaouen M, and Mansuy D (1984) The cytochrome P-450 metabolite complex derived from troleandomycin: properties in vitro and stability in vivo. *Chemico-biological interactions* **51:**371-376.

Diehl H, Capalna S, and Ullrich V (1969) The photochemical action spectrum of the carbon monoxide inhibited hydroxylation of cyclohexane by rat liver microsomes. *FEBS letters* **4:**99-102.

Drlica K and Zhao X (1997) DNA gyrase, topoisomerase IV, and the 4-quinolones. *Microbiology and molecular biology reviews : MMBR* **61:**377-392.

Edlund PO and Baranczewski P (2004) Identification of BVT.2938 metabolites by LC/MS and LC/MS/MS after in vitro incubations with liver microsomes and hepatocytes. *Journal of pharmaceutical and biomedical analysis* **34:**1079-1090.

Endo K, Helmkamp GM, Jr., and Bloch K (1970) Mode of inhibition of beta-hydroxydecanoyl thioester dehydrase by 3-decynoyl-N-acetylcysteamine. *The Journal of biological chemistry* **245:**4293-4296.

Faber MS and Fuhr U (2004) Time response of cytochrome P450 1A2 activity on cessation of heavy smoking. *Clinical pharmacology and therapeutics* **76:**178-184.

FDA (2016) Preventable Adverse Drug Reactions: A Focus on Drug Interactions, https://www.fda.gov/drugs/developmentapprovalprocess/developmentresources/druginteractionslabeling/ucm110632.htm.

Fowler S and Zhang H (2008) In vitro evaluation of reversible and irreversible cytochrome P450 inhibition: current status on methodologies and their utility for predicting drug-drug interactions. *The AAPS journal* **10:**410-424.

Franklin MR (1974) The Formation of a 455 nm Complex during Cytochrome P-450-Dependent N-Hydroxyamphetamine Metabolism. *Molecular Pharmacology* **10:**975-985.

Fromel T, Kohlstedt K, Popp R, Yin X, Awwad K, Barbosa-Sicard E, Thomas AC, Lieberz R, Mayr M, and Fleming I (2013) Cytochrome P4502S1: a novel monocyte/macrophage fatty acid epoxygenase in human atherosclerotic plaques. *Basic research in cardiology* **108:**319.

Fuhr U, Anders EM, Mahr G, Sorgel F, and Staib AH (1992) Inhibitory potency of quinolone antibacterial agents against cytochrome P450IA2 activity in vivo and in vitro. *Antimicrobial agents and chemotherapy* **36:**942-948.

Fuhr U, Strobl G, Manaut F, Anders EM, Sorgel F, Lopez-de-Brinas E, Chu DT, Pernet AG, Mahr G, Sanz F, and et al. (1993) Quinolone antibacterial agents: relationship between structure and in vitro inhibition of the human cytochrome P450 isoform CYP1A2. *Mol Pharmacol* **43:**191-199.

Fuhr U, Wolff T, Harder S, Schymanski P, and Staib AH (1990) Quinolone inhibition of cytochrome P-450-dependent caffeine metabolism in human liver microsomes. *Drug Metab Dispos* **18:**1005-1010.

Fujioka Y, Kunze KL, and Isoherranen N (2012) Risk assessment of mechanism-based inactivation in drug-drug interactions. *Drug Metab Dispos* **40:**1653-1657.

Granfors MT, Backman JT, Neuvonen M, and Neuvonen PJ (2004) Ciprofloxacin greatly increases concentrations and cypotensive effect of tizanidine by inhibiting its cytochrome P450 1A2–mediated presystemic metabolism. *Clinical Pharmacology & Therapeutics* **76:**598-606.

Grimm SW, Einolf HJ, Hall SD, He K, Lim HK, Ling KH, Lu C, Nomeir AA, Seibert E, Skordos KW, Tonn GR, Van Horn R, Wang RW, Wong YN, Yang TJ, and Obach RS (2009) The conduct of in vitro studies to address time-dependent inhibition of drug-metabolizing

enzymes: a perspective of the pharmaceutical research and manufacturers of America. *Drug Metab Dispos* **37:**1355-1370.

Guengerich FP (2001) Common and uncommon cytochrome P450 reactions related to metabolism and chemical toxicity. *Chem Res Toxicol* **14:**611-650.

Hamel B, Mottet N, Audran M, Costa P, and Bressolle F (2000) Pharmacokinetics of enoxacin and its oxometabolite after multiple oral dosing and penetration into prostatic tissue. *The Journal of antimicrobial chemotherapy* **46:**993-996.

Hanson KL, VandenBrink BM, Babu KN, Allen KE, Nelson WL, and Kunze KL (2010) Sequential metabolism of secondary alkyl amines to metabolic-intermediate complexes: opposing roles for the secondary hydroxylamine and primary amine metabolites of desipramine, (s)-fluoxetine, and N-desmethyldiltiazem. *Drug Metab Dispos* **38:**963-972.

Harder S, Staib AH, Beer C, Papenburg A, Stille W, and Shah PM (1988) 4-quinolones inhibit biotransformation of caffeine. *European journal of clinical pharmacology* **35:**651-656.

Hendrychova T, Anzenbacherova E, Hudecek J, Skopalik J, Lange R, Hildebrandt P, Otyepka M, and Anzenbacher P (2011) Flexibility of human cytochrome P450 enzymes: molecular dynamics and spectroscopy reveal important function-related variations. *Biochimica et biophysica acta* **1814:**58-68.

Hollenberg PF, Kent UM, and Bumpus NN (2008) Mechanism-based inactivation of human cytochromes p450s: experimental characterization, reactive intermediates, and clinical implications. *Chem Res Toxicol* **21:**189-205.

Ito K, Hallifax D, Obach RS, and Houston JB (2005) Impact of parallel pathways of drug elimination and multiple cytochrome P450 involvement on drug-drug interactions: CYP2D6 paradigm. *Drug Metab Dispos* **33:**837-844.

Jeffery EH and Mannering GJ (1983) Interaction of constitutive and phenobarbital-induced cytochrome P-450 isozymes during the sequential oxidation of benzphetamine. Explanation for the difference in benzphetamine-induced hydrogen peroxide production and 455-nm complex formation in microsomes from untreated and phenobarbital-treated rats. *Mol Pharmacol* **23:**748-757.

Jones DR, Gorski JC, Hamman MA, Mayhew BS, Rider S, and Hall SD (1999) Diltiazem Inhibition of Cytochrome P-450 3A Activity Is Due To Metabolite Intermediate Complex Formation. *Journal of Pharmacology and Experimental Therapeutics* **290:**1116-1125.

Kalgutkar AS, Bauman JN, McClure KF, Aubrecht J, Cortina SR, and Paralkar J (2009) Biochemical basis for differences in metabolism-dependent genotoxicity by two diazinylpiperazine-based 5-HT2C receptor agonists. *Bioorganic & medicinal chemistry letters* **19:**1559-1563.

Kalgutkar AS, Dalvie DK, Aubrecht J, Smith EB, Coffing SL, Cheung JR, Vage C, Lame ME, Chiang P, McClure KF, Maurer TS, Coelho RV, Jr., Soliman VF, and Schildknegt K (2007) Genotoxicity of 2-(3-chlorobenzyloxy)-6-(piperazinyl)pyrazine, a novel 5-hydroxytryptamine2c receptor agonist for the treatment of obesity: role of metabolic activation. *Drug Metab Dispos* **35:**848-858.

Kinzig-Schippers M, Fuhr U, Zaigler M, Dammeyer J, Rusing G, Labedzki A, Bulitta J, and Sorgel F (1999) Interaction of pefloxacin and enoxacin with the human cytochrome P450 enzyme CYP1A2. *Clinical pharmacology and therapeutics* **65:**262-274.

Kosoglou T, Statkevich P, Johnson-Levonas AO, Paolini JF, Bergman AJ, and Alton KB (2005) Ezetimibe: a review of its metabolism, pharmacokinetics and drug interactions. *Clinical pharmacokinetics* **44:**467-494.

Kumar V, Rock DA, Warren CJ, Tracy TS, and Wahlstrom JL (2006) Enzyme source effects on CYP2C9 kinetics and inhibition. *Drug Metab Dispos* **34:**1903-1908.

Kunze KL and Trager WF (1993) Isoform-selective mechanism-based inhibition of human cytochrome P450 1A2 by furafylline. *Chem Res Toxicol* **6:**649-656.

Kurian JR, Bajad SU, Miller JL, Chin NA, and Trepanier LA (2004) NADH cytochrome b5 reductase and cytochrome b5 catalyze the microsomal reduction of xenobiotic hydroxylamines and amidoximes in humans. *J Pharmacol Exp Ther* **311:**1171-1178.

Larrey D, Funck-Brentano C, Breil P, Vitaux J, Theodore C, Babany G, and Pessayre D (1983) Effects of erythromycin on hepatic drug-metabolizing enzymes in humans. *Biochem Pharmacol* **32:**1063-1068.

Lesher GY, Froelich EJ, Gruett MD, Bailey JH, and Brundage RP (1962) 1,8-NAPHTHYRIDINE DERIVATIVES. A NEW CLASS OF CHEMOTHERAPEUTIC AGENTS. *Journal of medicinal and pharmaceutical chemistry* **91:**1063-1065.

Lin JH and Lu AY (1998) Inhibition and induction of cytochrome P450 and the clinical implications. *Clinical pharmacokinetics* **35:**361-390.

Lindeke B (1982) The non- and postenzymatic chemistry of N-oxygenated molecules. *Drug Metab Rev* **13:**71-121.

Luffer-Atlas D, Vincent SH, Painter SK, Arison BH, Stearns RA, and Chiu SH (1997) Orally active inhibitors of human leukocyte elastase. III. Identification and characterization of metabolites of L-694,458 by liquid chromatography-tandem mass spectrometry. *Drug Metab Dispos* **25:**940-952.

Maeda T, Takahashi K, Ohtsu N, Oguma T, Ohnishi T, Atsumi R, and Tamai I (2007) Identification of influx transporter for the quinolone antibacterial agent levofloxacin. *Molecular pharmaceutics* **4:**85-94.

Mansuy D, Gans P, Chottard JC, and Bartoli JF (1977) Nitrosoalkanes as Fe(II) ligands in the 455-nm-absorbing cytochrome P-450 complexes formed from nitroalkanes in reducing conditions. *European journal of biochemistry / FEBS* **76:**607-615.

Marchbanks CR, Mikolich DJ, Mayer KH, Zinner SH, and Dudley MN (1990) Pharmacokinetics and bioavailability of intravenous-to-oral enoxacin in elderly patients with complicated urinary tract infections. *Antimicrobial agents and chemotherapy* **34:**1966-1972.

Mayhew BS, Jones DR, and Hall SD (2000) An in vitro model for predicting in vivo inhibition of cytochrome P450 3A4 by metabolic intermediate complex formation. *Drug Metab Dispos* **28:**1031-1037.

McGinnity DF, Berry AJ, Kenny JR, Grime K, and Riley RJ (2006) Evaluation of time-dependent cytochrome P450 inhibition using cultured human hepatocytes. *Drug Metab Dispos* **34:**1291-1300.

Miller RR, Doss GA, and Stearns RA (2004) Identification of a hydroxylamine glucuronide metabolite of an oral hypoglycemic agent. *Drug Metab Dispos* **32:**178-185.

Mizuki Y, Fujiwara I, and Yamaguchi T (1996a) Pharmacokinetic interactions related to the chemical structures of fluoroquinolones. *The Journal of antimicrobial chemotherapy* **37 Suppl A:**41-55.

Mizuki Y, Fujiwara I, Yamaguchi T, and Sekine Y (1996b) Structure-related inhibitory effect of antimicrobial enoxacin and derivatives on theophylline metabolism by rat liver microsomes. *Antimicrobial agents and chemotherapy* **40:**1875-1880.

Mizuki Y, Kamaura M, Yamaguchi T, Sekine Y, and Hashimoto M (1989) Interaction of enoxacin with theophylline in rats. *Arzneimittel-Forschung* **39:**593-597.

Mizuki Y, Yamamoto K, Yamaguchi T, Fujii T, Miyazaki H, and Ohmori H (1996c) Intermolecular interactions of antimicrobial fluoroquinolones with purified rat liver CYP1A2 studied by proton nuclear magnetic resonance spectroscopy. *Xenobiotica* **26:**1057-1066.

Mulder GJ, Nagelkerke JF, Tijdens RB, Wijnands WJ, and Van der Mark EJ (1988) Inhibition of the oxidative metabolism of theophylline in isolated rat hepatocytes by the quinolone antibiotic enoxacin and its metabolite oxoenoxacin, but not by ofloxacin. *Biochem Pharmacol* **37:**2565-2568.

Naeem A, Badshah SL, Muska M, Ahmad N, and Khan K (2016) The Current Case of Quinolones: Synthetic Approaches and Antibacterial Activity. *Molecules (Basel, Switzerland)* **21:**268.

Nakamura R, Yamaguchi T, Sekine Y, and Hashimoto M (1983) Determination of a new antibacterial agent (at-2266) and its metabolites in plasma and urine by high-performance liquid chromatography. *Journal of Chromatography B: Biomedical Sciences and Applications* **278:**321-328.

Nelson DR (2013) A world of cytochrome P450s. *Philosophical Transactions of the Royal Society B: Biological Sciences* **368**.

O'Neil IA, Cleator E, and Tapolczay DJ (2001) A convenient synthesis of secondary hydroxylamines. *Tetrahedron Letters* **42:**8247-8249.

Obach RS, Walsky RL, Venkatakrishnan K, Gaman EA, Houston JB, and Tremaine LM (2006) The utility of in vitro cytochrome P450 inhibition data in the prediction of drug-drug interactions. *J Pharmacol Exp Ther* **316:**336-348.

Ogliaro F, de Visser SP, Cohen S, Sharma PK, and Shaik S (2002) Searching for the Second Oxidant in the Catalytic Cycle of Cytochrome P450: A Theoretical Investigation of the Iron(III)-Hydroperoxo Species and Its Epoxidation Pathways. *Journal of the American Chemical Society* **124:**2806-2817.

Okuda K, Weber P, and Ullrich V (1977) Photochemical action spectrum of the co-inhibited 5beta-cholestane- 3alpha, 7alpha, 12alpha-triol 26-hydroxylase system. *Biochemical and biophysical research communications* **74:**1071-1076.

Omura T and Sato R (1964) THE CARBON MONOXIDE-BINDING PIGMENT OF LIVER MICROSOMES. I. EVIDENCE FOR ITS HEMOPROTEIN NATURE. *The Journal of biological chemistry* **239:**2370-2378.

Orr ST, Ripp SL, Ballard TE, Henderson JL, Scott DO, Obach RS, Sun H, and Kalgutkar AS (2012) Mechanism-based inactivation (MBI) of cytochrome P450 enzymes: structure-activity relationships and discovery strategies to mitigate drug-drug interaction risks. *Journal of medicinal chemistry* **55:**4896-4933.

Ortiz de Montellano PR (2005) *Cytochrome P450: Structure, Mechanism, and Biochemistry*. Kluwer Academic/Plenum Publishers, New York.

Parkinson A, Kazmi F, Buckley DB, Yerino P, Ogilvie BW, and Paris BL (2010) System-dependent outcomes during the evaluation of drug candidates as inhibitors of cytochrome P450 (CYP) and uridine diphosphate glucuronosyltransferase (UGT) enzymes: human hepatocytes versus liver microsomes versus recombinant enzymes. *Drug metabolism and pharmacokinetics* **25:**16-27.

Pershing LK and Franklin MR (1982) Cytochrome P-450 metabolic-intermediate complex formation and induction by macrolide antibiotics; a new class of agents. *Xenobiotica* **12:**687-699.

Pessayre D, Larrey D, Vitaux J, Breil P, Belghiti J, and Benhamou J-P (1982) Formation of an inactive cytochrome P-450 Fe(II)-metabolite complex after administration of troleandomycin in humans. *Biochemical Pharmacology* **31:**1699-1704.

Polasek TM, Elliot DJ, Somogyi AA, Gillam EM, Lewis BC, and Miners JO (2006) An evaluation of potential mechanism-based inactivation of human drug metabolizing cytochromes P450 by monoamine oxidase inhibitors, including isoniazid. *British journal of clinical pharmacology* **61:**570-584.

Reh R, Ozols J, and Clement B (2008) Involvement of stearoyl-CoA desaturase in the reduction of amidoxime prodrugs. *Xenobiotica* **38:**1177-1190.

Rendic S (2002) Summary of information on human CYP enzymes: human P450 metabolism data. *Drug Metabolism Reviews* **34:**83-448.

Roberts ES, Vaz AD, and Coon MJ (1991) Catalysis by cytochrome P-450 of an oxidative reaction in xenobiotic aldehyde metabolism: deformylation with olefin formation.

Proceedings of the National Academy of Sciences of the United States of America **88:**8963-8966.

Rodriguez RJ, Proteau PJ, Marquez BL, Hetherington CL, Buckholz CJ, and O'Connell KL (1999) Flavin-containing monooxygenase-mediated metabolism of N-deacetyl ketoconazole by rat hepatic microsomes. *Drug Metab Dispos* **27:**880-886.

Rosenthal I (1976) The synthesis of 18O-enriched KO2. *Journal of Labelled Compounds and Radiopharmaceuticals* **12:**317-318.

Sang H, Janzen EG, and Lewis BH (1996) Mass Spectrometry and Electron Paramagnetic Resonance Study of Free Radicals Spontaneously Formed in Nitrone−Peracid Reactions. *The Journal of Organic Chemistry* **61:**2358-2363.

Sarkar M, Polk RE, Guzelian PS, Hunt C, and Karnes HT (1990) In vitro effect of fluoroquinolones on theophylline metabolism in human liver microsomes. *Antimicrobial agents and chemotherapy* **34:**594-599.

Silverman R (1988) *Mechanism-Based Enzyme Inactivation: Chemistry and Enzymology*. CRC Press, Boca Raton, FL.

Smith DM (2007) Uncovering mechanisms to improve predictions: The alteration in CYP2C9 kinetics by albumin and identifying the cause of the drug-drug interaction between enoxacin and CYP1A2, in: *Medicinal Chemistry*, University of Washington, Seattle, WA, USA.

Soars MG, McGinnity DF, Grime K, and Riley RJ (2007) The pivotal role of hepatocytes in drug discovery. *Chemico-biological interactions* **168:**2-15.

Spaldin V, Madden S, Pool WF, Woolf TF, and Park BK (1994) The effect of enzyme inhibition on the metabolism and activation of tacrine by human liver microsomes. *British journal of clinical pharmacology* **38:**15-22.

Stein GE (1988) The 4-quinolone antibiotics: past, present, and future. *Pharmacotherapy* **8:**301-314.

Thesing J and Mayer H (1957) Cyclische Nitrone, II. Über die Polymeren des 2.3.4.5-Tetrahydro-pyridin-N-oxyds und verwandte Verbindungen. *Justus Liebigs Annalen der Chemie* **609:**46-57.

Tong Z, Chandrasekaran A, DeMaio W, Espina R, Lu W, Jordan R, and Scatina J (2010) Metabolism of vabicaserin in mice, rats, dogs, monkeys, and humans. *Drug Metab Dispos* **38:**2266-2277.

Trepanier LA and Miller JL (2000) NADH-dependent reduction of sulphamethoxazole hydroxylamine in dog and human liver microsomes. *Xenobiotica* **30:**1111-1121.

Tucker GT, Houston JB, and Huang SM (2001) Optimizing drug development: strategies to assess drug metabolism/transporter interaction potential--towards a consensus. *British journal of clinical pharmacology* **52:**107-117.

Tudela J, Garcia Canovas F, Varon R, Garcia Carmona F, Galvez J, and Lozano JA (1987) Transient-phase kinetics of enzyme inactivation induced by suicide substrates. *Biochimica et biophysica acta* **912:**408-416.

Ullrich V and Schnabel KH (1973) Formation and binding of carbanions by cytochrome P-450 of liver microsomes. *Drug Metab Dispos* **1:**176-183.

Uno T, Kondo H, Inoue Y, Kawahata Y, Sotomura M, Iuchi K, and Tsukamoto G (1990) Synthesis of antimicrobial agents. 3. Syntheses and antibacterial activities of 7-(4-hydroxypiperazin-1-yl)quinolones. *Journal of medicinal chemistry* **33:**2929-2932.

VandenBrink BM and Isoherranen N (2010) The role of metabolites in predicting drug-drug interactions: focus on irreversible cytochrome P450 inhibition. *Current opinion in drug discovery & development* **13:**66-77.

Vaz AD, Pernecky SJ, Raner GM, and Coon MJ (1996) Peroxo-iron and oxenoid-iron species as alternative oxygenating agents in cytochrome P450-catalyzed reactions: switching by

threonine-302 to alanine mutagenesis of cytochrome P450 2B4. *Proceedings of the National Academy of Sciences of the United States of America* **93:**4644-4648.
Vaz ADN, Roberts EA, and Coon MJ (1991) Olefin formation in the oxidative deformylation of aldehydes by cytochrome P-450. Mechanistic implications for catalysis by oxygen-derived peroxide. *Journal of the American Chemical Society* **113:**5886-5887.
Venkatakrishnan K, Obach RS, and Rostami-Hodjegan A (2007) Mechanism-based inactivation of human cytochrome P450 enzymes: strategies for diagnosis and drug-drug interaction risk assessment. *Xenobiotica* **37:**1225-1256.
Venkatakrishnan K, von Moltke LL, and Greenblatt DJ (1998) Human cytochromes P450 mediating phenacetin O-deethylation in vitro: validation of the high affinity component as an index of CYP1A2 activity. *Journal of pharmaceutical sciences* **87:**1502-1507.
Vincent TA (2005) The Quinolones: Past, Present, and Future. *Clinical Infectious Diseases* **41:**S113-S119.
Wang K and Guengerich FP (2013) Reduction of aromatic and heterocyclic aromatic N-hydroxylamines by human cytochrome P450 2S1. *Chem Res Toxicol* **26:**993-1004.
Werringloer J and Estabrook RW (1973) Evidence for an inhibitory product-cytochrome P-450 complex generated during benzphetamine metabolism by liver microsomes. *Life sciences* **13:**1319-1330.
Wienkers LC and Heath TG (2005) Predicting in vivo drug interactions from in vitro drug discovery data. *Nature reviews Drug discovery* **4:**825-833.
Wijnands WJ, van Herwaarden CL, and Vree TB (1984) Enoxacin raises plasma theophylline concentrations. *Lancet (London, England)* **2:**108-109.
Wijnands WJ, Vree TB, and van Herwaarden CL (1986) The influence of quinolone derivatives on theophylline clearance. *British journal of clinical pharmacology* **22:**677-683.
Wrighton SA, Maurel P, Schuetz EG, Watkins PB, Young B, and Guzelian PS (1985) Identification of the cytochrome P-450 induced by macrolide antibiotics in rat liver as the glucocorticoid responsive cytochrome P-450p. *Biochemistry* **24:**2171-2178.
Yamaguchi T, Suzuki R, and Sekine Y (1984) PHARMACOKINETICS OF A NEW ANTIBACTERIAL AGENT AT-2266 III PLASMA LEVELS AND URINARY EXCRETION OF AT-2266 AND ITS METABOLITES IN MAN. *CHEMOTHERAPY* **32:**109-116.
Yamano K, Yamamoto K, Kotaki H, Takedomi S, Matsuo H, Sawada Y, and Iga T (1999) Correlation between in vivo and in vitro hepatic uptake of metabolic inhibitors of cytochrome P-450 in rats. *Drug Metab Dispos* **27:**1225-1231.
Yates P, Eng H, Di L, and Obach RS (2012) Statistical methods for analysis of time-dependent inhibition of cytochrome p450 enzymes. *Drug Metab Dispos* **40:**2289-2296.
Yin W, Doss GA, Stearns RA, Chaudhary AG, Hop CE, Franklin RB, and Kumar S (2003) A novel P450-catalyzed transformation of the 2,2,6,6-tetramethyl piperidine moiety to a 2,2-dimethyl pyrrolidine in human liver microsomes: characterization by high resolution quadrupole-time-of-flight mass spectrometry and 1H-NMR. *Drug Metab Dispos* **31:**215-223.
Yin W, Mitra K, Stearns RA, Baillie TA, and Kumar S (2004) Conversion of the 2,2,6,6-tetramethylpiperidine moiety to a 2,2-dimethylpyrrolidine by cytochrome P450: evidence for a mechanism involving nitroxide radicals and heme iron. *Biochemistry* **43:**5455-5466.
Yoshimoto FK, Jung IJ, Goyal S, Gonzalez E, and Guengerich FP (2016) Isotope-Labeling Studies Support the Electrophilic Compound I Iron Active Species, FeO3+, for the Carbon–Carbon Bond Cleavage Reaction of the Cholesterol Side-Chain Cleavage Enzyme, Cytochrome P450 11A1. *Journal of the American Chemical Society* **138:**12124-12141.
Zhang H, Amunugama H, Ney S, Cooper N, and Hollenberg PF (2011) Mechanism-based inactivation of human cytochrome P450 2B6 by clopidogrel: involvement of both covalent modification of cysteinyl residue 475 and loss of heme. *Mol Pharmacol* **80:**839-847.

Zhao P, Kunze KL, and Lee CA (2005) Evaluation of time-dependent inactivation of CYP3A in cryopreserved human hepatocytes. *Drug Metab Dispos* **33:**853-861.

Zhou S, Yung Chan S, Cher Goh B, Chan E, Duan W, Huang M, and McLeod HL (2005) Mechanism-based inhibition of cytochrome P450 3A4 by therapeutic drugs. *Clinical pharmacokinetics* **44:**279-304.